STUDIES OF MEAN REYNOLDS STRESS MODELS OF TURBULENT FLOW

Thesis by

Philip Eric Wood

In Partial Fulfillment of the Requirements

for the Degree of

Doctor of Philosophy

California Institute of Technology

Pasadena, California

1978

(Submitted May 24, 1978)

ACKNOWLEDGMENTS

It must be nearly impossible to spend four or five years in graduate school and not acquire a long list of people who in some way have contributed to either your academic or personal well being. I would like to use this opportunity to express my sincere appreciation to these people for their kindness and interest in my career.

I would like to thank my adviser, Professor L. Gary Leal for suggesting my research problem and for his guidance throughout its completion. I am greatly indebted to Professors Philip Saffman, E. John List and Anafol Roshko for taking the time to share some of their knowledge of turbulence with me. Particular thanks also go to Dr. Fausto Millinazzo for his help with parts of the numerical solutions.

I am grateful to Dr. Ted Rhodes and Dr. Carl Gall of the Chemical Engineering Department at the University of Waterloo for encouraging me to attend graduate school. The Chemical Engineering faculty at Caltech are also acknowledged for their interest in me and for encouraging me to realize my career ambition.

I would like to acknowledge the financial support given by the California Institute of Technology in the form of Graduate Research and Teaching Assistantships and computing funds.

I benefitted from the friendship with the graduate students in the Chemical Engineering Department and special thanks go to my

colleagues in Dr. Leal's research group for our discussions of both a scientific and esoteric nature. The members and pastors of Knox United Presbyterian Church are gratefully acknowledged for their continuous support and fellowship.

Finally I would like to express my heartfelt thanks to my wife, Barbara. Her faith in me and her love and understanding made it all worthwhile.

To Barbara . . .

ABSTRACT

In this thesis a second order turbulence model is described which calculates the mean Reynolds stresses and dissipation rate for homogeneous and slightly inhomogeneous shear flows. The higher order terms which appear in the exact differential (transport) equations for the Reynolds stresses and dissipation rate are approximated in terms of the mean velocity gradient, Reynolds stresses and dissipation rate using some of the principles of invariant modeling. The unknown coefficients appearing in the models for the higher order terms were estimated by a systematic evaluation of the available experimental data for homogeneous turbulence. The model was used to calculate the Reynolds stresses for homogeneous shear flow, homogeneous strain and the decay of initially anisotropic turbulence.

The model was further tested by calculating the mean velocity and Reynolds stresses for two inhomogeneous free shear flows, the two dimensional turbulent jet and the two dimensional wake. The governing model equations were transformed into similarity form. A calculation procedure is described for the solution of the resulting set of nonlinear ordinary differential equations.

A simplified version of the mean Reynolds stress model was developed and it was also used to model the plane jet and wake.

TABLE OF CONTENTS

LIST OF TABLES

LIST OF FIGURES

Figure Page

CHAPTER 1

INTRODUCTION

1.1 Turbulence Modeling

There are many problems of technological interest where it would be advantageous to be able to numerically simulate or calculate a turbulent fluid flow. At the most fundamental level, it is of course well known that such flows are described completely by the Navier-Stokes equations (even the smallest length scales of a turbulent flow are orders of magnitude larger than the mean free path or molecular length scales of the fluid). However, the large spread between the smallest and largest length scales of a turbulent flow renders any direct attempt to numerically solve these equations completely impractical. Fortunately, in many cases, it is sufficient to be able to predict only certain mean (or time-averaged) features of the flow and the equations of motion can be considered in a more tractable, time-average form. The major difficulty with this approach is that the resulting equations for the time-averaged, statistical features of the flow are not closed. For example, the equations describing the mean velocity field contain the time average of the second moment, $\overline{u_i u_j}$, of the random fluctuations of the velocity about the mean and this quantity (which is known as the Reynolds stress) is itself known. Likewise, the governing equation for this "second-order" quantity contains unknown "third-order" velocity and pressure moments.

Although one can always derive new equations for these new higher-order moments, the new equations will then contain even higher-order moments. In all, an infinite set of differential equations would be required to "close" the system. This is the well known "turbulence closure problem."

This thesis is concerned with the development of an approximate closure of the time-average moment equations for turbulent flow. Such closure approximations, when based upon a combination of rigorous mathematics, intuition and experimental observation, are known as "turbulent models." At the simplest level of approximation, no differential equations are used except the equation for the mean velocity field, and the unknown mean Reynolds stresses are expressed as algebraic functions of the local mean field variables. Such a closure is called the Mean Velocity Field (MVF) closure. The next possible level of closure is at the second order and is known as the Mean Reynolds Stress (MRS) closure. Here the governing differential equations are retained both for the mean velocity and the Reynolds stresses, and the third order correlations which appear in the latter are expressed in terms of the first-order (mean field) and second-order quantities. These MRS models may be expected to yield a more complete description of the turbulent flow (e.g. they yield predictions for both the mean field and second-order moments), but they can only be developed at the expense of much more experimental and empirical input than is necessary for the MVF closure.

In view of this added complexity, it is logical to question the motivation for the development of a second-order model especially

since the first-order (MVF) models give acceptable results for the mean velocity fields in many situations. This question was recently considered by Lumley (1976) in an unpublished manuscript. The basic limitation of the MVF closure is that it is strictly applicable only to homogeneous (or nearly homogeneous) turbulent flows (i.e. flows for which the turbulence quantities are not functions of position in the flow). Thus when the MVF closure is used for predictions of more inhomogeneous flows, such as atmospheric flows (cf. Lumley, Zeman and Siess, 1978) unphysical predictions may result.

The MRS closure also assumes a degree of homogeneity, but in this case the assumption is applied to the models for the third-order turbulence quantities. Hence the assumption of homogeneity in the MRS models is expected to have less influence on the mean field calculations than for the MVF models. There are other reasons for considering a MRS level closure. In many cases the driving mechanism behind a particular aspect of the fluid motion is the magnitude of the difference between the diagonal components of the Reynolds stress tensor (for example, secondary flow in a duct, cf. Gessner and Emery, 1976). Such differences are possible with MRS models but not MVF models in their conventional forms. MRS models are also valuable as a basis for the rational development of intermediate closure models which lie between the MVF and full MRS models in complexity (cf. the models derived by Hanjalic and Launder 1972, 1976 and Pope, 1975). Such intermediate models will in fact be discussed in Chapter 4 in the context of the complete hierarchy of turbulent models, ranging from the full MRS to the much simpler MVF, which may be generated

by the progressive addition of increasingly restrictive assumptions to the full MRS models.

In the remainder of this introductory chapter, we set the scene for the main task of this thesis, which is the development and testing of a full MRS closure scheme. In particular, in the next two subsections, we briefly describe previous attempts to develop computational methods for turbulent flows. These divide naturally into two parts; closure models for the time average equations (i.e. turbulent models of the type considered in this thesis), and attempts to solve the Navier-Stokes equations in a more direct manner.

1.2 Direct Simulation and Related Methods

The Navier-Stokes equations apply to turbulent as well as laminar flows. For an incompressible, isothermal, Newtonian fluid these equations may be written:

$$\tilde{u}_{i,i} = 0 \tag{1.2.1a}$$

$$\dot{\tilde{u}}_i + \tilde{u}_j\tilde{u}_{i,j} = -\frac{1}{\rho}\,\tilde{p}_{,i} + \nu\tilde{u}_{i,jj} \tag{1.2.1b}$$

Here, we use the Cartesian summation convention (i.e. all repeated indices are summed over i = 1,2,3). The overdot in the first term denotes time differentiation and a comma denotes differentiation with respect to the subscripted spatial variables which appear after the comma (e.g. $\tilde{u}_{i,j} = \partial\tilde{u}_i/\partial x_j$). $\tilde{u}_i$ and $\tilde{p}$ are the instantaneous velocity and pressure fields respectively and ν and ρ are the kinematic viscosity and the fluid density. At high Reynolds numbers, equation (1.2.1) cannot be solved either analytically or numerically. This is

because of the wide range of length scales present in a turbulent flow. The largest of these scales contain most of the turbulent energy and are comparable in size to the lateral dimension of the flow. In the turbulence literature these scales are called integral scales and are denoted, ℓ. An estimation of their size can be obtained, for example, by considering the instantaneous photos of a turbulent mixing layer by Brown and Roshko (1974). It is clear from their figure 5 for example that the extent of the largest "eddies" is roughly equal to the width of turbulent region. On the other hand, the smallest scales of motion, where the turbulence energy is converted into heat by viscous dissipation, contain almost no energy. These eddies are comparable in size to the Kolmogorov length scale, $\eta = (\nu^3/\varepsilon)^{1/4}$, where ε is the viscous dissipation. The ratio of the smallest to the largest scales is thus (cf. Tennekes and Lumley, 1972) $\eta/\ell \sim R_\ell^{-3/4}$ where R_ℓ is the Reynolds number based on turbulence quantities. As the Reynolds number increases the numerical mesh required to resolve the smallest scales becomes prohibitively fine relative to ℓ and current computer memory capacities are quickly exceeded. [An example of the actual quantitative sizes of the largest and smallest eddies for pipe flow is given in Leslie (1973) and estimates of the actual computer core requirements are given in Shaanan et al. (1975) and Leslie (1973)]. For this reason, direct computer solutions to (1.2.1) are not currently feasible even for the simplest fully turbulent flows.

Two alternatives to direct simulation have been developed that retain at least some of its philosophy. These are: (1) the

Sub Grid Scale Method and (2) the Spectral or Galerkin Method. These methods are briefly described in the following subsections of this introductory chapter.

1.2.1 Sub-Grid Scale (SGS) Modeling

In sub-grid scale modeling, the governing Navier-Stokes equations are averaged, but only over small volume elements which are, in fact, comparable in size to the numerical grid volume. In this case, the Navier-Stokes equations (1.2.1), take the form

$$\dot{\bar{\tilde{u}}}_i = -(\overline{\tilde{u}_i\tilde{u}_j})_{,j} - \frac{1}{\rho}\overline{\tilde{p}}_{,i} + \nu\bar{\tilde{u}}_{i,jj} \tag{1.2.2}$$

in which the over bar represents a sub-grid scale average

$$\bar{\tilde{u}}_i(\underline{x},t) = \frac{1}{\Delta x'\Delta y'\Delta z'}\int_{x-\frac{1}{2}\Delta x'}^{x+\frac{1}{2}\Delta x'}\int_{y-\frac{1}{2}\Delta y'}^{y+\frac{1}{2}\Delta y'}\int_{z-\frac{1}{2}\Delta z'}^{z+\frac{1}{2}\Delta z'}\tilde{u}_i(\xi,\eta,\zeta,t)d\xi d\eta d\zeta \tag{1.2.3}$$

and $\Delta x'$, $\Delta y'$ and $\Delta z'$ are averaging increments. When the instantaneous velocity $\tilde{u}_i$ is expressed as the sum of a sub-grid scale average velocity and a fluctuating component,

$$\tilde{u}_i = \overline{u_i} + u_i' \qquad (\overline{u_i'} = 0) \tag{1.2.4}$$

the flux quantity $\overline{\tilde{u}_i\tilde{u}_j}$, becomes simply

$$\overline{\tilde{u}_i\tilde{u}_j} = \overline{u}_i\overline{u_j} + \overline{u_i'u_j'} \ . \tag{1.2.5}$$

Thus, the velocity field, including turbulent contributions, for the scales of motion greater than the grid spacing is resolved explicitly

using finite difference formulae, and the requirement for a turbulent model is limited to the sub-grid scale "fluxes" $\overline{u_i' u_j'}$. Most of the calculations using this method have employed a simple MVF closure for this term

$$\overline{u_i' u_j'} = K_m(\bar{u}_{i,j} + \bar{u}_{j,i}) \tag{1.2.6}$$

where K_m is a sub-grid scale eddy coefficient for momentum. Calculations using this approach have recently been carried out for a variety of homogeneous flows by Kwak, Reynolds and Ferziger (1975) and Shaanan, Ferziger and Reynolds (1975). Their results are in qualitative agreement with experiments. Earlier, Deardorff (1970) used (1.2.6) and (1.2.2) to model turbulent channel flows. He also obtained good agreement with the experimental data of Laufer (1950).

The principal advantage of the SGS method over a full turbulent model is that the closure approximation is applied only to the smaller scale motion. Since the small scales most nearly meet the criteria for a closure model (given § 2.3) the SGS model should give better predictions than a MVF closure which is applied to the whole spectrum of length scales. The basic disadvantage of the SGS approach however is that it is limited in accuracy by the size of the grid volume which may be practically used for numerical calculations. Due to the great storage demands this method places on the memory core of the computer, only grids which involve 16^3 to 32^3 total nodes have been used in calculations. Thus, if the Reynolds number is very large the sub grid scales which are modeled will lie in the energy containing range of eddies and the results will be very much

influenced by the kind of closure approximation which is used to model the sub-grid scale stresses. Another limitation of the SGS method is truncation error which arises when a finite difference approximation is employed for the large scale motions. A method which avoids such errors is the spectral method described in the next section.

The accuracy of the SGS scheme may, of course, be improved if a more sophisticated model is used for the sub-grid Reynolds stresses. This approach was actually followed by Deardorff (1973), who calculated the mean velocity and temperature and turbulence quantities for the planetary boundary layer, using a second-order turbulence model (similar to that of Donaldson, 1972) for the sub-grid scale Reynolds stresses. His calculations were in reasonable agreement with the data but were very expensive to carry out, taking 350 hours on a CDC 7600 computer to simulate 24 hours of actual time. This was about 2.5 times longer than required for similar calculations using equation (1.2.6) to model the SGS stresses (Deardorff, 1972). Nevertheless, Deardorff (1973) felt that the additional expense was justified since the more sophisticated model gave much better predictions for the mean velocity and temperature fields as well as being able to predict the sub-grid scale stresses themselves. Indeed, the success of Deardorff's calculations using a second order model for the sub-grid scale Reynolds stresses provides further motivation for studying MRS closures.

1.2.2 Spectral or Galerkin Methods

To implement the SGS model some method of discretization is required. The most common has been to use finite differences at grid notes. This allows the governing partial differential equations to be transformed into sets of simultaneous difference equations. An alternative approach is to expand the dependent variables in a set of orthogonal functions and then introduce these expansions into the governing equations giving a set of ordinary differential equations for the coefficients. The expansion in a finite Fourier series, i.e., Galerkin's method is the most efficient for computations. The Fourier decompositions for the instantaneous velocity and pressure fields are,

$$\begin{matrix}\tilde{u}(\underline{x},t) \\ \tilde{p}(\underline{x},t)\end{matrix} = \sum_{\underline{k}=-K}^{\underline{k}=K} \begin{matrix}\underline{v}(\underline{k},t)\exp(i\underline{k}\cdot\underline{x}) \\ \pi(\underline{k},t)\exp(i\underline{k}\cdot\underline{x})\end{matrix} \tag{1.2.7}$$

where,

$\tilde{\underline{u}}$,p are the instantaneous velocity and pressure fields

$\underline{v}$,π are their Fourier coefficients

$\underline{k}$ is the integer wave number vector with three components k_1, k_2 and k_3 with $\underline{k} = 2\pi\underline{n}$, $n_i = 0, \pm 1 \pm 2, \ldots$

K is the "cut-off" wave number, $-2\pi K \leq k_i \leq 2\pi K$.

The Fourier decompositions are substituted into (1.2.1) resulting in a system of ordinary differential equations for the Fourier coefficients $\underline{v}$, i.e.

$$\left(\frac{\partial}{\partial t} + \nu k^2\right) v_\alpha(k) = \frac{-i}{2} P_{\alpha\beta\gamma}(\underline{k}) \sum_{\underline{p}=-\underline{K}}^{\underline{K}} v_\beta(\underline{p}) v_\gamma(\underline{k}-\underline{p}) \tag{1.2.8a}$$

$$k_\alpha v_\alpha(\underline{k}) = 0 \qquad (1.2.8b)$$

with

$$P_{\alpha\beta\gamma}(\underline{k}) = k_\beta\left(\delta_{\alpha\gamma} - \frac{k_\alpha k_\gamma}{k^2}\right) + k_\gamma\left(\delta_{\alpha\beta} - \frac{k_\alpha k_\beta}{k^2}\right)$$

Equations (1.2.8) for $\underline{v}$ are solved numerically. The accuracy of this method is limited primarily by the maximum wave number K which can be employed. If the length scales present in a turbulent flow can be thought of in terms of inverse wave number then a restriction on K results in a restriction on the smallest length scales that can be computed. Orszag (1969) shows that a limitation on K also limits the direct numerical calculation of turbulent flows to $R_\lambda \sim 20$ (where R_λ is the turbulent Reynolds number based on the Taylor microscale, cf. Tennekes and Lumley, 1972, p. 68).

Recently Schumann and Patterson studied the viscous decay of isotropic turbulence (Schumann and Patterson, 1975a) and the return to isotropy of initially anisotropic turbulence (Schumann and Patterson, 1975b) using the spectral method. Their calculated results are in qualitative agreement with the available experimental data. Quantitative comparisons are not possible because of the low calculated value of R_λ (~20) versus the much higher experimental value of R_λ (~50).

Spectral calculations are expensive to carry out. Even for K only equal to 16, Orszag (1969) showed that the total number of multiplications involved in the right hand side of (1.2.8a) is roughly 3×10^9. Allowing 1 μsec for each operation this would require

~1 hr. for the multiplications alone at each time step. Orszag (1969) showed that this time could be reduced by judicious use of the fast Fourier transform but calculation times are still excessive. Thus it is our opinion that spectral calculations will not be used to solve problems of practical importance for some time to come. Nevertheless, they may prove useful in more specific applications, including generation of "numerical data" which can be used in validating the less rigorous closure approximations such as those described in the next section of this thesis. In particular, many of the terms arising in the transport equations for the second order correlations in an MRS model are not amenable to direct experimental measurement. Hence models for these terms can normally be tested only indirectly through their effect on the predictions of other mean flow properties. On the other hand, the spectral method just described can, in principle generate any desired correlation via a "numerical experiment." Such numerical experiments not only have the potential to provide "data" for difficult to measure correlation-quantities, but they may also be less expensive than their laboratory counterparts.

In addition to the limitations of the two methods just described, Orszag suggests additional reasons for considering a turbulence closure model rather than performing direct simulation, (1) a successful turbulent theory implies a greater physical understanding of turbulent flow, and (2) the results obtained by direct simulation must be ensemble averaged before they can be compared with experimental data. For these reasons, the Navier-Stokes equations are

usually considered in their time averaged form and closure is obtained using one of the methods described in the next section.

1.3 Closure Methods

The methods most frequently used to approximate turbulent flows are called "closure" methods. In this approach the instantaneous velocity and pressure fields appearing in (1.2.1) are decomposed into a mean $\{U_i, P\}$ and a fluctuating $\{u_i, p\}$ part. Then the time averaged equations of motion can be expressed (for steady flow) in the form

$$U_i U_{i,j} = \frac{-1}{\rho} P_{,i} + (2\nu S_{ij} - \overline{u_i u_j})_{,j} \qquad (1.3.1a)$$

$$U_{i,i} = 0 \qquad\qquad u_{i,i} = 0 \qquad (1.3.1b)$$

where $S_{ij} = \frac{1}{2}(U_{i,j} + U_{j,i})$ is the mean strain rate. As it stands, equation (1.3.1) is not closed since the $\overline{u_i u_j}$ are unknowns (six in all) in addition to U_i and P. To close (1.3.1) additional relations must be provided for these "second order quantities" (called Reynolds stresses). The simplest level of closure is the Mean Velocity Field (MVF) closure. In this closure, the $\overline{u_i u_j}$ are assumed to be described by a Newtonian constitutive equation based on an assumed (but overly simplified) analogy between turbulent and laminar momentum transport, i.e.

$$\overline{u_i u_j} = \frac{1}{3} q^2 \delta_{ij} - 2K_T S_{ij} \qquad (1.3.2)$$

where $q^2 = \overline{u_i u_i}$ is a scalar which can be combined with the dynamic pressure and K_T is the so-called "eddy" momentum diffusivity. K_T is determined by reference to experiment and is found to change from one type of flow to another.

Eddy diffusivity assumptions, such as (1.3.2) have been used successfully in calculations for decades. Nevertheless, they are well known to give implausible results in many important situations, including atmospheric flows (cf. Lumley, Zeman and Siess, 1978). The main difficulty with the theory is that it is based on the assumption that the length and time scales of turbulent motion are all small compared to the length and time scales of the mean flow. In other words, the turbulence is assumed to be nearly homogeneous, allowing the turbulence quantities to be related to the mean flow quantities at the same location. Thus the eddy diffusion theory is a "local" theory and implicitly assumes that an equilibrium relationship exists between the mean and fluctuating fields. Hence when more than one length or time scale exists (e.g. the case for a sudden change in boundary conditions) the eddy diffusivity (gradient transport) concept will break down. Recently, Zeman and Lumley (1976), Lumley, Zeman and Siess (1978) and Meroney (1976) have given examples of the failure of the gradient transport theory in cases where the buoyant mean shear production of turbulent kinetic energy are of comparable magnitude. The limitations of gradient transport models were also studied, from a more fundamental point of view, by Corrsin (1974).

Models which attempt to alleviate some of the limitations of the MVF closure are the so-called second-order or mean Reynolds

stress (MRS)[1] closures. At this level, exact differential (transport) equations are constructed for the Reynolds stresses and the necessary closure assumptions are applied to the third order quantities that appear in these equations. These higher order terms describe the convection, production, dissipation and intercomponent energy transfer of the Reynolds stresses and must be expressed in terms of the mean field quantities and Reynolds stresses themselves if the system is to be mathematically closed (i.e. have the same number of differential equations as unknowns).

Second-order calculation methods for engineering and atmospheric applications have been under development for some time. The earliest models of Donaldson (1972), Daly and Harlow (1970), Hanjalic and Launder (1972) and Lumley and Khajeh-Nouri (1974) were applied to isothermal flows primarily for the purpose of testing the closure assumptions. Recently the modeling group at Imperial College, London, England has extended the model of Hanjalic and Launder (1972) to: (1) account for the presence of a solid boundary, (Launder, Reece and Rodi, 1975); (2) account for gravitational (buoyancy) effects, (Launder, 1975); and (3) account for decreasing Reynolds number, (Hanjalic and Launder, 1976). The invariant method of Lumley and Khajeh-Nouri (1974) was extended to atmospheric flows by Zeman and Lumley (1976) and Lumley, Zeman and Siess (1978). Wyngaard and his associates have also used Lumley's method for their studies of the planetary boundary

---

[1]For the isothermal cases considered in this thesis, the only second order quantities calculated are the mean Reynolds stresses, $\overline{u_i u_j}$.

layer (cf. Wyngaard (1975) for their most recent calculations and references to their earlier studies). Turbulent free shear flow and various atmospheric flow calculations using Donaldson's (1972) model are summarized in a report by Lewellen (1975). Daly (1974) extended the model of Daly and Harlow (1970) to study turbulent transition in a buoyancy driven convection flow.

In most of the above cases the model development and verification has not been systematic. Hence when the early isothermal versions of the models were extended to more complicated flow situations, a systematic method was not generally used for the addition of new terms. As a result, there is presently disagreement, not only in the form of the models used by the various modeling groups, but particularly in the magnitude of the parameters appearing in these models. The present thesis is concerned with the systematic development of a second order turbulence model. A brief outline of the steps taken to develop this model is given in the next section.

1.4 Development of a Second Order Model

The development of calculation methods for turbulent flow has been closely linked to the increase in computing capability of the modern day computer. In the first half of this century turbulent closures were limited to the Mean Velocity Field type because they could be used to obtain solutions for some flow situations without the aid of a computer. The current version of high speed computers has reduced the computational limitations on the choice of turbulence models and today turbulence models have been proposed which contain

dozens of differential equations (cf. André et al., 1976). Nevertheless, we are still faced with a serious question as to the number of differential equations which can be kept in a model before the benefits of increasing refinement are outweighed by decreasing understanding of the turbulence quantities which must be approximated in these equations.

In this thesis we will consider the development of a second order turbulence model. This level of closure represents a compromise between (1) the simple MVF closure which was indicated in previous sections to be incorrect in many situations, and (2) third order closures which not only require many more differential equations but also require much more experimental input than the second order model. Even at second order the necessary models for the higher order moments that appear in the Reynolds stress equations contain a relatively large number of unknown constants that must be determined from experimental data. Thus, the validity of a second order model will depend strongly on the quality of the experimental data on which it is based.

The systematic development of a usable second order calculation procedure (and the outline of this thesis) is conveniently described using the following flow chart suggested by Bradshaw (1972). Three independent inputs are required for the initial development of a "turbulence model": exact transport equations; inspiration and formalism; and, finally, careful use of available experimental data. The governing transport equations for the Reynolds stresses are presented in § 2.1. These are obviously common to all MRS model

developers (though it should be noted that different equations have been proposed for generating the length scale which is required for non-dimensionalization).

The large number of available MRS models are thus distinguished primarily by differences in the other two inputs. Until recently, comparatively little attention had been paid to a systematic development of the closure relationships. Instead, the general approach was to suggest ad hoc closures based on physical "intuition"

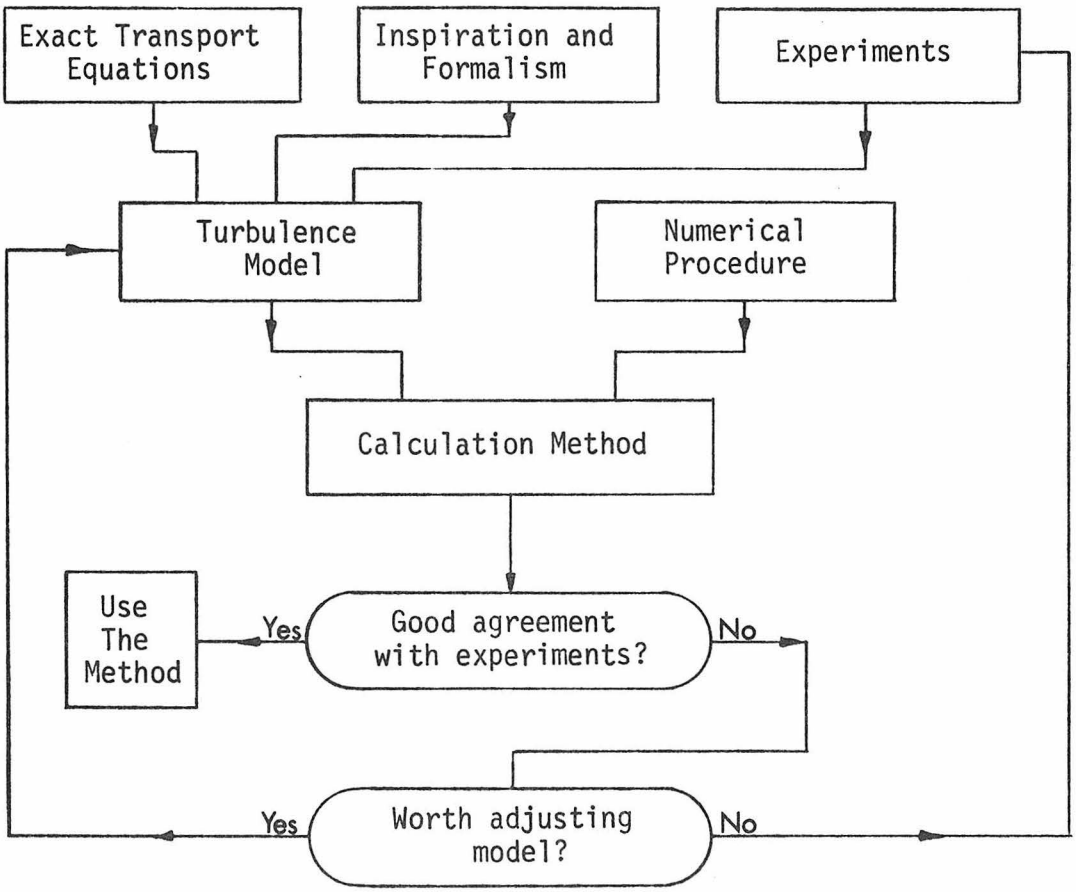

Figure 1.1.--Flow Chart for Model Development.

and dimensional analysis. All constants remaining in the resulting "model" equations were then adjusted to provide an optimal fit in some least squares sense to experimental data for a set of target flows. Since no systematic method was used to generate the model, no rational scheme existed for its improvement or extension if it did not provide a reasonable fit to the data. Furthermore, in our opinion, most of the previous modelers have devoted too little effort to the evaluation of the model constants. Models have typically been applied directly to complex flows with all of the constants adjusted simultaneously so that a reasonable fit to the experimental data results. As a consequence, however, the applicability of the models to other flows is uncertain, and in some instances models have been proposed which cannot predict even the simplest of wind-tunnel flows.

The more rational method used in this thesis to generate turbulence models for the third-order correlations was initiated in a series of papers by Lumley (Lumley, 1970, 1975a and Lumley and Khajeh-Nouri, 1974). The method was developed further in the theses of Cormack (1975) and Zeman (1975), and the final modeling scheme described in § 2.3 is a synthesis of the work of these earlier investigators. The models developed using the "rational" method are presented in sections 2.4 - 2.7. These models can be considered as consisting of two parts, (1) a term that is present, even in homogeneous flows and (2) corrections for inhomogeneity. In this thesis, only the homogeneous terms will be considered in detail. The reasons for this are two-fold. First, Pope (1978) and Cormack

(1975) have shown that the first contributions for inhomogeneity occur at order $\left(\frac{\ell}{L_0}\right)^2$, where ℓ is the integral length scale (a measure of large eddy size) and L_0 is some length scale which is characteristic of the inhomogeneity; for example, von Karman's scale

$$L_0 = (\partial U_1/\partial x_2)\Big/(\partial^2 U_1/\partial x_2^2). \tag{1.4.1}$$

Thus if the maximum eddy size is small compared to the scale of the inhomogeneity, the inhomogeneous contributions to the turbulence model will be negligible. Secondly, for a properly invariant second-order model, Cormack (1975) has shown that dozens of potential terms are possible at order $\left(\frac{\ell}{L_0}\right)^2$ in homogeneity. Since there are no <u>direct</u> experimental measurements of some of the higher order correlations and since the indirectly inferred values for these correlations are uncertain it is not prudent to use the information to estimate the great number of constants which arise at second order.

In addition to the rational method of model determination, a systematic method of parameter estimation was also undertaken. In Chapter 3 a method of parameter estimation is described which is comparable to the use of viscometric experiments in the material parameter determinations in rheology. By studying progressively more complicated flows the various physical phenomenon can be studied "one effect at a time" and the pertinent constants in the model can be determined uniquely. In particular, the homogeneous turbulent shear flow is shown to approach a unique structure for asumptotically long development times and this asymptotic structure can be used to

fix many of the parameters that appear in the homogeneous form of the model.

The homogeneous model developed by a consideration of homogeneous "viscometric" experiments is then tested by carrying out dynamic calculations for all types of homogeneous flows where adequate data is available for comparison. By proceeding in a stepwise fashion from a rational development of the models themselves to a systematic determination of the constants to a thorough testing of the model we feel that an optimal model can be developed for the available experimental data. This model will be "invariant" in the sense that it does not change under transformations of the co-ordinate axes and is also "invariant" in the sense that the constants, once determined for homogeneous flows, need not be adjusted when more complicated flow situations are encountered.

In Chapter 5 a numerical procedure for the calculation of self-similar turbulent free shear flows is developed using a mean Reynolds stress model. This allows a group of inhomogeneous flows to be simulated using the MRS model in its inhomogeneous form and compared to the available experimental data. Thus, the loop of model development and parameter determination by comparison with data outlined in Figure 1.1 is completed.

CHAPTER 2

PRINCIPLES OF MODEL DEVELOPMENT

2.1 Introduction

When the instantaneous velocity field is decomposed into mean and fluctuating components, $\tilde{u}_i = U_i + u_i$ an equation for the mean velocity field can be obtained by averaging the Navier-Stokes equations. As noted in the previous chapter, this equation

$$U_j U_{i,j} = \frac{-1}{\rho} P_{,i} + (2\nu S_{ij} - R_{ij})_{,j} \qquad (1.3.1a)$$

is not closed since it contains, in addition to the mean velocity and pressure, the additional unknowns, $R_{ij} = \overline{u_i u_j}$, which are known as the mean Reynolds stress components. Although a differential equation can be derived for R_{ij}, as indicated in Chapter 1, this equation in turn contains new, higher-order moments which are unknown and the system is still not closed. Indeed, the governing equations for the mean velocity and Reynolds stress fields can only be closed if some way is found to express the higher-order moments in terms of R_{ij}, U_i and appropriate characteristic length and velocity scales. Such closure relationships are, of course, not derived but rather developed from some initial hypothesis of functional form and the resulting equations are therefore "model" equations. When the closure approximation is applied to the unknown moments in the governing equation for R_{ij}, the result is a so-called "mean Reynolds stress (MRS)" model.

In this chapter, we derive governing equations for an MRS turbulence model. The starting point for this model is the exact equation for the velocity fluctuation, u_i, which is derived by subtracting (1.3.1a) from (1.2.1) to give

$$\dot{u}_i + U_j u_{i,j} + u_j u_{i,j} + u_j U_{i,j} = \frac{-1}{\rho} p_{,i} + R_{ij} + \nu u_{i,jj} \qquad (2.1.1a)$$

$$u_{i,i} = 0 \qquad (2.1.1b)$$

An equation for R_{ij} is determined by multiplying (2.1.1a) by u_j and averaging. Using continuity (2.1.1b), and rearranging, we obtain

$$R_{ij} + U_k (R_{ij})_{,k} = P_{ij} + \pi_{ij} + J'_{ijk,k} - D_{ij} \qquad (2.1.2a)$$

Here P_{ij} is the "production tensor,"

$$P_{ij} = -R_{ik} U_{j,k} - R_{jk} U_{i,k}; \qquad (2.1.2b)$$

π_{ij} is the "energy transfer" tensor,

$$\pi_{ij} = -\left(\overline{u_i p_{,j}} + \overline{u_j p_{,i}}\right)/\rho \; ; \qquad (2.1.2c)$$

and J'_{ijk} is the turbulent diffusion flux of R_{ij} in the x_k - direction,

$$J'_{ijk} = -\overline{u_i u_j u_k} + \nu R_{ij,k}. \qquad (2.1.2d)$$

Finally, D_{ij} is the viscous dissipation tensor,

$$D_{ij} = 2\nu \overline{u_{i,k} u_{j,k}} \; . \qquad (2.1.2e)$$

It may be noted that if (2.1.2) is contracted we obtain an equation for $q^2 = R_{ii}$, which will be called the "turbulent energy"[1] equation:

$$\dot{q}^2 + U_k(q^2)_{,k} = 2\mathcal{P} - 2\varepsilon + J^*_{k,k} \,. \tag{2.1.3}$$

Here $2\mathcal{P} = P_{ii}$, $J_k^* = J'_{iik}$ and $\varepsilon = D_{ii}$ is the isotropic dissipation rate (cf. Reynolds, 1976).

In later sections of this chapter the unknown moments appearing in (2.1.2), i.e. π_{ij}, J_{ijk} and D_{ij}, will be modeled in terms of: (1) the mean velocity gradient, (2) the mean Reynolds stresses and (3) the characteristic length and velocity scales of the turbulent flow. These variables will hereafter be called the "modeling variables." A necessary preliminary to the actual model development is a determination of appropriate characteristic length and velocity scales.

2.2 Characteristic Turbulent Length and Velocity Scales

Before the higher order moments appearing in (2.1.2a) can be modeled, one must have an appropriate characteristic length and velocity scale to render the model dimensionally consistent. An obvious choice for the velocity scale is,

$$u' = (q^2)^{\frac{1}{2}} \tag{2.2.1}$$

This is a better choice than $u' = (U_i U_i)^{\frac{1}{2}}$ because q^2 is invariant under Galilean transformations whereas $(U_i U_i)$ is not.

---

[1]Note that q^2 is actually twice the kinetic energy of the turbulent velocity fluctuations per unit volume.

If only a single length scale is used it must be a macro- or integral length scale. Some earlier modelers (notably Donaldson, 1972) specified such a length scale algebraically by considering the physics and geometry of the flow in question. The main drawback of this approach is that it is really only useful for flows in which a closure approximation much simpler than the MRS scheme is adequate. In cases where an explicit knowledge of the Reynolds stress field is important, it is often impossible to specify a length scale in any "a priori" fashion (notably in cases where the boundary conditions are changing rapidly with time or where secondary flow is important). One alternative approach, which has been adopted by many prior investigators to develop a transport equation for the length scale (or some quantity proportional to it) in a manner similar to that used to generate the R_{ij} - transport equation.

All of the approaches of this type which have been used so far, begin with the velocity fluctuation equation (2.1.1a). Wolfshtein (1970), Rodi and Spalding (1970) and Lewellen (1975) followed Rotta (1951) and derived an equation for the two-point velocity correlation, $R_{ii}(\underline{x},\underline{r}) = \overline{u_i(\underline{x})u_i(\underline{x} + \underline{r})}$, and then defined the integral length scale according to:

$$q^2L = c\int_{-\infty}^{\infty} R_{ii}(\underline{x},\underline{r})\, d\underline{r} \qquad (2.22)$$

A transport equation for q^2L is thus obtained by integrating the differential equation for $R_{ii}(\underline{x},\underline{r})$. Since equation (2.1.3) can be used to determine q^2, L is known implicitly.

Another quantity that can be used to generate a length scale is the dissipation rate, $\varepsilon = 2\nu\overline{u_{i,k}u_{i,k}}$. An advantage in using ε to define a length scale is that ε itself appears in the q^2 equation (2.1.3). Furthermore, it may be shown from dimensional considerations that

$$\varepsilon \sim \frac{(u')^3}{L}$$

Hence, using $(q^2)^{\frac{1}{2}}$ to estimate u', a length scale can be generated from the dissipation according to:

$$L = \frac{c(q^2)^{3/2}}{\varepsilon} \tag{2.2.3}$$

A transport equation for ε can be obtained by differentiating (2.1.1a) for the velocity fluctuation u_i with respect to x_j, multiplying the result by $2\nu u_{i,k}$, and then averaging. The result is

$$\begin{aligned}\dot{\varepsilon} + U_j\varepsilon_{,j} = &\underbrace{-2\nu\overline{u_{i,j}u_{j,k}u_{i,k}}}_{(i)} \quad \underbrace{- 2\nu^2\overline{u_{i,jk}u_{i,jk}}}_{(ii)} \\ &-2\nu(\overline{u_{i,j}u_{i,k}}\,U_{j,k} + \overline{u_{i,k}u_{j,k}}\,U_{i,j}) - 2\nu\overline{u_j u_{i,k}}U_{i,jk} \\ &-[\nu(\overline{u_j u_{i,k}u_{i,k}}) + 2\nu\,\overline{u_{j,k}p}_{,k} - \nu\varepsilon_{,j}]_{,j}\end{aligned} \tag{2.2.4}$$

Lumley and Khajeh-Nouri (1974) and Cormack (1975) applied an order of magnitude analysis to equation (2.2.4) and found that, for infinite Reynolds number, terms (i) and (ii) were $O(R_\ell^{\frac{1}{2}})$ with respect to the next largest terms. However, it is their difference that is important and the difference is the same order as the other terms in (2.2.4).

As a result of the order of magnitude analysis, equation (2.2.4) may be approximated, for large R_ℓ, by

$$\dot{\varepsilon} + U_j \varepsilon_{,j} = \Delta_\varepsilon - H_{j,j}. \tag{2.2.5a}$$

Here, $$\Delta_\varepsilon = 2\nu(\underbrace{\overline{u_{i,j}u_{j,k}u_{i,k}}}_{(i)} + \underbrace{\nu\overline{u_{i,jk}u_{i,jk}}}_{(ii)}) \tag{2.2.5b}$$

represents the balance between (i) the production of dissipation by vortex stretching, and (ii) the viscous destruction of dissipation, and

$$H_j = \nu(\overline{u_j u_{i,k} u_{i,k}} + 2\nu\overline{u_{j,k}p}_{,k} - \nu\varepsilon_{,j}) \tag{2.2.5c}$$

is the diffusive flux of ε in the x_j-direction. Obviously, if the turbulence is homogeneous H_j is negligible.

As was the case for the Reynolds stress transport equation, the terms Δ_ε and H_j must be expressed in terms of the modeling variables if the equation (2.2.5) is to be incorporated into a turbulence model.

Either of the equations, for ε or (q^2L) may be used to generate a transport equation for the length scale L. Indeed, with exception of models for the diffusion term, H_j, Bradshaw (1972) has shown that all of the proposals for length scale equations can be cast in <u>one</u> common form. In the present work, we utilize the dissipation equation because ε appears directly in the turbulent energy equation and also appears (see § 2.4) equally apportioned, in each of the equations for the normal Reynolds stress components (R_{11}, R_{22}

and R_{33}). In our opinion, another factor in favor of using the ε-equation is that it has more convenient boundary conditions than an equation for L would have in numerical calculations. In particular for free shear flows, ε approaches zero near the edge of the flow, but L approaches some finite (but unknown) value.

In section 2.6 the unknown moments appearing in (2.2.5) will be expressed as functions of the modeling variables. The method used to carry out this modeling is described in the next section.

2.3 The Modeling Method

The development of a second order (Reynolds stress) model requires that all of the higher-order moments, $\pi_{ij}(\underline{x},t)$, $D_{ij}(\underline{x},t)$ and $J'_{ijk}(\underline{x},t)$ in equation (2.1.1) and $\Delta_\varepsilon(\underline{x},t)$ and $H_j(\underline{x},t)$ in equation (2.2.5) be expressed as functions of the modeling variables. The most general form for such a model is:

$$Q_{ijk}(\underline{x},t) = \int_{-\infty}^{t} dt' \int_{-\infty}^{\infty}\int\int\int d\underline{\xi}\; F_{ijk}[U_{i,j}(\underline{x}+\underline{\xi},\tau),\; R_{ij}(\underline{x}+\underline{\xi},\tau),\; \varepsilon(\underline{x}+\underline{\xi},\tau)] \tag{2.3.1}$$

where $\tau = t-t'$, Q_{ijk} is any of the higher-order moments and F_{ijk} is a generalized functional of its arguments extending over the whole fluid and all previous time. Of course, in the general form, the model is useless for computation and the development of a simpler version is therefore mandatory. The basis for this development, in the present work is Lumley's (1967,1970) suggestion that the turbulence exhibits two of the properties of Coleman and Noll's (1961) "simple fluid" model, namely, (1) a fading memory for prior

configurations, and (2) a limited awareness of its surroundings. These assumptions allow the unknown general functionals at a point (2.3.1) to be expressed as a function of the second order quantities and their first few spatial derivatives, evaluated at the same point.

This crucial assumption of dependence only upon local flow properties is, of course, the very assumption for which the eddy viscosity hypothesis was discarded. It implies that the length scales of the modeled quantities are short relative to those of the mean flow, so that the local flow is nearly homogeneous (or in equilibrium). Implicit in all MRS models is the assumption that this hypothesis will have less effect on the mean flow properties when it is applied to the higher order moments than it does in the form of the eddy viscosity hypothesis.

Following Lumley and Khajeh-Nouri (1974), Cormack (1975) suggested the following rational scheme for approximating the third order moments in terms of the modeling variables.

(1) The stress R_{ij} is decomposed into a dimensionless deviator,

$$b_{ij} = \frac{R_{ij}}{q^2} - \frac{1}{3}\delta_{ij}. \qquad (2.3.2)$$

The term b_{ij} reflects the anisotropy of the turbulence. In the "rational" approach of Cormack (1975) and of Lumley and Khajeh-Nouri (1974), all terms in the model for any third-order moment are ordered with respect to their dependence on the anisotropic character of the turbulence. Scalars

such as q^2 and ε which are nonzero in isotropic turbulence are classified as zero-order in anisotropy. The deviator b_{ij}, which is zero for isotropic turbulence is then first-order in anisotropy while scalars such as the second and third principal invariants of b_{ij}. $II = b_{ij}b_{ji}$ and $III = b_{ij}b_{jk}b_{ki}$ are second and third order in anisotropy.

(2) The function representing any third-order moment at some point x in the flow is expressed via a Taylor series expansion in gradients of b_{ij}, q^2 and ε.

All terms in the expansion are then classified with respect to their dependence on the non-homogeneity of the turbulence. The local values of b_{ij}, etc. are non zero for homogeneous flow, and are hence zero-order in "inhomogeneity," while their gradients are first-order and so on to higher order in "inhomogeneity." The order of inhomogeneity depends upon the order of differentiation for a specific term.

(3) The tensor coefficients, which are functions of the local values of b_{ij}, q^2 and ε, are written in invariant form, in order of increasing anisotropy and inhomogeneity.

Lumley (1970) provided a method of determining how many invariants are required.

(4) Apply dimensional analysis to the coefficients using the length and velocity scales defined in § 2.2.

Application of the above rules is subject to the following limitations as noted by Cormack (1975) and Zeman (1975).

(a) The turbulence Reynolds number based on the integral length scale must be very large, i.e.

$$R_\ell = \frac{u'\ell}{\nu} = \frac{(q^2)^2}{\varepsilon\nu} >> 1 \tag{2.3.3}$$

Where ℓ is proportional to the integral length scale L, i.e., $\ell \sim \frac{(q^2)^{3/2}}{\varepsilon}$

(b) The turbulence length scale, ℓ, must be small compared with the distance to the nearest solid boundary, L_w, i.e.,

$$\frac{\ell}{L_w} << 1 \tag{2.3.4}$$

(c) The flow must be weakly inhomogeneous and anisotropic. This requires that

$$\frac{\ell}{L_0} << 1 \text{ and } II << 1. \tag{2.3.5}$$

Here ℓ is used as a measure of characteristic eddy dimension and L_0 characterizes the inhomogeneity of the mean flow.

Cormack (1975) carried out expansions for the unknown moments in equation (2.1.2) and (2.2.5) using the above rules. However he assumed that F_{ijk} in equation (2.3.1) was <u>not</u> a function of $U_{i,j}$.

This assumption was based on the observation that $U_{i,j}$ is directly dependent on the Reynolds stress field $R_{ij}(\underline{x},t)$ and so can be included in the functionality implicitly, using only ε, q^2 and R_{ij} in the modeled terms. It should be noted, however, that a unique relationship for computation of $U_{i,j}$ from R_{ij} does not exist for all types of flow. Furthermore, the mean velocity gradient arises explicitly in the exact integral expression for π_{ij}, thus demonstrating the convenience, if not quite the proven need, to retain $U_{i,j}$ explicitly as one of the independent modeling variables. In the following sections of this chapter models are derived for π_{ij}, Δ_ε and D_{ij} using the method outlined above with $U_{i,j}$ included as a modeling variable. Models for J_{ijk} and H_j have been developed by Cormack et al. (1977) and Launder, Reece and Rodi (1975) and their suggestions will be reviewed in § 2.7. Terms that appear in the functional expansion for π_{ij} and Δ_ε are of two types: (1) those which are present in homogeneous flows and (2) corrections to account for inhomogeneity. In the second order model developed here, terms of type (2) will be neglected. Pope (1978) and Rotta (1975) have shown that these terms are of order $\left(\frac{\ell}{L_o}\right)^2$ relative to the homogeneous terms. Hence for nearly homogeneous flows they will be negligible. Cormack (1975) has also shown that the first corrections to π_{ij} and Δ_ε are second order in inhomogeneity. At second order, however, there are far too many terms to be estimated sensibly from the limited data which are available for π_{ij} and Δ_ε.

2.4 The Dissipation Tensor D_{ij}

There have been only two proposals relating the dissipation tensor D_{ij} to the modeling variables. At very high Reynolds numbers there is a length scale separation between the largest and smallest eddies and it is assumed that the "energy cascade" process does not transmit the directional preferences of the large scale motion to the smaller dissipative eddies. Hence in the limit of infinite R_ℓ, the smallest eddies, where the dissipation occurs, are assumed to be in a state of local isotropy. In this case,

$$D_{ij} = \frac{2}{3} \delta_{ij} \varepsilon \tag{2.4.1}$$

As the turbulence Reynolds number decreases, however, the length scale range of energy containing eddies and that of the dissipative eddies begins to overlap and the dissipative process becomes anisotropic. Since no experiments have truly infinite R_ℓ, Daly and Harlow (1970), Donaldson (1972) and Mjolsness and Petschek (1977) have all proposed that the dissipation tensor be approximated in terms of ε, with a proportionality coefficient whose magnitude depends on the amount of turbulent energy in each component,

$$D_{ij} = \frac{2\overline{u_i u_j}}{q^2} \varepsilon \tag{2.4.2}$$

Equation (2.4.2) implies that the dissipative eddies are similar in structure to the energy containing ones, a fact which is true only in the limit $R_\ell \to 0$ (Hanjalic and Launder, 1977).

To accommodate both of the asymptotic expressions, Schumann and Patterson (1975) and Hanjalic and Launder (1976) have considered the combined form

$$D_{ij} = \frac{2}{3}\varepsilon\{(1-d)\delta_{ij} + \frac{3}{2}\frac{\overline{u_i u_j}}{q^2} d\} \qquad (2.4.3)$$

where d is a function of R_ℓ with asymptotic values $d \to 0$ for $R_\ell \to \infty$ and $d \to 1$ for $R_\ell \to 0$.

Since the model which is developed in this thesis is intended to approximate only high Reynolds number flows and since the anisotropic part of (2.4.3) could be included in the model for π_{ij} (see § 2.5) by a simple change in a constant, the isotropic formula, i.e. equation (2.4.1), will be used to model D_{ij} in dynamic calculations.

2.5 Modeling the Pressure-Velocity Correlation, π_{ij}

The pressure gradient-velocity interaction term in the Reynolds stress equation is,

$$\pi_{ij} = -(\overline{u_i p_{,j}} + \overline{u_j p_{,i}})/\rho \qquad (2.5.1)$$

It is convenient, for modeling purposes, to split π_{ij} into two parts, one corresponding to an energy transport term, and the other to inter-component energy redistribution. This is accomplished by expressing π_{ij} in the form

$$\pi_{ij} = T_{ij} - [(\overline{pu_i})_{,j} + (\overline{pu_j})_{,i}]/\rho. \qquad (2.5.2)$$

The term, $T_{ij} = \overline{p(u_{i,j} + u_{j,i})}/\rho$, which is called the "pressure-strain" correlation, is zero when i = j and thus does not influence the <u>total</u> energy at a point, but merely serves to redistribute the energy amongst the components of the Reynolds stress tensor. The second part of π_{ij} which is known as the "pressure-diffusion" term, corresponds to a net transport of kinetic energy. Since it cannot be measured independently, it is most conveniently modeled with the other transport terms in equation (2.1.2a), i.e. J'_{ijk}. Lumley (1975b) has argued that the decomposition (2.5.2) is not unique. In particular, he recommends the formation of a deviatoric part for π_{ij} by simply subtracting its trace. This gives

$$T_{ij}^* = -(\overline{p,_i u_j} + \overline{p,_j u_i})/\rho + \frac{2}{3}\delta_{ij}(pu_k),_k/\rho \qquad (2.5.3)$$

for the energy redistribution part and leaves $-\frac{2}{3}\delta_{ij}(\overline{pu_k}),_k/\rho$ for the energy transport term. In homogeneous turbulent flow the transport term, is, of course, zero and the models developed for T_{ij} or T_{ij}^* would be necessarily equal. Furthermore, since the homogeneous representation of T_{ij} of T_{ij}^* will be used even in moderately inhomogeneous situations, the choice between the two decompositions (2.5.2) or (2.5.3) is arbitrary. In the present work, we will adopt (2.5.2) since it is more common and thus more easily compared with previous models. Let us now turn to the development of a model for T_{ij}.

Rather than proceed formally as the modeling method would suggest, it is instructive in this case to express the fluctuating pressure in terms of the velocity field. This results in a closed integral form for T_{ij} in terms related only to the velocity field.

Although the resulting expression for T_{ij} must still be modeled, this procedure does allow for more physics to be incorporated into the model which is finally generated.

Therefore, let us begin with an equation for the fluctuating pressure, which can be obtained by taking the divergence of (2.1.1a). After rearrangement

$$\frac{1}{\rho}\nabla^2 p = -(S_1 + S_2) \tag{2.5.6}$$

where $S_1 = 2U_{i,j}u_{j,i}$ and $S_2 = (u_i u_j - \overline{u_i u_j})_{,ij}$. A formal solution to (2.5.6) is given by:

$$\frac{4\pi}{\rho} p = \iiint_V GS_1 dV + \iiint_V GS_2 dV \tag{2.5.7}$$

where the control volume V has zero fluctuations on its boundary and $G(\underline{x},\underline{r})$ is the Green's function for the Laplacian operator. Examination of (2.5.6) shows that pressure fluctuations are caused by two mechanisms:

(1) S_1, the interaction between the mean velocity gradient and the turbulent field, and

(2) S_2, the fluctuations of the Reynolds stress components about their mean values.

An equation for the pressure-strain correlation T_{ij}, is obtained by averaging $(u_{i,j} + u_{j,i})$ with p. The result, given by Rotta (1951), for points far from solid surfaces is

$$T_{ij} = \frac{1}{2\pi}\int_{Vol} U'_{\ell,m}\,\overline{u'_{m,\ell}(u_{i,j} + u_{j,i})}\frac{dVol}{\underline{x}} + \frac{1}{4\pi}\int_{Vol}\overline{(u_\ell u_m)'_{,\ell m}(u_{i,j} + u_{j,i})}\frac{dVol}{\underline{x}}$$

$$= T_{ij}^1 + T_{ij}^2 \tag{2.5.8}$$

In this expression, terms without primes are evaluated at the fixed point $\underline{x}_0$ while those with primes are evaluated at $\underline{x}_0 + \underline{x}$. Since there are two district sources of pressure fluctuations with apparently different dynamical behavior, the two terms T_{ij}^{1} and T_{ij}^{2} are modeled separately

A. The Rapid Part, T_{ij}^{1}

The term T_{ij}^{1} was given the designation "rapid" by Lumley (1975a) because it is related to the pressure contribution which derives from the interaction between the mean velocity gradient and the turbulent fluctuation field. This pressure corresponds, in principle, to the pressure appearing in the "rapid distortion" theory of Batchelor and Proudman (1954). The term, T_{ij}^{1}, can be approximated by utilizing the fact that the gradients of the velocity fluctuations (e.g. $u_{i,j}$) are largest for the smallest length scales, and $U_{\ell,m}$ is essentially constant on this scale. Thus, $U_{\ell,m}$ can be taken outside the integral in (2.5.8). If we also use the result of von Karman and Howarth (1938),

$$\overline{u_{i,j}u'_{m,\ell}} = -(\overline{u_i(\underline{x})u_m(\underline{x}+\underline{r})})_{,j\ell} \qquad (2.5.9)$$

then,

$$T_{ij}^{1} \simeq = \frac{1}{2\pi}\frac{dU_\ell}{dX_m}\left[\iiint_{Vol}\frac{\partial^2\overline{u_i(\underline{x})u_m(\underline{x}+\underline{r})}}{\partial r_\ell \partial r_j}\,\frac{dVol}{\underline{r}}\right. \qquad (2.5.10)$$

The dependence on $\frac{dU_\ell}{dX_m}$ is explicit but we need a model, either for the integral or (what is equivalent) for the velocity correlation

inside the integral. Three approaches have been advocated for modeling T_{ij}^{1}. A physical approach has been used by Wolfshtein and his co-workers [Naot, Shavit, and Wolfshtein (1973), Lin and Wolfshtein (1977)], who devise approximatations of varying complexity for the correlation functions $R_{im}(\underline{x},\underline{r}) = \overline{u_i(\underline{x})u_m(\underline{x} + \underline{r})}$, which are then integrated to determine T_{ij}^{1}. As an example, the result obtained for an isotropic correlation function is derived in appendix B. If the correlation model is allowed to depend linearly on the Reynolds stress the result obtained by Naot et al. (1973) is the same as that obtained by Launder, Reece and Rodi (1975) and Reynolds (1976) who model the integral as the most general fourth order tensor, linear in the Reynolds stress, which satisfies the continuity and symmetry constraints. The approach to modeling T_{ij}^{1} that we follow is consistent with the modeling method suggested in § 2.3. Thus, we formally expand the integral about the isotropic state using the small parameter b_{ij}. That is, we write

$$T_{ij}^{1} = \frac{2dU_{\ell}}{dx_m} B_{ij\ell m} \tag{2.5.11}$$

where $B_{ij\ell m}$ is a fourth order tensor. If we assume that $B_{ij\ell m}$ is isotropic, the result is

$$B_{ij\ell m} = \{- \frac{1}{15}\delta_{ij}\delta_{\ell m} + \frac{1}{10}(\delta_{i\ell}\delta_{jm} + \delta_{im}\delta_{\ell j})\} q^2, \tag{2.5.12}$$

which is exactly the same as that obtained by substituting the isotropic correlation function into equation (2.5.11) as shown in

appendix B. In appendix A, we derive the most general model for $B_{ij\ell m}$ which is linear[1] in the anisotropy tensor $\underline{\underline{b}}$. The resulting model,

$$B_{ij\ell m} = \{ -\frac{1}{15}\delta_{ij}\delta_{\ell m} + \frac{1}{10}(\delta_{i\ell}\delta_{jm} + \delta_{im}\delta_{\ell j}) + \alpha_0(\delta_{ij}b_{\ell m} + \delta_{\ell m}b_{ij}) - \frac{1}{3}(1 + 4\alpha_0)(\delta_{im}b_{j\ell} + \delta_{jm}b_{i\ell}) + \frac{1}{6}(2 - \alpha_0)(\delta_{j\ell}b_{im} + \delta_{i\ell}b_{jm})\} q^2 \tag{2.5.13}$$

contains a single coefficient α_0, which must be determined by reference to laboratory flows. When (2.5.13) is combined with the mean velocity gradient, the rapid part of T_{ij} can be expressed in a number of ways. The final model,

$$T_{ij}{}^1 = (\frac{4}{10} + 2\alpha_0)S_{ij}q^2 - 3\alpha_0 (R_{ik}S_{kj} + R_{jk}S_{ki} + \frac{2}{3}\delta_{ij}) - \frac{2}{3}(2 + \frac{7}{2}\alpha_0)(R_{ik}\Omega_{kj} + R_{jk}\Omega_{ki}) \tag{2.5.14}$$

is written in a form which emphasizes the physical contribution of the term to the Reynolds stress balance, (2.1.2a). We note that the production tensor, P_{ij}, (2.1.2b) in the Reynolds stress transport equation may be written in the alternative form,

$$P_{ij} = -(R_{ik}S_{kj} + R_{jk}S_{ki}) + (R_{ik}\Omega_{kj} + R_{jk}\Omega_{ki}).$$

---

[1]Reynolds (1976) shows that $B_{ij\ell m}$ cannot contain terms quadratic in $\underline{\underline{b}}$ hence $B_{ij\ell m}$ is accurate to second order in $\underline{\underline{b}}$.

Comparing this equation with (2.5.14), it is evident that T_{ij}^{1} contains terms proportional to those in the production tensor and will therefore modify the turbulence energy production in each Reynolds stress component by an amount which is determined by the value of α_0. In a shear flow, for example, R_{11} is the only normal stress component which has a non-zero production, P_{ij}. The other components, R_{22} and R_{33} receive their energy by transfer from R_{11} via T_{ij}. The effect of T_{ij}^{1} then is to make the energy production more isotropic.

The above model for T_{ij}^{1} (equation (2.5.14)) has also been obtained, using the methods described previously by Naot, Shavit and Wolfshtein (1973), Launder, Reece and Rodi (1975) and Reynolds (1976). Each of these authors predicts a different value of α_0 however. A method of accurately determining α_0 from homogeneous experimental data will be described in § 3.4.

Various simplifications to the equation (2.5.14) for T_{ij}^{1} have also been used in calculations. If only the isotropic contribution to the tensor $B_{ij\ell m}$ is retained, the resulting model for T_{ij}^{1}, given in appendix B, is

$$T_{ij}^{1} = \frac{2}{5} q^2 S_{ij} \qquad (2.5.15)$$

Lewellen (1975) reported that calculations carried out using (2.5.15) for T_{ij}^{1} indicated that the numerical coefficient $\frac{2}{5}$, gave erroneous predictions.

Since the primary effect of T_{ij}^{1} is to make the energy production more isotropic, Launder, Reece and Rodi (1975), suggested a simplified version of (2.5.14) where,

$$T_{ij}^{1} = \alpha_2(P_{ij} - \frac{2}{3}\delta_{ij}\mathcal{P}) \qquad (2.5.16)$$

This model has been used for calculations by Launder, Reece and Rodi (1975) and Launder (1975). They found that, for the flows considered, (2.5.16) gave predictions which were only slightly worse than those obtained using (2.5.14). It should be noted that all of the models (including (2.5.14)) contain only one constant. Furthermore, all of the models are added directly to the production tensor and there is no fundamental difference in the complexity of the resulting equation for R_{ij}. Thus, there is no significant saving computationally to using (2.5.15) or (2.5.16) instead of (2.5.14).

Zeman and Tennekes (1975) have suggested a form similar to our proposed model (2.5.14) except that they have different coefficients multiplying the mean strain and mean rotation terms. They claim that this allows the two effects (of mean strain and rotation) to be incorporated independently. However there is no fundamental reason, so far as we are aware, to believe that this added complication is necessary.

Recently Lin and Wolfshtein (1977) have proposed a model for T_{ij}^{1} that contains three coefficients. They claim that this model will also allow for wall effects. However, their only applications so far have been for homogeneous flows and in this case their predictions are no better than for the one constant model proposed here.

If wall bounded flows are to be modeled some modification of the model we have proposed for T_{ij}^{1} will be required. In particular, the exact expression corresponding to (2.5.8) contains a <u>surface</u>

integral which must be retained for points in the vicinity of a solid boundary. Possible models for this term have been suggested by Launder, Reece and Rodi (1975) and Irwin and Smith (1975). Since the present work is concerned only with the flow domain away from solid boundaries, this point is not considered further here.

Finally it should be pointed out that no inhomogeneous terms have been used in the proposed model for T_{ij}^{1}. The approximation in neglecting these terms is $\left(\frac{\ell}{L_0}\right)^2$, Pope (1978).

B. Return-to-Isotropy, T_{ij}^{2}

If the isotropic form of the two point velocity correlation is substituted into the expression (2.5.8) for T_{ij}^{2}, the result, after integration, is $T_{ij}^{2} = 0$. For non isotropic flows on the other hand, T_{ij}^{2} is definitely non zero. Thus the physical effect of T_{ij}^{2} is to cause the Reynolds stresses to become more isotropic. As a result, T_{ij}^{2} is commonly called the "return-to-isotropy" term. The tendency of anisotropic turbulence to return to an isotropic state has been verified experimentally. Even in a straining field, T_{ij}^{2} is believed to produce a tendency toward equalization of the normal Reynolds stresses.

Most modelers have followed Rotta (1951) and have assumed that the rate of return to isotropy is proportional to the departure of each component of the Reynolds stress tensor from its isotropic value, i.e.

$$T_{ij}^{2} = -\alpha_0 \varepsilon b_{ij} \qquad (2.5.17)$$

where $b_{ij} = R_{ij}/q^2 - \frac{1}{3}$.

Bradshaw (1968) indicated that the return to isotropy is not likely to be linear in b_{ij} and this conclusion can be supported using arguments given by Townsend (1976). Townsend accounts for a non linear return to isotropy via physical arguments which use the idea of a "dual" nature for turbulence structure. In this "model" it is assumed that the turbulence is made up of eddies of two sizes, (1) large energy containing eddies and, (2) small dissipative eddies. We can associate time scales with these eddies by considering the rate of strain associated with each. The large eddies are distorted by the mean rate of strain which is of order (u'/ℓ) (cf. Tennekes and Lumley, 1972). while the strain rate associated with the small scale fluctuations is of order (u'/λ). Here, λ is the "Taylor microscale" and is defined using the relationship,

$$\overline{\frac{\partial u_1}{\partial x_1}^2} = \frac{u'^2}{\lambda^2}$$

Thus λ is a measure of a length scale over which dissipation of energy is important and the length scale λ is much smaller than the integral scale ℓ. Hence the characteristic time scale for the smaller eddies is much <u>shorter</u> than that for the larger eddies, and it may be anticipated that the energy containing eddies return to isotropy on a time scale, $\tau_\ell \sim \frac{\ell}{u'}$, and which is much longer than that for the smaller eddies, $\tau_\lambda \sim \frac{\lambda}{u'}$. The longer time scale of the larger eddies leads to a kind of permanence of their structure. The smaller eddies on the other hand, have an anisotropic structure imposed on them by the next largest size of eddies, but this anisotropy departs quickly

when the straining is stopped. Townsend (1976, pp. 66-71) shows that this behavior leads to a non linear return to isotropy. Hence T_{ij}^2 should be non linear in b_{ij}. An appropriate non linear model can be developed by following the modeling rules that were suggested in § 2.3.

In general, T_{ij}^2 may be expressed in the functional form,

$$T_{ij}^2 = T_{ij}^2(R_{ij},\varepsilon,\nu) \ . \tag{2.5.18}$$

Note that the mean velocity gradient is not included as an argument for T_{ij}^2. In support of this simplification is the fact that the mean velocity gradient does not appear in the exact integral expression for T_{ij}^2. Furthermore, it is expected on physical grounds that T_{ij}^2 should not respond instantaneously to changes in $U_{\ell,m}$ but only after such canges are manifested in b_{ij}. Using dimensional analysis and (2.5.18) it follows that

$$T_{ij}^2 = \varepsilon\phi_{ij} \tag{2.5.19}$$

where ϕ_{ij} is a dimensionless function of R_{ij}, ε and ν i.e.

$$\phi_{ij}(R_{ij},\varepsilon,\nu) = \phi_{ij}\ (b_{ij},q^2,\varepsilon,\nu) = \phi_{ij}(\underline{\underline{b}},\ R_\ell) \tag{2.5.20}$$

where $R_\ell = q^4/\varepsilon\nu$. Finally, applying the principles of invariant modeling to ϕ_{ij} (for infinite Reynolds number), we obtain

$$\phi_{ij}(\underline{\underline{b}}) = f_1(II,III)b_{ij} + f_2(II,III)(b_{ij}^2 - \delta_{ij}II/3) \tag{2.5.21}$$

Equation (2.5.21), given originally by Lumley and Khajeh-Nouri (1974) is completely general since the Cayley-Hamilton theorem can be used to express any higher powers of $\underline{\underline{b}}$ in terms of $\underline{\underline{b}}$ and $\underline{\underline{b}}^2$. If the departure from anisotropy is small, the functions f_1 and f_2 can be approximated by linear combinations of the invariants, i.e.

$$f_1 = f_1^0 + f_1^1 II + \ldots, \quad f_2 = f_2^0 + f_2^1 II + \ldots \qquad (2.5.22)$$

The resulting model for T_{ij}^2, accurate to third order in anisotropy, is

$$T_{ij}^2 = -\beta_0 \varepsilon[(1.0 + \beta_1 II)b_{ij} + \beta_2(b_{ik}b_{kj} - \delta_{ij}II/3)] \qquad (2.5.23)$$

Equation (2.5.23) contains no inhomogeneous terms and as shown in Cormack (1975) none enter at first order in inhomogeneity. The first contributions for inhomogeneity occur only at second order and at this level, the most general model which is properly invariant contains 24 terms similar to those in (2.5.23). Thus, in our opinion, the extension of the model to second-order in inhomogeneity should be attempted only as a last resort.

Recently Lumley and Newman (1977) have made a detailed study of the return-to-isotropy problem and have derived an alternative non linear model for T_{ij}^2. Because of its complexity, however, the details of this model are given in appendix C. A graphical representation of the model, for a particular flow, is compared with the model proposed here, (2.5.23), in § 3.5.

2.6 Modeling the Source of Dissipation, Δ_ε

The first two terms on the right hand side of equation (2.2.5a) represent a balance between the production and destruction of dissipation. Since neither process can be measured, they are modeled together as a net "source" of dissipation. The scalar function Δ_ε must be modeled as a scalar function of the invariants of the modeling variables. A great deal of speculation has centered on the choice of invariants for inclusion in the functionality for Δ_ε. Lumley and Khajeh-Nouri (1974) and Cormack (1975) have both utilized the fact that the exact form of Δ_ε (equation 2.2.5b) does not contain mean velocity gradients to suggest that the model for Δ_ε should also not contain the mean velocity gradient as an independent variable. Hence the model proposed by those authors contains only turbulence quantities, i.e.

$$\Delta_\varepsilon = \Delta_\varepsilon(\underline{\underline{b}}, q^2, \varepsilon) = \frac{\varepsilon^2}{q^2} f_3(II, III) \qquad (2.6.1)$$

where f_3 is expanded as a linear combination of the invariants II and III. Part of the reasoning involved in the hypothesis of no dependence upon $U_{i,j}$ is the assumption that a knowledge of $\overline{u_i u_j}\ (\underline{x},t)$ implies an implicit knowledge of $U_i(\underline{x},t)$. This is not the case for homogeneous flows, however, and Lumley (1975a) has more recently included $U_{i,j}$ in the development of a model for Δ_ε. The same question was also considered by Reynolds (1974), who concluded that mean gradients should not be included in principle in the functionality of Δ_ε because the level of Δ_ε would then be determined by the features

of the large scale motions. He found, however, that he could not model even simple flows unless he included the mean velocity gradient as a modeling variable, and his final proposal for Δ_ε was exactly the same as that proposed by Hanjalic and Launder (1972) viz.,

$$\Delta_\varepsilon = \frac{\varepsilon^2}{q^2}\left(\psi_0 + \psi_* \frac{R_{ij}}{\varepsilon}\frac{dU_i}{dx_j}\right) \tag{2.6.2}$$

This latter model has, in fact, been used by most other modeling groups.

The uncertainty over the inclusion of the mean velocity gradients as a modeling variable for Δ_ε can be traced largely to the interpretation of the ε-equation. We consider (2.6.3) as an equation for a quantity that, (1) generates the integral length scale and, (2) equals the dissipation rate when the flow in question is in equilibrium. Thus, in spite of the fact that $\varepsilon = \nu \overline{u_{i,j}u_{i,j}}$ is largest for small scales and depends on the viscosity, the ε-equation (2.2.5a) is based on the dynamics of the large scale structure which is independent of viscosity.

This is best explained by reference to the dynamic equation for the energy spectrum, E(k). The integrated energy spectrum is $\int_0^\infty E(k)\, dk = q^2/2$. Hence E(k) represents the amount of turbulent kinetic energy between wave numbers k and k + dk. The wave number can be qualitatively related to the eddy size according to $k \sim 1/(\text{eddy size})$, and since most of the turbulent energy is in the large eddies, E(k) is centered around $k = 1/\ell$ and decreases in magnitude with increasing wave numbers. Townsend (1976) has shown that

the spectrum is in a state of equilibrium for wave numbers greater than k_e, where virtually all of the dissipation occurs, and can adjust quickly, relative to the time scale for mean velocity changes or decay, to changes in external conditions. Thus,

$$\text{for } k > k_e, \quad S(k_e) = 2\varepsilon \tag{2.6.3}$$

Here, $S(k_e)$ is the flux of energy through the equilibrium range and is independent of viscosity. $S(k_e)$ pertains to lower wave numbers than ε does because it is influenced by changes in $E(k)$ for $0 < k < k_e$. Hence we have demonstrated a link between the source of dissipation and the large scale motions. Specifically, at high Reynolds numbers, the dissipation ε is equal to the flux of energy out of the energy containing range of eddies.

Of course we do not expect that changes in energy transfer at a particular point in the flow are caused by changes in $E(k)$ at the same point since the characteristic time scale for such changes to be transmitted in wave number space is proportional to q^2/ε. However, as pointed out in § 2.3 the assumption of localness is consistent with mild inhomogeneity. Pope (1978) shows that it is the condition of homogeneity or what he calls "similarity"[1] (where the rate of strain and turbulent fields normalized by the characteristic length and velocity scales are constant) which allows the source of dissipation to be written:

---

[1]This is different from the "profile similarity" which is exhibited by free shear layers and described in § 5.2.

$$\Delta_\varepsilon = \frac{\varepsilon^2}{q^2} \psi(E_{ij}, \omega_{ij}, b_{ij}) \tag{2.6.4}$$

where $E_{ij} = \frac{1}{2} q^2/\varepsilon \, (U_{i,j} + U_{j,i})$ and $\omega_{ij} = \frac{1}{2} q^2/\varepsilon \, (U_{i,j} - U_{j,i})$ and ψ is a constant function of the invariants of E_{ij}, ω_{ij} and b_{ij}. When ψ is expanded in a linear combination of the invariants of its arguments, it can be written

$$\psi = \psi_0 + \psi_1 II + \psi_2\{\underline{\underline{bE}}\} + \psi_3\{\underline{\underline{E}}^2\} + \psi_4 \{\omega^2\} + \psi_5 \{\underline{\underline{E}}^3\} + \psi_6 \{\underline{\underline{\omega}}^2\underline{\underline{E}}\}$$

$$+ \psi_7 III + \psi_8 \{\underline{\underline{\omega}}^2\underline{\underline{b}}\} + \psi_9 \{\underline{\underline{b}}^2\underline{\underline{E}}\} + \psi_{10} \{\underline{\underline{b}}^2\underline{\underline{\omega}}\} + \ldots \tag{2.6.5}$$

Here, the curly brackets denote an invariant, for example $\{\underline{\underline{E}}^2\} = E_{ij}E_{ji}$. If E_{ij} and ω_{ij} are assumed to be first order in anisotropy, then the first line of (2.6.5) is second order in anisotropy and the remaining terms are third order.

In certain flows (notably flows which are nearly homogeneous), b_{ij} and E_{ij} can be related by a constitutative equation (see Pope, 1975, or Lumley, 1970), and in these cases

$$b_{ij} = C_* E_{ij} \tag{2.6.6}$$

so that $II = b_{ij}b_{ji} = C_*^2\underline{\underline{E}}^2$ and $b_{ij}E_{ji} = C_*\underline{\underline{E}}^2$ where C_* may also be a function of $\underline{\underline{b}}$ and $\underline{\underline{E}}$. Thus in equilibrium, the three invariants II, $\{\underline{\underline{E}}^2\}$ and $\{\underline{\underline{bE}}\}$ are proportional because they are measures of the same processes. This fact makes parameter estimation difficult because the coefficients ψ_i are usually determined from data for homogeneous flows where an expression like (2.6.6) applies. Furthermore, in the free shear flows which are commonly modeled, only one

component of $U_{i,j}$ is non-zero, namely $U_{1,2}$, in which case the two invariants $\{\underline{\underline{E}}^2\}$ and $\{\underline{\underline{\omega}}^2\}$ are identical. In these circumstances, it is impossible to distinguish between various terms in (2.6.5) and simple curve fits of the experimental data do not yield a unique choice for the optimal model.

The optimal form for terms involving II, $\{\underline{\underline{E}}^2\}$ and $\{\underline{\underline{b}}\ \underline{\underline{E}}\}$, as an example can only be determined by noting that the dynamic behavior of models containing II, $\{\underline{\underline{E}}^2\}$ and $\{\underline{\underline{b}}\ \underline{\underline{E}}\}$ will all be quite different. Thus the optimal form for ψ must ultimately be determined from the model performance in a dynamic calculation, rather than by means of simple curve fitting of ψ to experimental data. The model proposed here for subsequent study has terms of both types, mean strain and turbulent field,

$$\psi = \psi_0 + \psi_1 II + \psi_2\ \underline{\underline{b}}\ \underline{\underline{E}} \tag{2.6.7}$$

and is accurate to second-order in anisotropy. Rotta (1975) has shown that a model similar to (2.6.7) is also accurate to second order in homogeneity.

We have now proposed models for all of the terms required by a homogeneous representation of (2.1.2) and (2.2.5). The parameters appearing in the models for $T_{ij}^{\ 1}$, $T_{ij}^{\ 2}$ and Δ_ε will be determined from homogeneous turbulent experiments in Chapter 3. The models for J'_{ijk} and H_j are only required for inhomogeneous flows. They are discussed in the next section, for completeness, but will not be used

until the proposed model is used for calculations of turbulent shear flows in Chapter 5.

2.7 Models for the Diffusion Terms J_{ijk} and H_j

The only terms remaining in (2.1.2a) and (2.2.5) that need to be modeled are the diffusion terms J'_{ijk} and H_j. In a recent review, Cormack et al. (1978) studied all of the existing models for J'_{ijk} and suggested that the model originally proposed by Hanjalic and Launder (1972) be used for this term in numerical calculations. Hanjalic and Launder also proposed a model for the diffusive flux of dissipation, H_j. In this section we provide further discussion in support of the models proposed for H_j and J'_{ijk} by Hanjalic and Launder (1972).

If the transport part of the pressure-strain correlation (cf. equation (2.5.2)) is added to the other diffusion terms in (2.1.2a), the resulting equation for the "net diffusive flux" of R_{ij}, is:

$$J_{ijk,k} = -\frac{\partial}{\partial x_k}\{\overline{u_i u_j u_k} - \delta_{ik}\frac{\overline{u_j p}}{\rho} - \delta_{jk}\frac{\overline{u_i p}}{\rho} - \nu\frac{\partial R_{ij}}{\partial x_k}\}. \quad (2.7.1)$$

At high Reynolds numbers, the viscous term is negligible. Hanjalic and Launder (1972) use the experimental data of Irwin (1973), which demonstrates a balance between the diffusive flux of R_{ij} and $\overline{u_i u_j u_k}$, to argue further that the pressure terms are negligible. Since the term J_{ijk} would be modeled in the same way whether the pressure-terms are present or not (except for a change in model symmetry) it

is customary to neglect pressure-diffusion. We do so here, and model J_{ijk} as if it were,

$$J_{ijk,k} = (\overline{u_i u_j u_k})_{,k} \tag{2.7.2}$$

Chou (1945) was the first to suggest using exact differential equations for $\overline{u_i u_j u_k}$ to derive models for these terms. An exact equation for (2.7.2) obtained from (2.1.1a) is,

$$\frac{D\gamma_{ijk}}{Dt} + (\overline{u_i u_j u_k u_\ell})_{,\ell} - R_{ij}(R_{k\ell})_{,\ell} - R_{ik}(R_{j\ell})_{,\ell} - R_{jk}(R_{i\ell})_{,\ell}$$

$$+ U_{i,\ell}\gamma_{\ell jk} + U_{j,\ell}\,\gamma_{i\ell k} + U_{k,\ell}\,\gamma_{ij\ell}$$

$$= (\overline{p_{,i}u_j u_k} + \overline{p_{,j}u_i u_k} + \overline{p_{,k}u_k u_j}/\rho_0 + \nu(\overline{u_{i,pp}u_j u_k} + \overline{u_i u_{j,pp}u_k}$$

$$+ \overline{u_i u_j u_{k,pp}}) \tag{2.7.3}$$

For convenience, we have used γ_{ijk} to denote $\overline{u_i u_j u_k}$.

Hanjalic and Launder (1972) neglect the convective derivatives, the dissipative terms and the terms which depend on the mean velocity gradient in (2.7.3). These terms can be shown (using an order of magnitude analysis) to be about an order of magnitude smaller than the terms which are kept. The fourth-order velocity correlation is replaced by it's quasi-Gaussian form (Monin and Yaglom, 1971, p. 233) i.e.,

$$\overline{u_i u_j u_k u_\ell} = R_{ij}\cdot R_{k\ell} + R_{ik}R_{j\ell} + R_{i\ell}R_{jk} \tag{2.7.4}$$

Hanjalic and Launder then replace the pressure correlations by "relaxation" terms, i.e. the third-order term divided by the turbulent time scale. This leads to the following model for J_{ijk},

$$J_{ijk} = \frac{C_s q^2}{\varepsilon} \{R_{ij,\ell} R_{k\ell} + R_{ik,\ell} R_{j\ell} + R_{jk,\ell} R_{i\ell}\} \qquad (2.7.5)$$

Cormack, Leal and Seinfeld (1978) followed the modeling procedure outlined in § 2.3, keeping terms to second order in anisotropy and first order in inhomogeneity for J_{ijk}. The resulting model was a series in the gradients of q^2, ε and b_{ij} and contained 19 constants which were determined by curve fits of the model to the experimental profiles of J_{ijk} determined in four separate experiments. The number of constants was reduced to four by a systematic determination of the importance of each term (see Cormack, 1975, for details). The final recommended form of their model was

$$\begin{aligned} J_{ijk} = {} & C_1 \frac{q^4}{\varepsilon} M_{ijk\ell} q^2_{,\ell} + C_2 q^6/\varepsilon \, (b_{ik,j} + b_{ij,k} + b_{kj,i}) \\ & + C_3 q^4/\varepsilon \, (\delta_{ik} b_{j\ell} + \delta_{ij} b_{k\ell} + \delta_{jk} b_{i\ell}) q^2_{,\ell} + C_4 q^6/\varepsilon \\ & (b_{ik} b_{j\ell,\ell} + b_{ij} b_{k\ell,\ell} + b_{kj} b_{i\ell,\ell}) \end{aligned} \qquad (2.7.6)$$

where $M_{ijk\ell} = \delta_{ij}\delta_{k\ell} + \delta_{i\ell}\delta_{jk} + \delta_{ik}\delta_{j\ell}$. The form of the final proposed model is not too surprising. If one starts with (2.7.5) and makes the substitution, $R_{ij} = q^2(b_{ij} + 1/3\,\partial_{ij})$ the result is,

$$\begin{aligned} J_{ijk} = {} & \frac{C_s}{9} M_{ijk\ell} q^2_{,\ell} + \frac{C_s}{3} \frac{q^4}{\varepsilon} (b_{i\ell}\delta_{jk} + b_{j\ell}\delta_{ik} + b_{k\ell}\delta_{ij}) q^2_{,\ell} \\ & + \frac{C_s}{3} \frac{q^6}{\varepsilon} (b_{jk,i} + b_{ik,j} + b_{ij,k}) + C_s \frac{q^6}{\varepsilon} (b_{i\ell} b_{jk,\ell} + b_{j\ell} b_{ik,\ell} + b_{k\ell} b_{ij,\ell}). \end{aligned} \qquad (2.7.7)$$

Equation (2.7.7) is similar to the form suggested by Cormack et al. except for the last term in which the indices and differentiations are interchanged. Thus the greater predictive capability of the model of Cormack et al. (2.7.6) should be expected in that they use four parameters rather than a single parameter such as used in (2.7.5). It is instructive to note that when Cormack et al. fit equation (2.7.5) to the data used to generate their model, they determined that $C_s = 0.055$. This is exactly the same value of C_s that Launder, Reece and Rodi (1975) recently determined by a computer organization of dynamic calculations. Since predictions of free shear flows are relatively insensitive to the form of the model used for J_{ijk} (Launder, Reece and Rodi, 1975), the simpler one constant model (2.7.5) of Hanjalic and Launder (1972), will be used in favor of (2.7.6) when inhomogeneous flows are calculated in § 3.7. It may be noted that Cormack et al. <u>also</u> suggested using (2.7.5) for calculations of this type.

Hanjalic and Launder (1972) also proposed a "gradient-diffusion" form to model H_j in the dissipation equation. This model,

$$H_j = C_\varepsilon \frac{q^2}{\varepsilon} \overline{u_k u_\ell}\, \varepsilon_{,\ell} \qquad (2.7.8)$$

was also obtained by simplying an exact equation for the transport of H_j. Since free shear flow calculations have been shown to be relatively insensitive to the coefficient C_ε, (cf. Launder and Morse, 1977), (2.7.8) will be used to model H_j.

The coefficients C_s and C_ε were recently re-optimized by Launder, Reece and Rodi (1975). They determined that,

$$C_s = .055$$

$$C_\varepsilon = .075.$$

These constants will be used in the calculations of free shear flows in Chapter 5. In the next chapter, the constants appearing in the models for T_{ij}^{1}, T_{ij}^{2} and Δ_ε will be determined by considering homogeneous (one-dimensional) flows.

CHAPTER 3

MODELING HOMOGENEOUS TURBULENCE

3.1 Introduction

It was pointed out in Section 2.3 that turbulence exhibits some of the features of Coleman and Noll's (1961) "simple fluid" and the modeling of the unknown moments in the preceeding chapter proceeded in a manner analogous to that used to determine constitutive equations for non-Newtonian fluids. The analogy between turbulence modeling and rheology can be further extended to the development of a method for determining the unknown constants in the models (2.5.14, (2.5.23) and (2.6.2) for T_{ij} and Δ_ε. In rheology, simple experiments are designed, which exhibit a particular physical behavior, and allow the fluid mechanics to be described by a simplified form of the constitutive model. The constants appearing in this simplified model are then determined by reference to the experimental data. Such experiments are called rheometric and a classic example is the so-called Couette viscometer.

In second-order modeling, it is advantageous to adopt a similar strategy. In this case, the analog of the rheometric experiments are homogeneous turbulent flows that are each designed to exhibit particular physical features of turbulent flows. In order of increasing complexity the following homogeneous experiments can be used to estimate the parameters in the models for T_{ij} and Δ_ε.

The last flow can be subdivided into (a) irrotational and, (b) shear flows in order to determine the effect of solid body rotation.

Table 3.1

Turbulent Viscometric Experiments

	Flow	Physical Phenomenon Exhibited
1.	Isotropic turbulence with constant mean velocity.	Turbulence is dissipative so that turbulence energy decays.
2.	Anisotropic turbulence with constant mean velocity.	Relaxation effect, tendency-to-isotropy, faster decay of energy due to increased energy transfer.
3.	Homogeneous turbulence with constant velocity gradient.	Transfer of energy from mean flow to turbulence and inter-component energy transfer.

Although most flows of practical interest are inhomogeneous, the important features of the energy transfer process and length scale dynamics are similar whether the flow is inhomogeneous or not. This being the case, the comparative simplicity of the governing equations for homogeneous flows render them extremely valuable for model initialization. It may be added that Pope (1978), Rotta (1975) and Cormack (1975) have all shown that the homogeneous representations of the models for T_{ij} and Δ_ε are accurate to $O\left(\frac{\ell}{L_o}\right)^2$, i.e. the first corrections for inhomogeneity occur only at second order in the ratio of integral length scale to the scale of the inhomogeneity.

For homogeneous turbulent flows, the governing Reynolds equations developed in Chapter 2 reduce to:

$$\frac{\partial R_{ij}}{\partial t} = - R_{ik}U_{j,k} - R_{jk}U_{i,k} + T_{ij} - \frac{2}{3}\delta_{ij}\varepsilon \qquad (3.1.1)$$

$$\frac{\partial \varepsilon}{\partial t} = \Delta_\varepsilon = - \frac{\varepsilon^2}{q^2} (\psi_0 + \psi_1 II + \psi_2 \underline{\underline{b}} \underline{\underline{S}}_1) \tag{3.1.2}$$

where

$$T_{ij} = \left(\frac{4}{10} + 2\alpha_0\right) S_{ij} q^2 - 3\alpha_0 (R_{ik} S_{kj} + R_{kj} S_{ki} + \frac{2}{3} P\delta_{ij})$$

$$- \frac{2}{3} (2 + \frac{7}{2} \alpha_0)(R_{ik}\Omega_{kj} + R_{jk}\Omega_{ki})$$

$$- \beta_0 \varepsilon \left[(1 + \beta_1 II) b_{ij} + \beta_2 (b_{ij}^2 - \frac{II\delta_{ij}}{3})\right]$$

If a flow were truly homogeneous, all of the terms in the above equations would be independent of position in the flow. However, unless dissipation and production balance exactly, the total energy and length scale will actually vary with position. Indeed, the most common experimental approximations to homogeneous turbulence, namely "wind tunnel" flows, are <u>not</u> strictly homogeneous in the streamwise direction. Nevertheless, if certain conditions are met regarding the degree of inhomogeneity,[1] the turbulent flow at any cross-section of a <u>wind tunnel</u> is known to approximate homogeneous turbulence (i.e., "turbulence in a box") that has existed for a time equal to the convection time,

$$t = \int_0^x \frac{d\xi}{U_1(\xi)} \quad . \tag{3.1.3}$$

[1]Those conditions are given in Townsend (1976, p. 51) and Champagne, Harris and Corrsin (1970) and generally require that the turbulent scales be smaller than the scales of the mean flow.

Thus, if $U_1(x)$ has small lateral variations, the partial time derivatives in (3.1.1) and (3.1.2) can be replaced by convected time derivatives for purposes of comparison with laboratory produced homogeneous turbulence.

In the following two sections the available homogeneous experiments will be described. Then, in subsequent sections, the parameters in the models for T_{ij} and Δ_ε will be determined by best-fit to their experimental values from these experiments. Finally, the complete homogeneous model will be tested by comparison with dynamic calculations for all of the homogeneous experiments. As a preliminary to these considerations, we first consider the decay of isotropic (and homogeneous) turbulence.

3.2 Determination of ψ_0

In the limiting case of isotropic turbulence, the governing equations (3.1.1, 3.1.2) reduce to:

$$\dot{\varepsilon} = - \psi_0 \frac{\varepsilon^2}{q^2} \qquad \dot{q}^2 = - 2\varepsilon \tag{3.2.1}$$

This set of equations can be solved simultaneously to give [cf Reynolds (1976)]

$$q^2 = q_0^2 \, (1 + t/t_0)^{-n} \quad \Rightarrow \quad \varepsilon = \varepsilon_0 \, (1 + t/t_0)^{-(n+1)} \tag{3.2.2}$$

with $\quad t_0 = \dfrac{n q_0^2}{2\varepsilon_0} \quad$ and $\quad n = \dfrac{2}{\psi_0 - 2}$.

Here, q_0^2 and ε_0 are initial values. Thus, from an experimental study of

q^2 in the initial period of decay, the coefficient ψ_0 can be determined. Early experiments, [Batchelor and Townsend (1948)] suggested n = 1.0, thus giving $\psi_0 = 4.0$. Later however, Comte-Bellot and Corrsin (1966) took care to obtain better isotropy and found that n varied randomly between 1.15 and 1.3 for various grid types and mean velocities. Recently, Lumley and Newman (1977) have carefully reconsidered all of Comte-Bellot and Corrsin's experiments (both isotropic and slightly anisotropic) and found the following empirical expression for ψ,

$$\psi = 3.78 - 2.77\, R_\ell^{-\frac{1}{2}} - 9.09\, II \qquad (3.2.3)$$

This suggests a high Reynolds number asymptote for n of n = 1.12.

In an effort to obtain a theoretical estimate for n, Reynolds (1976) proposed a model for the energy spectrum E(k). Using the inertial subrange approximation, $E(k) \sim k^{-5/3}$ for the high wave number region and the form $E(k) \sim Ak^m$ for low wave numbers, Reynolds found that the value of n depended on the parameter m. For m = 4 (which is exact in the limit $k \to 0$), the coefficient n is $\frac{10}{7}$. Reynolds, however, argues that m should be two, thus giving n = 1.2 which is in reasonable agreement with the empirical estimate of n = 1.12 given by Lumley and Newman (1977).

The value $\psi_0 = 3.78$, which is the high Reynolds number isotropic limit of (3.2.3) is also very close to the value $\psi_0 = 3.80$ which was used in turbulence model calculations by Launder, Reece and Rodi (1975) and Zeman (1975). As a consequence of the experimental and theoretical evidence cited above, and the precedent of this earlier work the value $\psi_0 = 3.80$ will therefore be adopted throughout this chapter. Although the

precise value adopted for ψ_0 may not in itself be too important, it must be pointed out that the remaining constants in Δ_ε depend strongly on ψ_0. Thus, any future change in the value for ψ_0 can only be adopted if all the other constants in Δ_ε are altered simultaneously.

3.3 Homogeneous Turbulence Data

A turbulence model can only be as good as the experimental data on which it is based. In this section, we describe the experimental data which are to be used for parameter estimation and model verification in the present study. These data are basically of three kinds, (1) Return-to-isotropy of anisotropic turbulence, (2) homogeneous irrotational strain and (3) homogeneous rectilinear shear flow. The study of the homogeneous shear flow is the most important because it most closely approximates the shear flow situations encountered in engineering applications. Furthermore, it has been the subject of more experimental study than the other two flows. However, the data for all three types of homogeneous turbulent flow have played an important role in the model development which is reported in this chapter of the thesis.

A. Return-to-Isotropy of Anisotropic Turbulence

In the absence of mean strain, it has been illustrated (Section 2) that the pressure fluctuations will act to drive anisotropic turbulence towards its more probable isotropic state. Furthermore, the rate of return to isotropy depends on the degree of anisotropy. Indeed, it was shown in § 2 that the proposed model (2.5.23) for T_{ij}^2 will be non linear in the tensor b_{ij} which measures the departure from anisotropy.

A large set of experimental results is available for use in model development which reflect the physical picture for the decay of anisotropy in turbulent flows which was sketched in the preceding chapter. The classic example of weakly anisotropic turbulence is "grid turbulence". Here, the flow, after passing through a grid of bars, is axisymmetric but not isotropic, i.e. $\overline{u_1^2} > \overline{u_2^2} = \overline{u_3^2}$. Experiments are available which show that this anisotropy is slow to disappear. For example, Comte-Bellot and Corrsin (1966) have shown that the ratio $\overline{u_1^2}/\overline{u_2^2}$ decreases only from 1.25 to 1.12 (i.e., II diminishes from .004 to .001) in a distance downstream, which is sufficient for the total kinetic energy to decay by a factor of 25.

More strongly anisotropic turbulence may be created by passing grid turbulence through a distorting duct, and this is the source of the majority of strongly anisotropic decay data which is suitable for modeling. Tucker and Reynolds (1968) used a plane distorting duct which has a constant cross-sectional area (hence, a constant mean streamwise velocity), but changes in shape. In this flow (described in detail in part B of this section) an appropriate measure of the deviation from isotropy is the "structural" parameter, K, defined as

$$K = \frac{\overline{u_{max}^2} - \overline{u_{min}^2}}{\overline{u_{max}^2} - \overline{u_{min}^2}}$$

where u_{max} and u_{min} are the largest and smallest of the cross stream intensities. Necessarily for isotropic turbulence, K = 0. Tucker (1970) found, for three experiments, that K decayed rapidly in the region

immediately downstream of the straining section, but approached the asymptotic value K = 0.30 on a much longer time scale than would be inferred from this initial decay rate (see Figure 3.5). This time dependent behavior is, of course, consistent with the arguments of the preceding chapter which discussed the existence of two time scales for the return to isotropy.

Uberoi (1956, 1957) and Mills and Corrsin (1959) created anisotropic turbulence by passing grid turbulence through an axisymmetric contraction. This has the effect of increasing the transverse intensities relative to the streamwise intensity. The data of Mills and Corrsin (1959) and Uberoi (1956, 1957) for the region downstream of the contraction is similar to that of Tucker (1970) in that, K initially decays very rapidly but then only slowly approaches an asymptotic value. However, only one of Uberoi's flows had a sufficiently long test section for K to actually attain an asymptotic value. In this case, Uberoi (1957) found that K approached zero (see Figure 3.7).

The decay of axisymmetric strongly anisotropic turbulence was also studied numerically by Schumann and Patterson (1975) using the spectral method described in Section 1.2. Their results are qualitatively similar to those of Uberoi (1957), Mills and Corrsin (1959) and Tucker and Reynolds (1968). However, K approaches an asymptotic value of K = 0.28 which is consistent with Mills and Corrsin (1959) and Tucker and Reynolds (1968), but at variance with the Uberoi result. Unfortunately the turbulent Reynolds number of Schumann and Patterson's flow is in the range $20 < R_\ell < 30$, which makes it far too low for use as a rheometric experiment for the high R_ℓ limit which is the focus of our present paper.

Their data, however, do support the R_ℓ dependent model suggested by Lumley and Newman (1977) which will be used later for comparison with our proposed model.

B. Irrotational Strain

A second class of flows which is used in the present study primarily for model verification (rather than model development) is the evolution of strongly anisotropic flow in the presence of mean strain. Most studies of this class have also included data from the post-straining period and were thus mentioned in the previous section.

For present purposes the rate of strain for any of the common irrotational straining flows may be written in the form

$$S_{ij} = \left(\frac{dU_i}{dx_j}\right) \begin{bmatrix} 1 & 0 & 0 \\ 0 & F & 0 \\ 0 & 0 & -1-F \end{bmatrix}$$

where $F = \dfrac{dU_2/dx_2}{dU_1/dx_1}$ is the "strain-type" parameter. The co-ordinate axes are chosen such that,

$$\frac{dU_1}{dx_1} > 0 \qquad -\frac{1}{2} \leq F \leq 1$$

(i.e., there is always an extension in the x_1-direction and a compression in the x_3-direction). There different strain types have been considered.

(i) Plane Strain, F = 0

The duct which creates this strain is shown schematically in Table 3.12. The duct cross-section remains constant so the distortion is confined to the two cross-stream directions. Since the straining occurs in a plane perpendicular to the flow direction, this flow was called a lateral distortion by Tucker and Reynolds. The physics of this flow is conveniently described by considering two eddies lying along the principal strain axes of the mean flow as illustrated in Figure 3.1.

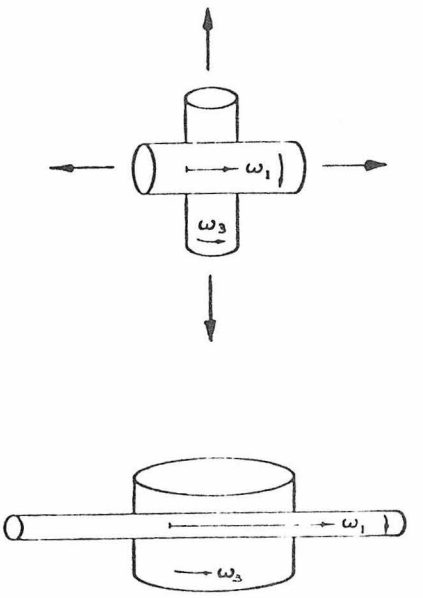

Figure 3.1. Vorticity stretching in a plane strain.
(a) before straining (b) after straining

The vorticity component ω_1 is increased due to vortex stretching, thus leading to a corresponding increase in u_2 and u_3. However, ω_3

is decreased, causing a decrease in u_1 and u_2. The net result, then, is that $\overline{u_3^2}$ increases and $\overline{u_1^2}$ decreases while the streamwise component $\overline{u_2^2}$ remains constant.

Plane irrotational straining flows have been studied experimentally by several investigators. A convenient measure of the potential for vortex stretching, and thus for induced anisotropy in a particular mean flow is provided by the total strain, $\tau_s \cong t\left(\frac{\partial U_1}{\partial x_2}\right)$ for a spatially uniform strain rate. Here t is the total time of application of the strain on a particular fluid element. Among the investigators of plane straining flow, Townsend (1954) achieved a total strain of 4.0, Tucker and Reynolds (1968) a total strain of 6.0 and Maréchal (1972) achieved $\tau_s = 13.3$. The change in the structural parameter K for each of these investigations is shown in Figure 3.2. The results are consistent except for those of Townsend which depart from the others and level-off for $\tau_s > 2$.

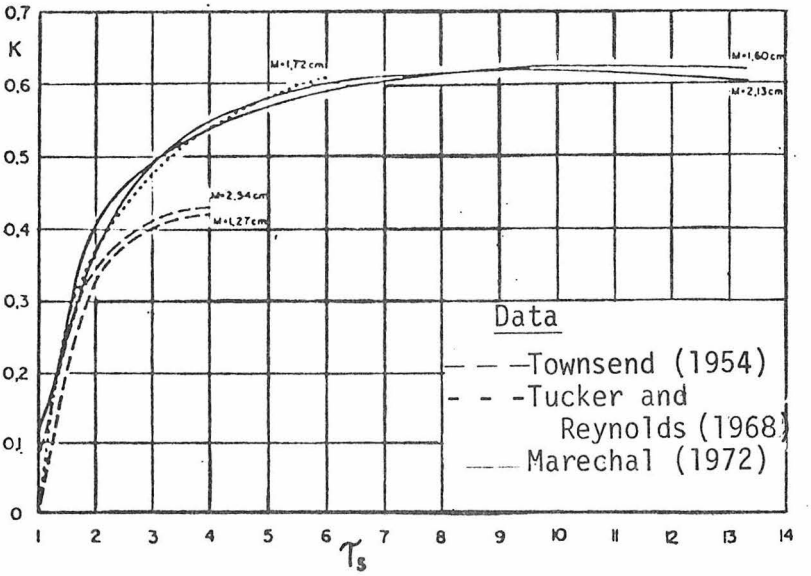

Figure 3.2.--Development of Structural Parameter k Versus Total Strain for Plane Lateral Strains. (Taken from Marechal, 1972).

The most complete set of experiments are those of Tucker (1970) [a portion of his results were published in Tucker and Reynolds (1968) and Reynolds and Tucker (1975)]. Tucker (1970) performed 3 experiments in the same wind tunnel for various initial conditions and Reynolds numbers. These conditions are summarized in Table 3.2.

Table 3.2

Experimental Conditions - Plane Strain - Tucker (1970)

Experiment	U_o(ft/sec)	Grid Type	$Re_M = \frac{U_o M}{\nu}$
1	20	½" square	6,780
2	20	diamond perforated	5,850
3	40	diamond perforated	11,700

The results for K are consistent for all three experiments, (shown in Figure 3.16) and independent of Reynolds number. We will use Tucker's (1970) data for comparison with numerical calculations in Section 3.7.

Reynolds and Tucker (1975) also studied a second type of plane strain in which the plane of the strain includes the streamwise direction, i.e. is in the longitudinal plane. This duct is shown schematically in Table 3.12. In this case the duct contracts in cross-section, hence the fluid is accelerated. However, the velocity gradient is constant and the same definition for total strain τ_s can be used. Two experiments of this type, with total strains 2.8 and

5.7 were reported in Reynolds and Tucker (1975).

(ii) The Axisymmetric Contraction, $F = -\frac{1}{2}$

The distorting duct which creates an axisymmetric contraction is shown schematically in Table 3.12. Again the cross-sectional area is decreasing so that the mean velocity is accelerating, but in this case, as distinct from the longitudinal strain, both of the cross-stream intensities are compressed. Thus an eddy lying along the tunnel axis is elongated resulting in a large increase in ω_1 (due to vortex stretching) so that both $\overline{u_2^2}$ and $\overline{u_3^2}$ increase (equally) relative to $\overline{u_1^2}$. This flow was studied experimentally by Uberoi (1956), Mills and Corrsin (1959) and Reynolds and Tucker (1975). The total strains obtained by these experimenters are given in the following table

Table 3.3

Total Strains, Axisymmetric Contraction

Investigator	Total Strain, τ_s
Uberoi (1956) a.	4.0
b.	9.0
c.	16.0
Mills and Corrsin (1959)	4.0
Reynolds and Tucker (1975)	5.8

A plot of the structural parameter K versus the total strain τ, Figure 3.21, suggests an essential difference between the flows of

Uberoi (1956) and Reynolds and Tucker. The test section in Uberoi's experiment was quite short ($\sim$ 2 ft.) whereas that of Reynolds and Tucker was much longer ($\sim$ 8 ft.). Thus, in Uberoi's case the application of the mean strain was over a shorter period of time than for Reynolds and Tucker, hence the natural tendency towards isotropy (cf Section 3.3A) prevents the latter flow from attaining the large valves of K obtained by Uberoi for a given total strain. A quantitative estimate of this effect may be obtained by comparing 1/(strain rate) to the anisotropic decay time for the two flows. The inverse strain rate is $t_s = (\partial U_1/\partial X_1)^{-1}$, whereas the time scale for return-to-isotropy is proportional to $t_d = \left[q^2/\varepsilon\right]_{t=0} =$

$\left[\frac{-q^2}{(dq^2/dt)}\right]_{t=0}$. Thus, the ratio $T_0 = t_d/t_s = (dU_1/dx_1)\left[\frac{-q^2}{\partial q^2/\partial t}\right]_0$ provides a useful measure of the degree of anisotropy which could be induced in a given mean flow for any given total strain. The values of T_0 for Uberoi (1956) and Tucker and Reynolds (1975) are compared in Table 3.4.

Table 3.4

Time Scale Ratios for Axisymmetric Contractions

Flow		T_0
Uberoi (1956)	$\tau_s = 4.0$	5.0
Uberoi	$\tau_s = 9.0$	13.35
Reynolds and Tucker	$\tau_s = 5.8$	.95

The effect on parameter estimation of the obvious dependence of K on T_0 will be discussed in Section 3.7.

(iii) The Equivalent Diffuser

If a distorting duct increases in cross-sectional area it is called a diffuser. In a symmetrical diffuser F = 1. However, since the mean velocity in a diffuser decreases with downstream distance, the Reynolds number decreases. It may also be noted that the initial velocity must be low enough to prevent separation if the diffuser experiment is to be successful. These two facts explain why the diffuser flow is not often studied. However, a related flow which has been studied is that of Tucker (1970), who considers a duct which is increasing in cross-sectional area while still expanding in one direction in such a manner that F should ideally be unity (F = 1). Experimentally, Reynolds and Tucker found F_e = 0.47 in their "equivalent" diffuser.

C. Homogeneous Shear Flow

A third class of flows which we shall utilize for turbulence model development is homogeneous shear flow. To create this flow experimentally, fluid is passed through some "flow generator" which has a varying resistance to flow from the bottom of the duct to the top. After an initial period of development, a flow with a constant mean velocity gradient is produced. Thus, on the duct centerline, this flow is the experimental analog to "pure shear flow in a box" that has been sheared for a time, $t = x/U_c$ where U_c is the mean centerline velocity and x is the downstream flow distance. Thus, the total strain, defined in Section 3.3.B is

$$\tau = t \frac{dU_1}{dx_2} = \frac{x}{U_c} \frac{dU_1}{dx_2} \qquad (3.3.1)$$

The first attempts to generate a homogeneous shear flow in a wind tunnel were due to Rose (1966) and Champagne, Harris and Corrsin (1970), (hereafter called CHC). Both of these experiments suggested that the turbulent intensities initially decayed and then reached an "equilibrium" state where production and dissipation of energy just balanced, thus maintaining the intensities at constant values. An apparent paradox existed however since the macro- and micro- length scales were found to increase monotonically in the same region. Since increasing length scales suggest a decrease in dissipation rate, one would expect the turbulent kinetic energy to be increasing rather than constant as observed. More recent experiments have, in fact, shown that the apparently level values of the turbulent intensities in these initial experiments were due simply to the fact that the test sections used were too short. The turbulent intensities pass through a local minimum which happened to occur near the end of the test section.

One of these later studies was due to Mulhearn and Luxton (1970, 1975) who used a much larger test section (20 ft. long instead of 10 ft. for Rose and CHC). These authors did observe an increase in kinetic energy after a local minimum had been reached. However, they used a relatively low mean center-line velocity and the boundary layers on the walls were sufficiently thick to affect the development of the turbulent intensities. The authors' original report [Mulhearn and Luxton (1970)] suggested that the results were in doubt for streamwise distances greater

than 16 ft. In fact the final results were published [Mulhearn and Luxton (1975)] only for distances of less than 10 ft. for which no increase in turbulence energy was observed.

A second investigation of the same type was reported by Richards (1972) and Morton and Richards (1975), who studied shear flows with both quadratic and linear mean velocity profiles. Their principal finding was that the r.m.s. values of the intensities initially decayed, but then increased with increasing total strain τ. The total strain parameter τ can be interpreted as a dimensionless time or distance ratio and can be increased by either increasing the test section length, increasing $\frac{dU_1}{dx_2}$ or decreasing U_c. Using a 20 ft. test section Richards obtained a maximum total strain of $\tau = 5.6$, compared to a maximum of $\tau = 3.3$ obtained by CHC and Rose (1966).

Rather than physically extending their wind tunnel to obtain larger τ-values than those of CHC, Harris, Graham and Corrsin (1977) increased $\frac{dU_1}{dx_2}$ from 12.9 to 48 sec^{-1} while keeping U_c constant. This yielded a maximum value for τ of approximately 12. The turbulent intensity profiles again showed a substantial increase with total strain in agreement with the results of Mulhearn and Luxton (1970) and Richards (1972).

With so many different shear flow experiments, done under different experimental conditions, a method of determining the consistency of the experimental data is required. A first consistency check was suggested by Richards and Morton (1975) and consists of plotting the dimensionless longitudinal intensity, u_1/U_c normalized by its minimum value $\left[u_1/U_c\right]_{min}$ versus τ, the total strain. All of Richards (1972) data plus that of

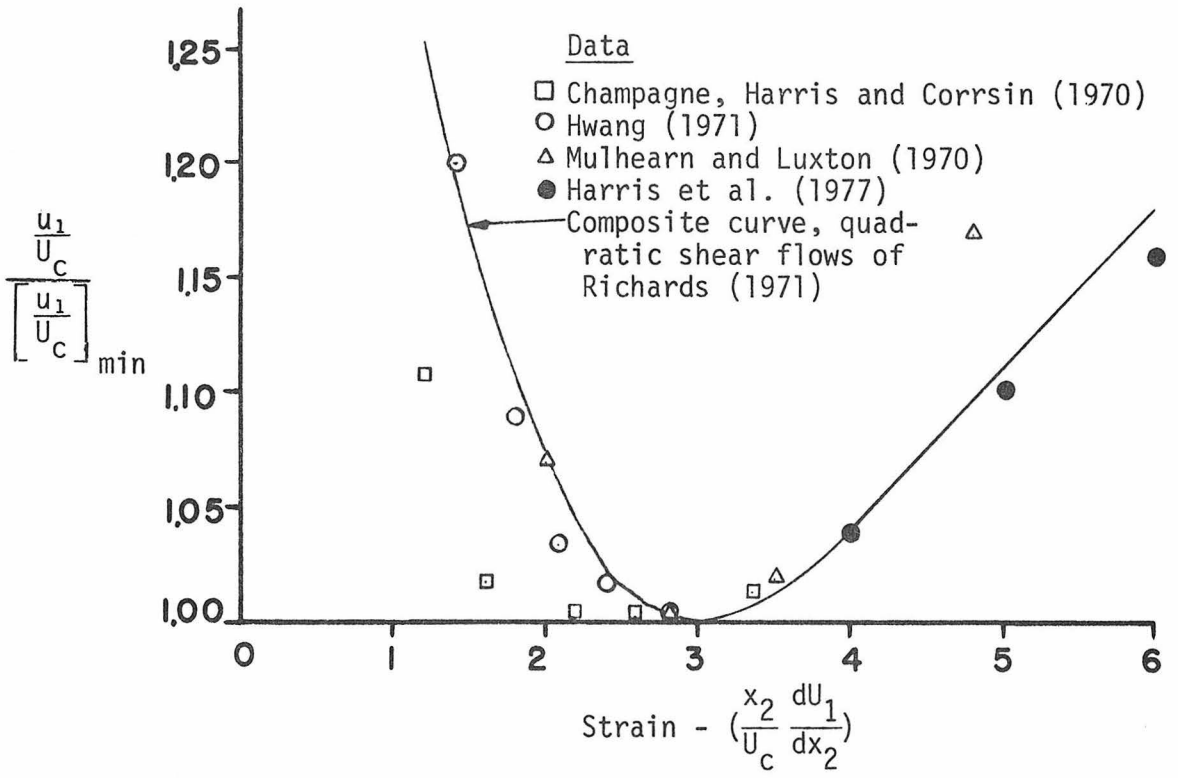

Figure 3.3.--Normalized Streamwise Turbulent Intensity Versus Total Strain for Several Homogeneous Shear Flows.

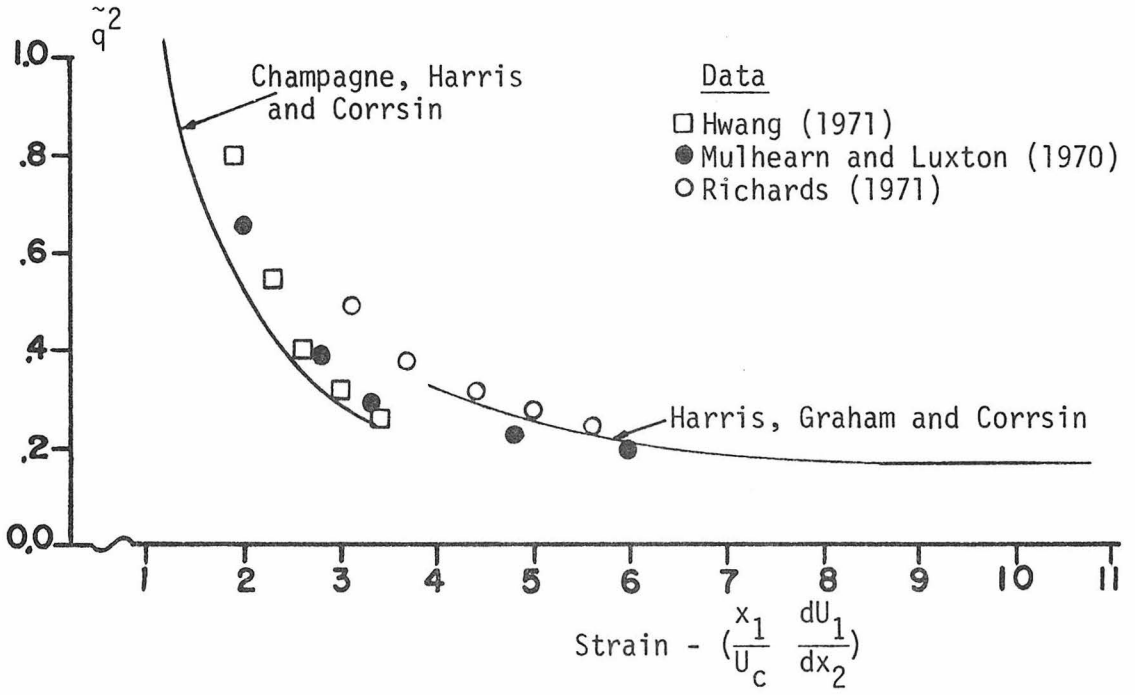

Figure 3.4.--Dimensionless Turbulence Energy Versus Total Strain For Homogeneous Shear Flow.

Hwang (1971), Rose (1966), CHC and Harris, Graham and Corrsin (1977) fall on approximately the same curve. The data of Mulhearn and Luxton (1970) exhibit too high an intensity after the minimum. One plausible suggestion for this behavior is that the wall boundary layers cause an increase in production, thus causing the turbulent intensities to be higher than in the other published studies.

A comparison of results for the two experiments of CHC and Harris, Graham and Corrsin (1977) shows that the intensities, non-dimensionalized with U_c, are "higher" for the latter, higher shear rate case. However, the centerline mean velocity cannot be the appropriate velocity scale because $\left(\frac{u_1}{U_c}\right)$ should not vary under Galilean transformation. Harris, Graham and Corrsin (1977) suggest an alternative characteristic velocity scale

$$U_* = L_1\Gamma \tag{3.3.2}$$

in which Γ is the mean shear rate, $\Gamma = \frac{dU_1}{dx_2}$ and L_1 is the longitudinal length scale defined by

$$L_1 = \int_0^\infty R_{11}(r_1,o,o)dr_1 \tag{3.3.3}$$

where

$$R_{11}(r_1,o,o) = \frac{\overline{u_1(\underline{x})\,u_1(\underline{x}+\underline{r})}}{\sqrt{\overline{u_1^2(\underline{x})}}\sqrt{\overline{u_1^2(\underline{x}+\underline{r})}}} \qquad \text{with } \underline{r} = (r_1,o,o)$$

is the two point velocity correlation coefficient.

In order to test the relevance of U_* as a characteristic velocity scale, we have plotted in Figure 3.4, the dimensionless turbulent energy

$\tilde{q}^2 = q^2/U_*^2$ as a function of total strain τ for all of the experiments described earlier in which L_1 was calculated. The points from all experiments fall on approximately the same curve when plotted in this fashion. Furthermore, for large T the data approach a constant non-zero value indicating that at sufficiently high rates of shear, an asymptotic state exists where $\tilde{q}^2$ is independent of T. The existence of such an asymptotic state is an extremely important discovery which plays a vital role in the turbulent model parameter estimation that is reported in the next section. The fact that earlier turbulence models were based on parameter estimations carried out in the non-asymptotic region of a local minimum of intensity means that they are almost certainly incorrect since it is only the asymptotic region which has unique values for the turbulence quantities (i.e., values which are independent of "initial" conditions upstream).

Turbulent data are thus required, for our purposes in the asymptotic region. Harris, Graham and Corrsin (1970) found that the components of the Reynolds stress tensor asymptotically approached a constant fraction of turbulent energy, i.e.

$$\frac{R_{ij}}{q^2} = a_{ij} \tag{3.3.4}$$

where a_{ij} is a matrix of constants. In all previous experiments the value of a_{ij} had still been changing at the end of the test section, though apparently tending towards the asymptotic values suggested by Harris, et al. In support of (3.3.4), Townsend (1976) determined that the energy containing eddies for all types of turbulent flows exhibit a "structural" similarity. As an index of structure Townsend (1976)

determined the values of a_{ij} (in 3.3.3) for a number of shear flows. These values are reproduced in Table 3.5a.

If flows with wall layers are excluded (a condition of the modeling method described in Section 2.3) the average values of the a_{ij} tensor are those given in Table 3.5, where they are compared to the asymptotic values obtained by Harris, et al.

Table 3.5b

Comparison of Stress Coefficients
for Turbulent Shear Flows

Flow	a_{11}	a_{22}	$-a_{12}$	std. dev.
All flows in Table 3.1 excluding wall layers	.44	.26	.15	.02
Harris, Graham and Corrsin	.50	.20	.15	

The results obtained for the homogeneous shear flow are in reasonable agreement with the average values of a_{ij} for the other shear flows. It may be noted that the value $a_{12} = -0.15$ was used by Bradshaw, Ferris and Atwell (1967) and Saffman (1970) in their earlier models.

In the following sections the existence of the asymptotic region for homogeneous shear flow and the values of a_{ij} obtained in that region will be used to:

(1) estimate α_0 in the model for T_{ij}^{1} (Eq. 2.5.14),

(2) determine a relationship between β_0, β_1 and β_2 in T_{ij}^{2} (Eq. 2.5.23) and,

Table 3.5a

Reynolds Stress Coefficients in Turbulent Shear Flow

Flow	a_{11}	a_{22}	$-a_{12}$
Boundary Layer			
a = 0			
outer layer	.54	.27	.13
inner layer	.60	.10	.12
a = - 0.15			
outer layer	.48	.28	.13
inner layer	.56	.17	.095
a = - 0.255			
outer layer	.48	.23	.14
inner layer	.54	.15	.07
Cylindrical Mixing Layer	.35	.30	.18
Plane Jet	.42	.30	.16
Plane Wake	.42	.32	.15
Plane Mixing Layer	.45	.26	.17
Pipe			
r = .5R	.47	.23	.14
near wall	.55	.115	.115
Channel Flow			
z = .1h	.62	.17	.205
z = .5h	.58	.20	.16

Notes

1. In boundary layer data, a is the exponent of the power law describing the variation in free stream velocity.
2. Sources of data: Boundary layer, Klebanoff (1955) and from Bradshaw (1967); cylindrical mixing layer, Bradshaw, Ferris Johnson (1964); Channel, Laufer (1950); pipe, Laufer (1955); plane jet, Bradbury (1965); plane wake, Townsend (1949); plane mixing layer, Liepmann and Laufer (1947).

(3) find ψ_1, ψ_2 in the dissipation equation (Eq. 3.1.2).

Then the return-to-isotropy data will be used to determine β_0 from which numerical values can be calculated for β_1 and β_2 using the results of (2) above. Finally, the resulting model will be tested on homogeneous strain and shear flows.

3.4 Determination of α_0, β_0, β_1 and β_2

The importance of using the homogeneous shear flow for parameter estimation is underscored by its structural similarity to many other turbulent shear flows (listed in Table 3.4). Townsend (1976) identifies a group of eddies larger than the dissipative eddies and smaller than the largest eddies (i.e., smaller than the eddies which are comparable to the scale of inhomogeneity of the mean flow). Townsend calls this middle range of eddies the "main turbulent motion" and argues that it is the universality of the structure of turbulence at this scale which gives the overall structural similarity evidenced in Table 3.4. It may be noted that these eddies are assumed to be small enough, compared to any inhomogeneity in the mean flow, that they are exposed to an approximately linear shear. Thus, the idealized homogeneous shear flow is expected to reflect much of the structure and dynamics of Townsend's (1976) "main turbulent motion" and parameter estimations based on it should have a degree of universality for the whole class of shear type flows.

Other modelers have used the homogeneous shear flow for parameter estimation, but all of them used the data of Champagne, Harris and Corrsin (1970, CHC) in the region of the local energy minimum. Indeed, Hanjalic and Launder (1972), Launder, Reece and Rodi (1975), Cormack

(1975) and Tennekes and Zeman (1975) all inferred from the CHC data that homogeneous shear flow reaches an equilibrium asymptotic state. In this case turbulent energy production is equal to dissipation and the Reynolds stress equations can be reduced to a non-linear set of algebraic equations independent of dissipation. The data of CHC in the "equilibrium region" then allow the parameters in the models for T_{ij}^{1} (Eq. 2.5.14) and T_{ij}^{2} (Eq. 2.5.23) to be determined explicitly.

This approach might at first sight appear to be valid, in spite of the fact that the flow does not attain an equilibrium, since a local minimum in the energy profile does exist and production does equal dissipation at least locally. However, the local minimum occurs at different values of the total strain for each component of the Reynolds stress tensor. More importantly, the fraction of the total kinetic energy in each component of the turbulent velocity field at the position of the relative minimum is not unique as the following table shows.

Table 3.6

Fraction of Energy in Each Reynolds Stress Component at Local Minimum

Experiment	$\overline{u_1^2}/q^2$	$\overline{u_2^2}/q^2$	$\overline{u_3^2}/q^2$
Champagne, Harris and Corrsin	.470	.245	.285
Rose	.437	.266	.297
Mulhearn and Luxton	.474	.218	.308
Richards	.416	.278	.306
Hwang[1]	.382	.291	.327

[1]Hwang's values are averaged over 3 experiments with 3 different grids.

Thus, earlier methods of parameter estimation, based on the data of CHC at the end of their test section, are clearly in error since the magnitudes of the component Reynolds stresses are not unique in this region. In what follows we present an alternative method of parameter estimation which is based on an examination of the Reynolds stresses in the truly asymptotic region of the homogeneous shear flow, which we have identified in Figure 3.4.

In the homogeneous shear flow, the only non-zero components of the mean rate of strain and vorticity tensors are:

$$S_{12} = S_{21} = \frac{1}{2}\frac{dU_1}{dx_2} \quad \text{and} \quad \Omega_{12} = -\Omega_{21} = \frac{1}{2}\frac{dU_1}{dx_2} \ .$$

Thus, the governing equations (Eqs. 3.1.1 and 3.1.2) may be written

$$U_c \frac{\partial R_{11}}{\partial x_1} = -\varepsilon\beta_0 \left((1 + \beta_1 II)b_{11} + \beta_2(b_{11}^2 + b_{12}^2 - II/3)\right) - \frac{\varepsilon}{3} + \left(\frac{4}{3}\alpha_0 - \frac{2}{3}\right) R_{12}\frac{dU_1}{dx_2} \qquad (3.4.1a)$$

$$U_c \frac{dR_{22}}{\partial x_1} = -\varepsilon\beta_0 \left((1 + \beta_1 II)b_{22} + \beta_2(b_{22}^2 + b_{12}^2 - II/3)\right) - \frac{\varepsilon}{3} - \left(\frac{10}{3}\alpha_0 + \frac{4}{3}\right) R_{12}\frac{dU_1}{dx_2} \qquad (3.4.1b)$$

$$U_c \frac{dq^2}{dx_1} = -2\left(R_{12}\frac{dU_1}{dx_2}\right) + \varepsilon \qquad (3.4.1c)$$

$$U_c \frac{dR_{12}}{dx_1} = -\varepsilon\beta_0 \frac{R_{12}}{q^2}\left(1 + \beta_1 II + \beta_2(b_{11} + b_{22})\right) + \left[\left(\frac{1}{5} + \alpha_0\right)q^2 - \left(\frac{2}{3} + \frac{8}{3}\alpha_0\right)R_{11} - \left(\frac{1}{3} + \frac{1}{3}\alpha_0\right)R_{22}\right]\frac{dU_1}{dx_2} \qquad (3.4.1d)$$

$$U_c \frac{d\varepsilon}{dx_1} = -\frac{\varepsilon^2}{q^2}\left(3.80 + \psi_1 II + \psi_2 \frac{R_{12}}{\varepsilon}\frac{dU_1}{dx_2}\right) \qquad (3.4.1e)$$

We anticipate that the total strain rate is the important independent dimensionless parameter. The turbulent energy is used to non-dimensionalize the stresses. Hence, we introduce the following dimensionless variables into (3.4.1),

$$\tau = \frac{x_1}{U_c}\frac{dU_1}{dx_2} \qquad R_{ij}' = \frac{R_{ij}}{q^2} \qquad \text{and} \qquad \varepsilon' = \frac{\varepsilon}{q^2 dU_1/dx_2} .$$

The resulting dimensionless Reynolds stress equations are:

$$\frac{dR_{11}'}{d\tau} = -\varepsilon'\beta_0\left[(1 + \beta_1 II)b_{11} + \beta_2\left(b_{11}^2 + b_{12}^2 - \frac{II}{3}\right)\right] - \frac{2}{3}\varepsilon' + \left(\frac{4}{3}\alpha_0 - \frac{2}{3}\right)R_{12}' + 2R_{11}'(R_{12}' + \varepsilon') \qquad (3.4.2a)$$

$$\frac{dR_{22}'}{d\tau} = -\varepsilon'\beta_0\left[(1+\beta_1 II)b_{22} + \beta_2\left(b_{22}^2 + b_{12}^2 - \frac{II}{3}\right)\right] - \frac{2}{3}\varepsilon'$$

$$- \left(\frac{10}{3}\alpha_0 + \frac{4}{3}\right) R_{12}' + 2R_{22}'(R_{12}' + \varepsilon') \qquad (3.4.2b)$$

$$R_{11}' + R_{22}' + R_{33}' = 1$$

$$\frac{dR_{12}}{d\tau} = -\varepsilon'\beta_0 R_{12}'\left(1 + \beta_1 II + \beta_2(b_{22} + b_{11})\right)$$

$$- \left[\left(\frac{2}{3} + \frac{8}{3}\right)\alpha_0 R_{11}' + \left(\frac{1}{3} + \frac{1}{3}\alpha_0\right)R_{22}' - \left(\frac{1}{5} + \alpha_0\right)\right]$$

$$+ 2R_{12}'(R_{12}' + \varepsilon') \qquad (3.4.2c)$$

The coefficients α_0, β_0, β_1 and β_2 may now be determined by reference to the asymptotic region of the homogeneous shear flow. The experimental results of Harris, Graham and Corrsin (1977) in this region indicate that both $\tilde{q}^2 = \frac{q^2}{L_1^2 r^2}$ and R_{ij}' approach constant values. Since L_1 is not calculated directly in the second order model considered here, it must be determined from the dissipation rate ε. Following Rotta (1951), Schumann and Patterson (1975) have suggested that ε and L_1 may be related according to:

$$\varepsilon = K_1 \nu \frac{q^2}{L_1^2} + K_2 \frac{\left(\frac{1}{3} q^2\right)^{3/2}}{L_1}$$

so that

$$\varepsilon = \frac{\left(\frac{1}{3} q^2\right)^{3/2}}{L_1} \left(K_1' \cdot \frac{1}{R_{L_1}} + K_2 \right) , \qquad (3.4.3)$$

Thus, if $R_{L_1} >> 1$, the first term is negligible and we only need K_2 to determine L_1 from ε. In the following table, values of K_2 and R_{L_1} are calculated from the experiments of Richards (1975) and Harris, Graham and Corrsin (1977).

Table 3.7

K_2 Determination from (3.4.3)

Richards		Harris, Graham and Corrsin	
R_{L_1}	K_2	R_{L_1}	K_2
1285	1.13	629	1.15
1384	1.09	743	1.00
1490	1.04	850	.82
1605	.97	1150	.89
1726	.90	1235	.87
1857	.84	1385	.91
1924	.83		

The average value of K_2 is in the range $0.90 < K_2 < 1.00$. In the

asymptotic limit $R_{L_1} \to \infty$, if $L_1 = K_2 \frac{\left(\frac{1}{3} q^2\right)^{3/2}}{\varepsilon}$, then q^2 and ε can be expressed in terms of q^2 and :

$$\tilde{q}^2 = \frac{q^2}{L_1^2 \Gamma^2} = \frac{27}{K_2^2} \frac{\varepsilon^2}{(q^2)^2} = \frac{27}{K_2^2} \varepsilon'^2 \qquad (3.4.4)$$

Now the R_{ij}' approach a constant, so that $\frac{dR_{ij}'}{d\tilde{\tau}} = 0$ for large T. Thus, we may ignore the left hand side of Eq. (3.4.2) to obtain a linear set of algebraic equations in the constants α_0, β_0, β_1 and β_2 in which the R_{ij}' are known from the asymptotic values which were obtained experimentally and ε' is calculated from (3.4.4) since $\tilde{q}^2$ also has an asymptote. Hence, (3.4.2) for the Reynolds stresses becomes,

$$- \varepsilon' \left[\beta_1' b_{11} + \beta_2' (b_{11}^2 + b_{12}^2 - II/3)\right] - \frac{2}{3} \varepsilon' + \left(\frac{4}{3} \alpha_0 - \frac{2}{3}\right) R_{12}' + 2R_{11}'(R_{12}' + \varepsilon') = 0 \qquad (3.4.5a)$$

$$- \varepsilon' \left[\beta_1' b_{22} + \beta_2' (b_{22}^2 + b_{12}^2 - II/3)\right] - \frac{2}{3} \varepsilon' - \left(\frac{10}{3} \alpha_0 + \frac{4}{3}\right) R_{12}' + 2R_{22}'(R_{12}' + \varepsilon') = 0 \qquad (3.4.5b)$$

$$- \varepsilon' R_{12}' \left[\beta_1' + \beta_2'(b_{11} + b_{22})\right] - \left[\left(\frac{2}{3} + \frac{8}{3}\alpha_0\right) R_{11}' + \left(\frac{1}{3} + \frac{1}{3}\alpha_0\right) R_{22}' - \left(\frac{1}{5} + \alpha_0\right)\right] + 2R_{12}'(R_{12}' + \varepsilon') = 0 \qquad (3.4.5c)$$

Note that β_0, β_1 and β_2 appear only in the independent groupings:

$$\beta_1' = \beta_0(1 + \beta_1 II)$$

and

$$\beta_2' = \beta_0\beta_2$$

so that we can, at most determine β_1 and β_2 in terms of β_0 from the homogeneous shear flow data. The quantities R_{ij}' and ε' appearing in (3.4.5) have the following measured asymptotic values.

Table 3.8

Asymptotic Values of Reynolds Stresses in Homogeneous Shear Flows

R_{11}'	R_{22}'	R_{33}'	R_{12}'	ε'
.500	.200	.300	-.150	.0755

Notes.

(1) $b_{ij} = R_{ij}' - \frac{1}{3}\delta_{ij} \Rightarrow II = b_{ij}b_{ji} = .09167$

(2) $\varepsilon' = .0755$ corresponds to a value of $K_2 = 0.9$ in Eq. (3.4.4), if $K_2 = 1.0$, then $\varepsilon' = .0839$.

Solving Eqs. (3.4.5) using the values in Table 3.8, gives the following parameter estimates:

$$\alpha_0 = -0.333$$

$$\beta_1' = 4.144$$

$$\beta_2' = -6.926$$

The value of α_0 is independent of the value used for ε' and is relatively insensitive to changes in R_{11}' and R_{22}'. Increasing ε' from 0.0755 to 0.0839, a 10% increase, results in a - 5% change in β_1' and a 10% increase in β_2'. Since both of these terms multiply higher order corrections to T_{ij}^2, this amount of uncertainty is not excessive.

Other modellors use a form similar to Eq. (2.5.14) for the rapid part of the pressure-strain correlation. The values of α_0 in these earlier models are summarized in Table 3.9.

Table 3.9

Parameter Estimates of α_0 in T_{ij}^1 Model

Predictor	Value of α_0
Present	- .333
Reynolds (1976)	- .300
Launder (1975)	- .332
Launder, Reece and Rodi (1975	- .291
Naot, Shavit and Wolfshtein (1973)	- .266
Lumley (1975)	- .491

Notes.

(1) The result of Launder was given as tentative with no indication of how it was determined.

(2) The α_0 value of Lumley (1975) is by far the largest and was determined by reference to "rapid strain" analysis. This value is too extreme for use in a general model, but later in this chapter a flow with approximately rapid strain will be modelled and it will be shown that a larger value of α_0 is required in these extreme cases.

The value of α_0 determined by Zeman and Tennekes (1975) was not included in Table 3.9 because they separated the effects of mean strain and mean rotation in their model. Furthermore, they estimate their parameters using both a homogeneous shear flow and several wall bounded flows. We believe that this appraoch is incorrect because the Reynolds stresses in a turbulent boundary layer approach a different set of asymptotic values than for a homogeneous shear flow (cf. Table 3.4).

In the next section, the value of β_0 will be determined from a consideration of the return-to-isotropy flows. With β_0 known, the constants β_1 and β_2 can be determined from the estimated values of β_1' and β_2' which were given earlier, i.e.

$$\beta_1 = \frac{45.208}{\beta_0} - 10.909$$

$$\beta_2 = -\frac{6.926}{\beta_0} \quad .$$

3.5 Determination of β_0

In the absence of mean strain, the model for the pressure-strain

correlation T_{ij}, reduces to the return-to-isotropy part, T_{ij}^{2} (Eq. 2.5.23). The only coefficient so far undetermined in this expression is β_0 which can be obtained by studying the decay of anisotropic turbulence. For this problem, the governing Eqs. (3.1.1) and (3.1.2) reduce to the simple form,

$$U_1 \frac{\partial R_{ij}}{\partial x_1} = -\varepsilon\beta_0\left[(1 + \beta_1 II)b_{ij} + \beta_2\left(b_{ik}b_{kj} - \frac{II}{3}\delta_{ij}\right)\right] - \frac{2}{3}\delta_{ij}\varepsilon \quad (3.5.1)$$

$$U_1 \frac{\partial \varepsilon}{\partial x_1} = -\frac{\varepsilon^2}{q^2}(3.80 + \psi_1 II) \quad (3.5.2)$$

It was suggested in Section 3.3 that a distinction can be made between the rate of decay for weakly and strongly anisotropic turbulence. The use of weak anisotropy will be considered first and β_0 will be determined. The resulting model will then be tested by predicting strongly anisotropic turbulent decay to determine whether any adjustments in the parameters are required.

The return-to-isotropy for weak anisotropy is most conveniently studied by considering an equation for the anisotropy tensor b_{ij}, which may be deduced from Eq. (3.5.1).

$$\frac{q^2}{\varepsilon} U_1 \frac{db_{ij}}{dx_1} = -\left\{(\beta_0 - 2 + \beta_0\beta_1 II)b_{ij} + \beta_2\beta_0\left(b_{ij}b_{kj} - \frac{II}{3}\delta_{ij}\right)\right\} \quad (3.5.3)$$

For small b_{ij} (i.e., only weakly anisotropic turbulence), the higher order terms can be neglected, leaving the linear model:

$$\frac{db_{ij}}{d\tau} = (\beta_0 - 2)b_{ij} \qquad (3.5.4)$$

where

$$\tau = \left(\frac{q^2 U_1}{\varepsilon}\right)^{-1} dx_1$$

It is clear from (3.5.4) that β_0 must be greater than 2.0 for isotropy to be restored (unless the only restoring mechanisms are nonlinear in b_{ij}). However, β_0 should not be too much greater than 2.0 because the return is weak in the weak anisotropy limit (c.f. Section 3.2A).

From Table I of Comte-Bellot and Corrsin (1966) β_0 may be determined. The average for all of the experiments considered by Comte-Bellot and Corrsin is $\beta_0 = 2.5$ and this value will be used for the testing on strongly anisotropic flows which is considered next.

Using the result obtained in Section 3.6 that $\psi_1 = -16.4$ for strongly anisotropic decay in the absence of mean velocity gradients, Eqs. (3.1.1) and (3.1.2) were solved numerically. The equations were integrated forward using the CIT subroutine MODDEQ for the initial conditions given in Table 3.10.

Table 3.10

Initial Conditions for Strongly Anisotropic Flows

Experiment	K	ε_0
Tucker and Reynolds (1968)	.620	$.521 \times 10^{-5}$ in.$^{-1}$
Uberoi (1957)	.600	$.210 \times 10^{-5}$ in.$^{-1}$

In Figure 3.5 the K values from Tucker and Reynolds (1968), three experiments are compared to the model predictions for three different values of β_0. The value $\beta_0 = 3$ gives best agreement with the data, but all three values give comparable results over the initial half of the decay. In Figure 3.6, other models are compared to the same data. Two of these models are linear in β_0, but have different values of β_0, namely 3.0 and 4.0. The value $\beta_0 = 3$ was proposed by Launder, Reece and Rodi (1975) and represents a consensus of all the values summarized in Launder (1975, Table 1.2). The value, $\beta_0 = 4.0$ gives the best agreement for a linear model. The non linear model of Launder (1975) under predicts the return giving nearly the same profile as the linear model with $\beta_0 = 3$.

In Figure 3.7 the experimental K-values determined from Uberoi's (1956, 1957) experiments are compared to predictions for $\beta_0 = 2.5$. Of the two cases considered, the rate of return is too rapid in one and too slow in the other. This behavior may be partly explained by reference to the recent return-to-isotropy model of Lumley and Newman (1977). They found that, although the return is not linear in b_{ij}, it does not increase without bound as b_{ij} increases. Instead, there is a local maximum rate of return at a particular value of II.

Their model is described in Appendix C and is shown graphically in Figure 3.8, along with several others for the case of return-to-isotropy of axisymmetric turbulence. For this case, the quantity $\frac{T_{11}}{b}$ is sufficient to characterize the return-to-isotropy, i.e. if $b_{11} = b$ then $b_{22} = b_{33} = -\frac{b}{2}$ hence $II = \frac{3}{2} b^2$ and $T_{22} = -T_{11}/2 = T_{33}$.

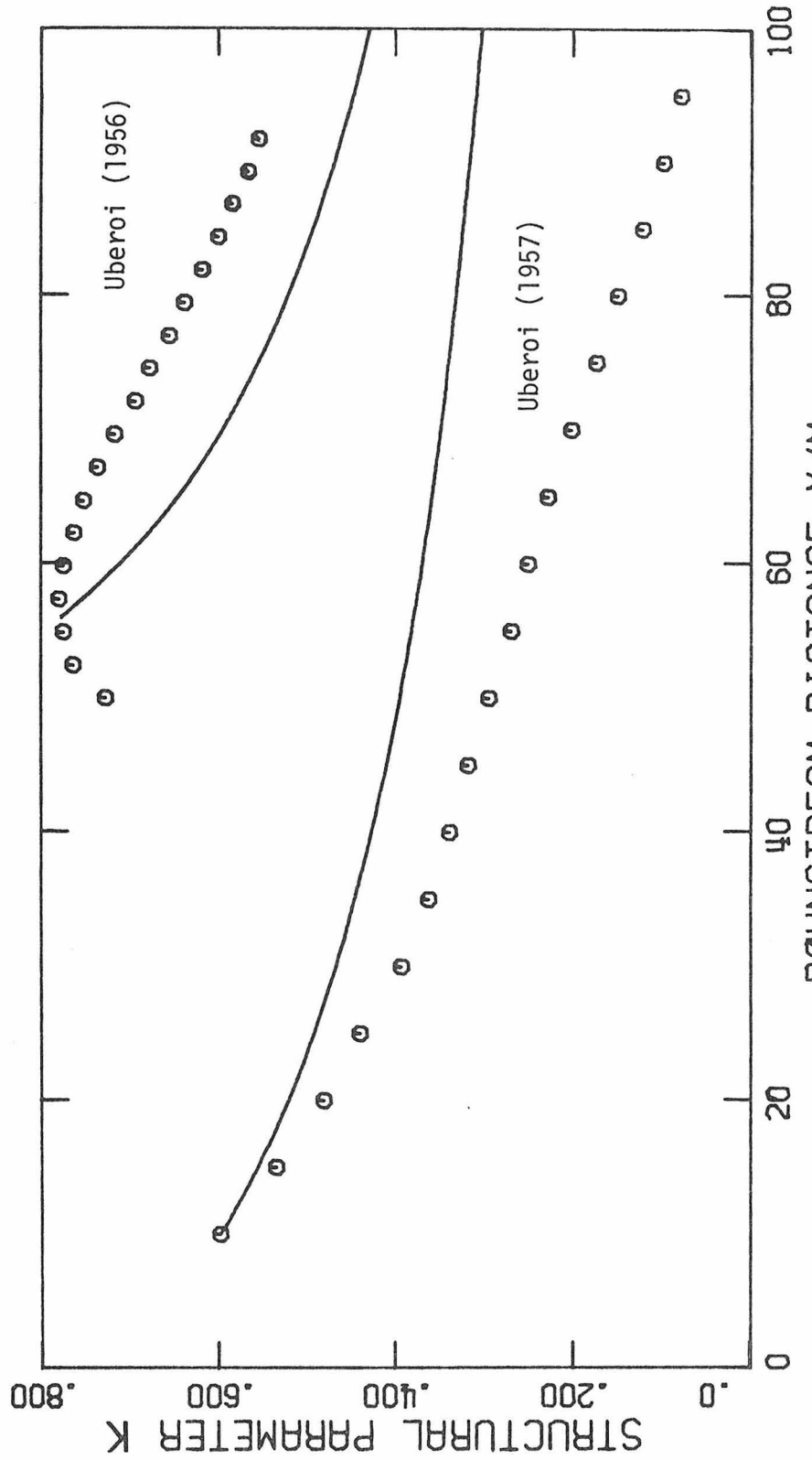

Figure 3.7.--Return-To-Isotropy Calculations for Flows of Uberoi (1956, 1957).

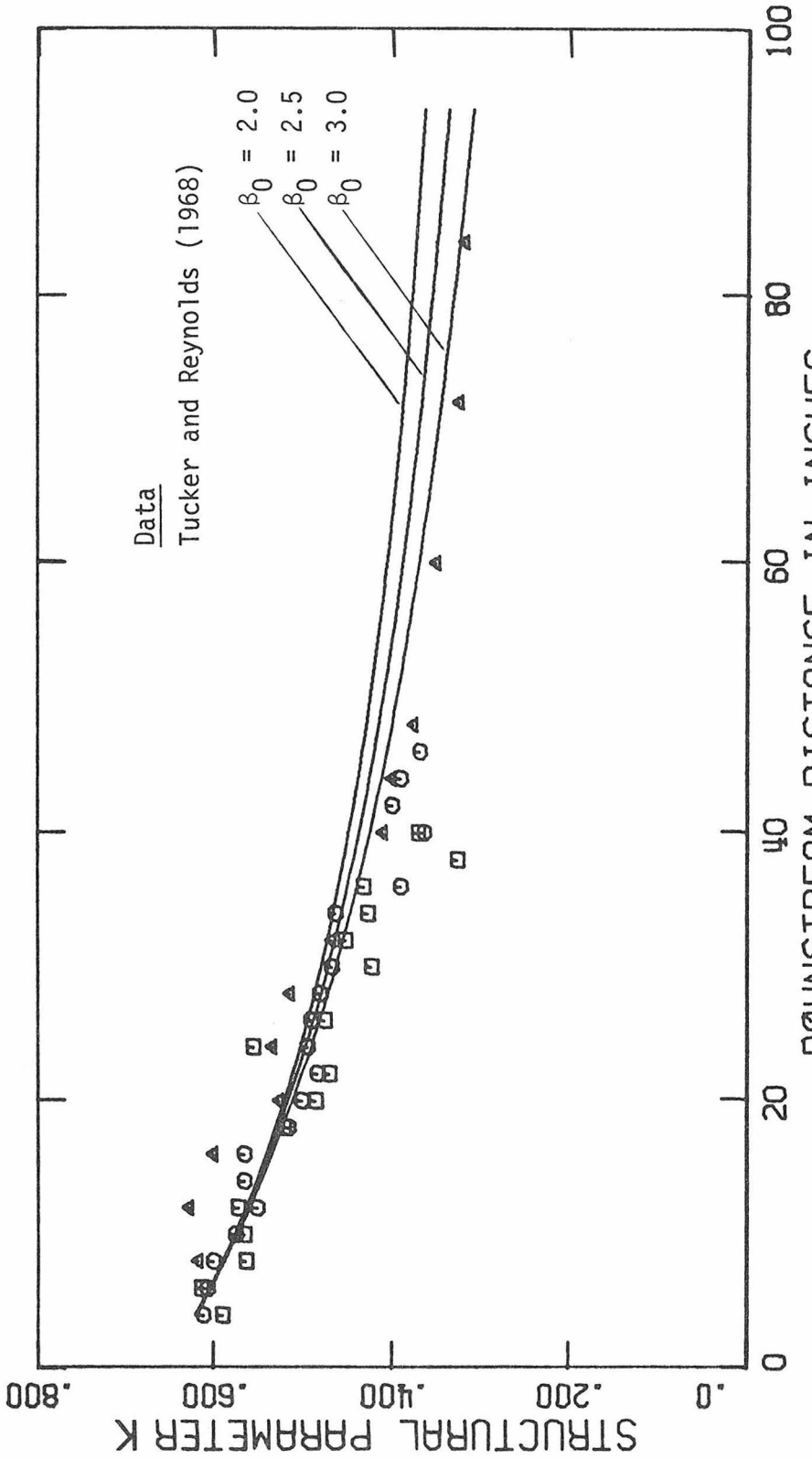

Figure 3.5.--Return To Isotropy Calculations Using Present Model With Different β_0 Values.

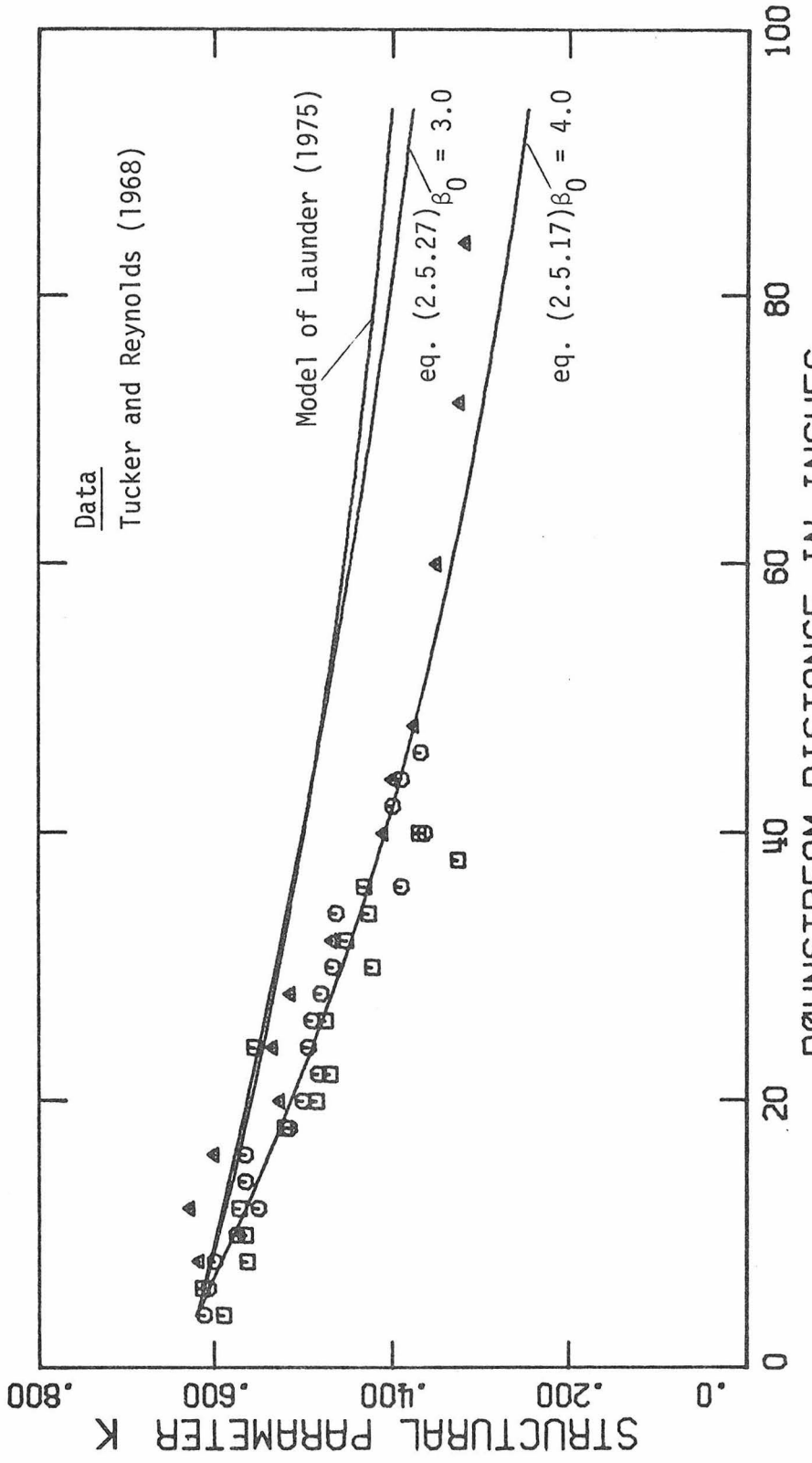

Figure 3.6.--Return to Isotropy Calculations Using the Linear Model, equation (2.5.17) and Launder's (1975) Model.

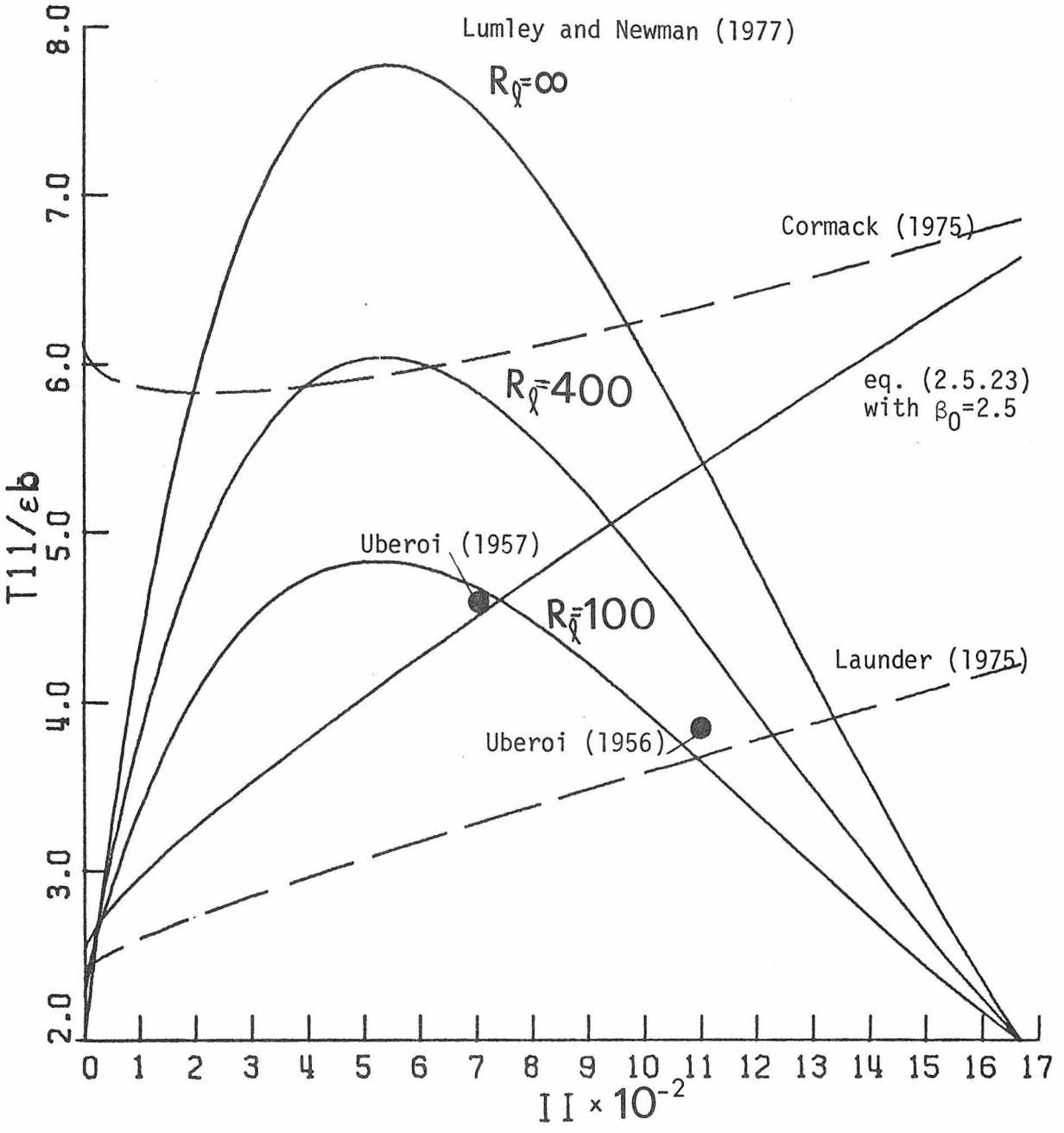

Figure 3.8.--Magnitude of $T_{11}/\varepsilon b$ Versus the Second Invariant, II, for Various Return to Isotropy Models. Data Points are Initial Values for the Flows of Uberoi.

The model of Lumley and Newman is capable of predicting all of the flows of Uberoi [see Lumley and Newman (1977) Figures 3 - 11]. The Uberoi flow with Re_M = 3710 initially has II = .11 and $R_\ell \sim 200$. The present model predicts a much higher value of $T_{11}/\varepsilon b$ than Lumley and Newman and K, therefore initially decays too rapidly as Figure 3.7 shows. The other Uberoi flow (1957) with Re_M = 10,000, initially has II = .07 and $R_\ell \sim 100$. In this case the two models are initially in approximate agreement. As II decreases, however, the Lumley-Newman model predicts a faster rate of return that is not realized using the present model. It is also clear that a linear model with β_0 = 3.0 will predict too small a value for $T_{11}/\varepsilon b$ which explains the under predicted return-to-isotropy in Figure 3 for Tucker and Reynolds (1968) flow. The same thing is true for Launder's (1975) non linear model. In Figures 3.9 and 3.10 the decay of the Reynolds stresses for the two Uberoi flows is shown. These figures further illustrate that the rate of return is initially too rapid in one case [Uberoi (1956)] and too slow in the other [Uberoi (1957)].

As was mentioned in § 2.5, the model of Lumley and Newman (1977) for T_{ij}^2 cannot easily be used in calculations because of its eigenvalue formulation and dependence on Reynolds number. Furthermore, most laboratory flows have Reynolds numbers in the range $100 < R_\ell < 400$, and in this range the present model represents a reasonable compromise between the Lumley and Newman model and the overly simplified linear model.

In summary, the present model for T_{ij}^2 works reasonably well in both weakly and strongly anisotropic flows with the same value,

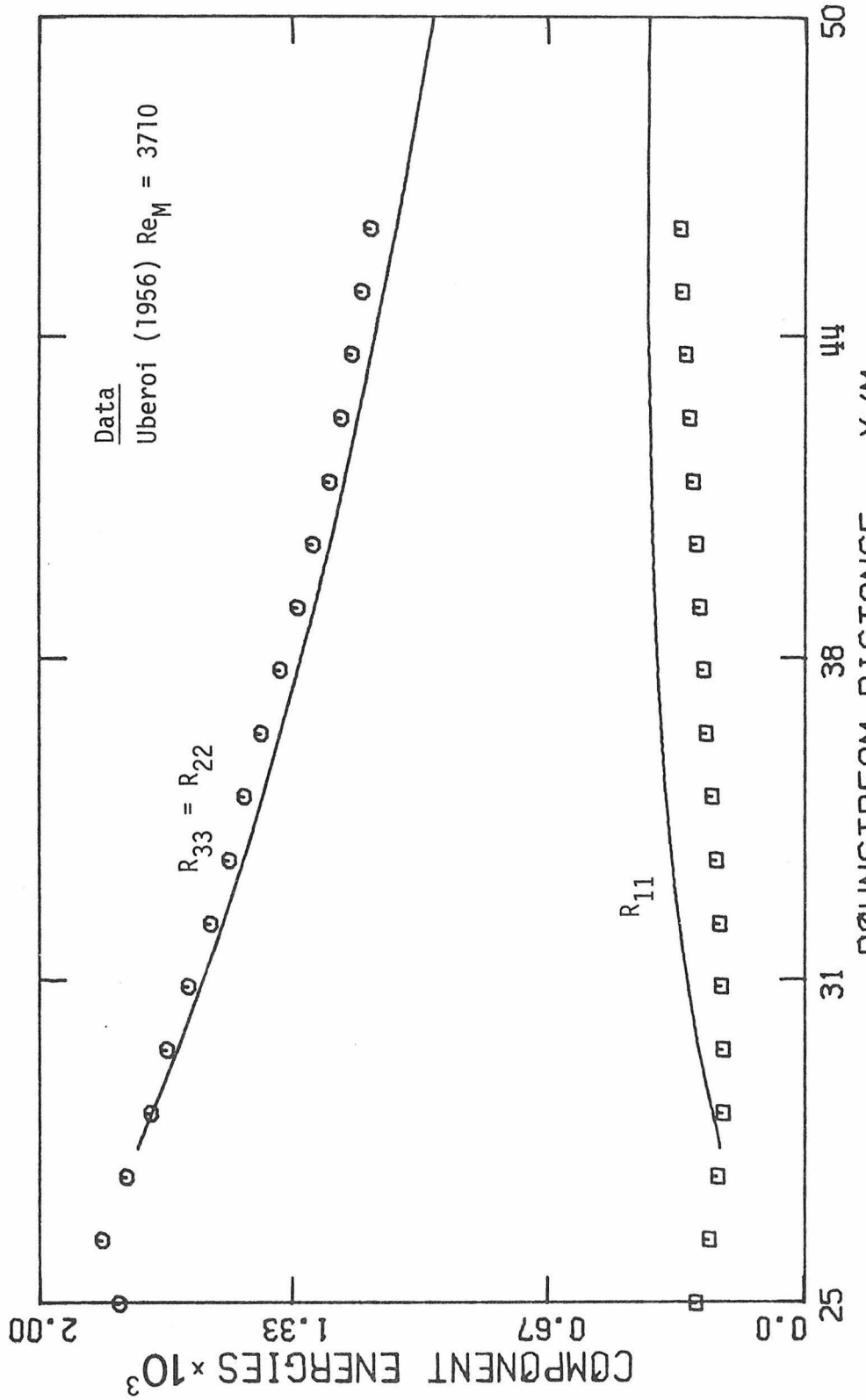

Figure 3.9.--Decay of Anisotropic Turbulence; _____, Present Model Predictions.

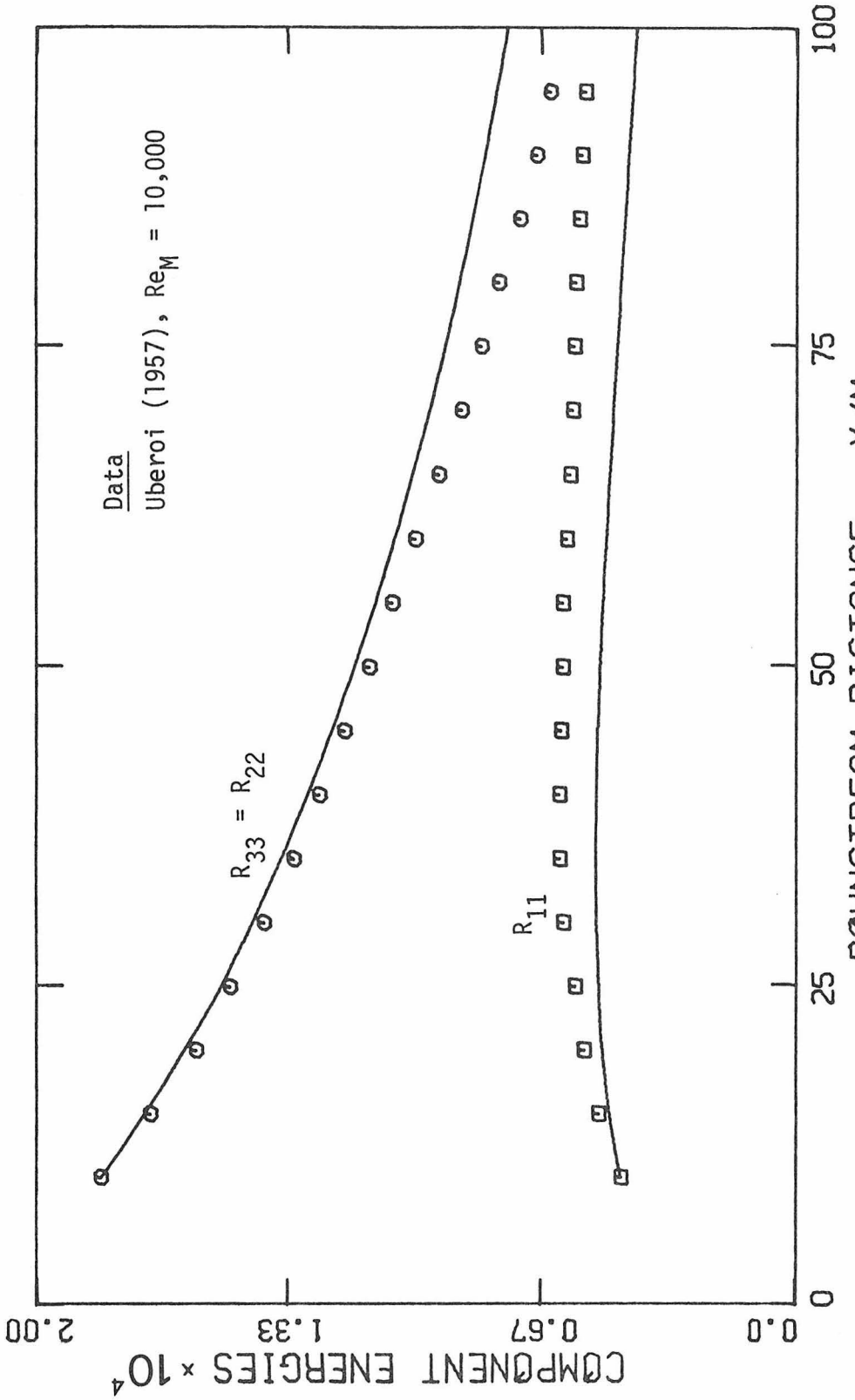

Figure 3.10.--Decay of Anisotropic Turbulence; _____ Present Model Predictions (equation 2.5.23) Predictions.

$\beta_0 = 2.5$. It does not work particularly well when II is very large, but these cases lie outside of the hypotheses used in § 2.3 to generate the model.

In later sections it will be shown that the non linear return to isotropy model derived here works well in calculations of homogeneous shear and homogeneous strain flows. In these cases, the rapid part of the pressure-strain model (i.e., T_{ij}^{1}) dominates T_{ij}^{2}. Before predictions of these flows can be calculated, the parameters ψ_1 and ψ_2 in the dissipation Eq. (3.1.2) must be evaluated. This is carried out in the next section.

3.6 Determination of ψ_1 and ψ_2

The only constants as yet undetermined in the model are ψ_1 and ψ_2 in the dissipation equation (3.1.2). These constants can also be determined by reference to homogeneous flows. However, in none of these flows is the dissipation rate actually measured. So, to obtain the constants directly, the dissipation must be calculated by difference from the kinetic energy equation and then substituted into equation (3.1.2) which can then be solved for Δ_ε. This method is inaccurate because it necessitates two differentiations of the energy data. A more convenient way to determine ψ_1 and ψ_2 is to integrate equations (3.1.1) forward in x to determine the energy (q^2) profile. The calculated values of q^2 are then compared to the experimental values and estimates of ψ_1 and ψ_2 are determined by minimizing the objective function,

$$\Phi = (q^2_{calc} - q^2_{exp})^2 \qquad (3.6.1)$$

using the CIT subrouting LSQENP which is a non linear least squares regression routine.

Initially the plane strain flows of Tucker (1970) were used to determine ψ_1 and ψ_2. These results are given in Table 3.11.

Table 3.11

Determination of ψ_1 and ψ_2 from Data of Tucker (1970)

Experiment	ψ_1	ψ_2
# 1	- 14.26	1.581
# 2	56.20	8.7357
# 3	36.24	3.097

These estimates show no consistency whatsoever and the reason for this was alluded to in § 2.6. Since II and $(\underline{\underline{bS}}_1)$ are both a measure of the production of dissipation, a high correlation exists between ψ_1 and ψ_2. A convenient way of studying the two terms separately is to consider flows for which the production is zero (i.e., the decay of anisotropic turbulence).

For the case of weakly anisotropic turbulence, Lumley and Newman (1977) found that $\psi_1 = - 9.09$. The more strongly anisotropic flows of Uberoi (1965,1957) suggest that $\psi_1 = - 16.4$. In both cases though, the estimate of ψ_1 is very uncertain and depends on the initial value

of the dissipation rate used to start the integration. Typically, a 1% change in the initial dissipation rate gives a 5% change in ψ_1. About all that can be said about ψ_1 is that it should be negative; that is, anisotropic turbulence decays faster than isotropic turbulence.

The asymptotic nature of the homogeneous shear flow after prolonged strain can also be used to determine the constants ψ_1 and ψ_2. It was shown in § 3.4 that the dimensionless energy,

$$\tilde{q}^2 = \frac{q^2}{L_1^2 \Gamma^2} = \frac{27}{K_1^2} \varepsilon'^2 \qquad (3.6.2)$$

approached a constant value. Thus, ε' must be constant. An equation for ε', similar to those for R_{ij}', (3.4.2), can be determined from equations (3.1.1) and (3.1.2), and is

$$\frac{d\varepsilon'}{dt} = -(3.80 + \psi_1 II)\varepsilon' - \psi_2 \varepsilon' R_{12}' + 2\varepsilon'(\varepsilon' + R_{12}') \qquad (3.6.3)$$

Since R_{12}' and II become asymptotically constant, the above equation can be integrated, giving

$$\frac{(2 - \psi_2)R_{12}' - (3.80 - 2. + \psi_1 II)\varepsilon'}{\varepsilon'} = C_1'' e^{(\psi_2 - 2)R_{12}'} \qquad (3.6.4)$$

where C_1'' depends on the initial conditions. R_{12}' is negative, so that if $\psi_2 > 2.0$, the exponential decays to zero and ε' approaches the constant value.

$$\varepsilon' = \frac{(\psi_2 - 2)R_{12}'}{-(1.80 + \psi_1 II)} \qquad (3.6.5)$$

Using the experimental values from Table (3.8), equation (3.6.5) can be solved to give a locus of possible pairs of values for ψ_1 and ψ_2.

Table 3.12

ψ_1, ψ_2 Values Determined from Homogeneous Shear Flow

ψ_1	ψ_2
0.0	2.90
- 4.0	2.72
- 8.0	2.54

The first value of ψ_2, ψ_2 = 2.90 is very close to the value of ψ_2 = 2.88 which was obtained by Launder, Reece and Rodi (1975) on the basis of a computer optimization for both homogeneous and free shear flows.

If the ε-equation, (3.1.2), is transformed into an equation for an integral length scale using $L' = \frac{(q^2)^{3/2}}{\varepsilon}$, then

$$\frac{dL'}{dt} = \frac{(q^2)^{1/2}}{\varepsilon} P(3 - \psi_2) + (q^2)^{1/2}(- 3 + \psi_0 + \psi_1 II) \qquad (3.6.6)$$

where $P = R_{12}\Gamma$ and L' is proportional to the longitudinal integral length scale would be independent of the mean shear rate. This result

is consistent with the findings of Harris, Graham and Corrsin (1977). Instead, a comparison of the integral length scale, L_1, obtained from their experiments, with the similar result from the lower shear rate flow of Champagne, Harris and Corrsin (1970), shows that the growth of the length scale is independent of the total strain (see Figure Harris, Graham and Corrsin, 1977). Bradshaw (1977) has also indicated that the eddy length <u>scale</u>, as distinct from the eddy <u>shape</u>, is controlled by the turbulent mixing term (the second term in 3.6.6) rather than the mean strain. The best way to study eddy shapes is to consider the correlation function defined by,

$$R_{11}(r_1, r_2, r_3, \tau) = \frac{\overline{u_1(\underline{x},t)u_1(\underline{x}+\underline{r},t+\tau)}}{\sqrt{\overline{u_1^2(\underline{x})}}\ \sqrt{\overline{u_1^2(\underline{x}+\underline{r})}}} \qquad (3.6.7)$$

The integral length scale, L_1, is related to R_{11} by the equation

$$L_1 = \int_0^\infty R_{11}(r_1,0,0;0)dr_1.$$

In Figure (3.11) the correlation functions for the two homogeneous shear flows are compared. Since the curves are nearly coincident, despite the considerable differences in total strain, it is suggestive, as indicated above, that the strain rate is not an important parameter for scale growth. Possibly typical eddy shapes can be determined by considering the spatial iso-correlation contours $[R_{11}(r_1,r_2,0;0)]$ in the (r_1,r_2) plane. In Figure 3.12, the particular correlation coefficients $R_{11} = 0.4, 0.5$ are plotted for both the low total strain flow of CHC and the higher total strain homogeneous shear flow of Harris, Graham and

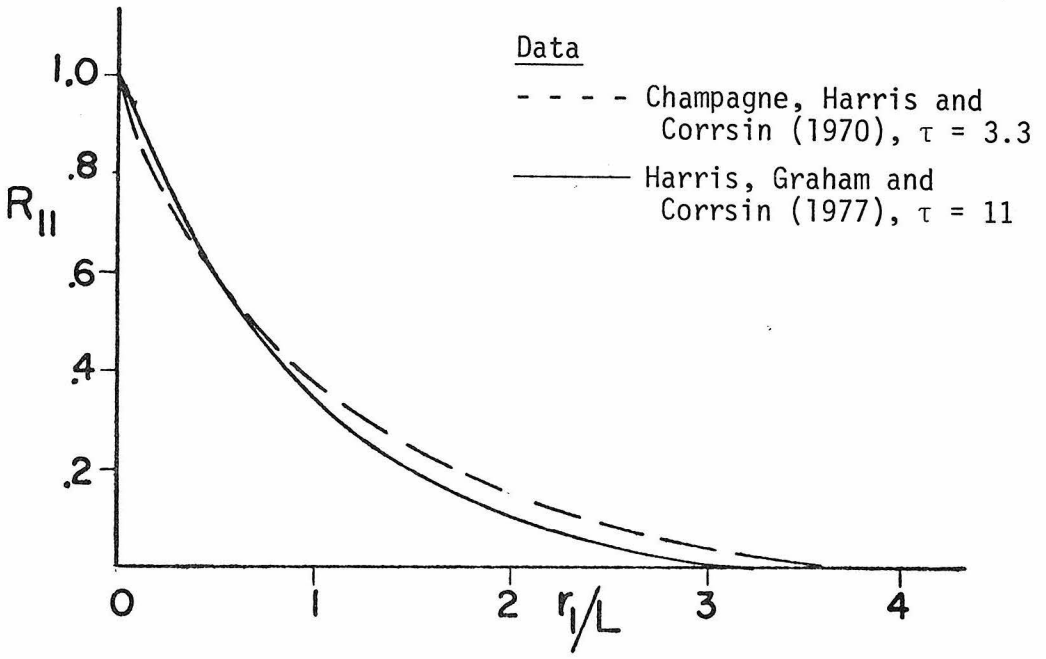

Figure 3.11.--Similarity of Two-Point Velocity Correlation, $[R_{11}(r_1,0,0_j0)]$ for Two Values of Total Strain, τ.

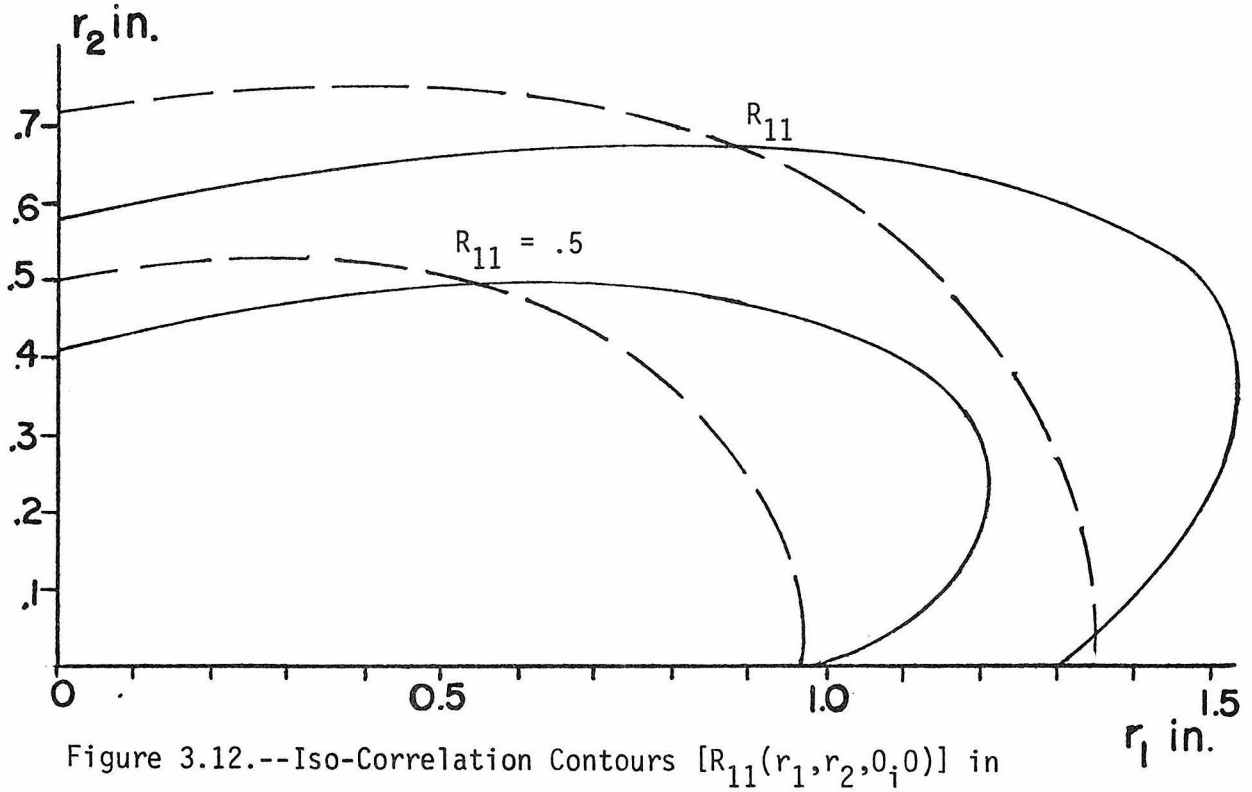

Figure 3.12.--Iso-Correlation Contours $[R_{11}(r_1,r_2,0_i0)]$ in the (r_1,r_2) Plane. Data as in Figure 3.11.

Corrsin (1977). The extent of the eddies is comparable in both cases, but in the high shear case, the oval shape is more tilted (13^{o} relative to the r_1-axis) than for the weaker shear case. The contours of the high shear case are typical of those observed in a turbulent boundary layer [cf. Sabot and Comte-Bellot (1972)].

A model for the integral length L', was derived by Rodi and Spalding (1970) and Rotta (1975) by integrating the $R_{ij}(\underline{x},\underline{r})$ equation. These models have terms proportional to the energy production P and may be written for illustrative purposes as

$$\frac{dL'}{dt} = \frac{L'}{q^2}(\psi_2' - 2.0)\, P + \begin{array}{c}\text{turbulent mixing and} \\ \text{diffusion terms}\end{array} \qquad (3.6.8)$$

For the integral length scale development to be independent of the mean strain in <u>this</u> model, ψ_2' must be equal to two. By studying a wide range of free shear flows, Rodi and Spalding determined that $\psi_2' = 2.0$ and Rotta (1975) gave $\psi_2' = 1.96$.

The above theoretical and experimental evidence suggests that the integral length scale dynamics should be approximately independent of mean strain. In the present dissipation model [Equation (3.1.2)] , this requires ψ_2 to be approximately 3.0. For preliminary calculations, we thus adopt the pair of values $\psi_1 = 0.0$ and $\psi_2 = 2.9$ which are consistent with this requirement as well as the earlier analysis of homogeneous shear flow (cf. Table 3.12). A larger value for ψ_2 (e.g. $\psi_2 = 3.0$) would require <u>positive</u> values of ψ_1 and we have cited evidence earlier which suggested strongly that ψ_1 should be negative or zero, but definitely not positive. The estimates $\psi_1 = 0.0$, $\psi_2 = 2.9$ must be

tested further in dynamic calculations. Dynamic (model) predictions for homogeneous irrotational strain and homogeneous shear flow are given in the next section. In Chapter 5 model predictions will be compared to the available experimental data.

3.7 Homogeneous Model Verification

The homogeneous form of the model proposed in Chapter 2 and the parameter estimates of the present chapter must be tested in dynamic calculations. In this section the homogeneous flows described in § 3.3B,C will be modeled using the proposed model and in some cases compared to predictions made using other models. It is important to note that the irrotational straining flows described in § 3.3B were not used to determine the model constraints. Furthermore, only the asymptotic, large strain region of the homogeneous shear flow was used to estimate the constants. Hence, the dynamic calculations described in this section provide a strong test of the predictive capability of the model in dynamic calculations for a wide range of homogeneous flow situations. The first flows considered are the homogeneous straining flows described in § 3.3B.

A. Irrotational Straining Flows

The proposed model has the following form for homogeneous straining flows

$$\frac{dR_{\alpha\alpha}}{dx_1} = U^{-1}\left\{-2R_{\alpha\alpha}S_{\alpha\alpha} + \left(\frac{4}{10} + 2\alpha_0\right)S_{\alpha\alpha}q^2 - 3\alpha_0\left(2R_{\alpha\alpha}S_{\alpha\alpha} + \frac{2}{3}P\right)\right.$$

$$\left. - \varepsilon\beta_0\left[(1 + \beta_1 II)b_{\alpha\alpha} + \beta_2\left(b_{\alpha\alpha}^2 - \frac{II}{3}\right)\right] - \frac{\varepsilon}{3}\right\} \qquad (3.7.1)$$

$$\frac{d\varepsilon}{dx_1} = U^{-1}\left\{\frac{\varepsilon^2}{q^2}\left(-3.80 - \psi_1 II + \psi_2 P/\varepsilon\right)\right\} \qquad (3.7.2)$$

here α takes on the values, α = 1,2,3 (no summation) where,

$$S_{\alpha\alpha} = \frac{dU_\alpha}{dx_\alpha} \quad \text{and} \quad P = -R_{11}S_{11} - R_{22}S_{22} - R_{33}S_{33}.$$

The above equations were integrated forward in x_1 using the CIT program MODDEQ which is an accurate Runge-Kutta quadrature with an Adams-Moulton predictor-corrector for increased precision. The initial values of the variables used are given in Table 3.13. The method used to determine the initial dissipation and the equations used to determine the mean velocity for each flow are given in Appendix D.

i) Plane Strain

Predictions of the relative turbulent intensities for the lateral plane straining flows are compared with the data of Tucker (1970) for his three experiments in Figures 3.13 to 3.15. The agreement is excellent except near the end of the test section where the values of R_{33}/q^2 is under-predicted and those of R_{11}/q^2 are over-predicted. This disagreement may be due to the presence of boundary layers which

TABLE 3.12

Initial Values of Turbulence Quantities for Plane Strain Flows

Strain Type	Experimental Set-Up	Maximum Strain	$\frac{R_{11}}{q^2}$	$\frac{R_{22}}{q^2}$	$\frac{R_{33}}{q^2}$	$\frac{q^2}{U_0^2} \times 10^{-3}$	$\frac{\varepsilon}{U_0^2} \times 10^{-4}$
Plane lateral strain	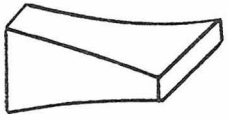	6.0	.42	.29	.29	2.636	.750
		6.0	.42	.29	.29	1.072	.316
		6.0	.42	.29	.29	1.101	.315
Plane longitudinal strain		5.8	.39	.30	.31	2.461	.727
		2.8	.41	.295	.295	2.685	.749
Axisymmetric contraction		6.0	.40	.30	.30	2.649	.670
Equivalent Diffuser		2.3	.390	.290	.320	2.894	.750

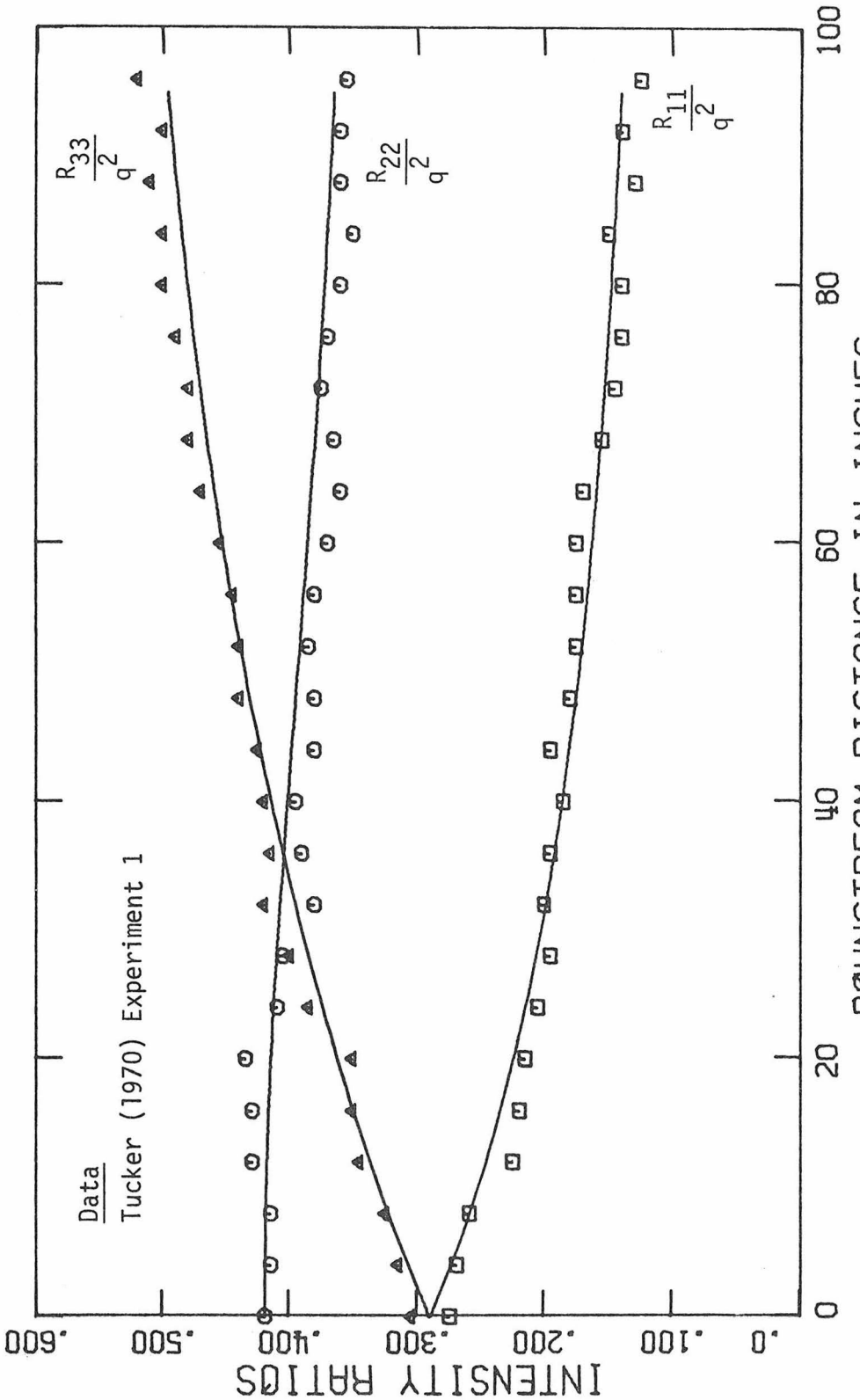

Figure 3.13.--Calculation of Relative Reynolds Stresses, $\frac{R_{ij}}{q^2}$: Plane Strain Flow.

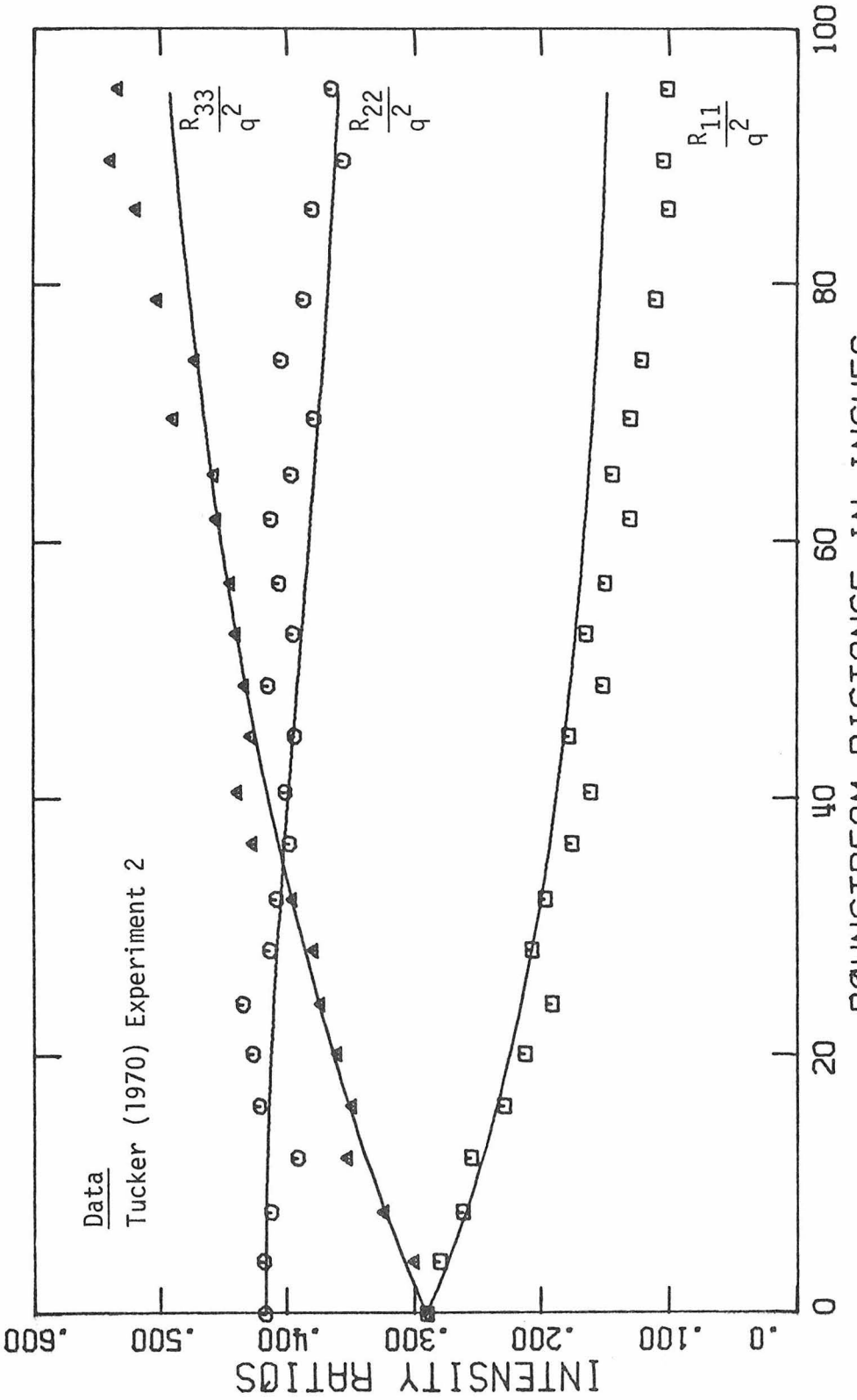

Figure 3.14.--Calculation of the Relative Reynolds Stresses, $\frac{R_{ij}}{q^2}$: Plane Strain Flow.

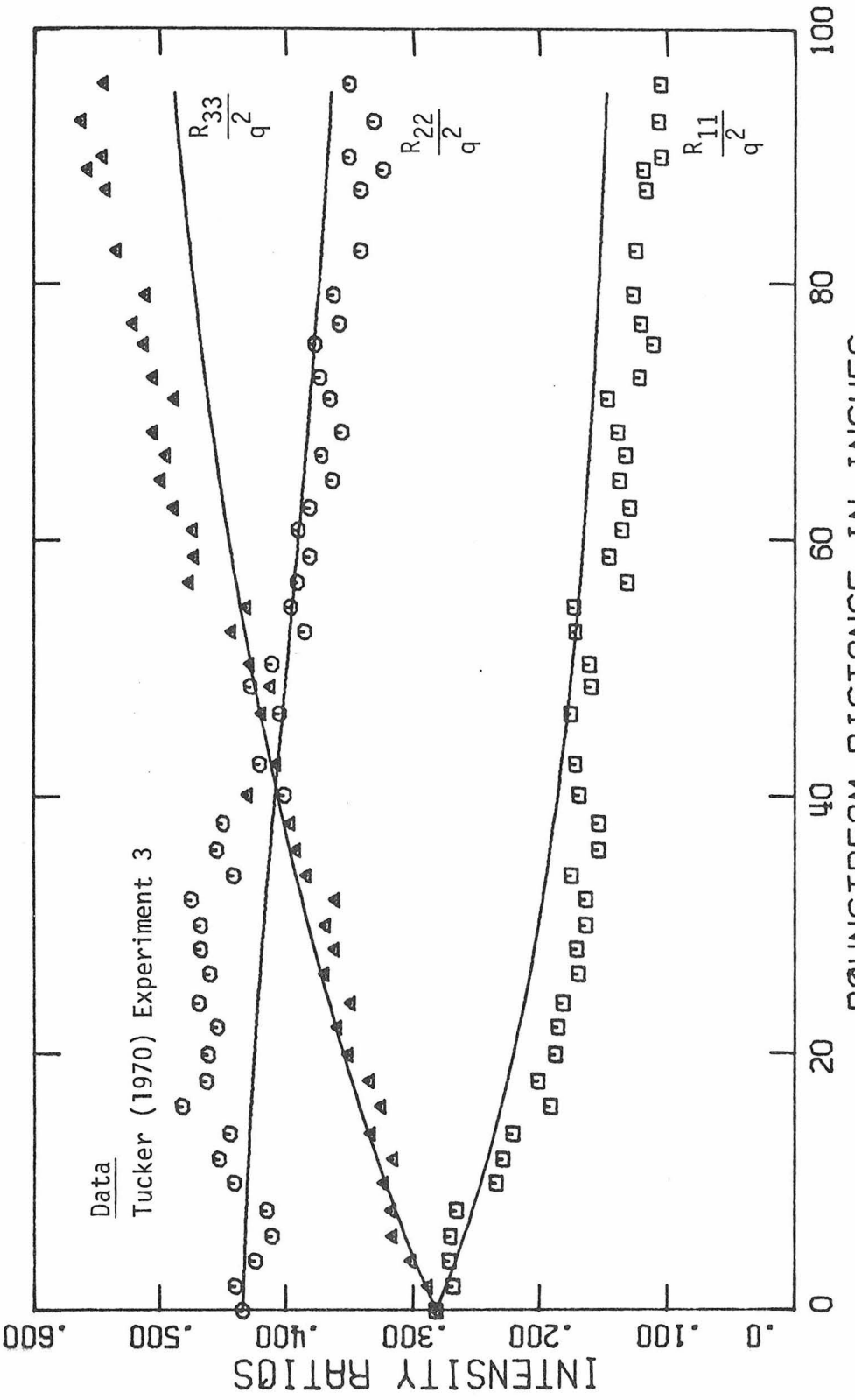

Figure 3.15.--Calculation of the Relative Reynolds Stresses, $\frac{R_{ij}}{q^2}$: Plane Strain Flow.

increase in thickness with downstream distance and inhibit the growth of R_{11}/q^2. In Figure 3.16 the structural parameter K is compared with predictions. This figure also shows the gradually worsening agreement between predictions and data toward the end of the test section. It should be observed that despite the different initial conditions used in each case (see Table 3.12) the three predictions are coincident. This suggests that the initial magnitudes of energy and dissipation are not important when the normalized intensities, R_{ij}/q^2 are considered.

The turbulent energy profile is shown in Figure 3.17. The effect of the distorting duct can be noted by comparing the energy profile which results when a strain is applied, to the case of pure decay (which gives a straight line decay or the logarithmic plot considered). The distortion causes energy to be transferred from the mean flow to the turbulence.

The agreement between predictions and data is good except towards the end of the duct where the turbulent energy is underestimated by the model. It seems likely that the experimental values are too high in this region since the presence of boundary layers on the walls of the duct will undoubtedly increase the production of turbulent energy.

The two longitudinal straining flows of Reynolds and Tucker (1975) are predicted in Figures 3.18 and 3.19. The agreement between predictions and data is good except for the R_{22} component. The model predicts that this term should remain about constant whereas the data shows a small but steady increase with increasing strain. No reason can be offered for this discrepancy.

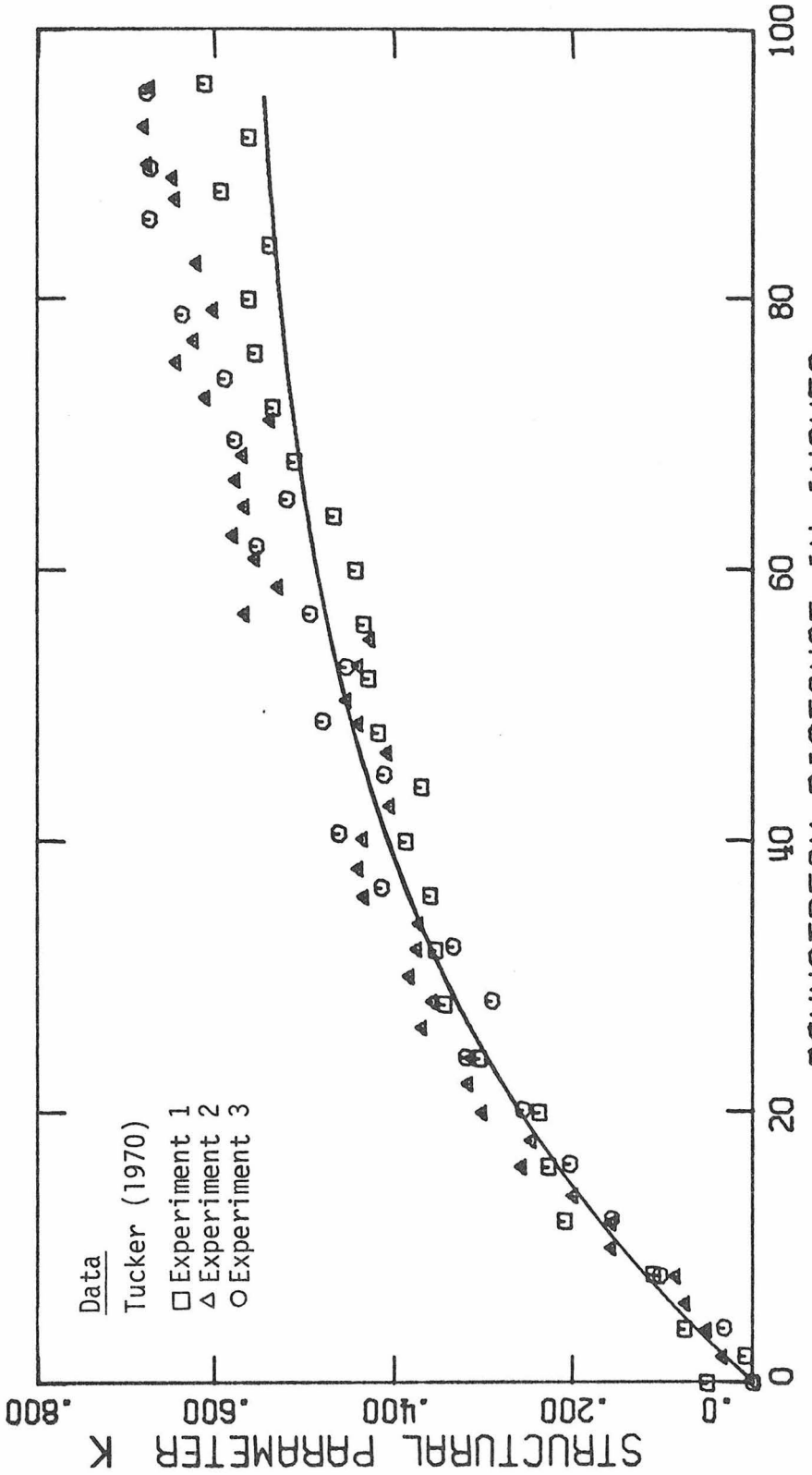

Figure 3.16.--Calculation of the Structural Parameter $k = \frac{R_{33} - R_{11}}{R_{33} + R_{11}}$ for the 3 Plane Strains of Tucker (1970).

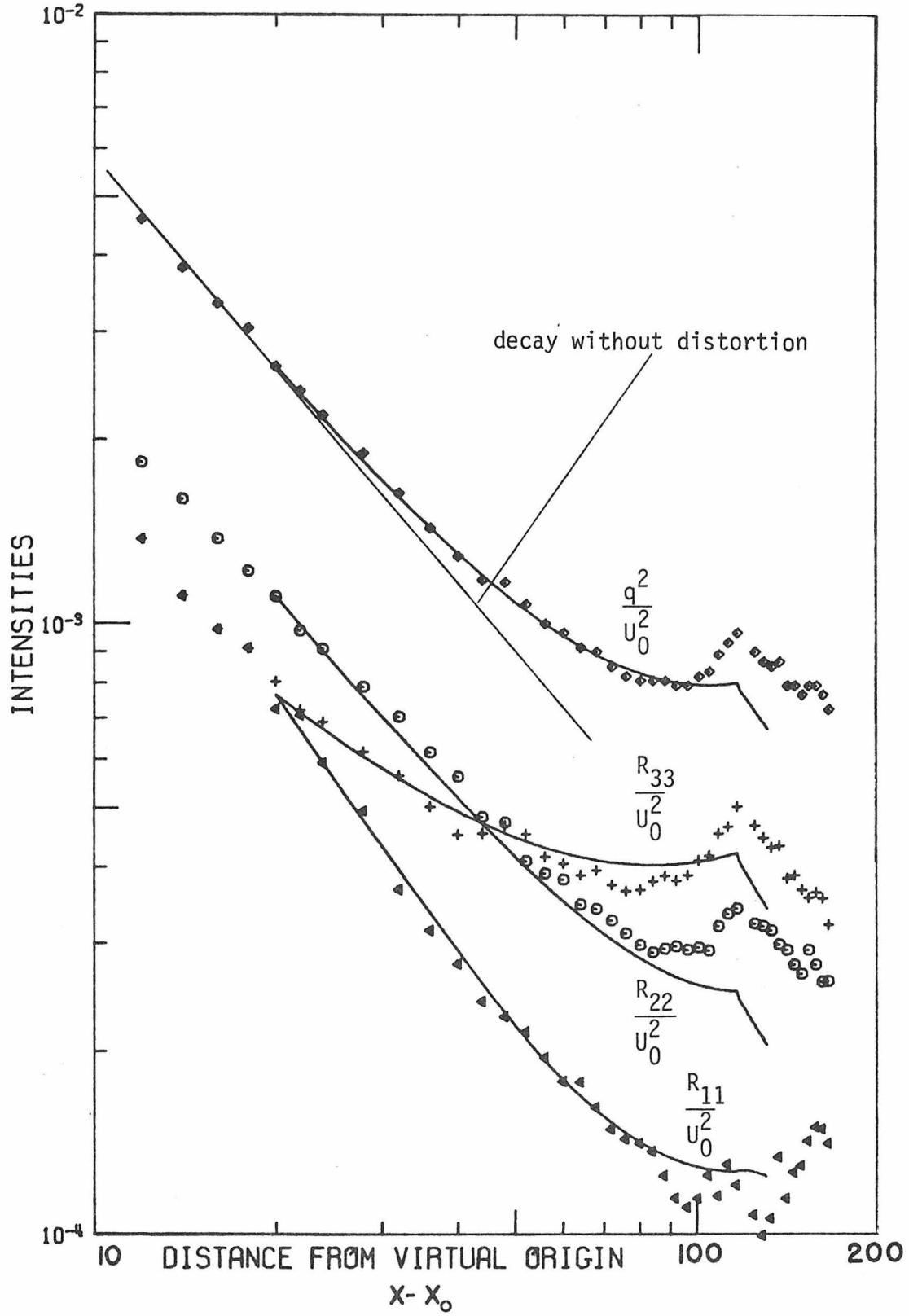

Figure 3.17.--Decay of Reynolds Stress Components and Turbulence Energy in Plane Distortion. Data of Tucker and Reynolds (1968).

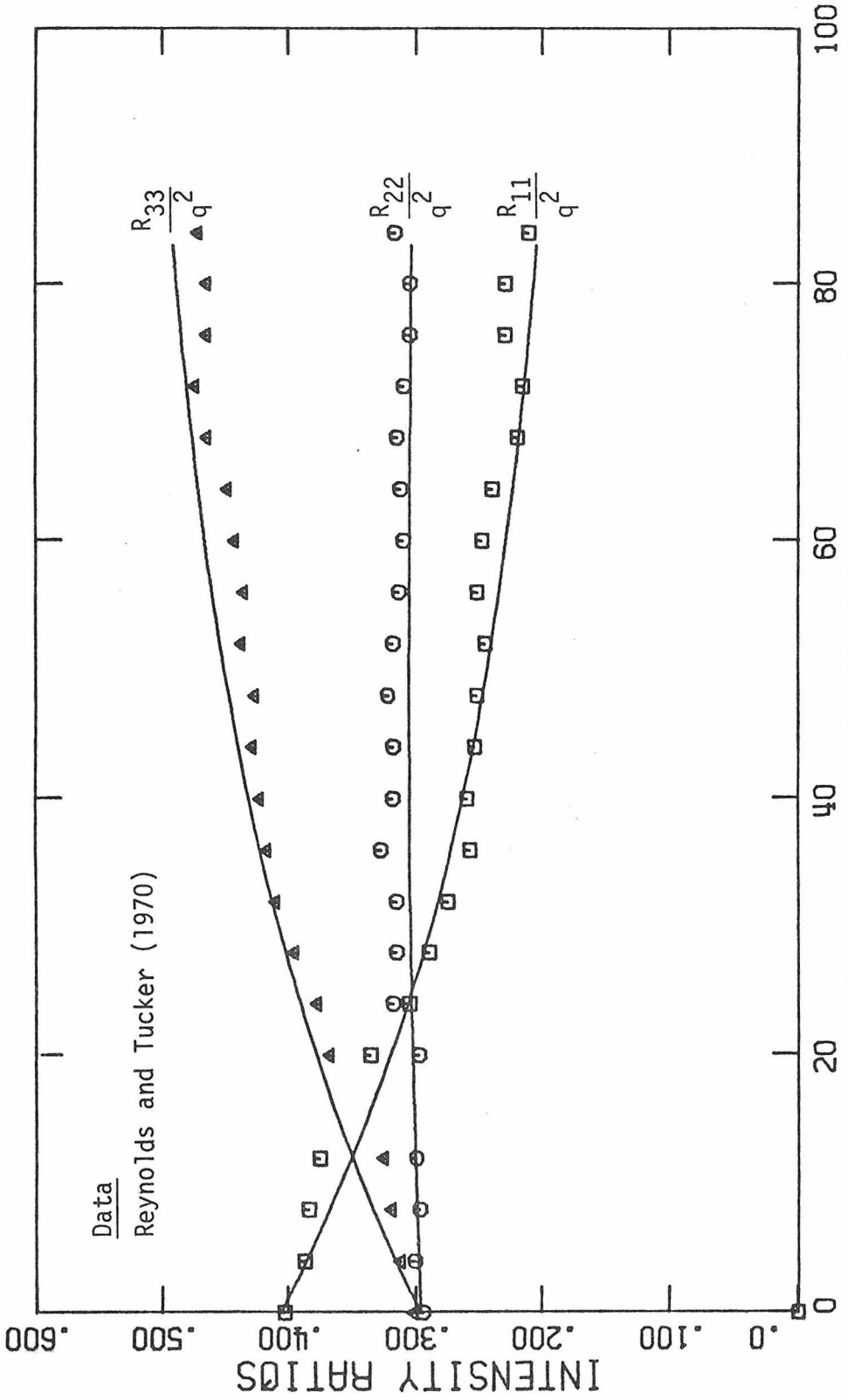

Figure 3.18.--Calculation of Relative Reynolds Stresses: Longitudinal Plane Strain, Lower Total Strain Case, $\tau_{max} = 2.3$.

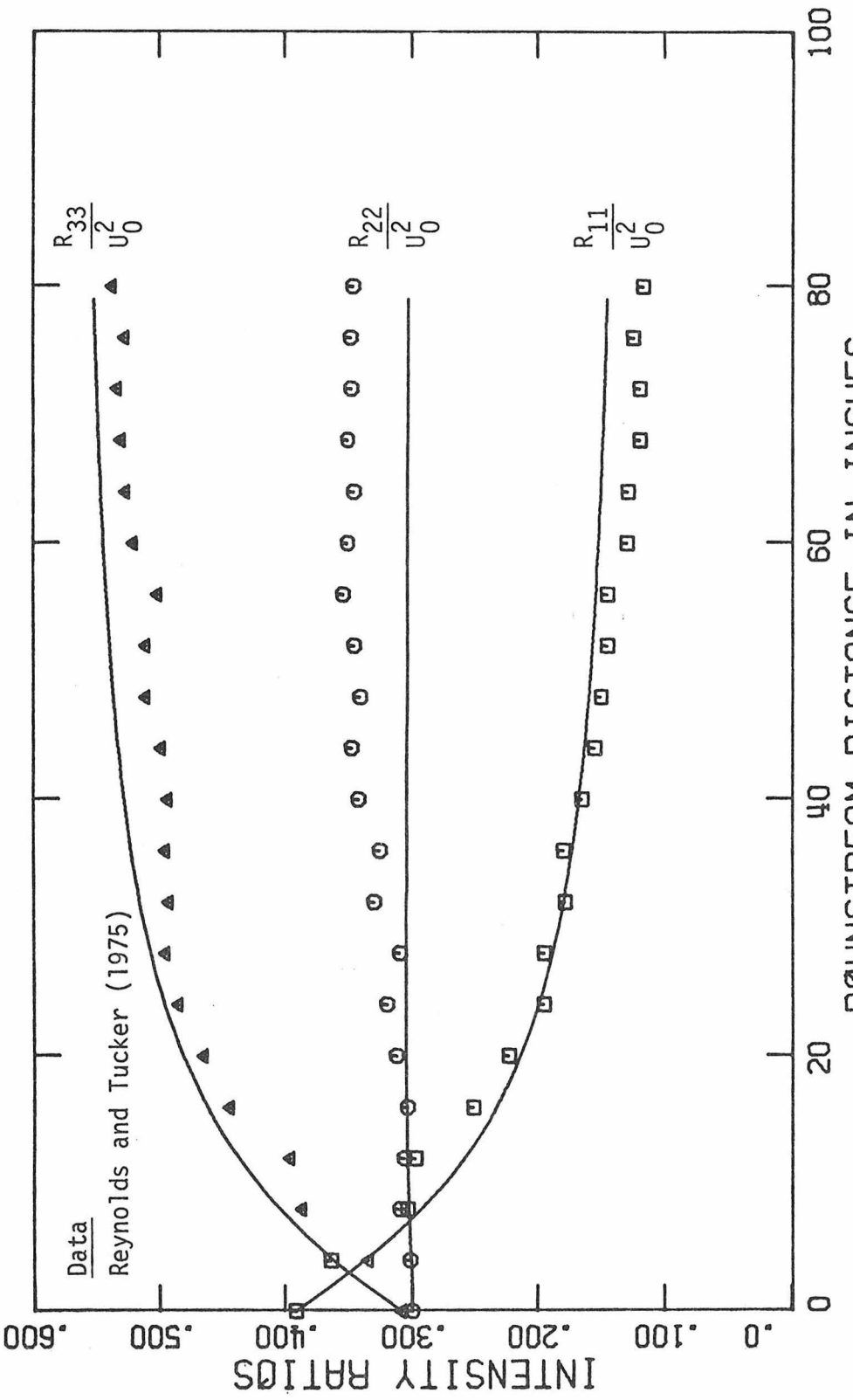

Figure 3.19.--Calculation of Relative Reynolds Stresses: Longitudinal Plane Strain Higher Total Strain Case, $\tau_{max} = 5.8$.

ii) Axisymmetric Contraction

The predicted relative stress levels for an axisymmetric contraction are compared to the data of Reynolds and Tucker (1975) in Figure 3.20. The predicted cross-stream quantities are slightly too high and the predicted streamwise stress is too low. This results in an overestimate of K as shown in Figure 3.21. However, when predictions are obtained for the more rapidly contracting duct of Uberoi (1956), the value of K is underestimated by the present model. This is illustrated in Figure 3.19. Calculations were also carried out using Lumley's (1975) estimation for α_0. Since Lumley based his estimate on a rapid strain analysis, it is not surprising that his value for α_0 gives better comparison with the data of Uberoi (1956). However, Lumley's value for α_0 represents an extreme, limiting case which would greatly overpredict K for the less rapid distortion considered by Reynolds and Tucker. The present model, in which α_0 was obtained from the asymptotic behavior of homogeneous shear flow thus appears to be a reasonable compromise between the extremely high value of Lumley (1975) and the lower values of Table 3.9 which were used by other investigators.

iii) Equivalent Diffuser

In Figure 3.22, model predictions for the equivalent diffuser flow are presented. As indicated in § 3.3B the ideal value of the strain rate parameter for this flow, F = 1.0, could not be obtained experimentally. The experimentally determined value Fe = 0.47 was used in the calculations to determine the rates of strain in the three

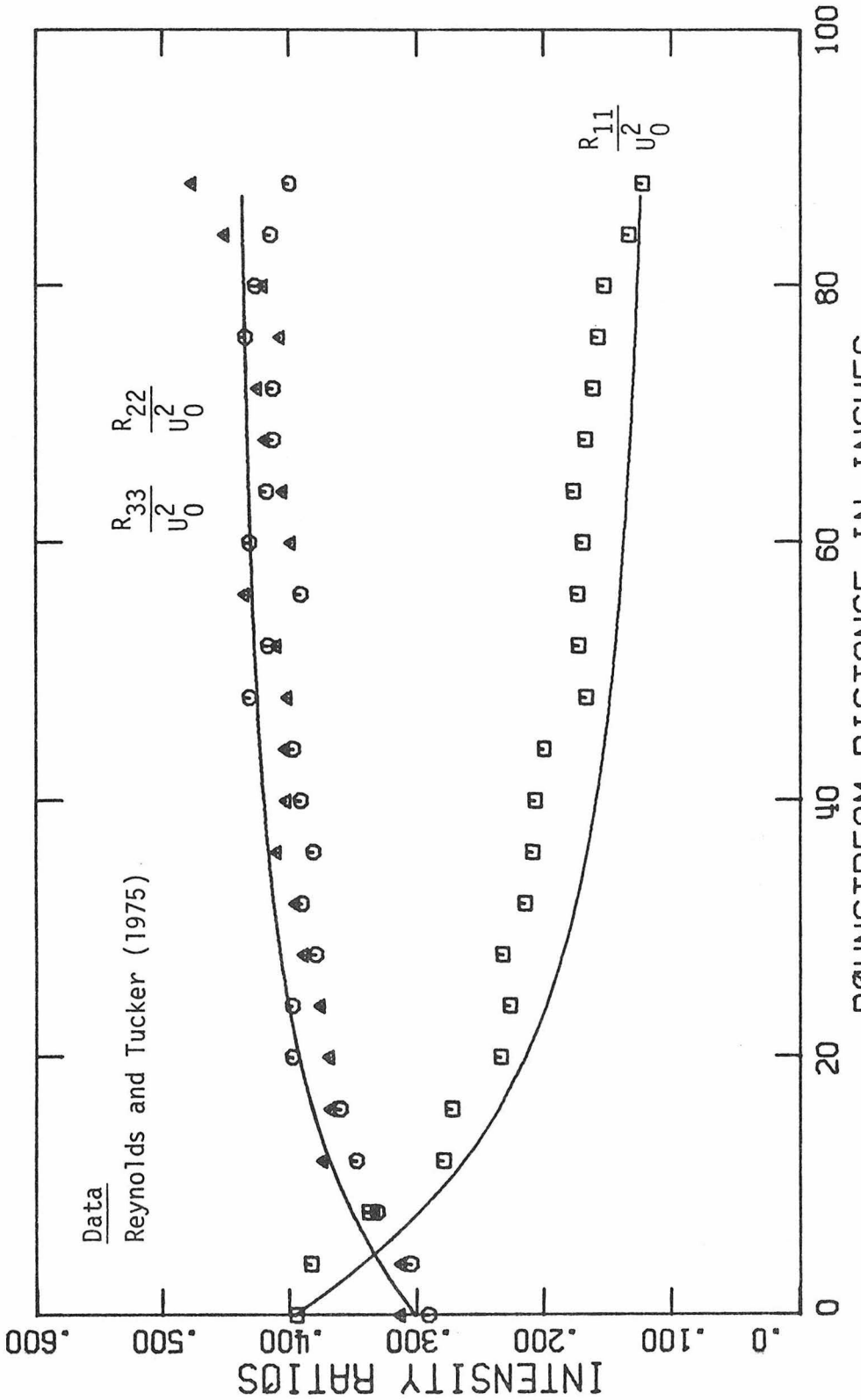

Figure 3.20.--Calculation of Relative Reynolds Stresses: Axisymmetric Contraction.

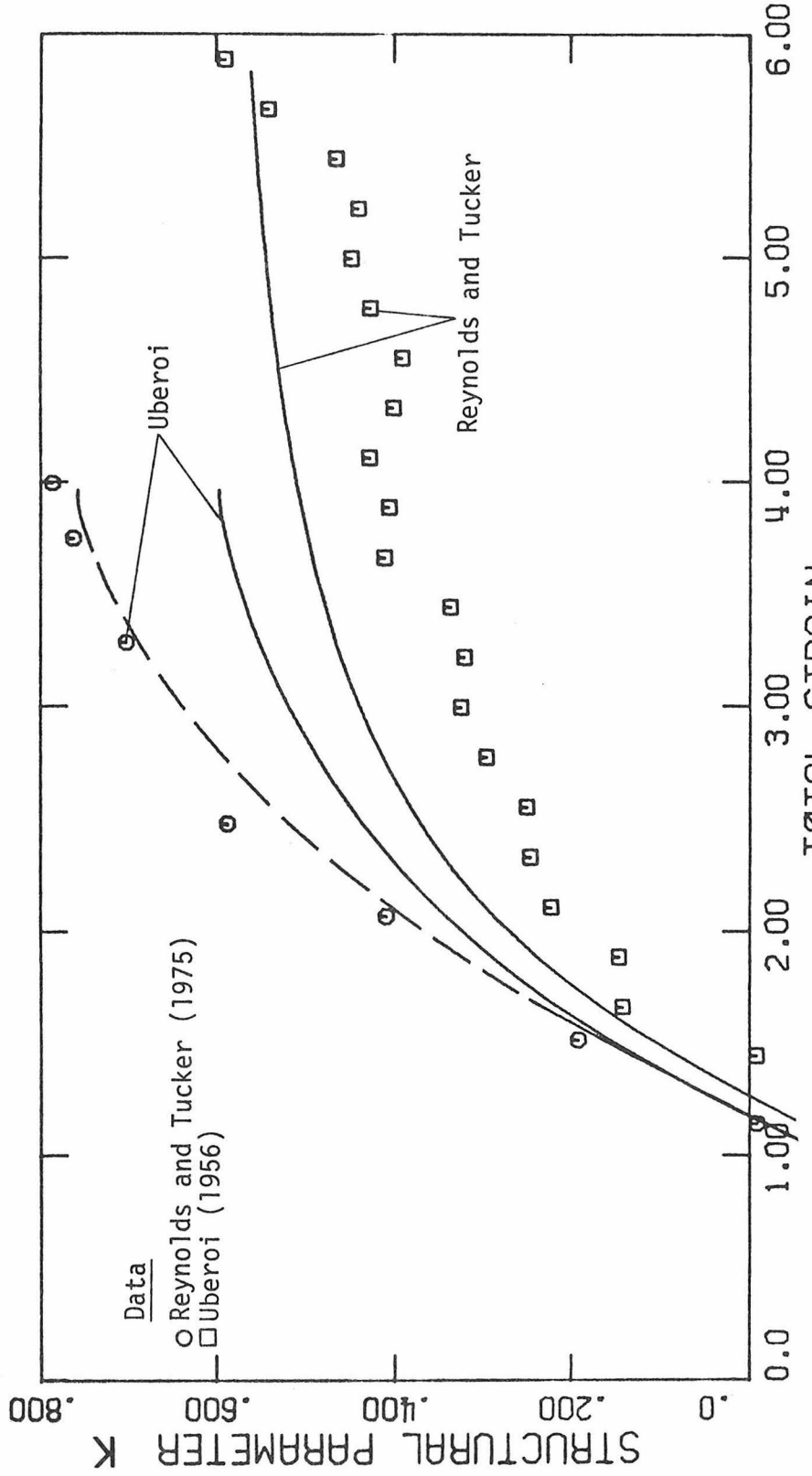

Figure 3.21.--Calculation of the Structural Parameter $k = \frac{R_{33} - R_{11}}{R_{33} + R_{11}}$ for the Axisymmetric Contractions of Uberoi (1956), and Reynolds and Tucker (1975). _____ Present Model, - - - Lumley's α_0 Value in eq. (2.5.23).

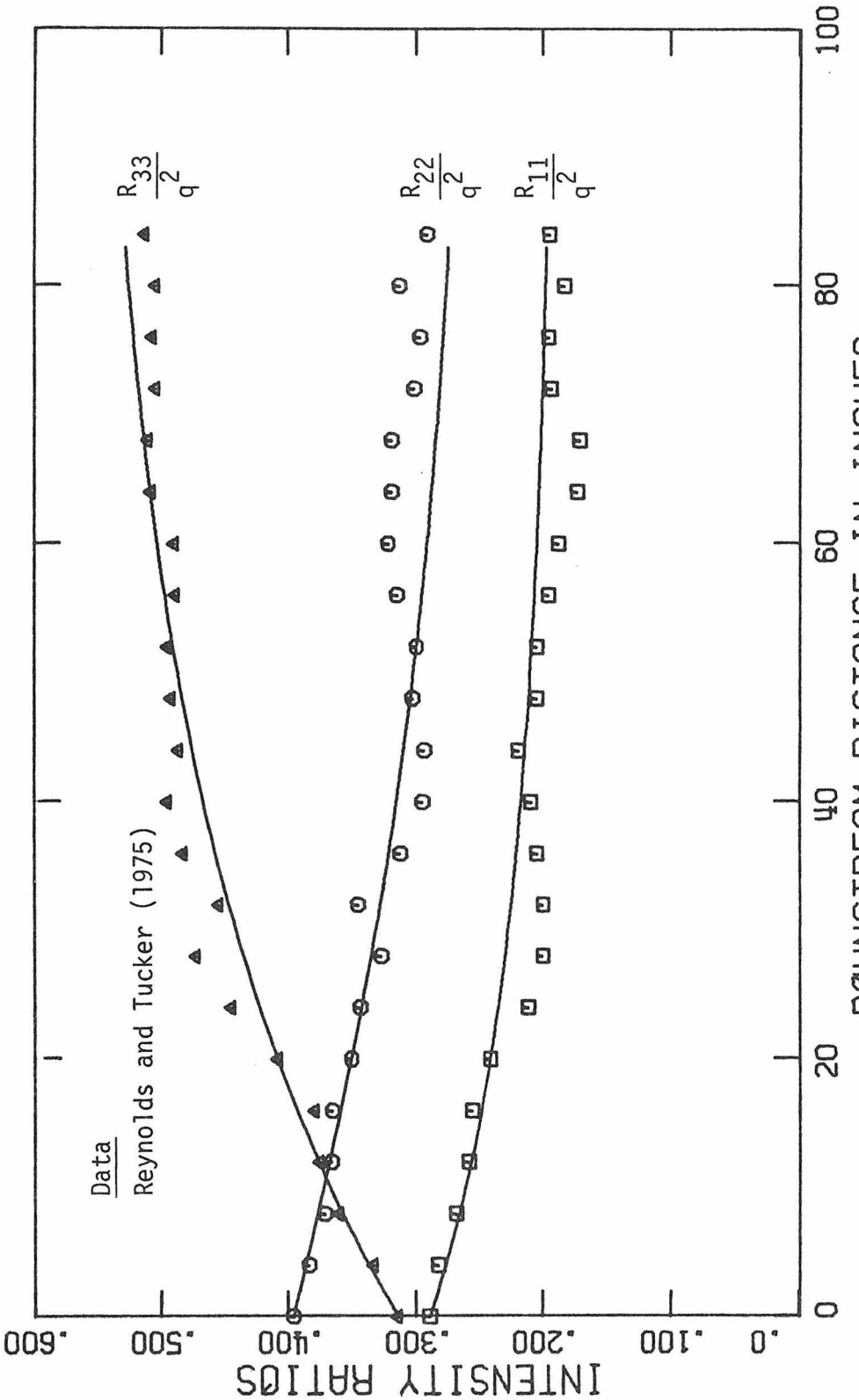

Figure 3.22.--Calculation of Relative Reynolds Stresses: Equivalent Diffuser.

coordinate directions. As shown in Figure 3.22 the agreement between predictions and data is excellent.

In summary, it may be concluded that the present model provides excellent predictions for homogeneous straining flows. In particular, the partitioning of the turbulent energy among the three normal stresses is well predicted as shown in Figures 3.13 - 3.15, 3.18, 3.19, 3.20 and 3.22.

Since the apportioning of the energy is primarily due to the model of the pressure-strain correlation, the good predictions shown in these figures are evidence of its validity.

B. Homogeneous Shear Flows

The governing equations for homogeneous shear flows were given in § 3.4, i.e. Equations (3.4.1a - e). As a further test of the homogeneous model, these equations were solved using the initial values given in Table 3.14 and the results compared with the data of CHC and Harris, Graham and Corrsin (1977). The predictions corresponding to these two sets of data are presented in Figures 3.23 and 3.24. The experimental studies of CHC and Harris et al. were chosen for comparison because they span the range from high to low total shear.

The lower shear rate case is well predicted although the predicted values of R_{11}/U_c^2 are somewhat lower than the data. This underprediction is, however, common to the models of Launder, Reece and Rodi (1975). Zeman (1975), and Cormack (1975). Since the higher total

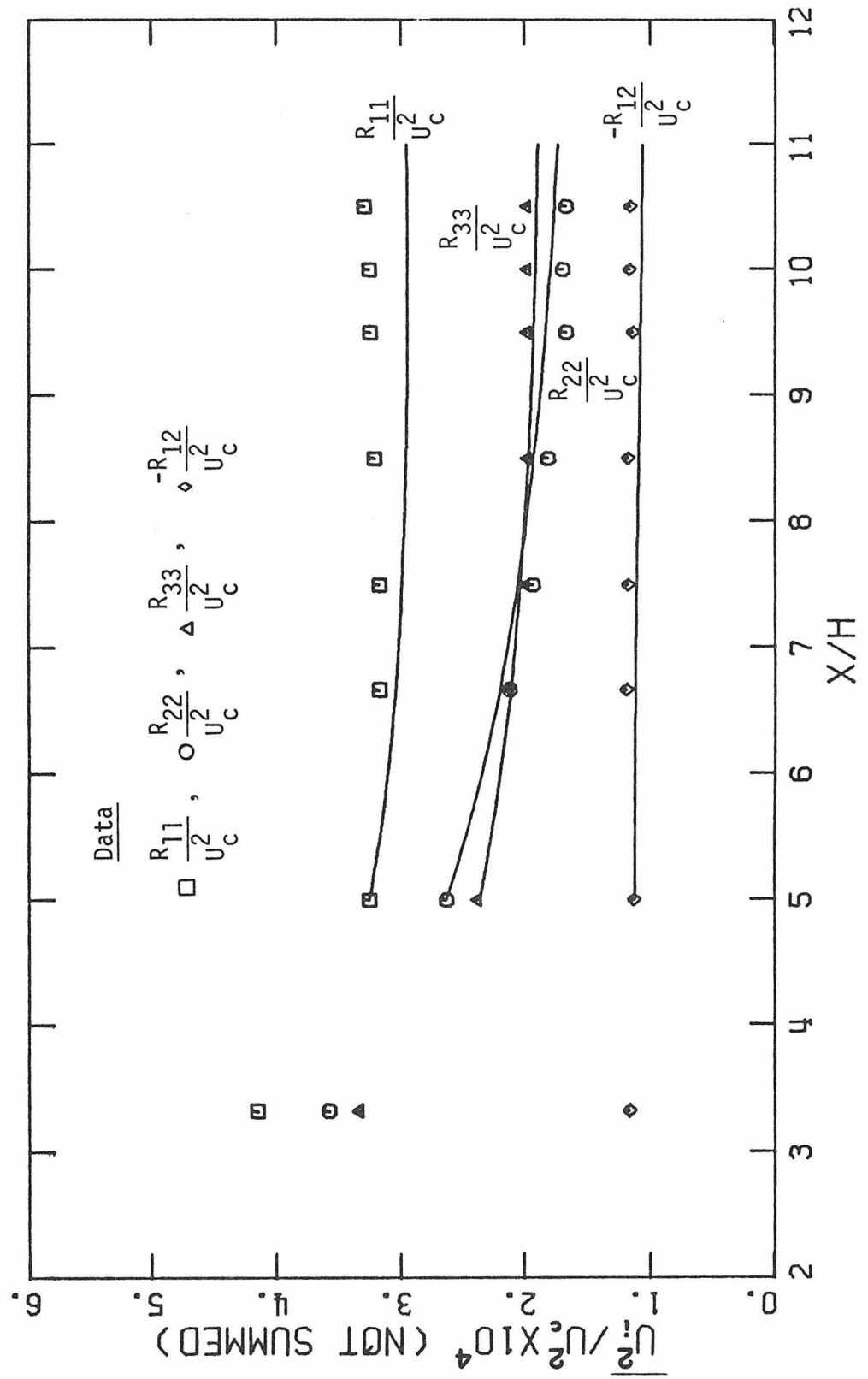

Figure 3.23.--Calculation of Homogeneous Shear Flow Using Present Model. Data of Champagne, Harris and Corrsin (1970).

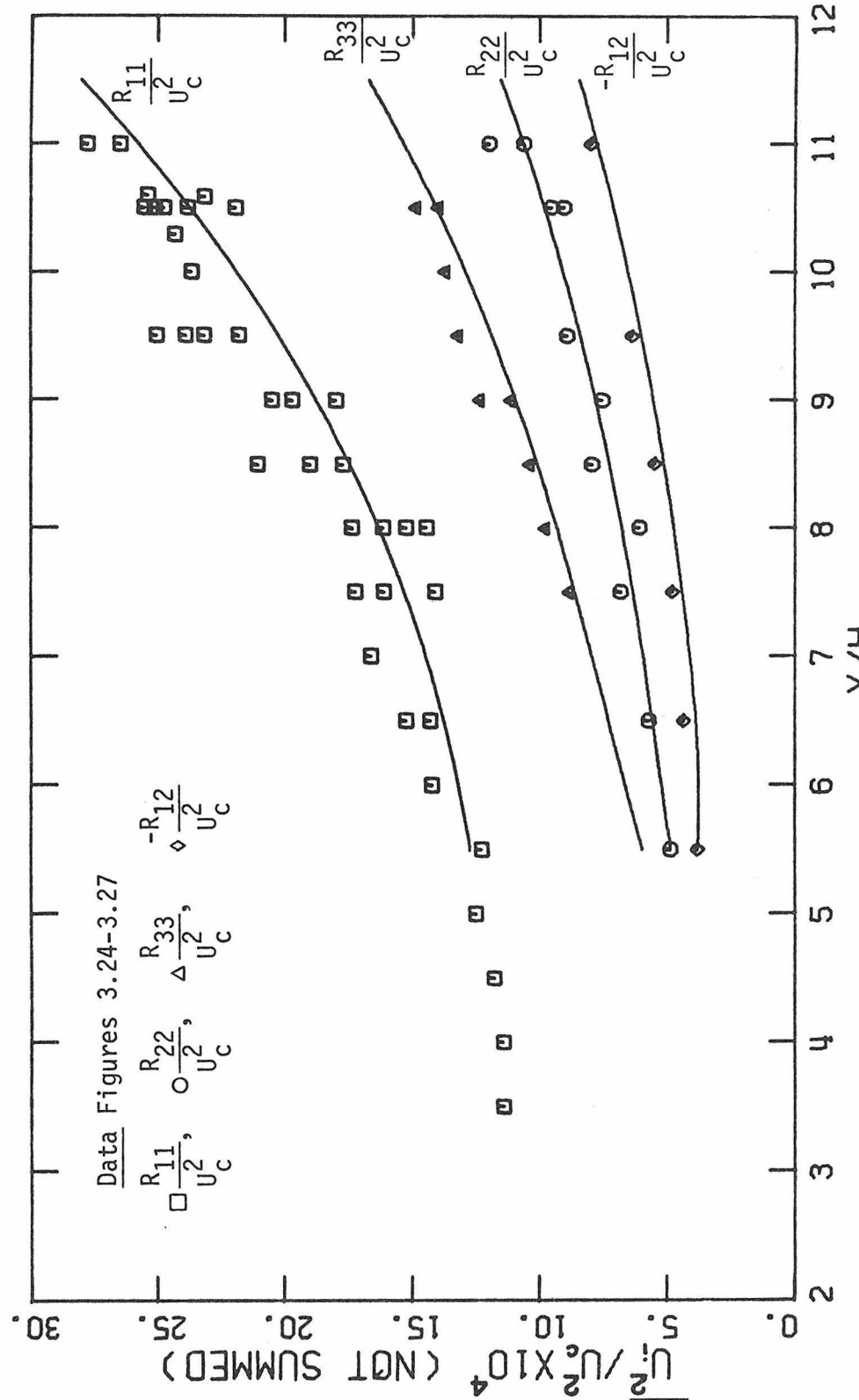

Figure 3.24.--Calculation of Homogeneous Shear Flow Using Present Model. Data of Harris, Graham and Corrsin (1977).

Table 3.14

Initial Conditions for Homogeneous Shear Flow

Experiment	R_{11}/U_c^2 x 10^{-3}	R_{22}/U_c^2 x 10^{-3}	R_{33}/U_c^2 x 10^{-3}	$-R_{12}/U_c^2$ x 10^{-3}	$\varepsilon/U_c^2\Gamma$ x 10^{-3}	τ_0
CHC	.33	.26	.244	.108	.256	1.585
Harris et al.	1.23	.484	.644	.377	.243	6.919

strain case more closely resembles inhomogeneous shear flows (see Harris et al. (1977) for a discussion). The good agreement between data and the present model predictions exhibited in Figure 3.22 is encouraging.

In Figures 3.25 to 3.27 the models of Donaldson (1972) (as modified by Lewellen, 1975), Launder, Reece and Rodi (1975) and Launder are used to predict the higher shear rate flow of Harris et al. The constants for these models, after each has been cast in the form of the present model, are given in Table 3.15. Only the model of Launder (1975) with predictions shown in Figure 3.28) gives agreement with the

Table 3.15

Homogeneous MRS Model Constants

Constant	Donaldson	Launder et al.	Launder	Present
α_0	-	- .291	- .330	- .333
β_0	8.0	3.0	2.4	2.5
β_1	0.0	0.0	3.33	7.17
β_2	0.0	0.0	-1.25	-2.98
ψ_0	3.67	3.8	3.8	3.8
ψ_2	2.96	2.88	2.88	2.9

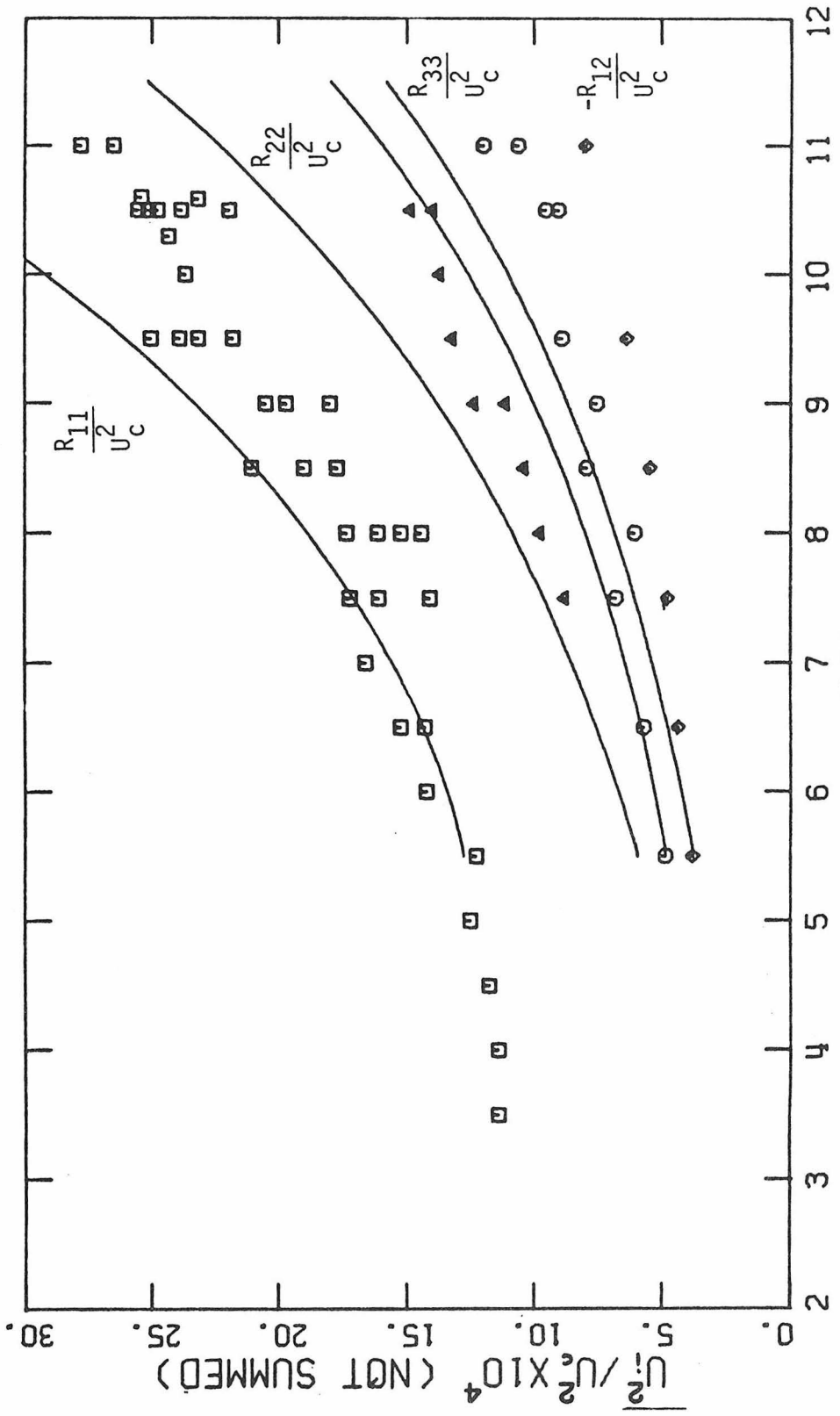

Figure 3.25.--Calculation of Homogeneous Shear Flow Using Model of Launder, Reece and Rodi (1975). Data of Harris, et al. (1977).

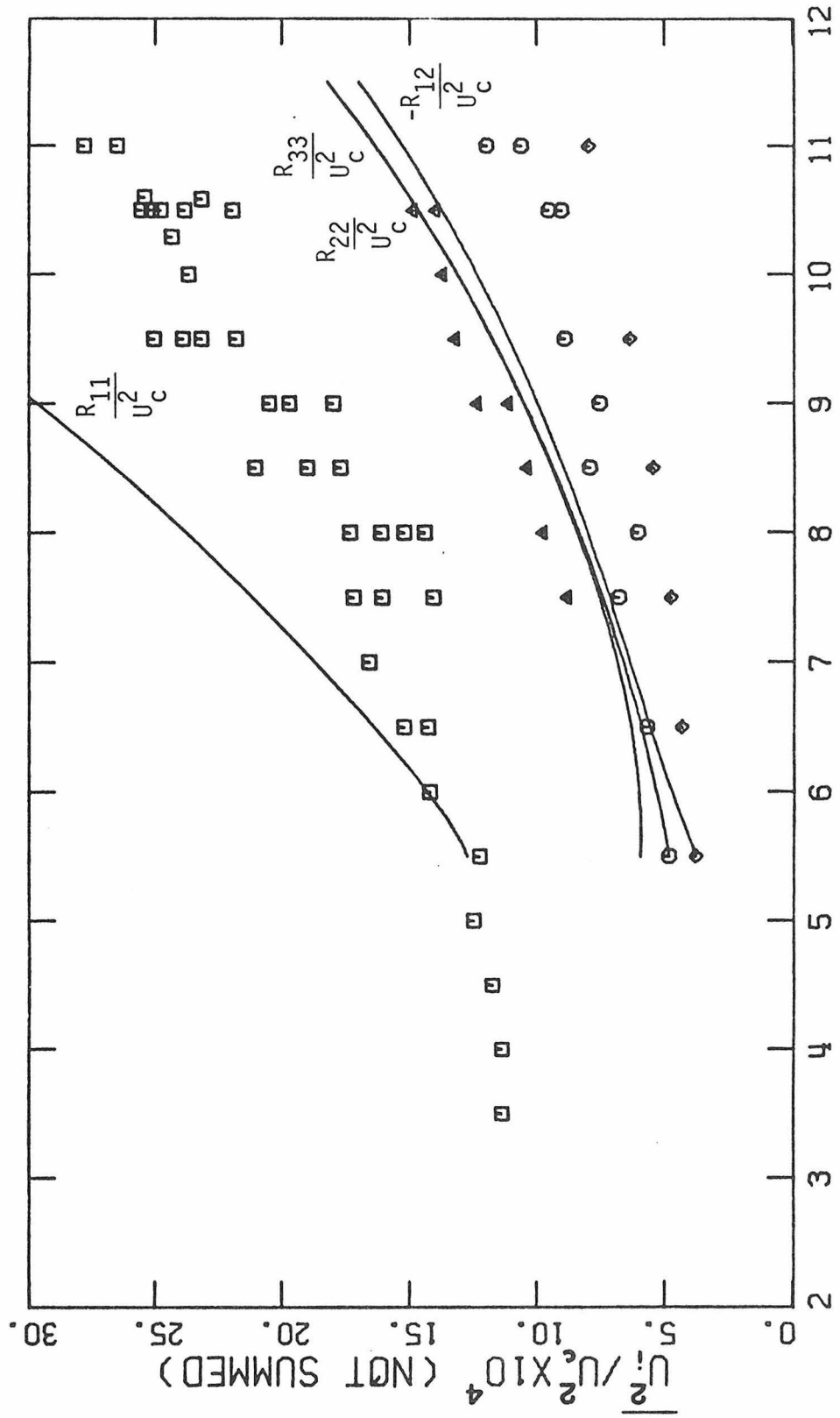

Figure 3.26.--Calculation of Homogeneous Shear Flow Using Model of Donaldson (1972). Data of Harris, et al. (1977).

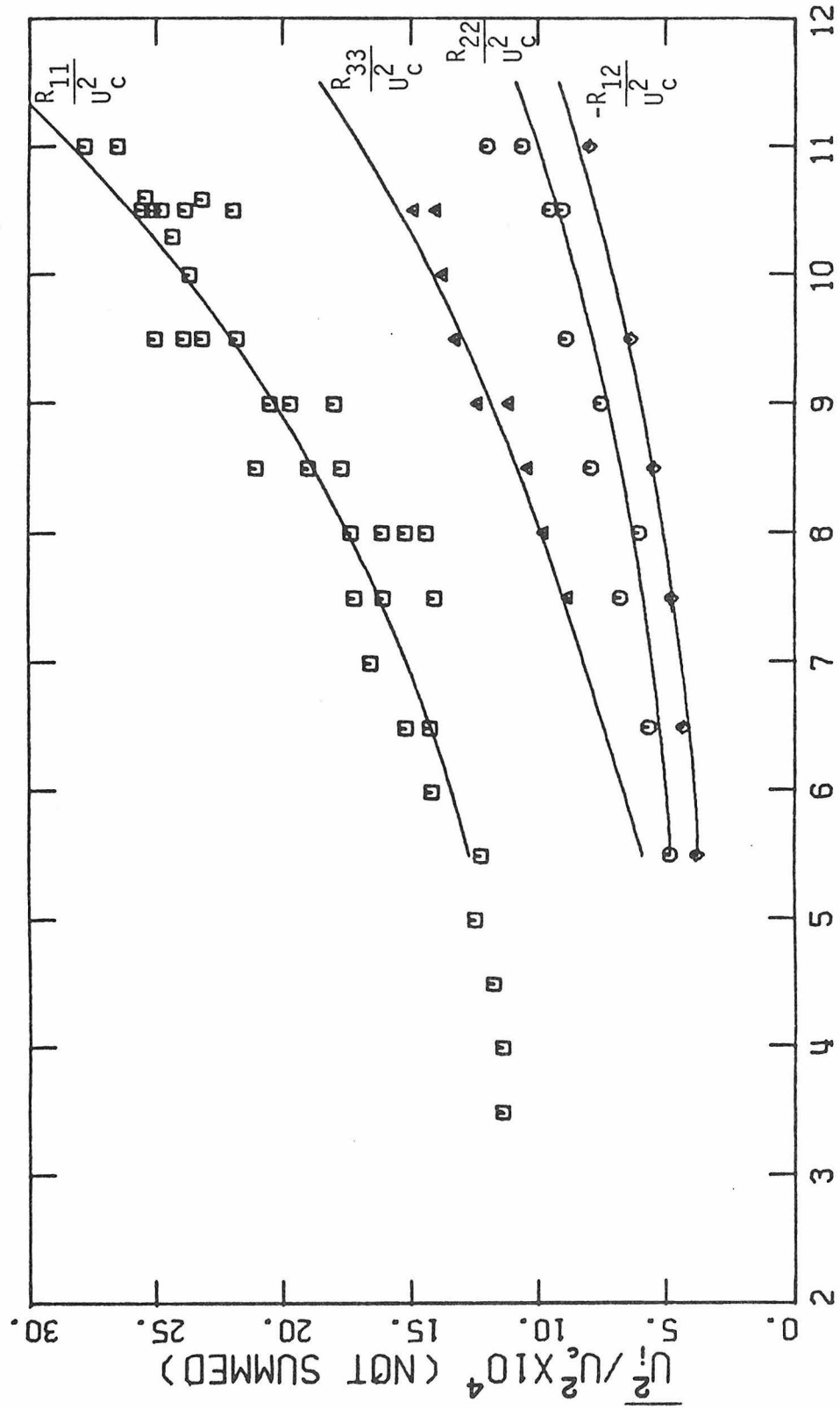

Figure 3.27.--Calculation of Homogeneous Shear Flow Using Model of Launder (1975). Data of Harris, et al. (1977).

data which are comparable with the present model. The models of Launder, Reece and Rodi (1975) and Donaldson predict stress profiles as much as 50% greater than the experimental values. These large values can be traced directly to the energy transfer term, T_{ij}' [Equation (2.5.24)]. T_{ij}' tends to cancel out some of the production of Reynolds shear stress R_{12}. In particular, the smaller absolute value of α_0 for the model of Launder, Reece and Rodi (cf. Table 3.15) allows for a greater production of R_{12} than the present model. This leads directly to the larger values of $|R_{12}|$ and hence production of turbulent energy. The increase in the production of turbulent energy manifests itself in the larger predictions for the stress as shown in Figure 3.25. The model of Donaldson (1972) has no term T_{ij}', hence his model predicts even greater values for the stresses (Fig. 3.26). Launder's model has a value of α_0 that is nearly equal to the present one (see Table 3.15) hence, predictions using his model (Fig. 3.27) are comparable to the present predictions for this flow.

The asymptotic values of the normalized stresses $R_{ij}'(R_{ij}' = R_{ij}/q^2)$ are given in the following table for each model.

Table 3.16

Predicted Asymptotic Normal Stresses for Homogeneous Shear Flow

Model	α_0	R_{11}'	R_{22}'	R_{33}'	$-R_{12}'$
Present	-.333	.500	.200	.300	.150
Launder (1975)	-.332	.512	.181	.307	.153
Launder et al. (1975)	-.291	.490	.212	.298	.187
Donaldson (1972)	n.a.	.579	.211	.211	.196

The asymptotic results are comparable except for the shear stress R_{12}'. However, in the inhomogeneous shear flows of interest (cf. Table 3.12) the shear stress, R_{12} is dominant. In Chapter 5 the model developed in Chapter 2 and the constants evaluated in this chapter will be used to predict some free shear flows. In these flows, the mean momentum equation reduces to,

$$U_1 \frac{\partial U_1}{\partial x_1} + U_2 \frac{\partial U_1}{\partial x_1} = - \frac{\partial R_{12}}{\partial x_2} \qquad (3.7.3)$$

where x_1 is the flow direction, x_2 is the direction of the mean velocity gradient and $\{U_1, U_2\}$ are the velocities in these directions. It is clear from Equation (3.7) that a correct prediction of R_{12} is essential since the mean velocity is calculated from it.

Calculations using a full Reynolds stress model are not trivial and as a result, a calculation procedure was initially developed using a model of less complexity. This model is derived in the next chapter.

CHAPTER 4

SIMPLIFIED TRANSPORT MODEL

4.1 Introduction

The difficulty of solving six to eight highly non linear partial differential equations has severely restricted the number of numerical studies of the full Reynolds stress, second-order turbulence models. Indeed, most of the numerical studies of turbulent flow to date have been carried out using simpler closure models. Since many of these simpler models can be derived by making suitable simplifications of the general Reynolds stress model, it is convenient at this time to consider simpler versions of the present MRS model and to discuss the limits of applicability of these simpler models.

Two types of simplified closure will be considered. They are: (1) The Algebraic Stress Model (ASM) and (2) The τ-k-ε model of Hanjalic and Launder (1972). The first of these results from a single assumption regarding the transport terms in the Reynolds stress equations. The second is less general being designed for use primarily on free shear flows where only the shear stress R_{12} affects the mean flow. This model does, however, retain a differential equation for R_{12}, hence it presents many of the computational difficulties associated with the full MRS model and can be used to test some of the constants evaluated in Chapter 3. In addition it can be

used to generate an initial guess for the solution of the full MRS model.

4.2 The Algebraic Stress Model (ASM)

The mean Reynolds stress model (MRS) developed in Chapter 2 may be written in the form,

$$\mathcal{D}_{ij} = \frac{D}{Dt} R_{ij} - J_{ijk,k} = P_{ij} + T_{ij}^{1} + T_{ij}^{2} - \frac{2}{3}\delta_{ij}\varepsilon \qquad (4.2.1)$$

Contraction on i and j then yields an equation for the kinetic energy, $k = \frac{1}{2} R_{ii}$

$$\mathcal{D}_{k} = \frac{Dk}{Dt} - \frac{1}{2} J_{iik,k} = \mathcal{P} - \varepsilon \qquad (4.2.2)$$

Here $\frac{D}{Dt} = \frac{\partial}{\partial t} + u_k \frac{\partial}{\partial x_k}$, $\mathcal{P} = -R_{\ell,m}U_{\ell,m}$ and P_{ij}, T_{ij}^{1}, T_{ij}^{2} and J_{ijk} are given by equations (2.1.2b), (2.5.14), (2.5.23) and (2.7.5) respectively. Inspection of (4.2.1) reveals that it is the advection and diffusion terms, denoted here by the "total transport" $_{ij}$, which make (4.2.1) a differential equation. If this term is eliminated (i.e. if advection balances diffusion) or if it may be approximated as a function of the remaining variables, then the Reynolds stresses could be determined from algebraic relationships of the form,

$$R_{ij} = f(R_{pq}, U_{\ell,m}, k, \varepsilon) \qquad (4.2.3)$$

At first sight it would seem that a reasonable first approximation would be to neglect the transport terms entirely, thus developing a model for nearly homogeneous flows. However, Pope (1978) points out that this approximation is inconsistent for even small departures

from inhomogeneity since the transport of R_{ij} or k is assumed zero, but equation (4.2.2) shows this to be untrue unless $\mathcal{P}$ equals ε.

The proposal of Rodi (1976) shows more physical insight. He assumes that,

$$\text{transport of } R_{ij} = \frac{R_{ij}}{k} \cdot \text{transport of } k$$

$$\text{i.e. } \mathcal{D}_{ij} = a_{ij}\mathcal{D}_k = a_{ij}\,(\mathcal{P}-\varepsilon) \tag{4.2.4}$$

where $a_{ij} = \frac{R_{ij}}{k}$ is the "normalized" stress. This relationship was motivated by the identity

$$\frac{DR_{ij}}{Dt} = a_{ij}\frac{Dk}{Dt} + \frac{kDa_{ij}}{Dt} \tag{4.2.5}$$

which implies that (4.2.4) will be a reasonable approximation for the advection terms in $\mathcal{D}_{ij}$ at least, if a_{ij} is approximately constant.

Putting (4.1.4) into (4.1.1) gives the following algebraic stress model

$$a_{ij}\,(\mathcal{P}-\varepsilon) = P_{ij} + T_{ij}^{\,1} + T_{ij}^{\,2} - \frac{2}{3}\,\delta_{ij}\varepsilon \tag{4.2.6}$$

Equation (4.2.6) is an <u>implicit</u> equation for the Reynolds stresses since both P_{ij} and T_{ij} contain non linear expressions involving the R_{ij}. Thus, at each grid point in a calculation, the set of simultaneous non linear algebraic equations (4.2.6) must be solved to determine the individual stresses, R_{ij}.

As an alternative Pope (1975) and Warsi and Amlicke (1976) express R_{ij} as an explicit function of the mean velocity gradient.

This yields an expression equivalent to the "effective diffusion" hypothesis described in § 1.3. In this case, however, a general effective viscosity results because it depends on both the mean rate of strain and mean rotation. At the lowest level of approximation this model takes the form,

$$R_{ij} = \nu_T (U_{i,j} + U_{j,i}) + \frac{2}{3} \delta_{ij} k \qquad (4.2.7)$$

where $\nu_T = C_\mu \frac{k^2}{\varepsilon}$. In this latter model, differential equations are kept for k (equation 4.1.2) and ε. Rodi (1976) shows that C_μ is not constant and suggests using the next order of approximation where C_μ is given by

$$C_\mu = \frac{2}{3} \frac{1-\gamma}{C_1} [1 - \frac{1}{C_1} (1 - \gamma \mathcal{P}/\varepsilon)]/[1 + \frac{1}{C_1} (\mathcal{P}/\varepsilon - 1)]^2 \qquad (4.2.8)$$

That is, the eddy diffusion coefficient is assumed to depend on the ratio of energy production to energy dissipation. In cases where $\mathcal{P} \simeq \varepsilon$ equation (4.2.8) reduces to the limiting form of (4.2.7).

The algebraic stress model will yield results equal to those of the Reynolds stress model in many applications. However, as shown in equation (4.2.6) it relies on many of the closure assumptions suggested for the MRS models. Hence only by properly validating the MRS models can we have confidence in the simpler models which are derived from it.

4.3 The τ-k-ε Model

The τ-k-ε model is a simplified version of the MRS model where, instead of a transport equation for each normal stress (R_{11},

R_{22}, R_{33}), only one equation for half of their sum is used. However the transport equation for the shear stress ($R_{12} = \tau$) is kept intact, so the resulting model retains many of the features of the full MRS model.

The τ-k-ε model was first proposed by Hanjalic and Launder (1972) who successfully applied it to a number of free shear and wall bounded flows. Subsequent calculations using the τ-k-ε model were carried out by Rodi (1972) for free shear flows and Hanjalic (1974) for duct flows. Recently Rotta (1975) has derived a similar model except that he uses an equation for the product ($q^2 L_1$) in place of an ε-equation.

The τ-k-ε model applies to cases where only the shear stress affects the mean flow. Thus we can deduce the governing equations by a consideration of the R_{12}, k and ε equations from the MRS model in boundary layer form. These equations are:

$$U_j \frac{dk}{dx_j} = - R_{12}\frac{dU_1}{dx_2} - \varepsilon + C_s \frac{\partial}{\partial x_2}\left[\frac{k}{\varepsilon}\left(R_{22}\frac{\partial}{\partial x_2}(k + R_{22}) + R_{12}\frac{\partial R_{12}}{\partial x_2}\right)\right] \tag{4.3.1a}$$

$$U_j\frac{\partial R_{12}}{\partial x_j} = \left[\left(\frac{2}{5} + 2\alpha_0\right)k - \left(\frac{2}{3} + \frac{8}{3}\alpha_0\right)R_{11} - \left(\frac{1}{3} + \frac{\alpha_0}{3}\right)R_{22}\right]\frac{dU_1}{dx_2}$$

$$- \beta_0 \frac{\varepsilon R_{12}}{2k}\left\{1 + \beta_1 II + \beta_2 (b_{11} + b_{22})\right\} \tag{4.3.1b}$$

$$+ C_s\frac{\partial}{\partial x_2}\left[\frac{k}{\varepsilon}\left(R_{12}\frac{\partial R_{22}}{\partial x_2} + 2R_{22}\frac{\partial R_{12}}{\partial x_2}\right)\right]$$

$$U_j \frac{\partial \varepsilon}{\partial x_j} = -1.90 \frac{\varepsilon^2}{k} - \psi_2 \frac{\varepsilon}{k} R_{12} \frac{dU_1}{dx_2} + C_\varepsilon \frac{\partial}{\partial x_2} \frac{k}{\varepsilon} R_{22} \frac{\partial \varepsilon}{\partial x_2} \qquad (4.3.1c)$$

where x_1 is the streamwise direction and x_2 is the direction of the mean velocity gradient. The principal assumption inherent in this model is similar to that of the ASM; that is, the normalized stresses, $a_{ij} = \frac{R_{ij}}{k}$ are constant across the width of the flow. Experimental results for free shear flows (cf. Rodi (1972) for a review of experimental data) show that the normalized stresses are approximately constant across the central portion of the shear flow. So, if the R_{ij} are expressed as functions of k, i.e.

$$R_{ij} = a_{ijk}, \qquad (4.3.2)$$

and substituted into equations (4.3.1a-c) the normal stress terms can be eliminated. Initially, it was felt that the a_{ij} values obtained in the asymptotic region of the homogeneous shear flow would be suitable for use on general shear flows. However, R_{22} and R_{33} are more nearly equal for the case of free shear flows than for the homogeneous flow. Thus, from a consideration of the normalized stress values for free shear flows, the following values for a_{ij} were assumed.

Table 4.1.--Normalized Stresses for Free Shear Flows.

a_{11}	a_{22}	a_{33}	a_{12}
.95	.45	.60	-0.30

The values of a_{ij} are substituted into equation (4.3.2) to obtain estimates of R_{ij}. These values are then substituted into equation (4.3.1). The parameter estimates for α_0, β_0, β_1, β_2, ψ_2, C_s and C_ε, determined in Chapter 3 are then inputted into (4.3.1) to yield the following model,

$$U_j \frac{\partial \tau}{\partial x_j} = - \gamma_1 k \frac{dU_1}{dx_2} - \gamma_2 \frac{\varepsilon}{k} \tau + \gamma_3 \frac{\partial}{\partial x_2} \frac{k^2}{\varepsilon} \frac{\partial \tau}{\partial x_2} \tag{4.3.3a}$$

$$U_j \frac{\partial k}{\partial x_j} = - \tau \frac{dU_1}{dx_2} - \varepsilon + \gamma_4 \frac{\partial}{\partial x_2} \frac{k^2}{\varepsilon} \frac{\partial k}{\partial x_2} \tag{4.3.3b}$$

$$U_j \frac{\partial \varepsilon}{\partial x_j} = - \gamma_5 \frac{\varepsilon}{k} \tau \frac{dU_1}{dx_2} - \gamma_6 \frac{\varepsilon^2}{k} + \gamma_7 \frac{\partial}{\partial x_2} \frac{k^2}{\varepsilon} \frac{\partial \varepsilon}{\partial x_2} \tag{4.3.3c}$$

The parameters γ_i are compared with those of Rodi (1972) in Table 4.2.

Table 4.2.--Constants γ_i in the τ-k-ε Model.

Model	γ_1	γ_2	γ_3	γ_4	γ_5	γ_6	γ_7
Present	.135	1.50	.10	.10	1.45	1.90	.082
Rodi (1972)	.252	2.80	.10	.09	1.45	2.00	.082

If the advection and diffusion terms of the τ-equation balance, the remaining terms can be combined to give,

$$\tau = C_\mu \frac{k^2}{\varepsilon} \frac{dU_1}{dx_2} \tag{4.3.4}$$

$$C_\mu = .09$$

Equation (4.3.4) is the same as the limiting form of the algebraic stress model. Hence in free shear flows where advection and diffusion terms do balance, the predictions of the τ-k-ε, ASM and MRS models will be the same.

Our main purpose in studying the τ-k-ε model is that it provides a stepping stone to the solutions of the full MRS model. After solving the equations (4.3.3a-c), estimates for the normal stresses were determined from equation (4.3.2) and the calculated values of k. These profiles were then used as initial guesses for the MRS calculations which are described in the next chapter.

CHAPTER 5

SIMILARITY SOLUTIONS OF FREE SHEAR FLOWS

As a final test, the model developed in Chapter 2 and the parameter estimates determined in Chapter 3 will be used to predict two free shear flows, the plane turbulent jet and plane turbulent wake. The free shear flow, despite its relatively simple appearance exhibits certain features which make its prediction a demanding and yet fair test of the present turbulence model. In the first place, these flows contain regions of both strong and weak mean strain which make them a more sensitive test of the parameter estimates of Chapter 3 than wall-bounded flows. This is because the characteristic length and velocity scales for a free shear flow must develop on their own whereas these scales in wall bounded flows are dominated by the strong-strain, near-wall region. Secondly, the inhomogeneity and anisotropy of the free shear flow is not too great, the turbulence Reynolds numbers are high and the flows are not affected by solid boundaries so that important assumptions in the model development (cf. § 2.3) are met. Finally, these flows can be considered rheometric (as described in § 3.3) in the sense that the inhomogeneity is not added at the expense of including other complications (temperature or buoyancy effects for example) which have not yet been considered in the model development.

From an experimental point of view the free shear flow is well documented. The results of several investigators are summarized by Halleen (1964) and Newman (1967) and a critical assessment of the recent data was made in a recent review by Rodi (1976). An important experimental feature of free shear flows, is their tendency to become self similar after the initial period of development. Here we use the following definition of similarity given in Rodi (1976): "A flow is self similar when one velocity scale and one length scale are sufficient to render its time averaged quantities dimensionless functions of one geometric variable only." This feature not only facilitates the comparison of the measured and calculated profiles but allows one to calculate asymptotic values of the mean velocity and turbulent stresses of the flow without requiring an accurate estimate of their initial profiles.

The fact that these flows become self-similar has not been directly utilized so far in turbulence model calculations. Traditionally, the governing model equations, which are parabolic partial differential equations (p.d.e.'s), are solved by allowing assumed initial profiles for the turbulence quantities to develop in the downstream direction until they become self similar (at which point they will be independent of the initial conditions). One problem with this method is that, as the flow develops, it grows continually wider and hence requires more and more grid points as the numerical integration proceeds. In flows such as the two dimensional wake behind a circular cylinder, for example, the experimental profiles do not become self similar until the flow has travelled over 500

cylinder diameters downstream. At this point the wake is very wide and requires a great many grid points.

Free shear flows have been predicted by most modelers as test calculations for their Reynolds stress models. Hanjalic and Launder (1972) and Launder, Reece and Rodi (1975) predicted mean velocity and stress profiles for the plane jet and mixing layer. Lumley and Khajeh-Nouri (1974) applied their model to the plane wake and Lewellen (1975) used Donaldson's (1972) model to study various plane and axisymmetric free shear flows. All of the above authors, however, solved the governing equations in the form of p.d.e.'s.

In this chapter, we obtain numerical predictions for free shear flows using the governing Reynolds stress equations in their similarity form. That is, assuming that the flow is in the similarity regime, the governing partial differential equations are transformed into a coupled set of ordinary differential equations. These equations have boundary conditions at two points in the flow and the overall problem is thus an example of the class of "non linear two-point boundary-value problems." In the present study, we have used the accurate finite difference scheme proposed by Keller (1974) for this type of problem, which is known as Keller's Box Scheme.

A basic feature of this scheme is that the governing equations are initially written as a system of first-order differential equations. The first derivatives are then replaced by their finite difference (centered Euler) analogs and the resulting set of $N(J + 1)$ non linear algebraic equations (where, N = number of first order equations, $J + 1$ = number of grid nodes) are solved using Newton's

method. Because of the nature of the governing equations, the solutions are confined to a finite region of the similarity variable space, and it is necessary to calculate the width of this region as an eigenvalue in the solution set.

There are several basic advantages to solving the ordinary differential equations instead of the original set of partial differential equations. Mathematically, uniqueness and consistency theorems have been proven for the numerical solution of ordinary equations (Keller, 1974; White, 1974). In contrast, it is not yet clear whether the partial differential equations will yield unique asymptotic solutions for arbitrary initial conditions. Another difficulty with the full p.d.e.'s is that the solutions may take a long downstream distance to reach asymptotic values in which the influence of the initial profiles has vanished. Launder (1975) reported a case where the governing equations for the round jet took several thousand jet diameters of downstream calculation before becoming self similar. Such problems are obviously avoided in solving the self similar equations directly. Perhaps the most important feature of the present calculation scheme is that whole families of solutions for each flow can be determined for various values of the model parameters using analytic continuation. Thus the sensitivity of the solution to changes in the parameters can be determined quickly, easily and at a great savings in computation time.

Three different methods for solving the similarity equations were initially investigated. These were, (1) shooting, (2) relaxation

and (3) Keller's Box Scheme. Keller's Box Scheme was ultimately chosen for the following reasons,

(1) Ease of programming. The basic method of solution is the same for all of the flows considered. Only a different sub-program containing the governing equations, boundary conditions and a Jacobian matrix of these equations differentiated with respect to each variable is required for each flow calculated.

(2) Accuracy and convergence. The scheme is second order accurate in the grid spacing, h and h can be non uniform if desired. Thus engineering accuracy can be obtained on rather coarse grids. The accuracy can be further improved by the application of Richardson extrapolation if required. Newton's method for solving the difference equations exhibits quadratic convergence so that the compution is rapid once the solution is in the neighborhood of the final result.

In this chapter the computation scheme is described and is used to solve the governing self-similar Reynolds stress equations for two dimensional jets and wakes. The numerical solution of high order boundary-value problems, such as that associated with the Reynolds stress model, is far from trivial. Hence, the calculation scheme was initially developed and tested using the simpler τ-k-ε model. This model was described in the last chapter. One advantage of first considering the τ-k-ε model is that the solutions obtained using it can serve as initial guesses for the turbulence quantities when a full Reynolds stress model is used. Thus the solution is considered in two stages.

In the following sections, the characteristic length and velocity scales are derived for jets and wakes, and are used to transform the governing equations into their similarity form. Then, in § 5.4 we discuss boundary conditions, and, in § 5.5 the basic computation scheme. Finally, this computation scheme is used to obtain profiles for the turbulent stresses and mean velocity using both the τ-k-ε model and the full MRS model. These profiles are compared to the available experimental data and this comparison is used as the basis for a critical assessment of the model performance.

5.2 Characteristic Length and Velocity Scales

The governing equations for wakes and jets are obtained by application of "boundary-layer" approximations to the full elliptic model equations. In particular, we assume that the flow is "slowly developing" in the downstream direction so that streamwise derivatives can be neglected relative to cross-stream derivatives. Application of the similarity transformation to the resulting equations reduces the problem from a coupled set of parabolic partial differential equations (p.d.e.'s) to a coupled set of ordinary differential equations (o.d.e.'s).

The similarity variables for jets and wakes can be determined from a consideration of the mean momentum equation and the momentum integral. Applying the boundary layer assumptions to the time averaged Navier-Stokes equations (equation 1.3.1) yields

$$U\frac{\partial U}{\partial x} + V\frac{\partial U}{\partial y} = U_E \frac{\partial U_E}{\partial x} - \frac{\partial}{\partial y} R_{12} - \frac{\partial}{\partial x}(R_{11} - R_{22}) \qquad (5.2.1)$$

$$\frac{\partial U}{\partial x} + \frac{\partial V}{\partial y} = 0 \qquad (5.2.2)$$

Here, U_E is the free stream velocity (note $U_E = 0$ for jets in a quiescent ambient). The spatial coordinates x and y are in the streamwise and cross-stream direction of the flow directions respectively. The corresponding mean velocities are denoted as U and V. The Reynolds stresses R_{11}, R_{22} and R_{12} are determined by model equations which will be given later. Integrating (5.2.1) over the flow cross-section yields

$$\frac{\partial}{\partial x}\int_0^\infty [U(U-U_E) + (R_{11}-R_{22})]\, dy + \frac{dU_E}{dx}\int_0^\infty (U-U_E)\, dy = 0 \qquad (5.2.3)$$

If the free stream velocity is constant, equation (5.2.3) implies that the excess momentum flux,

$$M = \rho\int_{-\infty}^{\infty} U(U-U_E)\, dy \qquad (5.2.4)$$

is a constant, independent of downstream distance, x. In deriving (5.2.4), the streamwise gradient of the normal stress difference $(R_{11}-R_{22})$ has been neglected on the grounds that it is usually negligible compared to the shear stress, R_{12}. The kinematic momentum flux $M'(= \frac{M}{\rho})$ can be positive, negative or zero, corresponding to:

(a) $M' > 0$: jets ($M' = J$)

(b) $M' < 0$: wakes ($M' = -D$)

(c) $M = 0$: flow behind a self propelled body.

The similarity length and velocity scales are determined from equations (5.2.1 - 4.2.4). The derivation is very similar for both jets and wakes, hence only the plane jet case will be described in detail. The results for the plane wake will be presented in tabular form.

5.2.1 The Plane Jet

The plane jet flow is shown schematically in Figure 5.1. In general the global parameters are J, the kinematic momentum flux per unit slot width and ν, the kinematic viscosity. At high Reynolds number, however, the flow becomes independent of viscosity so that all of the ostensible date are contained in J which has the units,

$$[J] = \text{velocity}^2 \times \text{length} \tag{5.2.5}$$

Ignoring the normal stress difference and introducing the stream function ψ, defined by

$$U = \frac{\partial \psi}{\partial y} = \psi_y \qquad\qquad V = -\frac{\partial \psi}{\partial x} = -\psi_x,$$

the continuity equation (5.2.2) is satisfied exactly and (5.2.1) becomes,

$$\psi_y \psi_{xy} - \psi_x \psi_{yy} = \tau_y \tag{5.2.6}$$

where $\tau = R_{12}$. The momentum integral (5.2.4) is

$$J = 2\int_0^\infty U^2 dy \tag{5.2.7}$$

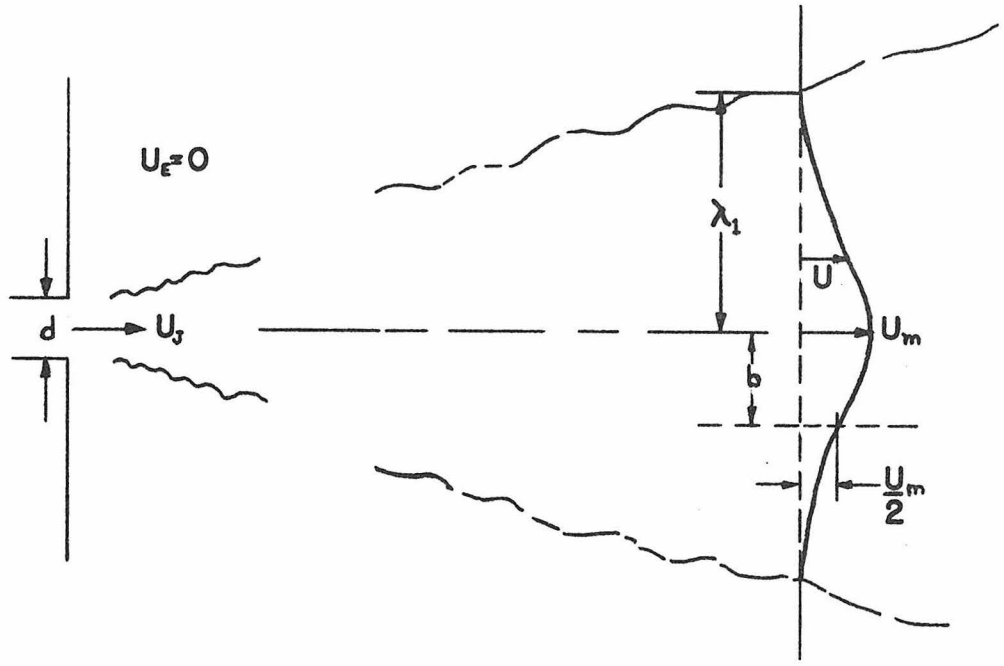

Figure 5.1.--Definition Sketch for the 2-Dimensional Jet.

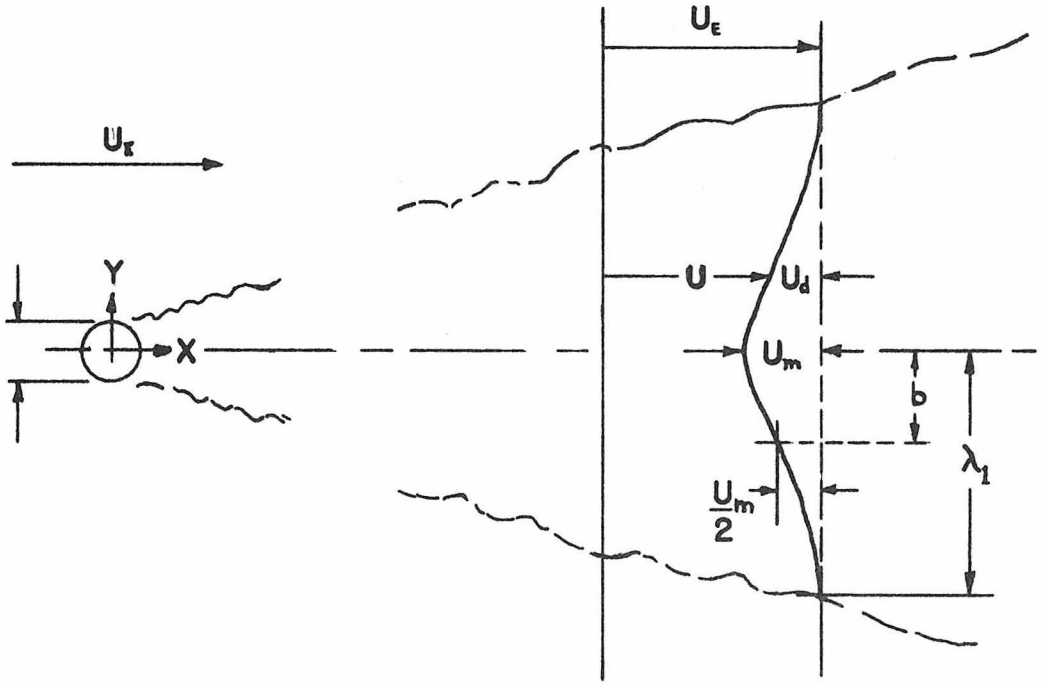

Figure 5.2.--Definition Sketch for the 2-Dimensional Wake.

Now let us seek a similarity transformation in which the local velocity scale Us(x) and length scale $\ell(x)$, are both to be determined. Thus we introduce

$$\psi = U_s \ell \, f(\eta)$$

and

$$\tau = U_s^2 \, g(\eta) \qquad (5.2.8)$$

with

$$\eta = \frac{y}{\ell(x)}$$

Both $f(\eta)$ and $g(\eta)$ are assumed to be dimensionless functions of the single similarity co-ordinate η. With the transformation (5.2.8), the equation (5.2.6) becomes

$$\left(\frac{\ell}{U_s}\frac{dU_s}{dx}\right) f'f' - \left(\frac{1}{U_s}\frac{dU_s \ell}{dx}\right) ff'' = - g' \quad . \qquad (5.2.9)$$

Here, the prime refers to differentiation with respect to η. For similarity to exist the non-dimensional coefficients in brackets must either be constant or zero (in particular, <u>independent</u> of x). Thus we assume

$$\frac{\ell}{U_s}\frac{dU_s}{dx} = \text{constant}_1; \qquad \frac{d\ell}{dx} = \text{constant}_2 \qquad (5.2.10)$$

The solution for (5.2.10) subject to (5.2.5) is

$$\ell = \lambda_1 x \qquad U_s = \lambda_2 \left(\frac{J}{x}\right)^{\frac{1}{2}} \qquad (5.2.11)$$

The constants λ_1 and λ_2 remain to be defined. Using (5.2.11), equations (5.2.9) and 5.2.4) become

$$\frac{\lambda_1}{2}(ff')' = g' \tag{5.2.12}$$

$$\lambda_2^2\lambda_1\int_0^\infty (f')^2\, d\eta = \frac{1}{2} \quad . \tag{5.2.13}$$

In addition, the mean streamwise and cross-stream velocities are:

$$U = \psi_y = \lambda_2 \left(\frac{J}{x}\right)^{\frac{1}{2}} f'(\eta) \tag{5.2.14}$$

$$V = -\psi_x = \lambda_2\lambda_1\left(\frac{J}{x}\right)^{\frac{1}{2}}(\eta f' - \frac{1}{2}f) \quad . \tag{5.2.15}$$

These results and those obtained for the plane wake by following the same procedure are summarized in Table 5.1.

Table 5.1.--Similarity Variables for Plane Jets and Wakes.

Flow	$\ell(x)$	$U_s(x)$	$[U/U_s(x)]^*$	V/U_s
Plane Jet	$\lambda_1 x$	$\lambda_2 \left(\frac{J}{x}\right)^{\frac{1}{2}}$	$f'(\eta)$	$\lambda_1(\eta f' - \frac{1}{2}f)$
Plane Wake	$\lambda_1 \left(\frac{Dx}{U_E^2}\right)^{\frac{1}{2}}$	$\lambda_2 \left(\frac{D}{x}\right)^{\frac{1}{2}}$	$f(\eta)$	—

*The velocity U, of the plane wake is actually the velocity defect $U_d = (U_E - U)$.

5.2.2 Plane Wake

The plane wake flow is shown schematically in Figure 5.2. The plane wake is approximately self-similar only when the mean velocity defect (U_d) is much smaller than the free stream velocity U_E. In this case the mean momentum equation (5.2.1) reduces to

$$U_E \frac{\partial U}{\partial x} = - \frac{\partial \tau}{\partial y} \tag{5.2.16}$$

Introducing the similarity transformation

$$\frac{U_E - U}{U_s(x)} = f(\eta) \tag{5.2.17}$$

and the similarity scales for the wake as defined in Table 5.1, we obtain the governing mean momentum equation,

$$\frac{1}{2} \lambda_1 (\eta f)' = -g' \tag{5.2.18}$$

which is to be solved subject to the momentum constraint

$$2\lambda_2^2 \lambda_1 \int_0^\infty f(\eta)\, d\eta = 1 \tag{5.2.19}$$

Equations (5.2.12), (5.2.13), (5.2.18) and (5.2.19) apply to both the full Reynolds stress model and the simplified τ-k-ε model. These equations are solved simultaneously with the model equations given in the next section.

5.3 Governing Model Equations in Similarity Form

The similarity equations for the mean velocity derived in the previous section (equations (5.2.12) and (5.2.18)) cannot be solved

without further discussion because each contains the dimensionless shear stress $g(\eta)$ as an unknown. Of course $g(\eta)$ can be specified in principle from the turbulence model equation describing its transport. However, this equation contains all of the other Reynolds stresses as unknowns. Thus, in general a full set of transport equations is required for each non zero component of the Reynolds stress tensor. These equations define a set, which will henceforth be called the governing equations.

As a means of testing the calculation method and expediting the calculation of the full MRS model equations, the simplified τ-k-ε model described in § 4.2 was also employed. In this model, the transport equation for the shear stress τ, depends only on the turbulent kinetic energy k, (where $k = \frac{1}{2}(R_{11} + R_{22} + R_{33})$) and the dissipation rate ε. As we have seen (cf. equation (4.3.3)) these quantities are also described by transport equations.

In this section the governing equations for both the mean Reynolds stress (MRS) model and simpler τ-k-ε model will be transformed into a set of ordinary differential equations using the similarity scales derived in the last section.

5.3.1 The τ-k-ε Model

Let us first consider the τ-k-ε model for the case of the plane jet and plane wake. For these flows we apply boundary-layer assumptions to the full τ-k-ε model which was developed in § 4.2 to yield

$$\underset{(i)}{U\frac{\partial\tau}{\partial x}} + \underset{}{V\frac{\partial\tau}{\partial y}} = \underset{}{-} \underset{(ii)}{\lambda_1 k\frac{dU}{dy}} \underset{}{-} \underset{(iii)}{\lambda_2 \frac{\varepsilon}{k}\tau} + \underset{(iv)}{\lambda_3 \frac{\partial}{\partial y}\frac{k^2}{\varepsilon}\frac{\partial\tau}{\partial y}} \tag{5.3.1a}$$

$$\underset{(i)}{U\frac{\partial k}{\partial x}} + \underset{}{V\frac{\partial k}{\partial y}} = \underset{}{-} \underset{(ii)}{\tau\frac{dU}{dy}} \underset{}{-} \underset{(iii)}{\varepsilon} + \underset{(iv)}{\gamma_4 \frac{\partial}{\partial y}\frac{k^2}{\varepsilon}\frac{\partial k}{\partial y}} \tag{5.3.1b}$$

$$\underset{(i)}{U\frac{\partial\varepsilon}{\partial x}} + \underset{}{V\frac{\partial\varepsilon}{\partial y}} = \underset{}{-} \underset{(ii)}{\gamma_5 \frac{\varepsilon}{k}\tau\frac{dU}{dy}} \underset{}{-} \underset{(iii)}{\gamma_6\frac{\varepsilon^2}{k}} + \underset{(iv)}{\gamma_7 \frac{\partial}{\partial y}\frac{k^2}{\varepsilon}\frac{\partial\varepsilon}{\partial y}} \tag{5.3.1c}$$

The numbered terms have the following physical significance, (i) = ADVECTION, (ii) = PRODUCTION, (iii) = DISSIPATION and (iv) = DIFFUSION. In order to proceed further, we apply the similarity transformation (5.2.b) with $\ell(x)$ and $U_s(x)$ given in Table 5.1, plus the additional similarity forms

$$k = U_s^2 p(\eta) \qquad \text{and} \qquad \varepsilon = \frac{U_s^3}{\ell} m(\eta) \tag{5.3.2}$$

for the turbulent kinetic energy and dissipation functions. With these transformations, the governing partial differential equations are transformed into a set of non linear ordinary differential equations for the unknown functions $f(\eta)$, $g(\eta)$, $p(\eta)$ and $m(\eta)$. The various terms in these latter equations are given for each flow in Table 5.2. The full equations are reconstructed from Table 5.2 by duplicating (5.3.1) in the form,

$$\text{ADVECTION} = \text{PRODUCTION} - \text{DISSIPATION} + \text{DIFFUSION}. \tag{5.3.5}$$

Thus, for example, the similarity equation for the turbulent energy (k) for the plane jet flow is,

Table 5.2.--Governing Similarity Equations: τ-k-ε Model.

Flow	Equation	Advection	Production	Diffusion	Dissipation	
2-D Jet	k	$-\lambda_1(pf' + \frac{1}{2}p'f)$	$-gf''$	$\gamma_4(\frac{p^2p'}{m})'$	m	(5.3.3a)
	τ	$-\lambda_1(gf' + \frac{1}{2}g'f)$	$-\gamma_1 pf''$	$\gamma_3(\frac{p^2g'}{m})'$	$\gamma_2\frac{mg}{p}$	(5.3.3b)
	ε	$-\frac{\lambda_1}{2}(5mf' + m'f)$	$-\gamma_5\frac{mgf''}{p}$	$\gamma_7(\frac{p^2m'}{m})'$	$\gamma_6\frac{m^2}{p}$	(5.3.3c)
2-D Wake	k	$-\lambda_1(\frac{\eta p'}{2} + p)$	gf'	$\gamma_4(\frac{p^2p'}{m})'$	m	(5.3.4a)
	τ	$-\lambda_1(\frac{\eta g'}{2} + g)$	$\gamma_1 pf'$	$\gamma_3(\frac{p^2g'}{m})'$	$\gamma_2\frac{mg}{p}$	(5.3.4b)
	ε	$-\lambda_1(\frac{\eta m'}{2} + 2m)$	$\gamma_5\frac{mgf'}{p}$	$\gamma_7(\frac{p^2m'}{m})'$	$\gamma_6\frac{m^2}{p}$	(5.3.4c)

$$\lambda_1(pf' + \tfrac{1}{2}p'f) = - gf'' - m + \gamma_4(\frac{p^2p'}{m})' \qquad (5.3.3a)$$

5.3.2 The MRS Model

Predictions of the turbulence quantities and mean velocity for the jet and wake were also carried out using the full MRS model. The governing MRS equations developed in Chapter 2, after application of the boundary layer assumptions are given in Table 5.3. Rather than write transport equations for each of the normal stresses (R_{11}, R_{22}, R_{33}) differential equations are given for R_{11} and R_{22} plus an equation for k. The third normal Reynolds stress component R_{33} can be calculated from,

$$R_{33} = 2k - R_{11} - R_{22} \qquad (5.3.7)$$

The parameters ($\alpha_0, \beta_0, \beta_1, \beta_2$ and ψ_2) were determined in Chapter 3. For convenience these are listed in Table 5.7 (in § 5.7). We follow the same approach as was used for the simple model to transform the governing equations into their similarity forms. Of course, similarity functions are required for the individual Reynolds stresses in addition to the functions for $\tau = R_{12}$, k and ε which were defined in equation (5.3.2). The complete set is,

$$R_{11} = U_s^2 h(\eta), \qquad R_{22} = U_s^2 e(\eta)$$
$$R_{12} = U_s^2 g(\eta), \qquad k = U_s^2 p(\eta) \quad \text{and} \quad \varepsilon = \frac{U_s^3}{\ell} m(\eta) \qquad (5.3.8)$$

plus the mean velocity terms given in Table 5.1. With these transformations, the governing partial differential equations are

Table 5.3.--Governing Partial Differential Equations: Reynolds Stress Model.

$$U_j\frac{\partial R_{11}}{\partial x_j} = -2R_{12}\frac{\partial U}{\partial y} + (\frac{4}{3}\alpha_0 + \frac{4}{3})R_{12}\frac{\partial U}{\partial y} - \beta_0\varepsilon[(1.0 + \beta_1 II)b_{11} + \beta_2(b_{11}^2 + b_{12}^2 - \frac{II}{3})]$$

$$+ C_s\frac{\partial}{\partial y}\frac{k}{\varepsilon}(2R_{12}\frac{\partial R_{12}}{\partial y} + R_{22}\frac{\partial R_{11}}{\partial y}) - \frac{2}{3}\varepsilon \qquad (5.3.6a)$$

$$U_j\frac{\partial R_{22}}{\partial x_j} = -(\frac{4}{3} + \frac{10}{3}\alpha_0)R_{12} - \beta_0\varepsilon[(1.0 + \beta_1 II)b_{22} + \beta_2(b_{22}^2 + b_{12}^2 - \frac{II}{3})] + 3C_s\frac{\partial}{\partial y}\frac{k}{\varepsilon}(R_{22}\frac{\partial R_{22}}{\partial y}) - \frac{2}{3}\varepsilon \qquad (5.3.6b)$$

$$U_j\frac{\partial k}{\partial x_j} = -R_{12}\frac{\partial U}{\partial y} + C_s\frac{\partial}{\partial y}\frac{k}{\varepsilon}[R_{12}\frac{\partial R_{12}}{\partial y} + R_{22}(\frac{\partial R_{22}}{\partial y} + \frac{\partial k}{\partial y})] - \varepsilon \qquad (5.3.6c)$$

$$U_j\frac{\partial R_{12}}{\partial x_j} = -R_{12}\frac{\partial U}{\partial y} + [(\frac{4}{10} + 2\alpha_0)k - (\frac{2}{3} + \frac{8}{3}\alpha_0)R_{11} - (\frac{1}{3}\alpha_0 - \frac{2}{3})R_{22}] - \beta_0\varepsilon\frac{R_{12}}{k}[1.0 + \beta_1 II + \beta_2(b_{11} + b_{22})]$$

$$+ C_s\frac{\partial}{\partial y}\frac{k}{\varepsilon}(R_{12}\frac{\partial R_{22}}{\partial y} + 2R_{22}\frac{\partial R_{12}}{\partial y}) \qquad (5.3.6d)$$

$$U_j\frac{\partial \varepsilon}{\partial x_j} = -\psi_2\frac{\varepsilon}{k}R_{12}\frac{\partial U}{\partial y} - (\psi_0 + \psi_1 II)\frac{\varepsilon^2}{k} + C_\varepsilon\frac{\partial}{\partial y}(\frac{k}{\varepsilon}R_{22}\frac{\partial}{\partial y}) \qquad (5.3.6e)$$

$$b_{ij} = R_{ij}/k - \frac{2}{3}\delta_{ij} \qquad II = b_{ij}b_{ji}$$

NOTE: For the wake, $U_1 = U_E$, and U_2 is negligible.

transformed into the following sets of differential equations for the plane jet and wake.

A. Governing Similarity Equations--Plane Jet.

$$-\lambda_1(hf' + \frac{h'f}{2}) = -\zeta_1 gf'' - t_{11} - \frac{2}{3}m + r' \qquad (5.3.9a)$$

$$-\lambda_1(ef' + \frac{e'f}{2}) = -\zeta_2 gf'' - t_{22} - \frac{2}{3}m + s' \qquad (5.3.9b)$$

$$-\lambda_1(pf' + \frac{p'f}{2}) = -gf'' - m + t' \qquad (5.3.9c)$$

$$-\lambda_1(gf' + \frac{g'f}{2}) = -(\zeta_3 p + \zeta_4 h + \zeta_5 e)f'' - t_{12} + u' \qquad (5.3.9d)$$

$$-\frac{\lambda_1}{2}(5mf' + m'f) = -\psi_2\frac{mg}{p}f'' - (\psi_0 + \psi_1 II)\frac{m^2}{p} + v' \qquad (5.3.9e)$$

where,

$$r = C_s\frac{p}{m}(2gg' + eh') \qquad (5.3.10a)$$

$$s = 3C_s p/_m ee' \qquad (5.3.10b)$$

$$t = C_s\frac{p}{m}(gg' + ee' + ep') \qquad (5.3.10c)$$

$$u = C_s p/_m(ge' + 2eg') \qquad (5.3.10d)$$

$$v = C_\varepsilon p/_m em' \qquad (5.3.103)$$

and

$$t_{11} = \beta_0 m[(1 + \beta_1 II)b_{11} + \beta_2(b_{11}^2 + b_{12}^2 - II/_3)] \qquad (5.3.11a)$$

$$t_{22} = \beta_0 m[(1 + \beta_1 II)b_{22} + \beta_2(b_{22}^2 + b_{12}^2 - II/3)] \qquad (5.3.11b)$$

$$t_{12} = \beta_0 \frac{mg}{p}[1 + \beta_1 II + \beta_2(b_{11} + b_{22})] \qquad (5.3.11c)$$

The coefficients $\beta_0, \beta_1, \beta_2, C_s, C, \psi_0, \psi_1$ and ψ_2 are all given in Table 5.7. The coefficients ζ are all related to the coefficients α_0 according to,

$$\zeta_1 = -(\frac{2}{3} - \frac{4}{3}\alpha_0), \quad \zeta_2 = (4/3 + 10/3\alpha_0), \quad \zeta_3 = -(4/10 + 2\alpha_0)$$

$$\zeta_4 = (2/3 + 8/3\alpha_0) \text{ and } \zeta_5 = (1/3\ \alpha_0 - 2/3) \qquad (5.3.12)$$

and α_0 is also given in Table 5.7.

B. Governing Similarity Equations--Plane Wake.

$$-\lambda_1(\frac{\eta h'}{2} + h) = \zeta_1 g f' - t_{11} - \frac{2}{3}m + r' \qquad (5.3.13a)$$

$$-\lambda_1(\frac{\eta e'}{2} + e) = \zeta_2 g f' - t_{22} - \frac{2}{3}m + s' \qquad (5.3.13b)$$

$$-\lambda_1(\frac{\eta p'}{2} + p) = g f' - m + t' \qquad (5.3.13c)$$

$$-\lambda_1(\frac{\eta g'}{2} + g) = (\zeta_3 p + \zeta_4 h + \zeta_5 e)f' - t_{12} + u' \qquad (5.3.13d)$$

$$-\lambda_1(\frac{\eta m'}{2} + 2m) = \psi_2 \frac{mgf'}{p} - (\psi_0 + \psi_1 II)\frac{m^2}{p} + v' \qquad (5.3.13e)$$

Here, the variables, r,s,t,u and v are given by equations (5.3.10), t_{11}, t_{12} and t_{22} are given by (5.3.11) and coefficients ζ_i are given by (5.3.12) respectively.

The similarity equations, either for the simple model, given in Table 5.2 or the full MRS model given by equations (5.3.9) or (5.3.13), together with the mean momentum equations and integral constraints must be solved numerically, subject to boundary conditions. The boundary conditions are listed at the end of the next section.

5.4 Boundary Conditions

Turbulent shear flows increase in width with downstream distance due to the process of entrainment. Irrotational fluid acquires vorticity from the turbulent fluid by viscuous diffusion and this vorticity is then increased by vortex stretching. This process leads to a sharp interface separating the turbulent/non-turbulent regions which can be treated as a front propagating into the non-turbulent zone. Instantaneous "spark" photographs of real turbulence (cf. Figure 5, Brown and Roshko, 1974) do show the existence of such a sharp interface.

Saffman (1970) has shown that the turbulent model equations in some way reflect this behavior. Near the outer edge of the flow, advection balances diffusion. Thus for example the energy equation (5.3.1b) of the τ-k-ε model, becomes

$$V\frac{\partial k}{\partial y} \sim \gamma_4 \frac{\partial}{\partial y}\frac{k^2}{\varepsilon}\frac{\partial k}{\partial y} \qquad (5.4.1)$$

In the irrotational zone, k and ε vanish by definition and the "diffusivity" $\gamma_4\frac{k^2}{\varepsilon}$ also vanishes in this region. Under these conditions, Laundau and Lifshitz (1959, § 51) show that the diffused quantity (k), occupies only a finite space and propagates as a front

into the irrotational zone. Thus the turbulence model equations produce a sharp, smooth and steady boundary between the turbulent and non-turbulent regions. In experiments, on the other hand, this boundary is corrugated in appearance and unsteady. The computational boundary is shown schematically in Figure 5.3.

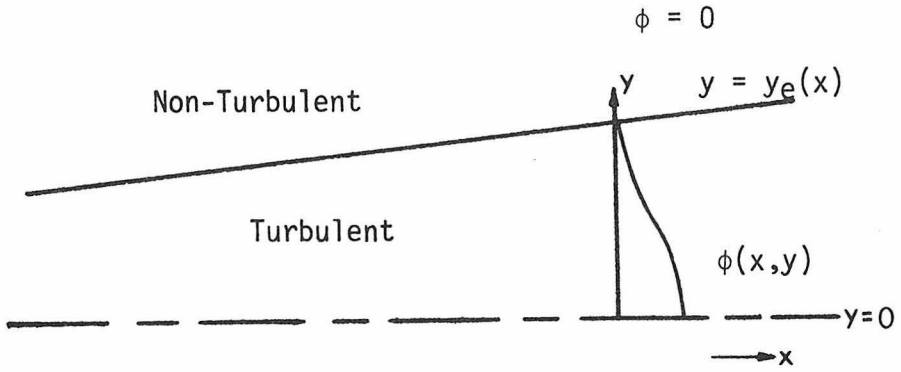

Figure 5.3.--Computational Boundaries for Free Shear Flow.

In Figure 5.3, $\phi(x,y)$ represents any diffused turbulent quantity (e.g. k or ε). The solution to equation (5.4.1), or its counterpart for τ and ε, is not analytic for all y, but is singular along the line $y = y_e(x)$ as required by the fact that the diffusivity vanishes at this point. We avoid the problem of non-analytic solutions, however , by only considering the solution space $0 < y < y_e$ and then applying the boundary conditions at $y = 0$ and $y = y_e(x)$. The location of $y_e(x)$ is then calculated as part of the solution of the problem.

In § 5.2, the similarity length scale, $\ell(x)$, contained a multiplier λ_1 which was not defined. If this is now chosen so that $\ell(x)$ is the half-width of the turbulent region, then in the plane jet case for example the location of the singularities is the locus

of points $y_e = \lambda_1 x$, corresponding to $\eta = \eta_e = 1$. Thus the domain of the solution in η-space is [0,1] and the half-width of the flow region is determined by treating η as an eigenvalue.

Since λ_1 is a constant, its governing equation is

$$\lambda_1' = 0$$

and the value of λ_1 is determined by means of the integral constraint. If we introduce the new variable z, such that (for the plane jet),

$$z(\eta) = \int_0^\eta \left(f'(\eta)\right)^2 d\eta \tag{5.4.3}$$

then the integral constraint for the jet (equation 5.2.13) becomes

$$\lambda_1 z(1) = \frac{1}{2} \tag{5.4.4}$$

where the unknown multiplier λ_2 in (5.2.13) has been set equal to one. The integral constraint is then incorporated into the governing equations by introducing the differential equation

$$z' = (f')^2 \tag{5.4.5}$$

and the two additional boundary conditions

$$z(0) = 0 \qquad z(1) = \frac{1}{2\lambda_1} . \tag{5.4.6}$$

The similar equations for the plane wake are

$$z = \int_0^\eta f(\eta)d\eta \rightarrow \quad z' = f \tag{5.4.7}$$

with $$z(0) = 0 \qquad \text{and} \qquad z(1) = \frac{1}{2\lambda_1} . \tag{5.4.8}$$

Again for convenience λ_2 has been set equal to unity. The remaining boundary conditions arise from the symmetry of the flow at $\eta = 0$ and the vanishing of the turbulence quantities at $\eta = 1$. These are, at $\eta = 0$, $p' = h' = e' = f = g = m' = z = 0$ and at $\eta = 1$, $p = h = e = m = g = f' = 0$, $z = \frac{1}{2\lambda_1}$ for the plane jet and, at $\eta = 0$, $p' = h' = e' = m' = g = z = 0$ and at $\eta = 1$, $p = h = e = m = g = f = 0$, $z = \frac{1}{2\lambda_1}$ for the plane wake.

5.5 Description of the Calculation Scheme

The coupled sets of non linear ordinary differential equations described in the previous section must be solved numerically. Since these equations have boundary conditions at both ends of the computational domain, they form what is called a "non linear two-point boundary-value problem." These problems are difficult to solve, especially for large sets of coupled equations. However, an accurate finite difference method has been developed by Keller (1974) and this is the approach which we have used to solve our problem. Keller's scheme, in the context of our present problem is discussed in this section.

The governing equations are solved as a coupled set of first order differential equations. To decompose the similarity equations given in section § 5.3 (i.e. equations (5.3.9) - (5.3.13)) into a system of first order equations, it is convenient to consider the "diffusion" terms as separate variables. For the τ-k-ε model, we define t, v and u, according to

$$t = \gamma_4 \frac{p^2 p'}{m} \quad (5.5.1a) \qquad v = \gamma_7 \frac{p^2 m'}{m} \quad (5.5.1b) \qquad u = \gamma_3 \frac{p^2 g'}{m} \quad (5.5.1c)$$

These may be rearranged to give the set of first order equations

$$p' = \frac{mt}{\gamma_4 p^2} \quad (5.5.2a)$$

$$m' = \frac{mv}{\gamma_7 p^2} \quad (5.5.2b)$$

$$g' = \frac{mu}{\gamma_3 p^2} \quad (5.5.2c)$$

The similarity forms of the diffusion variables have already been defined for the MRS model (equation 5.3.10). These equations can be solved algebraically to give the following set of first order equations,

$$e' = \frac{m}{C_s p} \left(\frac{s}{3e}\right) \quad (5.5.3a)$$

$$g' = \frac{m}{C_s p} \left(\frac{u}{2e} - \frac{gs}{3e}\right) \quad (5.5.3b)$$

$$h' = \frac{m}{C_s p} \left(\frac{r}{e} - \frac{2g}{e}\left(\frac{u}{2e} - \frac{gs}{3e}\right)\right) \quad (5.5.3c)$$

$$p' = \frac{m}{C_s p} \left(\frac{t}{e} - \frac{g}{e}\left(\frac{u}{2e} - \frac{gs}{3e}\right) - \frac{s}{3e}\right) \quad (5.5.3d)$$

$$m' = \frac{mv}{C_\varepsilon p e}$$

The governing equations for each flow are considered separately.

5.5.1 The Plane Jet

A. τ-k-ε Model

The mean momentum equation for the jet

$$\frac{\lambda_1}{2}(ff')' = g' \tag{5.2.12}$$

is written as two simultaneous first-order equations

$$f' = w \tag{5.2.4a}$$

$$w' = \frac{2g}{\lambda_1 f} - \frac{h^2}{\lambda_1} \tag{5.5.4b}$$

Then defining the vector $\underset{\sim}{y}$,

$$\underset{\sim}{y}^T = \{u,f,v,t,g,z,p,m,w,\lambda_1\} \tag{5.5.5}$$

the governing equations (5.5.4), (5.5.2) and (5.3.3) for the plane jet may be written as the following system of first order differential equations,

$$\underset{\sim}{y}' - \underset{\sim}{F}(\underset{\sim}{y},\eta) = 0 \tag{5.5.6a}$$

with separated end-point conditions,

$$B_0\underset{\sim}{y}(0) = C_0 \qquad\qquad B_1\underset{\sim}{y}(1) = C_1 \tag{5.5.6b}$$

Here,

$$\begin{bmatrix} \lambda_1(gw + g'f/2) - \gamma_1 pw' - \gamma_2 mg/p \\ -w \\ \lambda_1(5mw + fm')/2 - \gamma_5 mgw'/p - \gamma_6 m^2/p \end{bmatrix}$$

$$F(\underset{\sim}{y},\eta)=\begin{bmatrix} \lambda_1(pw + p'f/_2) - gw' - m \\ -mu/\gamma_3 p^2 \\ \\ - w^2 \\ - mt/\gamma_4 p^2 \\ -mv/\gamma_7 p^2 \\ -2g'/\lambda_1 f + w^2/f \\ 0 \end{bmatrix}$$

and B_0 and B_1 are the 5 x 10 matrices

$$B_0 = \begin{bmatrix} 0 & 1 & & & & & & & & \\ 0 & 0 & 1 & & & & & & & \\ 0 & 0 & 0 & 1 & & & & 0 & & \\ 0 & 0 & 0 & 0 & 1 & & & & & \\ 0 & 0 & 0 & 0 & 0 & 1 & & & & \end{bmatrix} \qquad B_1 = \begin{bmatrix} 0 & 0 & 0 & 1 & & & & & & \\ 0 & 0 & 0 & 0 & 1 & & & & & \\ 0 & 0 & 0 & 0 & 0 & 1 & & 0 & & \\ 0 & 0 & 0 & 0 & 0 & 0 & 1 & & & \\ 0 & 0 & 0 & 0 & 0 & 0 & 0 & 1 & & \end{bmatrix}$$

and,

$$C_0^T = \{0, 0, 0, 0, 0\}, \quad C_1^T = \{0, 1/2\lambda_1, 0, 0, 0\}.$$

B. MRS Model

The mean momentum equation is decomposed into the same set of first-order equations that were used for the τ-k-ε model (i.e. equation 5.5.4). The vector $\underset{\sim}{y}$ in this case is

$$\underset{\sim}{y}^T = \{u, f, v, t, r, s, g, z, p, m, h, e, w, \lambda_1\} \qquad (5.5.7)$$

and the governing equations (5.5.4), (5.5.3) and (5.3.9) can again be written as a first order system of the general form (5.5.6a,b). Here, $\underset{\sim}{F}(\underset{\sim}{y},\eta)$ is given by

$$
\underset{\sim}{F}(\underset{\sim}{y},\eta)=\begin{bmatrix}
\lambda_1(gw + g'f/_2) - (\zeta_3 p + \zeta_4 h + \zeta_5 e)w' - t_{12} \\
-w \\
\lambda_1(5mw + m'f)/_2 - \psi_2 mgw'/_p - (\psi_0 + \psi_1 II)m^2/_p \\
\lambda_1(pw + p'f/_2) - gw' - m \\
\lambda_1(hw + h'f/_2) - \zeta_1 gw' - t_{11} - 2/_3\, m \\
\lambda_1(ew + e'f/_2) - \zeta_2 gw' - t_{22} - 2/_3\, m \\
-\frac{m}{C_s p}\left(\frac{u}{2e} - \frac{gs}{3e}\right) \\
-w^2 \\
-\frac{m}{C_s p}\,\frac{t}{e} - \frac{g}{e}\left(\frac{u}{2e} - \frac{gs}{3e}\right) - \frac{s}{3e} \\
-\frac{mv}{C_\varepsilon pe} \\
-\frac{m}{C_s p}\,\frac{r}{e} - \frac{g}{e}\left(\frac{u}{2e} - \frac{gs}{3e}\right) \\
-\frac{m}{C_s p}\left(\frac{s}{3e}\right) \\
-\frac{2g'}{\lambda_1 f} + \frac{w^2}{f} \\
0
\end{bmatrix}
$$

where the variables t_{11}, t_{12} and t_{22} are defined in equations (5.3.11a, b, c). B_0 is a 7 x 14 matrix with the following non-zero elements: $B_0(1,2) = B_0(2,3) = B_0(3,4) = B_0(4,5) = B_0(5,6) = B_0(6,7) = 1$, and B_1 is also a 7 x 14 matrix with the non-zero elements, $B_1(1,7) = B_1(2,8) = B_1(3,9) = B_1(4,10) = B_1(5,11) = B_1(6,12) = 1$. Finally, C_0 and C_1 are given by $C_0^T = \{0,0,0,0,0,0,0\}$, $C_1^T = \{0,1/2\lambda_1,0,0,0,0,0\}$.

5.5.2 The Plane Wake

A. τ-k-ε Model

For the case of the plane wake, the momentum equation is already first order in f' and can be written as:

$$f' = -\frac{2g'}{\lambda_1 \eta} - \frac{f}{\eta} \tag{5.5.8}$$

The vector $\underset{\sim}{y}$ has one less component than its counterpart for the jet, i.e.

$$\underset{\sim}{y}^T = \{v,\ t,\ g,\ z,\ p,\ m,\ f,\ u,\ \lambda_1\} \tag{5.5.9}$$

and the governing equations (5.5.8), (5.5.2) and (5.3.4) can again be expressed in terms of a first-order system of the type (5.5.6a,b). For the case of a wake $\underset{\sim}{F}(\underset{\sim}{y},\eta)$ is given by,

$$\begin{bmatrix} \lambda_1(\eta m'/_2 + 2m) + \gamma_5 g m f'/_p - \gamma_6 m^2/_p \\ \lambda_1(\eta p'/_2 + p) + g f' - m \end{bmatrix}$$

$$\underset{\sim}{F}(\underset{\sim}{y},\eta)=\begin{bmatrix} -mu/\gamma_3 p^2 \\ -f \\ -mt/\gamma_4 p^2 \\ -mv/\gamma_7 p^2 \\ \frac{2g}{\lambda_1} + \frac{f}{\eta} \\ \lambda_1(\eta g'/_2 + g) - \gamma_1 mg/_p + \gamma_2 pf' \\ 0 \end{bmatrix}$$

The boundary conditions are contained in B_0 a 4 x 9 matrix, B_1 a 5 x 9 matrix and the vectors C_0 and C_1, i.e.

$$B_0\underset{\sim}{y}(0) = C_0 \qquad \text{and} \qquad B_1 y(1) = C_1$$

where

$$B_0 = \begin{bmatrix} 1 & 0 & & & \\ 0 & 1 & 0 & 0 & \\ 0 & 0 & 1 & 0 & \\ 0 & 0 & 0 & 1 & 0 \end{bmatrix} \qquad B_1 = \begin{bmatrix} 0 & 0 & 1 & 0 & & & \\ 0 & 0 & 0 & 1 & 0 & 0 & \\ 0 & 0 & 0 & 0 & 1 & 0 & 0 \\ 0 & 0 & 0 & 0 & 0 & 1 & 0 \\ 0 & 0 & 0 & 0 & 0 & 0 & 1 & 0 \end{bmatrix}$$

and,

$$C_0^T = \{0,\ 0,\ 0,\ 0\} \qquad C_1^T = \{0,\ 1/_{2\lambda_1},\ 0,\ 0,\ 0\}\ .$$

B. MRS Model

For the plane wake the dependent similarity variables for the MRS model are $\underset{\sim}{y}$, where

$$\underset{\sim}{y}^T = \{v,\ t,\ r,\ s,\ g,\ z,\ p,\ m,\ h,\ e,\ f,\ u,\ \lambda_1\} \tag{5.5.10}$$

In this case the governing equations (5.5.8), (5.5.3) and (5.3.13) also comprise the first-order system

$$\underset{\sim}{y}' - \underset{\sim}{F}(\underset{\sim}{y},\ \eta) = 0$$

where,

$$\underset{\sim}{F}(\underset{\sim}{y},\eta) = \begin{vmatrix} \lambda_1(\eta m'/_2 + 2m) + \psi_2 mgf'/_p - (\psi_0 + \psi_1 II)m^2/_p \\ \lambda_1(\eta p'/_2 + p) + gf' - m \\ \lambda_1(\eta h'/_2 + h) + \zeta_1 gf' - t_{11} - \frac{2}{3}m \\ \lambda_1(\eta e'/_2 + e) + \zeta_2 gf' - t_{22} - \frac{2}{3}m \\ -\frac{m}{C_s p}\ \frac{t}{e} - \frac{g}{e}\left(\frac{u}{2e} - \frac{gs}{3e}\right) - \frac{s}{3e} \\ -\frac{mv}{C_\varepsilon pe} \\ -\frac{m}{C_s p}\ \frac{r}{e} - \frac{g}{e}\left(\frac{u}{2e} - \frac{gs}{3e}\right) \\ -\frac{ms}{C_s p}\left(\frac{s}{3e}\right) \\ \frac{2g'}{\lambda_1 \eta} + \frac{f}{\eta} \end{vmatrix}$$

$$\begin{bmatrix} \lambda_1(\eta g'/_2 + g) + (\zeta_3 p + \zeta_4 h + \zeta_5 e)f' - t_{12} \\ \\ 0 \end{bmatrix}$$

The boundary conditions are given by

$$B_0 \underset{\sim}{y}(0) = C_0 \qquad \text{and} \qquad B_1 \underset{\sim}{y}(1) = C_1.$$

Here, B_0 is a 6 x 13 matrix with the non-zero elements: $B_0(1,1) = B_0(2,2) = B_0(3,3) = B_0(4,4) = B_0(5,5) = B_0(6,6) = 1$, B_1 is a 7 x 13 matrix with the following non-zero elements: $B_1(7,5) = B_1(9,7) = B_1(10,8) = B_1(11,9) = B_1(12,10) = B_1(13,11) = 1$ and C_0 and C_1 are vectors with the components: $C_0^T = \{0, 0, 0, 0, 0, 0\}$, $C_1^T = \{0. \ 1/2\lambda_1, 0, 0, 0, 0, 0\}$.

5.5.3 Numerical Scheme

We thus desire to numerically solve a system of first order differential equations of the general form,

$$\underset{\sim}{y}' - \underset{\sim}{F}(\underset{\sim}{y}(\eta), \eta) = 0 \qquad (5.5.6a)$$

subject to the boundary conditions

$$B_0 \underset{\sim}{y}(0) = C_0 \qquad B_1 \underset{\sim}{y}(1) = C_1 \qquad (5.5.6b)$$

Here $\underset{\sim}{y}$ is a vector containing the η dependent similarity functions and $\underset{\sim}{F}$, B_0, B_1, C_0 and C_1 were given in the four previous subsections for the cases being considered. For generality it will be assumed that there are p boundary conditions at $\eta = 0$ and $q = n - p$ boundary conditions at $\eta = 1$.

To solve the system (5.5.6) numerically we use the centered Euler (or box) scheme proposed and analyzed by Keller (1974). We briefly outline Keller's method here. A more detailed discussion can be found in the thesis of White (1974).

We first define a uniform mesh on the interval [0,1].

$$\eta_0 = 0 \qquad \eta_j = jh_\Delta \qquad j = 1, 2, \ldots J \qquad h_\Delta = \frac{1}{J} \tag{5.5.11}$$

Applied to (5.5.6) the centered Euler scheme is then the set of difference equations

$$\frac{1}{h_\Delta}[\underset{\sim}{u}_j - \underset{\sim}{u}_{j-1}] - F(\eta_{j-\frac{1}{2}}, \frac{1}{2}[\underset{\sim}{u}_j + \underset{\sim}{u}_{j-1}]) = 0 \quad 1 \leq j \leq J \tag{5.5.12a}$$

$$\eta_{j-\frac{1}{2}} \equiv \eta_j - h/2$$

with boundary conditions

$$B_0\underset{\sim}{u}_0 = C_0 \qquad\qquad B_1\underset{\sim}{u}_J = C_1 \tag{5.5.12b}$$

Here $\underset{\sim}{u}_j$ is the computed approximation to $\underset{\sim}{y}(\eta_j)$. Henceforth, $\underset{\sim}{u}_j$ will be understood to be an n-vector and written u_j. Furthermore, the average of $\underset{\sim}{y}$ over a grid interval will be written

$$\bar{u}_j = \frac{1}{2}[u_j + u_{j-1}] \tag{5.5.13}$$

Now, defining the "maxi-vector" $\underset{\sim}{U}$ of $n(J + 1)$ components

$$\underset{\sim}{U} = \begin{bmatrix} u_0 \\ \vdots \\ u_j \\ \vdots \\ u_J \end{bmatrix}$$

we require the solution to the following set of non-linear algebraic equations,

$$\Phi(\underset{\sim}{U}) = \begin{bmatrix} B_0 u_0 - C_0 \\ \vdots \\ (u_j - u_{j-1}) - hF(\eta_{j-\frac{1}{2}}, \bar{u}_j) \\ \vdots \\ B_1 u_J - C_1 \end{bmatrix} = 0 \qquad (5.5.15)$$

The system (5.5.15) is solved using Newton's iterative method. The Newton iterates are defined by

$$U^{\nu+1} = U^{\nu} + \delta U^{\nu} \qquad (5.5.16)$$

where U^{ν} is an approximation to U*, the desired root of (5.5.15), and δU^{ν} is a correction factor which is intended to bring $U^{\nu+1}$ closer to U*. At each iteration, we attempt to choose δU^{ν} so that

$$\Phi(U^{\nu+1}) = 0 \qquad (5.5.17)$$

The choice of δU^{ν} is obtained by expressing $\Phi(U^{\nu+1})$ in terms of $\Phi(U^{\nu})$ and δU^{ν} via a Taylor series expansion,

$$\Phi(U^{\nu} + \delta U^{\nu}) = \Phi(U^{\nu}) + \frac{\partial \Phi(U^{\nu})}{\partial U} \delta U^{\nu} + \ldots . \qquad (5.5.18)$$

Thus, retaining only the linear term, the correction matrix δU^{ν}, can be estimated at each step of the iteration from the equation,

$$\frac{\partial \Phi(U^{\nu})}{\partial U^{\nu}} \cdot \delta U^{\nu} = - \Phi(U^{\nu}) \qquad (5.5.19)$$

where $\frac{\partial \Phi}{\partial u}$ is the Jacobian matrix of Φ evaluated at U^{ν}. The Jacobian matrix can be calculated by blocks, that is,

$$\frac{\partial \Phi(U^{\nu})}{\partial U} = \frac{\partial \Phi_i}{\partial U_j} \quad .$$

Using (5.5.12), this gives

$$\frac{\partial \Phi}{\partial U} = \begin{bmatrix} B_0 & & & \\ -L_1 & R_1 & & \\ & \ddots & \ddots & \\ & & -L_J & R_J \\ & & & B_1 \end{bmatrix} \qquad (5.5.20)$$

where

$$L_j = I + \frac{h}{2} \frac{\partial f}{\partial y} (\eta_{j-\frac{1}{2}}, \bar{u}_j)$$

$$R_j = I - \frac{h}{2} \frac{\partial f}{\partial y} (\eta_{j-\frac{1}{2}}, \bar{u}_j)$$

Equations (5.5.19) and (5.5.20) define a <u>linear</u> system that must be solved at each iteration ot obtain the correction matrix δU^{ν}.

Following Keller (1974), the banded matrix (5.5.20) can be regarded as "block tridiagonal)

$$\frac{\partial \Phi}{\partial U} = [B_j, A_j, C_j] \qquad (5.5.21)$$

in which B_j, A_j and C_j are n x n matrices which are easily identified by comparing (5.5.21) and (5.5.20). This is illustrated symbolically in the following equation,

$$\frac{\partial \Phi}{\partial U} = \begin{bmatrix} B_0 & & & & \\ -L_1 & R_1 & & & \\ & -L_2 & R_2 & & \\ & & & -L_J & R_J \\ & & & & B_1 \end{bmatrix} \tag{5.5.22}$$

The dotted boxes represent the new blocks (B_j, A_j, C_j) hence $\frac{\partial \Phi}{\partial U}$ can be written in "block-tridiagonal" form

$$\frac{\partial \Phi}{\partial U} = \begin{bmatrix} A_1 & C_1 & & & \\ B_2 & A_2 & C_2 & & \\ & \ddots & \ddots & \ddots & \\ & & B_j & A_j & C_j \\ & & & B_{J+1} & A_{J+1} \end{bmatrix} \tag{5.5.23}$$

It is clear from (5.5.22) that the last q-rows of each B_j and the first p-rows of each C_j are all zeros.

The system of equations (5.5.19) may now be solved in an efficient manner for the correction matrix by taking account of the tridiagonal nature of the Jacobian matrix. To illustrate the method used, let us examine a linear system of order n(J+1) which has the form

$$A \underset{\sim}{X} = \underset{\sim}{R} \tag{5.5.24}$$

where $\mathbf{A}$ represents the block tridiagonal matrix (5.5.21) and $\underset{\sim}{X}^T = (\underset{\sim}{x}_1, \cdots \underset{\sim}{x}_{J+1})$, $\underset{\sim}{R}^T = (\underset{\sim}{r}_1, \cdots \underset{\sim}{r}_{J+1})$. To solve (5.5.24), $\mathbf{A}$ is factored into the form

$$\mathbf{A} = \mathbf{L}\mathbf{U} \ , \quad \mathbf{L} = \left[\beta_j, \delta_j, \underset{\sim}{0}\right] \qquad \mathbf{U} = \left[\underset{\sim}{0}, \alpha_j, \gamma_j\right] \tag{5.5.25}$$

Here α_j, β_j, γ_j and $\underset{\sim}{0}$ are all n x n matrices, with $\underset{\sim}{0}$ having all elements equal to zero. and are block-lower and block-upper triangular matrices. The equation (5.5.24) may thus be replaced by the two systems of equations

$$\mathbf{L}\underset{\sim}{Y} = \underset{\sim}{R} \tag{5.5.26a}$$

$$\mathbf{U}\underset{\sim}{X} = \underset{\sim}{Y} \tag{5.5.26b}$$

The factorization (5.5.25) is defined in terms of a series of recursion relations for the β_j, δ_j, α_j and γ_j which can be obtained by carrying out the multiplication of $\mathbf{LU}$ and comparing with $\mathbf{A}$. The result is

$$\begin{aligned} \delta_1\alpha_1 &= A_1 \\ \delta_j\gamma_j &= C_j \qquad 1 \le j \le J \\ \beta_j\alpha_{j-1} &= B_j \qquad 2 \le j \le J+1 \\ \delta_j\alpha_j &= A_j - \beta_j\gamma_{j-1} \qquad 2 \le j \le J+1 \end{aligned} \tag{5.5.27}$$

The solution to (5.5.24) is then obtained by solving

$$\delta_1 \underset{\sim}{y}_1 = \underset{\sim}{r}_1 \qquad\qquad \alpha_{J+1} \underset{\sim}{x}_{J+1} = \underset{\sim}{y}_{J+1}$$

$$\delta_j \underset{\sim}{y}_j = \underset{\sim}{r}_j - \beta_j \underset{\sim}{y}_{j-1} \quad 2 \leq j \leq J+1 \qquad \alpha_j \underset{\sim}{x}_j = \underset{\sim}{y}_j - \gamma_j \underset{\sim}{x}_{j+1} \quad J \geq j \geq 1 \tag{5.5.28}$$

It may be noted that δ_j and α_j are not uniquely determined by (5.5.27). Indeed, Keller (1974) distinguished four possible factorizations. The choice $\delta_j = I$ was used in (5.5.28) because it allows a form of partial pivoting. The method outlined in this paragraph may be applied directly to the solution of the linear system (5.5.19) and a new estimate ($U^{\nu+1}$) generated for the solution of (5.5.15) from the correction matrix. The Newton iteration scheme is continued until two successive iterates satisfy a given error criteria.

5.5.4 Continuation and Embedding

In solving non linear problems, a major difficulty is obtaining an initial guess U^0 which is in the "domain of convergence" for Newton's method. Generally speaking, the initial iterate must be within O(h) of the exact finite difference solution for Newton's method to converge. In order to partially circumvent this problem, solutions were initially obtained on a rather coarse net with only 26 nodes. Then by linearly interpolating between points this solution provides an order (h) initial estimate for the solution on a 51-point grid. The two-dimensional jet equations, given in section § 5.2.1A were solved on 26, 51 and 101-point grids. The computed profiles were insensitive to the number of grid points. Hence the wake solutions were all obtained on grids with 26 nodes.

Even on a coarse grid it is difficult to obtain an adequate initial guess for convergence. Two methods were used in the present work to generate an initial estimate for the solution. If a solution for some problem had not previously been obtained for some set of the model constants, the following embedding method was used to generate the initial iterate. A parameter ε' was defined such that:

$$G(U) = (1-\varepsilon')\ \Phi\ (U) + \varepsilon'\Phi\ (U^0) = 0 \qquad (5.5.29)$$

Then, starting with $\varepsilon' = 1$, any initial guess U^0 is an exact solution to (5.5.29). The calculation proceeds by gradually decreasing ε', with the "initial" guess for each ε' being the previously obtained solution at $\varepsilon' + \delta\varepsilon'$. When ε' reaches zero, we have a solution of the original problem (5.5.16).

Once a solution has been obtained, it can be used as an initial guess for other solutions in which the constants of the turbulence model are varied. In this way whole families of solutions for various values of the model constants can be obtained with little computational effort. In the following sections the calculation scheme which we have described will be used to obtain similarity solutions for the plane jet and plane wake using both the τ-k-ε and MRS models. Solutions for these two flows were also obtained by Rodi (1972) for a τ-k-ε model using the Patankar-Spalding (1970) numerical scheme. Thus the present calculation method can be verified by comparing Rodi's original solutions with solutions computed here using Rodi's (1972) τ-k-ε model.

5.6 Experimental Data for Plane Jets and Wakes

Free shear flows have been the subject of a relatively large number of experimental studies. These range from a simple determination of the mean velocity profile to more complete studies where all of the non-zero components of the Reynolds stress tensor and even some of the higher order turbulent correlations have been measured. The most comprehensive review and critical evaluation of experimental data, for the plane turbulent jet and wake which are considered here, is that of Rodi (1976). This review, however, was based on the available data as of 1972 and requires updating.

In the following section, the available experimental data for the plane jet and wake are considered and the "best" or consensus data for these experiments are chosen as "target" cases for comparison with the numerical predictions in the next section. The plane jet and plane wake are considered separately. In each case, an attempt is made to identify the "best" available data for: (i) the characteristic length and velocity scales which must be used to non dimensionalize the experimental profiles, (ii) the "spreading rate" (defined later), (iii) the mean velocity profile, and (iv) profiles for the second-order turbulence quantities (i.e. the Reynolds stresses). Except where noted, our independent evaluation of the data available today has led us to agree with the recommendations of Rodi (1976) as to the optimal choices for comparison with the numerically calculated results.

5.6.1 Two-Dimensional Jets

A. Characteristic Scales.

It was pointed out in § 5.2 that two characteristic scales (ℓ, U_s) are required to form the dimensionless similarity variables. The most convenient characteristic scales for use in experimental data reduction are somewhat different than those defined in § 5.2 (i.e. λ_1 and λ_2 in equation (5.2.1) for use in the computational scheme. The scales commonly used to non-dimensionalize the experimentally determined turbulence quantities for a jet are determined from the lateral distribution of the mean axial velocity U(x,y) measured at several streamwise locations. As shown in Figure 5.1, these are:

(1) the "centerline" velocity, $U_m = U(x,0)$, and

(2) the jet "half-width," b(x) determined from

$$U(x, \pm b(x)) = \frac{1}{2} U(x,0) = \frac{1}{2} U_m \qquad (5.6.1)$$

In order to establish the relationship (if any exists) between these "experimental" length and velocity scales, and the characteristic scales (ℓ, U_s) of the similarity variables, we may examine the behavior of U_m and b in the far downstream similarity regime. In particular, if one plots experimental values for $\left(\frac{U_J}{U_m}\right)^2$ vs. $\frac{x}{d}$, the result is a straight line. Similarly if the normalized half-widths $\frac{b(x)}{d}$, calculated using (5.6.1), are plotted versus the dimensionless distance from the jet orifice, $\frac{x}{d}$, a straight line of the form;

$$\frac{b(x)}{d} = K_1\left(\frac{x}{d} + K_2\right) \qquad (5.6.2)$$

can be fitted to the experimental data in the similarity regime. It follows that U_m varies as $x^{-\frac{1}{2}}$ and $b(x)$ as x. This is precisely the functional dependence which was shown in equation (5.2.11) to pertain for similarity scales U_s and ℓ. Thus, a direct relationship exists between the similarity scales used in the computational scheme and the experimental values U_m and b. The centerline mean velocity can be determined in the calculations directly from equation (5.2.14), i.e.

$$U_m = \left(\frac{J}{x}\right)^{\frac{1}{2}} f'(0).$$

The location of the half-width is then found by determining the value of η (call it $\eta_{\frac{1}{2}}$) for which $f(\eta_{\frac{1}{2}}) = \frac{1}{2} f(0)$. The similarity variable, $\tilde{\eta} = y/b(x)$ is then used for comparing the computations with experiment. These experimental scales can then be used to rescale the calculated similarity variables according to:

$$\tilde{f}(\tilde{\eta}) = \frac{f(\eta)}{f(\eta)} \qquad \tilde{p}(\tilde{\eta}) = \frac{p(\eta)}{[f(0)]^2} \qquad \tilde{g}(\tilde{\eta}) = \frac{g(\eta)}{[f(0)]^2}$$

B. <u>The Spreading Rate</u>.

The coefficient K_1 in (5.6.2) is known as the "spreading rate" of the jet, while $x_0 = -K_2 d$ is the virtual origin of the similarity region. Newman (1965) reviewed the plane jet experiments and determined an average spreading rate of $K_1 = 0.11$. Rodi (1976) included data through (1972) in his more recent review and the

average value of K_1 determined from his table 7 is, $K_1 = 0.104$. The most comprehensive study of the spreading rate of plane turbulent jets is that of Kotsovinos (1976). By considering more than a dozen existing experiments plus his own experimental study (Kotsovinos, 1977), Kotsovinos concluded that the linear spreading law (equation 5.6.2) was not valid. Instead, he proposed the following curve fit to the available data (see Figure 5, Kotsovinos, 1976a) as a "weakly non linear" spreading law,

$$\frac{b(x)}{d} = 0.228 + 0.913\left(\frac{x}{d}\right) + 0.00005101\left(\frac{x}{d}\right)^2 + 0.000000331\left(\frac{x}{d}\right)^3 \tag{5.6.3}$$

Bradshaw (1977) however, in a rebuttal to Kotsovinos (1976a), showed that the apparently non linear behavior hypothesized by Kotsovinos was due to draughts in the room in which the experiments were being carried out. These draughts arise because of the continuous recirculation of fluid being entrained in the jet. Bradshaw showed that if the jet induced room draughts scaled with U_J (the jet exit velocity) then a spreading law of the form

$$\frac{db}{dx} = \left(\frac{db}{dx}\right)_0 + C_2 \frac{U_J}{U_m} \tag{5.6.4}$$

would occur. Fitting (5.6.4) to the comprehensive set of data used by Kotsovinos (1976a), Bradshaw found that C_2 was approximately constant (for all of the experiments considered) at $C_2 \simeq 5 \times 10^{-3}$ and

$$K_1 = \left(\frac{db}{dx}\right)_0 = .0913 \tag{5.6.5}$$

Thus, in our opinion, the spreading rate $K_1 = .0913$ is the most reliable current estimate from experiments and will be used for comparison with numerical calculations in the next section.

C. The Mean Velocity Profile.

Rodi (1976) compared the mean velocity data of several investigators (cf. Figure 12, Rodi, 1976) and found that the data are in good agreement except near the edge of the jet. Since hot wires are known to give inaccurate readings in regions of small mean velocity (Rodi, 1972), the data of Robbins (1971) obtained using an impact tube, was judged to be the best by Rodi (1976). We agree with this suggestion and thus use the points taken by Rodi (1976) from Robbins' (1971) original data for comparison with our numerical mean velocity calculation.

D. Second-Order Turbulence Quantities.

The turbulence kinetic energy profiles from five experiments are plotted together in Figure 5.4. Although the agreement is not good, it will be noted that the profiles of Gutmark and Wygnanski (1976), Heskestad (1965), and Bradbury (1965) form a group which is in relative agreement but greater in magnitude than those of Robbins (1971) and Patel (1970). The recently determined kinetic energy profile of Bashir (1973) also falls within the envelope containing the higher data. Since most of the experimental results fall within this envelope and since the two lower curves were not published (except in thesis form), the envelope of the higher data will be used for comparisons in § 5.7.

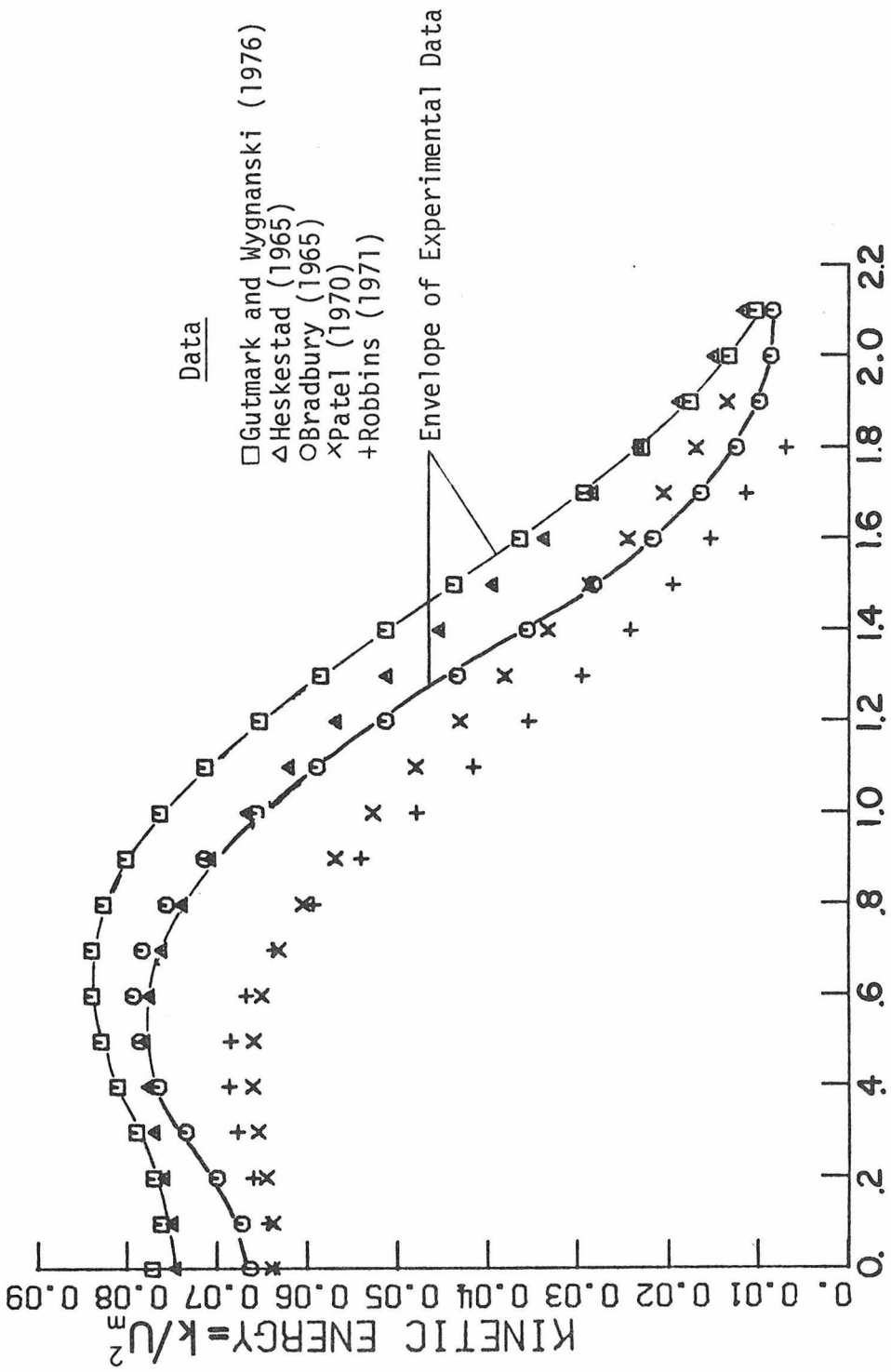

Figure 5.4.--Experimental Determinations of the Turbulent Kinetic Energy: Plane Jet.

We have chosen Heskestad's (1965) experimental determination of the relative intensities (R_{ij}/k) for comparison with our numerical predictions. The data are shown with model predictions (to be discussed in § 5.7) in Figure 5.16. The relative intensities, rather than the absolute values of the Reynolds stresses were used for comparison with numerical calculations, because the various experiments show very little agreement on the absolute values of the individual normal stress components. This is true, in spite of the fact that the kinetic energy profiles (i.e. $k = R_{ii}/2$) are in relative agreement. Since the data for the normal stresses are so inconsistent, only qualitative comparisons between predictions and experiment can be made in the next section.

The shear stress (R_{12}) measurements for the three investigators whose data are included in the turbulent energy envelope (i.e. Bradbury, 1965; Heskestad, 1965; and Gutmark and Wygnanski, 1976) will be used as the target experimental data.

5.6.2 Two-Dimensional Wakes

A. The Turbulent Velocity and Length Scales.

The characteristic length and velocity scales which are commonly used for reduction of experimental data for turbulent wakes are shown in Figure 5.2. Their definition is similar to that used for the plane jet except that the mean velocity defect profile plays the role of the mean velocity profile for the jet. The mean velocity defect U_d is defined as

$$U_d(x,y) = U_E - U(x,y)$$

Table 5.4.--Plane Wakes Behind Circular Cylinders.

Experimenter	Range x/d	$[\phi(\frac{b}{x-x_0})]^{\frac{1}{2}}$	$\frac{u_1'}{U_m}$	$\frac{u_2'}{U_m}$	$\left[\frac{-R_{12}}{U_m^2}\right]_{max}$ exp.	$\left[\frac{-R_{12}}{U_m^2}\right]_{max}$ calc.
Pfeil and Eifler (1975)						
near wake	0- 200	.363	-	-		
far wake	150-1000	.273	.27	.21	.035	.041
Townsend (1956)	80- 950	.298	.27	.31	.0505	.051
Everitt (1971)	120- 800	.334	.26	-	.0364	.050
Alexopoulos and Keffer (1968)	40- 228	.41	.30	-	.033	.055
Reichardt (1942)	30-1200	.353	-	-	-	-
Ermhaus (1970)	80- 240	-	-	-	.035	-
Builtjes (1977)	180- 500	-	.30	-	.038	.045
Uberoi and Freymuth (1969)	25- 800	-	.31	-	-	-
Okamoto et al. (1977)	< 200	.367	-	-	-	-

where U_E is the mean free-stream velocity and U(x,y) is the exact mean velocity. The velocity half-width b(x), calculated using equation (5.6.1) is again used as the characteristic length scale.

Experiments (cf. Townsend, 1956) show that the mean velocity profile becomes self similar for downstream distances $\frac{x}{d} > 80$. However, the turbulence quantities take much longer to become self-similar only for $\frac{x}{d} > 500$ and higher order correlations only for $\frac{x}{d} > 1000$ (Townsend, 1949). At such great distances downstream, the mean velocity defect is quite small and turbulent measurements are difficult to obtain. Consequently, measurements of turbulence quantities in the plane wake do not agree well from one experiment to another.

B. Spreading Rate.

For large distances downstream, the half-width of the mean velocity defect profile varies as $x^{\frac{1}{2}}$. Thus a plot of the normalized half-width squared versus the distance downstream yields a straight-line in the similarity region which can be described by

$$\frac{(b/d)^2}{C_w} = K_1^2\left(\frac{x}{d} + K_2\right) . \qquad (5.6.6)$$

Here C_w is the "drag coefficient" defined by,

$$D' = \frac{1}{2} C_w U_E^2 d \qquad (5.6.7)$$

where D' is the kinematic drag force per unit length (defined in equation (5.2.4)). The coefficient K_1 could be used to define the

spreading rate of the wake but this is not frequently done in the literature. The most common definition is

$$S_1 = \frac{b}{[\theta(x-x_0)]^{\frac{1}{2}}} \tag{5.6.8}$$

Here, S_1 is the spreading rate, x_0 is the virtual origin and $\theta = \frac{C_w d}{2}$ is the so-called "momentum thickness." Using (5.6.7), the momentum thickness can be expressed in terms of the drag, i.e.

$$\theta = U_E^2 D \tag{5.6.9}$$

thus,

$$S_1 = \frac{b}{\left[\frac{D(x-x_0)}{U_E^2}\right]^{\frac{1}{2}}} \tag{5.6.10}$$

This form is convenient for use in the present investigation because it is closely related to the similarity variable η defined in section 5.2, i.e.

$$\eta = \frac{y}{\lambda_1 \left[\frac{Dx}{U_E 2}\right]^{\frac{1}{2}}} \tag{5.6.11}$$

If we denote the position where $y = b$ as $\eta_{\frac{1}{2}}$, it may be seen then that S_1 can be calculated from

$$S_1 = \lambda_1 \eta_{\frac{1}{2}} \tag{5.6.12}$$

The spreading rate, defined by equation (5.6.10) requires a knowledge of the drag coefficient C_w and the virtual origin x_0. Since these quantities are often not given explicitly in the literature, Rodi (1976) suggested the alternative definition

$$S_2 = \frac{U_E}{U_m} \left(\frac{db}{dx}\right) \tag{5.6.13}$$

However, S_2 calculated in this way depends on both the wake width and centerline velocity, i.e. it contains both a length and velocity scale making it less suitable as a measure of spreading rate.

Experimental determinations of the spreading rate S_1 are in apparent conflict. This is illustrated in Table 5.4 where it may be seen that S_1 values range from .27 to .40 for the several experiments which are listed. Fortunately, however, the recent experimental study of Pfeil and Eifler (1975) can be used to resolve the conflict. These authors show that <u>two</u> distinct regions exist where the half width varies as $x^{\frac{1}{2}}$ as illustrated in the following figure which is taken from their paper. In the near-wake, up to approximately $\frac{x}{d} = 180$, the straight line defined by (5.6.6) describes the spreading behavior with $K_1 = 0.257$ and $K_2 = 0.0$. However, in the far-wake, $200 < \frac{x}{d} < 800$ the slope of the line $(b/d)^2/C_w$ vs x/d changes and it is suggested that $K_1 = 0.193$ and $K_2 = 100.0$. The experimental results of the other investigators listed in Table 5.4 verify this behavior. The results of Okamoto et al. (1977) and Schlichting (1930) extend up to $\frac{x}{d} \simeq 200$ and estimates of S_1 determined from their data are consistent with those of Pfeil and Eifler in the near wake

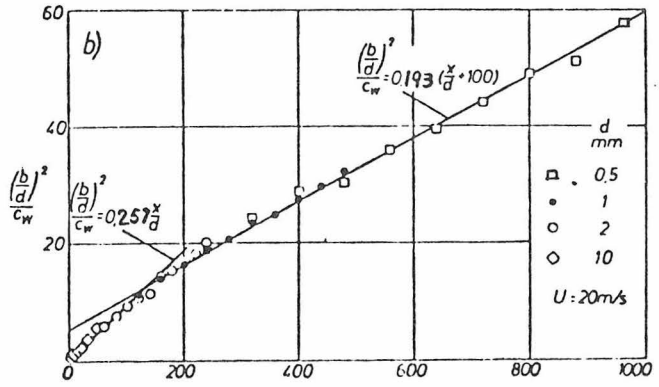

Figure 5.5.--Spreading Rate Two-Dimensional Jet. Source of Data; Pfeil and Eifler (1975).

region. The results of Townsend (1956) extend up to $\frac{x}{d} \simeq 1000$ and the value of S_1 determined from his mean velocity profile, $S_1 = 0.298$ is in closer agreement with the far wake value, $S_1 = .273$ determined from Pfeil and Eifler's data. However, Townsend (1956) does not show a plot like Figure 5.5. so the presence of two regions in his wake could not be verified.

Since assumptions pertinent to the small velocity defect, far-wake were used in the calculations (described earlier), the spreading rate applicable to the asymptotic far wake region will be used for comparison with calculations. The results of Pfeil and Eifler (1975) and Townsend (1956) indicate that

$$.273 \leq S_1 \leq .298.$$

C. Mean Velocity.

As recommended in Rodi (1976) the mean velocity defect measurements of Townsend (1956) will be used for comparison with numerical predictions in the next section. The actual data points used (eg. Figure 5.12) are taken at regular intervals from a curve "faired" through Townsend's experimental data.

D. Second-Order Turbulence Quantities.

Only a few of the investigators listed in Table 5.4 measured all of the non-zero components of the Reynolds stress tensor. Hence the available data for the kinetic energy profile is sparse. The turbulent kinetic energy profiles of three investigators are given in Figure 5.6. The data of Fabris (1974) was taken from Libby (1976), and that of Everitt (1971) from Rodi (1976). Except on the wake-axis, these recent results are comparable. The kinetic energy profile of Townsend (1956) is probably too high (particularly on the wake centerline). This hypothesis is supported by the considerations of the next several paragraphs.

The r.m.s. values of the normalized streamwise Reynolds stress component [i.e. $\frac{u_1}{U_m} = \frac{R_{11}^{\frac{1}{2}}}{U_m}$] are listed in Table 5.4 for several of the experiments. The value $\frac{u_1}{U_m} = 0.27$ obtained by Townsend (1956) agrees well with the recent determination of Pfeil and Eifler (1975). However, the experimental determinations of Uberoi and Freymuth (1969) and Builtjes (1977) are approximately 10 percent greater (i.e. $\frac{u_1}{U_m} = .3$). Although these might suggest that the results of Townsend and Pfeil and Eifler are too low, the results of Uberoi

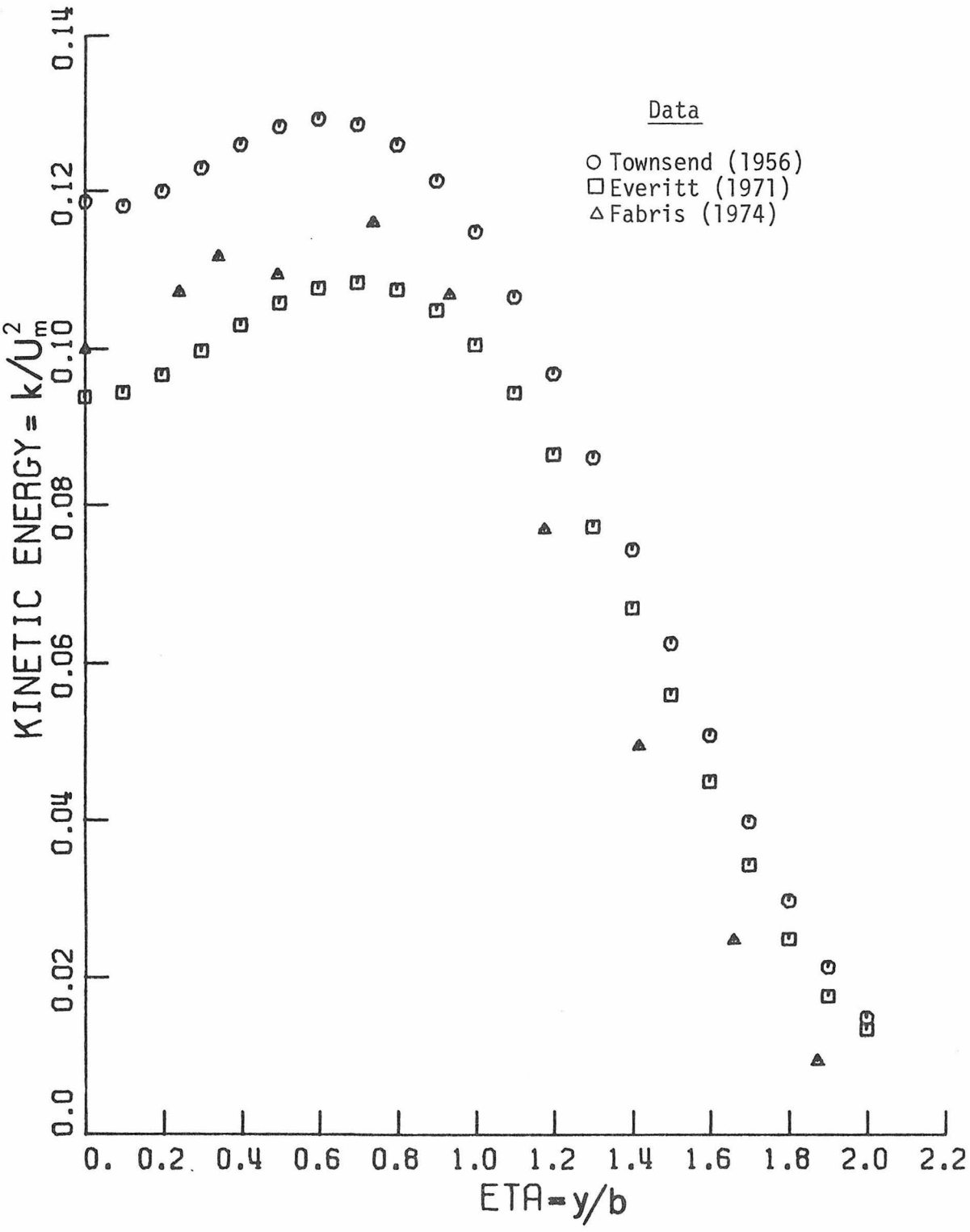

Figure 5.6.--Experimental Determinations of Turbulent Kinetic Energy: Plane Wake.

and Freymuth (1969) and Builtjes (1977) are incomplete in the sense that only the single normal stress component R_{11}, was measured. Furthermore, the $h(\tilde{n}) = \frac{R_{11}}{U_m^2}$ profiles of Townsend and Pfeil and Eifler (1975) are in close agreement as shown in Figure 5.7. Hence these two profiles will be used for comparison with calculations in § 5.7.

Only Townsend (1956) and Pfeil and Eifler (1975) measured the R_{22} component of the Reynolds stress tensor in the far-wake region and their results are in substantial disagreement. Townsend reported a centerline value for $e(\tilde{n}) = \frac{R_{11}}{U_m^2}$ of 0.0965, whereas Pfeil and Eifler found $e(0) = 0.0441$ as shown in Table 5.5. It should be noted, however, that Townsend's (1956) result yields $R_{22} > R_{11}$ on the wake centerline and this result is contrary to <u>all</u> other wake studies where the Reynolds stress components were measured. These studies include the wake behind a thin flat plate, investigated by Chevray and Kovasznay (1969), which is not listed in Table 5.4. For this reason, we believe that the results of Pfeil and Eifler for R_{22} are more likely to be correct than those of Townsend (1956) and we adopt them for purposes of numerical comparison. The <u>only</u> available data for the $d(\tilde{n}) = \frac{R_{33}}{U_m^2}$ component are those of Townsend (1956). Hence these must be used for comparison with our numerical results. The centerline values of the normalized Reynolds stresses are compared in the following table.

A turbulent kinetic energy can be determined from Table 5.5. The normalized turbulent energy on the centerline is

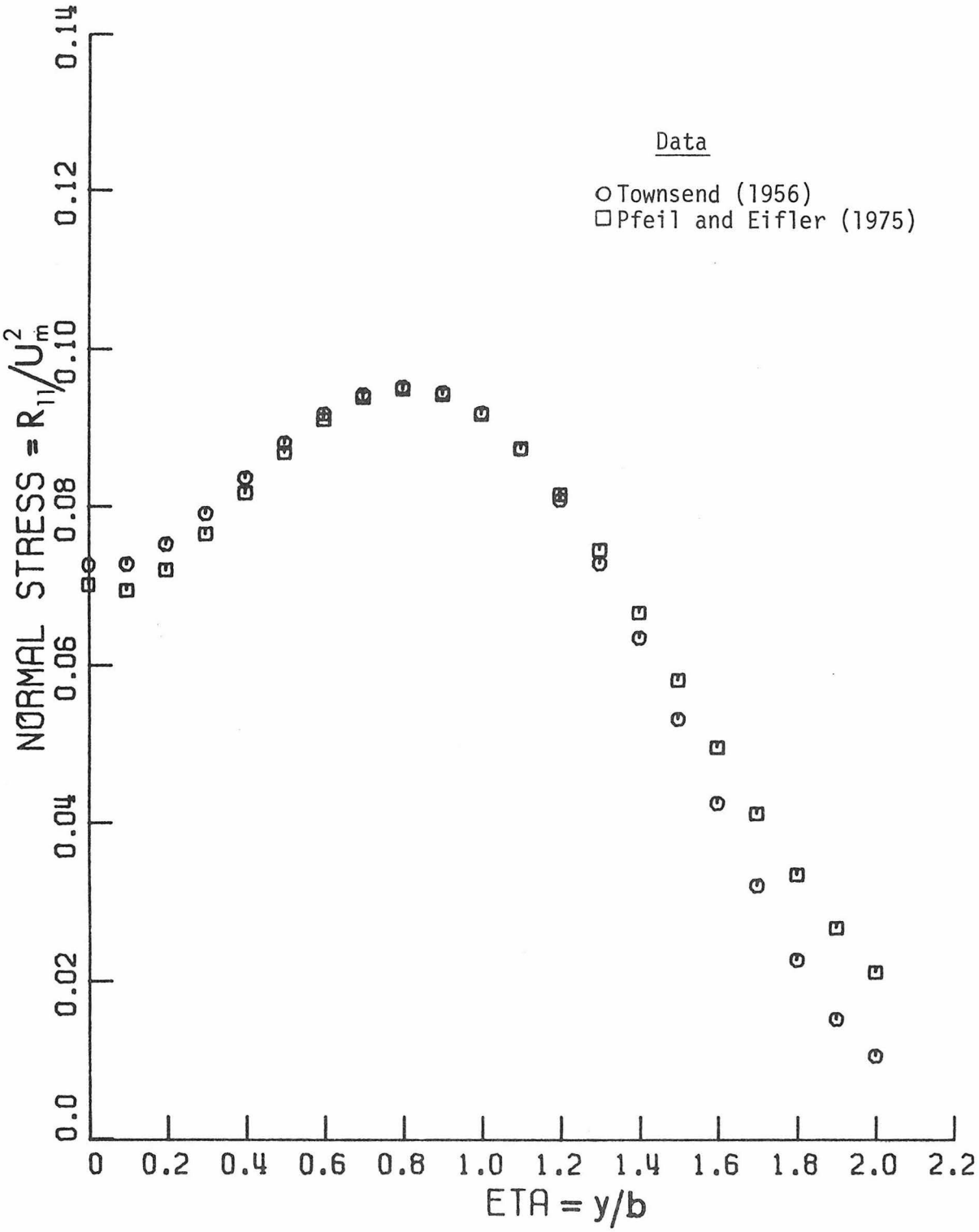

Figure 5.7.--Experimental Determinations of Streamwise Normal Stress Component: Plane Wake.

Table 5.5.--Normalized Reynolds Stresses on Wake Centerline.

	$\frac{R_{11}}{U_m^2}$	$\frac{R_{22}}{U_m^2}$	$\frac{R_{33}}{U_m^2}$
Magnitude on Centerline	.0728	.0441	.0678
Source of data	Pfeil and Eifler (1975) Townsend, (1956)	Pheil and Eifler	Townsend

$\frac{k(0)}{U_m^2} = h(0) + e(0) + d(0) = 0.0923$. This is in agreement with the results of Everitt shown in Figure 5.6.

All three of the kinetic energy profiles shown in Figure 5.6 will be used for comparison with the calculations in the next section and the normal stresses determined by the experimenters identified in Table 5.5 will also be used. As was the case for the jet, only qualitative comparisons with the data can be made because of the uncertain quality of the data.

The maximum values of the Reynolds shear stress $\frac{R_{12}}{U_m^2}$ obtained in several investigations are given in Table 5.4. These results are in good agreement with each other but in each case, they are substantially smaller than the maximum shear stress that can be calculated from the mean momentum equation. No reasons are offered in any of the experimental papers for this discrepancy. The shear stress profile of Pfeil and Eifler was chosen for comparison with

our numerical results because, for the most part, we have used their other turbulent profiles as our target cases.

In the next section, the experimental results described here for the jet and wake will be compared with the profiles predicted using the MRS model.

5.7 Similarity Solutions for Plane Jets and Plane Wakes

The ability to predict the turbulence quantities for a turbulent free shear flow is a demanding test for any turbulence model. In this section, the predicted mean velocity and second-order turbulence profiles for the two dimension jet and wake are calculated using both the τ-k-ε and MRS models and the results compared to the experimental data described in the last section. As a preliminary, the numerical scheme described in § 5.5 was tested by carrying out calculations using Rodi's (1972) τ-k-ε model, equation (4.3a,b,c), and comparing the results to Rodi's original numerical profiles which were obtained by a different method. Next, the τ-k-ε model developed in Chapter 4, with the constants determined there (see Table 4.2), was also used to predict profiles for the quantities, U, τ and k. These calculations were primarily intended to obtain an initial iterate for the full MRS model. However, the τ-k-ε model is of some interest in itself and the results of these calculations are compared with the available experimental data. Finally, calculations are obtained using the full MRS model.

5.7.1 Validation of the Calculation Procedure

As a preliminary to obtaining solutions of the plane wake and jet flow problems using the models developed in Chapters 2, 3 and 4 of this thesis, solutions were obtained for the τ-k-ε model of Rodi (1972) using the computational techniques which were described in the earlier sections of this chapter. In particular, Rodi's (1972) model was transformed to similarity form and the resulting boundary-value problem was solved using Keller's "box" scheme. The primary purpose of these initial calculations was to verify the accuracy and computational utility of the proposed numerical algorithm for a case where the solution was known. The original calculations of Rodi (1972) utilized the governing model equations in their full parabolic p.d.e. form and employed an explicit finite difference method developed by Patankar and Spalding (1970) for boundary-layer calculations. The method integrates by marching forward (i.e. downstream), starting at some initial station where profiles are assumed for U, τ, k and ε. Some distance downstream the calculated profiles become self-similar (hence independent of the initial profiles) and the integration is terminated.

The computed profiles of mean velocity, turbulent energy and shear stress for the plane jet are compared for the two calculation methods in Figure 5.8. The turbulence quantities (τ, k, U) have all been normalized by the mean centerline velocity (which is the velocity scale most commonly used by experimenters) and are plotted against the dimensionless similarity co-ordinate, $\tilde{\eta} = y/b(x)$, where b(x) is the velocity "half-width." The solid lines are predictions obtained

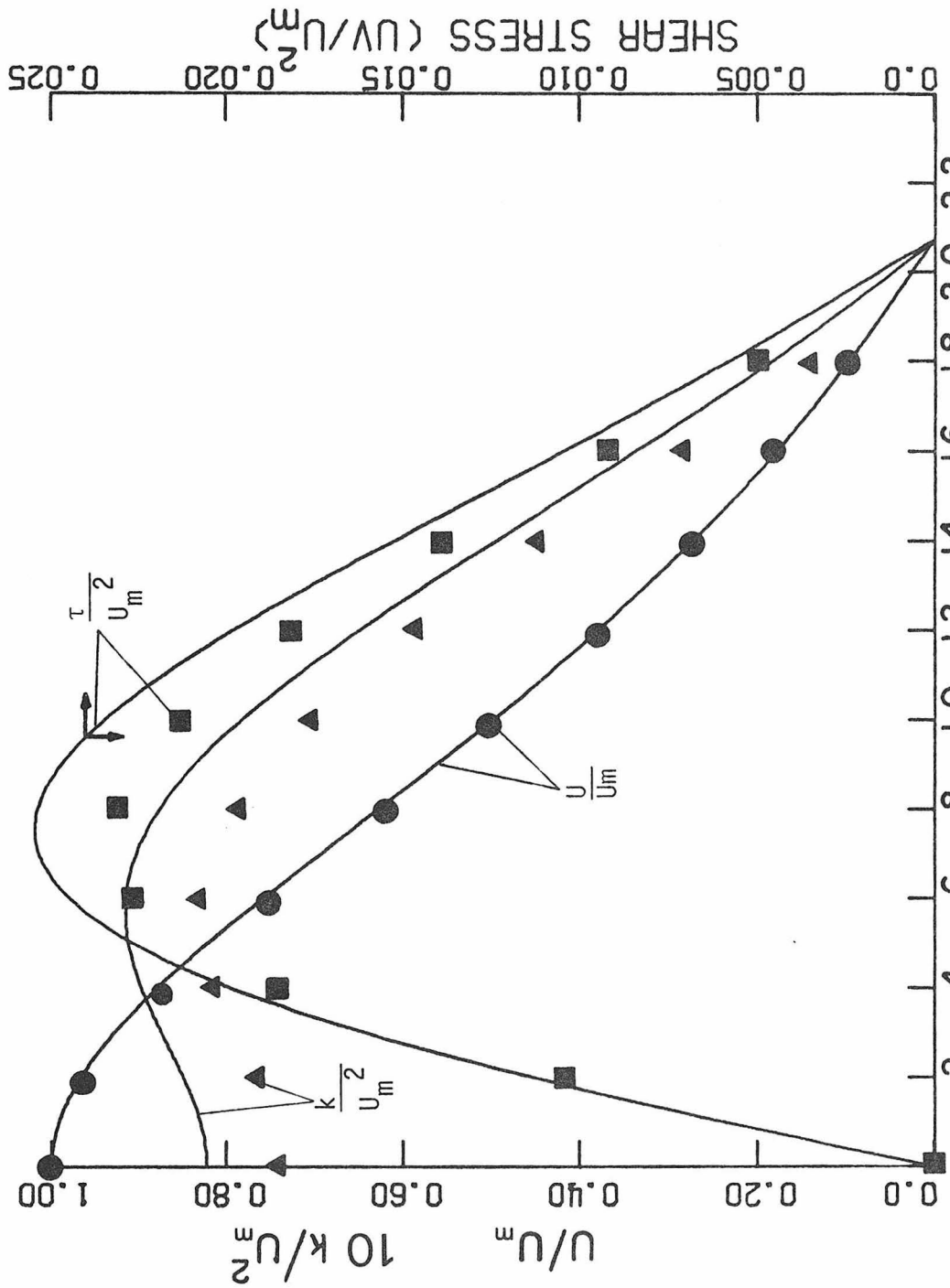

Figure 5.8.--τ-k-ε Model Predictions, Plane Jet. Points are Calculated Results of Rodi (1972), Lines are Present Calculations.

from Rodi's (1972) model by solving the similarity equations using the calculation scheme which is developed in § 5.5 of this thesis. The points are the original results given by Rodi (1972) for the self-similar region using exactly the same τ-k-ε model.

The normalized mean velocity profiles plotted in Figure 5.8 are coincident. However, the kinetic energy and shear stress profiles determined by Rodi are approximately 10 percent lower than those obtained using the present scheme. The reason for this discrepancy may be due to differing estimates of the centerline jet velocity for the two cases. In the current method, the mean centerline velocity is given directly using the similarity function $f(\eta)$

$$\text{i.e.} \qquad f(0) = \frac{U_m}{(J/x)^{\frac{1}{2}}} = 2.4 \qquad (5.7.1)$$

Rodi does not report a calculated value for the centerline velocity. It may be noted, however, that a 5 percent decrease in $f(0)$ would cause the kinetic energy and shear stress profiles to become coincident.

In Figure 5.9 the calculated profiles for the plane wake are shown. The mean velocity defect, turbulent energy and shear stress, all normalized by the mean velocity defect, are compared with Rodi's (1972) original profiles. Here again the two mean velocity profiles are coincident, while the turbulent energy and shear stress predicted by Rodi are about 10 percent less than those obtained using the present computational scheme.

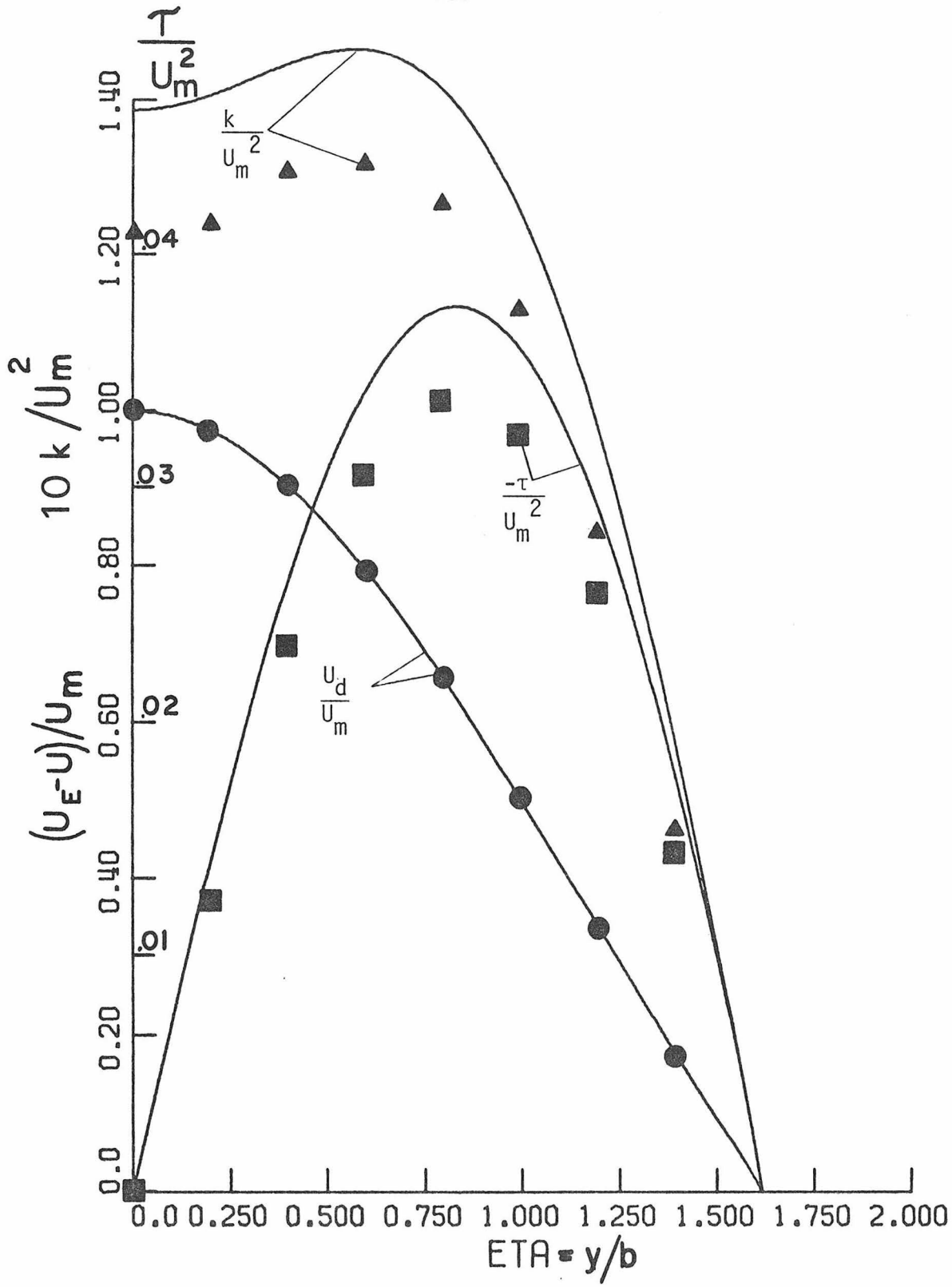

Figure 5.9.--τ-k-ε Model Predictions, Plane Wake. Points are Calculations of Rodi (1972), Lines are Present Calculations.

In Table 5.6 the spreading rates, defined in § 5.6 (equation (5.6.2) for the jet and equation (5.6.13) for the wake), are compared for the two calculation schemes. It is evident that the predicted rates of spread are essentially the same. Thus, apart from a deduced discrepancy in the predicted centerline mean velocity, the present calculation scheme yields predictions which are in agreement with those of Rodi (1972) who used an entirely different approach.

Table 5.6.--Calculated Spreading Rates.

Method	Jet	Wake
Present	.117	.072
Rodi (1972)	.114	.069

5.7.2 Simple Model Solutions

In an effort to determine an initial guess for the MRS calculations the τ-k-ε model derived in Chapter 4 was used to predict profiles for U, τ, k and ε for the plane jet and plane wake. These predictions are compared to the experiments and to the present predictions using Rodi's (1972) estimate of the constants (given in Table 4.2) in Figures 5.10 - 5.13. Specifically, in Figure 5.10 the calculated mean velocity and shear stress profiles for the plane jet are compared with the best experimental data as outlined in the previous section as well as with the profiles from Rodi's (1972) model (these are identical to the profiles in Figure 5.8). The kinetic energy profile is compared to the envelope of experimentally

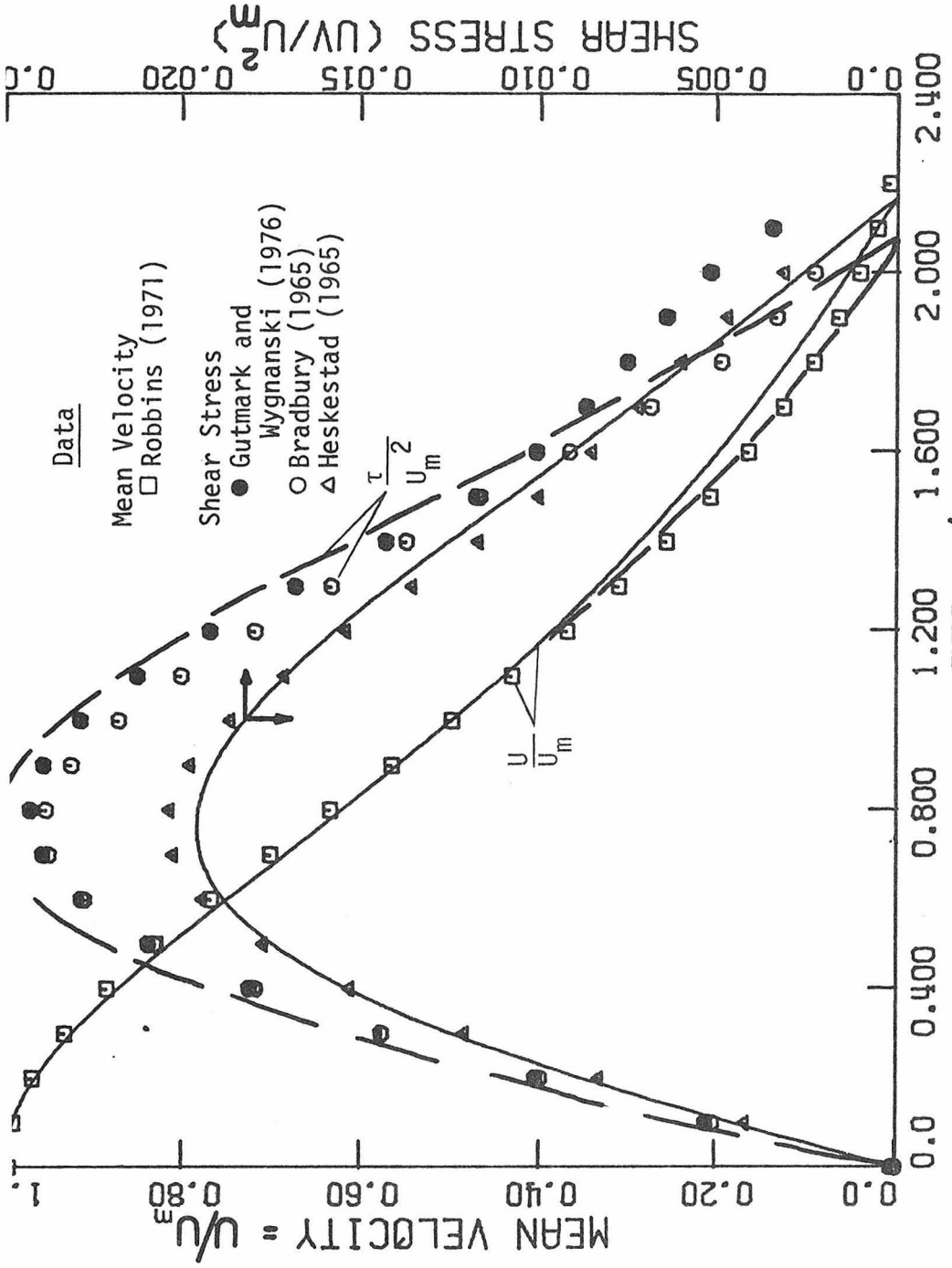

Figure 5.10.--τ-k-ε Model Calculations of the Mean Velocity and Shear Stress for the Plane Jet, ———, Present Model; - - - , Rodi (1972) Model.

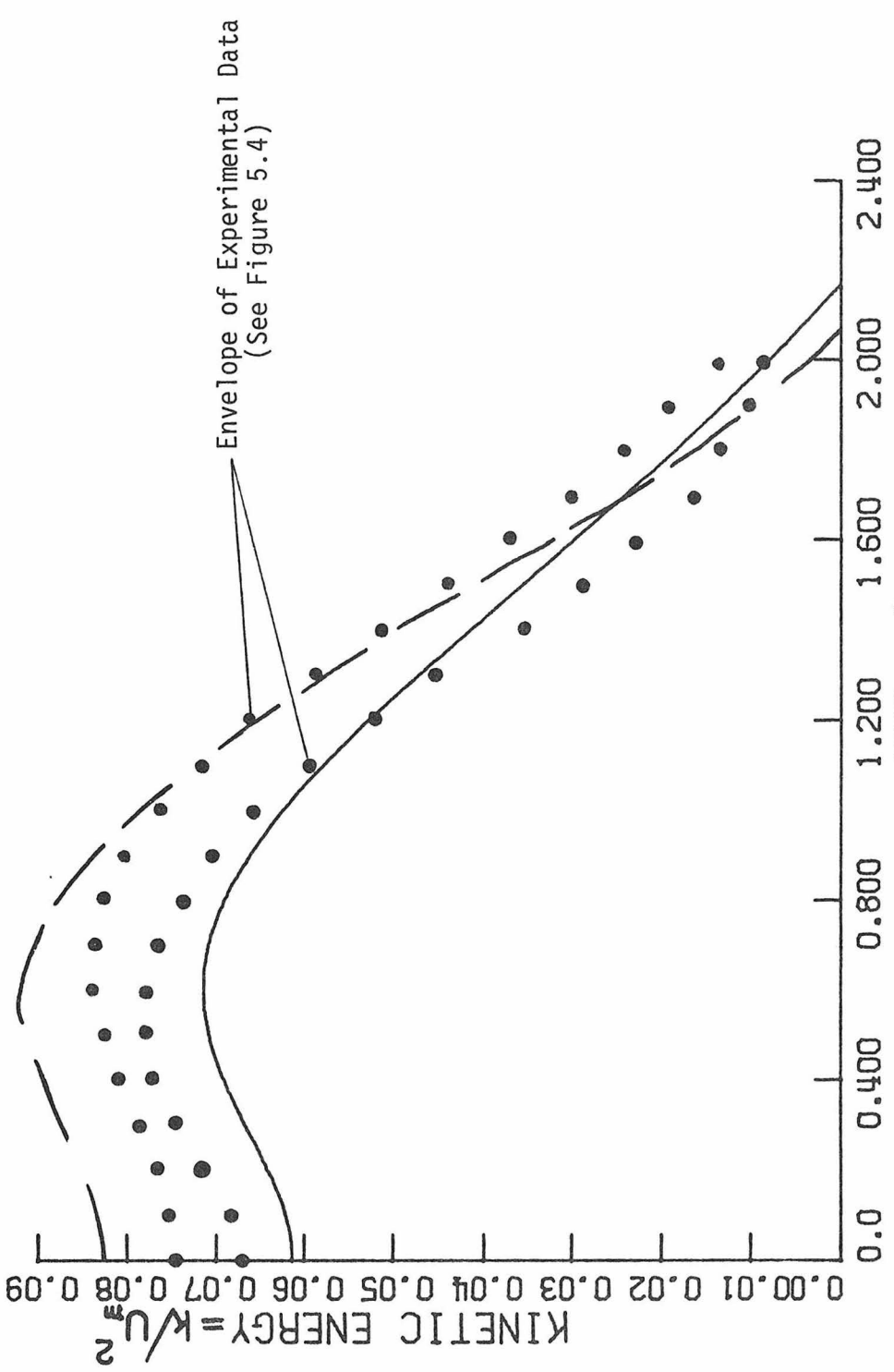

Figure 5.11.--τ-k-ε Model Calculations of the Kinetic Energy for the Plane Jet, _____, Present Model; - - - - - Rodi (1972) Model.

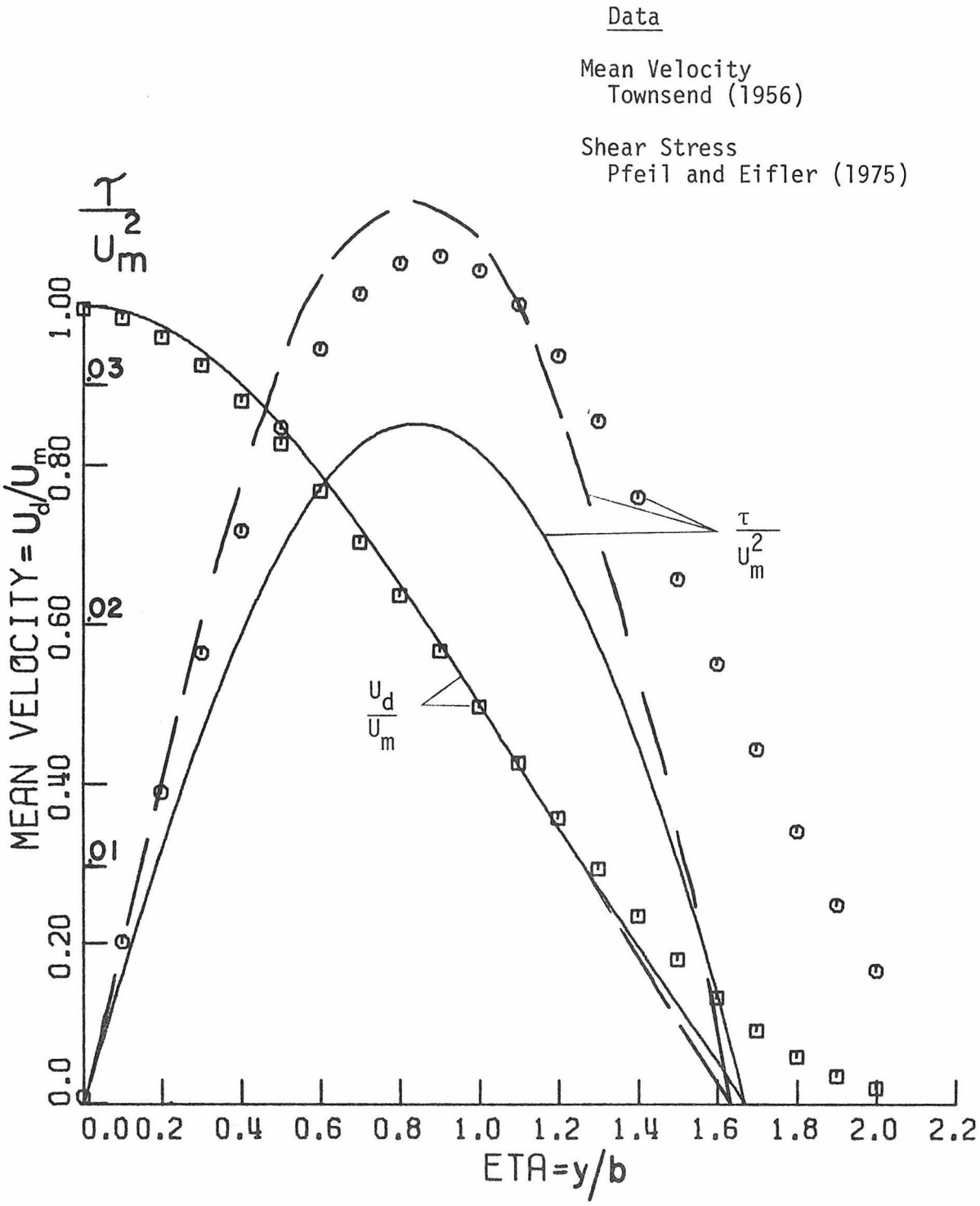

Figure 5.12.--τ-k-ε Model Calculations of the Mean Velocity and Shear Stress for the Plane Wake, _____, Present Model; - - - -, Rodi (1972) Model.

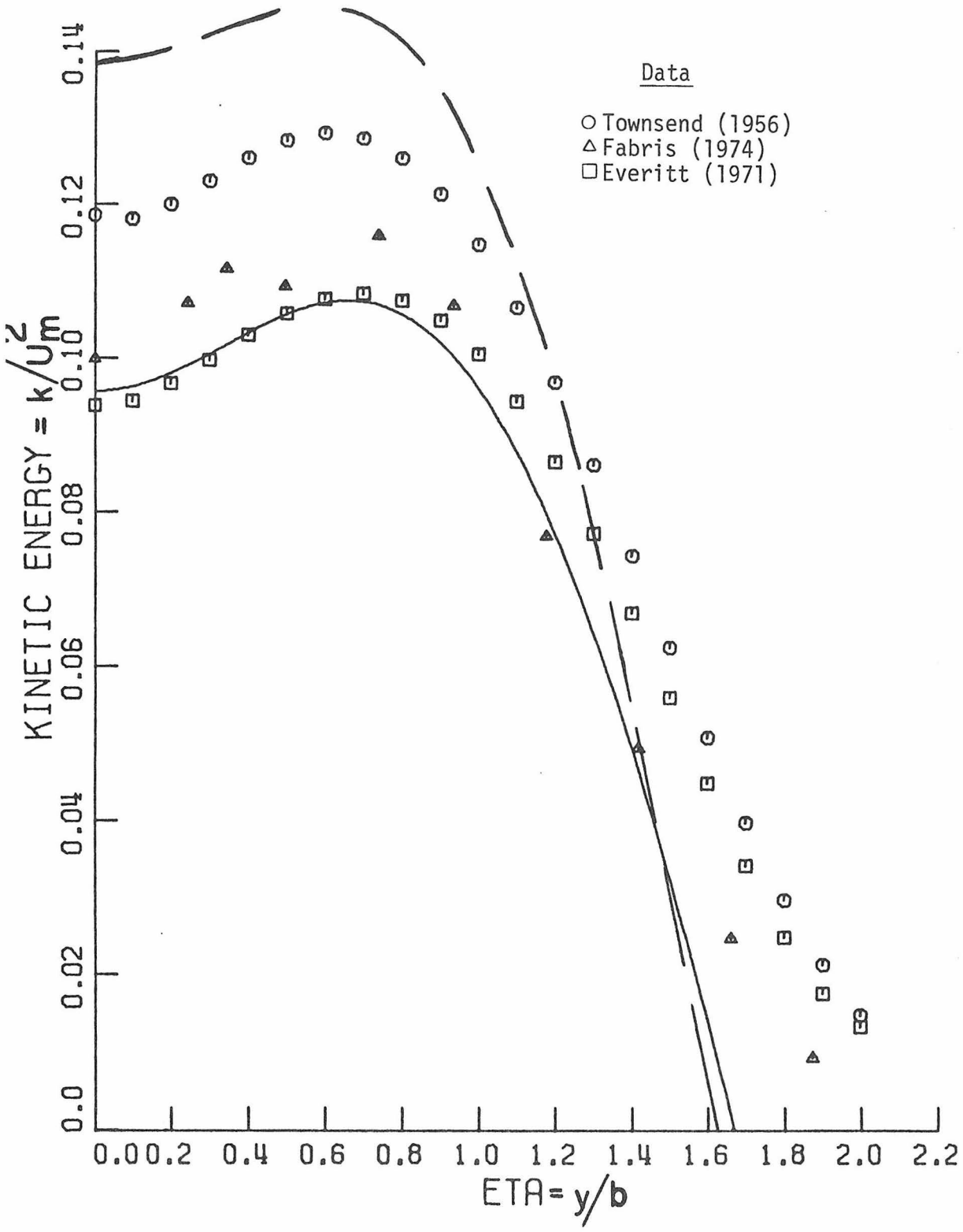

Figure 5.13.--τ-k-ε Model Calculations of Kinetic Energy for the Plane Wake, _____, Present Model; - - - -, Rodi (1972) Model.

determined turbulent energy and to the results using Rodi's constants in Figure 5.11. These comparisons are repeated for the plane turbulent wake in Figure 5.12 and 5.13. The results for both flows using our present τ-k-ε model are closely comparable to the predictions for the full MRS model and these will, therefore, be discussed in detail in the next section. However, it is worth noting here that the present τ-k-ε model, which is based on the parameter estimations of Chapter 3, provides a somewhat better estimate of the turbulence profiles (i.e. τ and k) than the Rodi (1972) model.

5.7.3 MRS Model Predictions

The solutions obtained in the previous section using the τ-k-ε model were used to generate our initial guess for the full Reynolds stress calculations. Initial profiles for the individual normal stress components were determined from the equation, $R_{ij} = a_{ij}\, k$, where the coefficients a_{ij} are the same as those used to construct the τ-k-ε model (and given in Table 4.1). The governing MRS model equations and boundary conditions were given previously in § 5.5.1B for the jet and § 5.5.2B for the plane wake. The model constants determined in Chapter 3, are repeated for convience in Table 5.7. Also shown, for purposes of comparison, are the coefficients suggested by Launder, Reece and Rodi (1972, called LRR hereafter). The present model contains some terms not present in the LRR model. These are denoted by a coefficient of zero in the LRR model. The LRR model has undergone more complete testing on isothermal flows than any other model and provides the best predictions of these flows. Hence,

Table 5.7.--Values of Coefficients Used in MRS Models.

Coefficient	MODEL	
	Present	Launder, Reece and Rodi (1975)
α_0	- .333	- .291
β_0	1.25	1.5
β_1	1.79	0.0
β_2	-1.39	0.0
C_s	0.11	0.11
ψ_0	1.90	1.90
ψ_2	1.45	2.88
C_ε	0.15	0.15

NOTE: All of the numerical values of the coefficients in Table 5.7 are local to Chapter 5 because the kinetic energy $k(=\frac{1}{2}q^2)$ has been used to non-dimensionalize the equations instead of q^2 and the numerical factor $\frac{1}{2}$ has been absorbed into the coefficients.

the LRR model provides a useful basis for comparison with the results from our present model. It is important to note, however, that LRR determined some of the constants in their model by optimizing the predictions for a number of flows, including the turbulent jet. The present model on the other hand, is determined entirely by the (mainly asymptotic) data for homogeneous flows.

The calculated profiles of the turbulence quantities for the plane jet are presented in Figures 5.14 to 5.16. Also shown, for purposes of comparison, are the "best" available experimental data (discussed earlier in this chapter). In Figure 5.14 we compare the

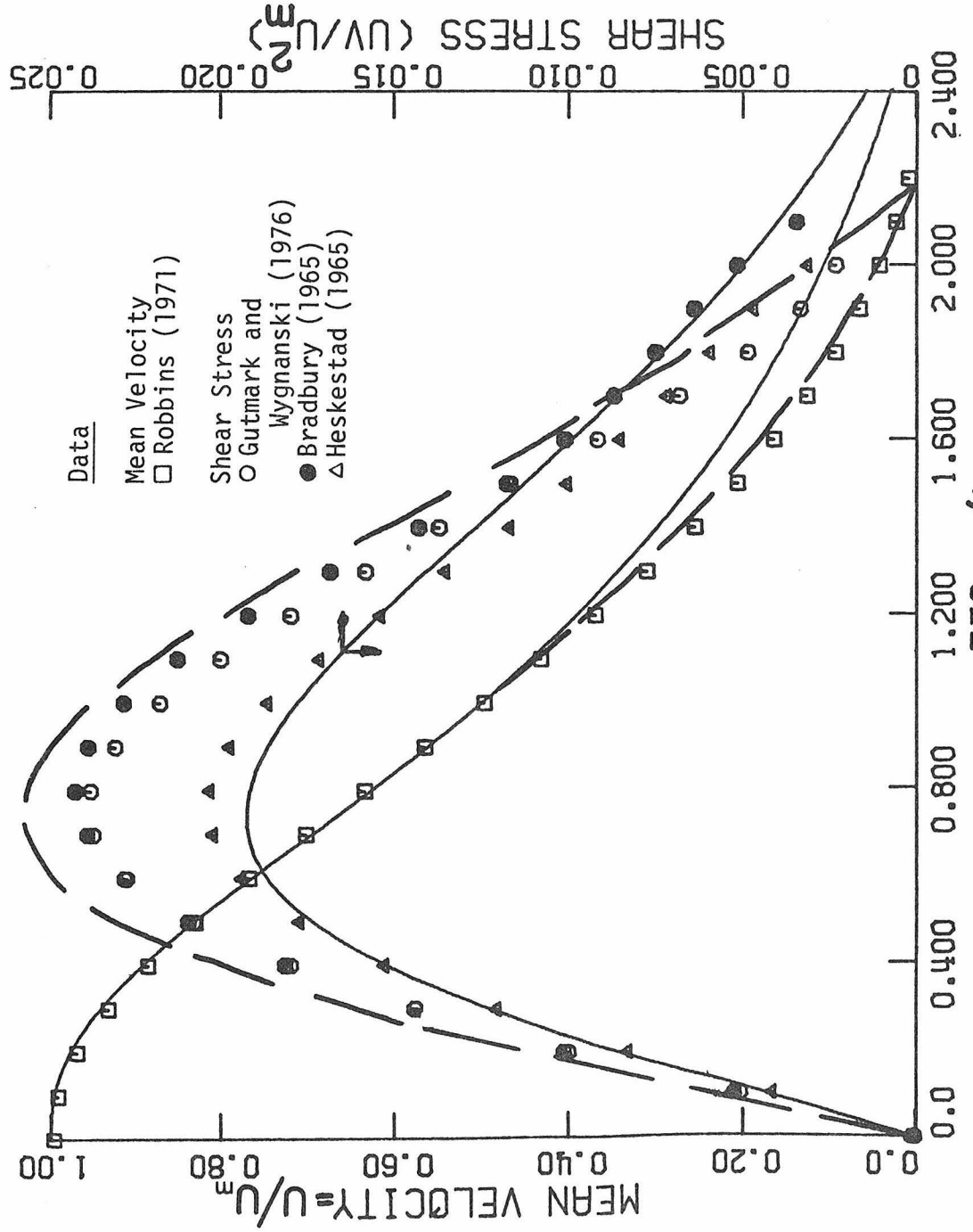

Figure 5.14.--MRS Model Calculations of the Mean Velocity and Shear Stress for the Plane Jet, ——, Present Model; - - - -, Model of LRR.

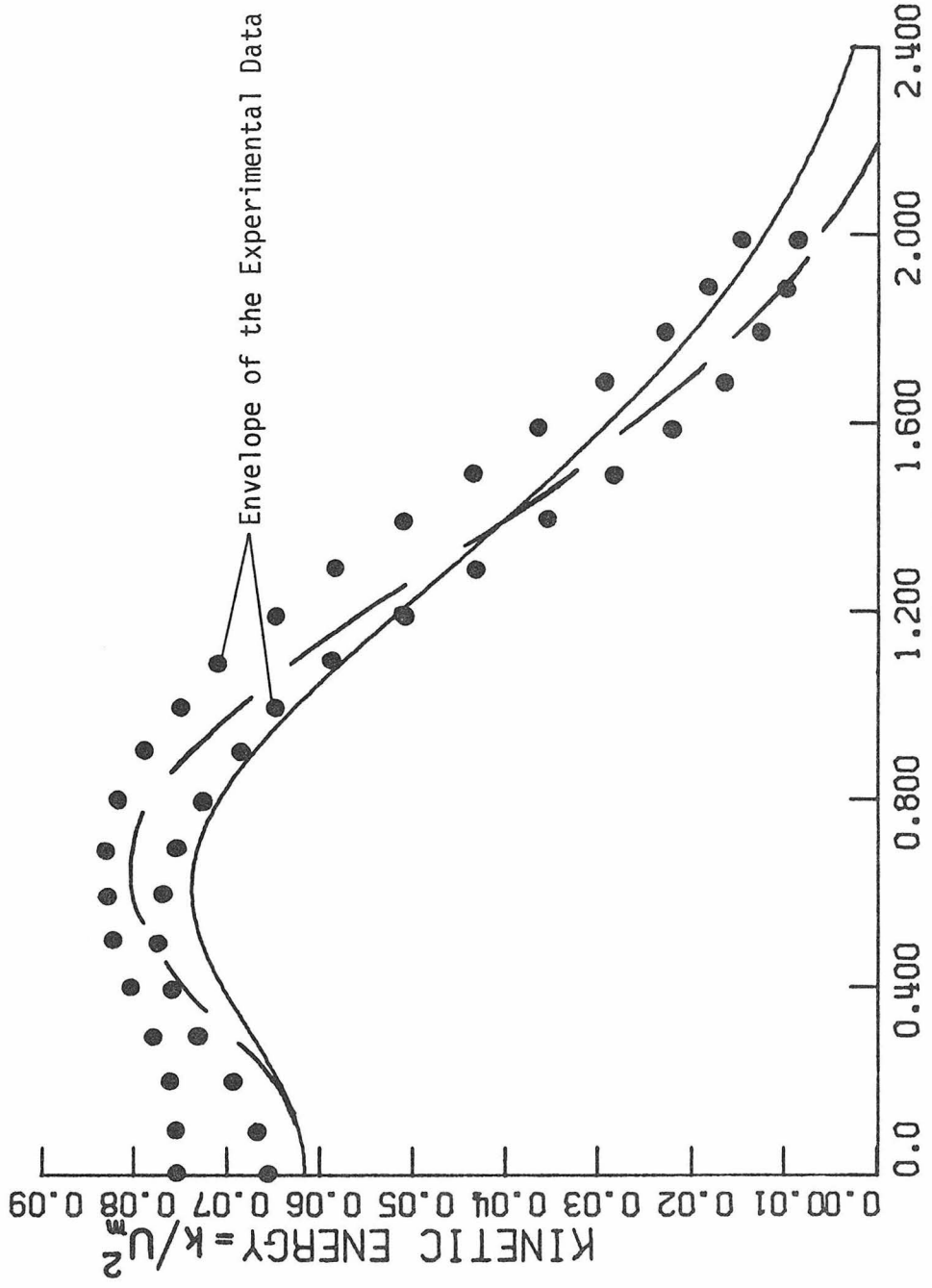

Figure 5.15.--MRS Model Calculation of Kinetic Energy for Plane Jet. Lines have same meaning as Figure 5.14.

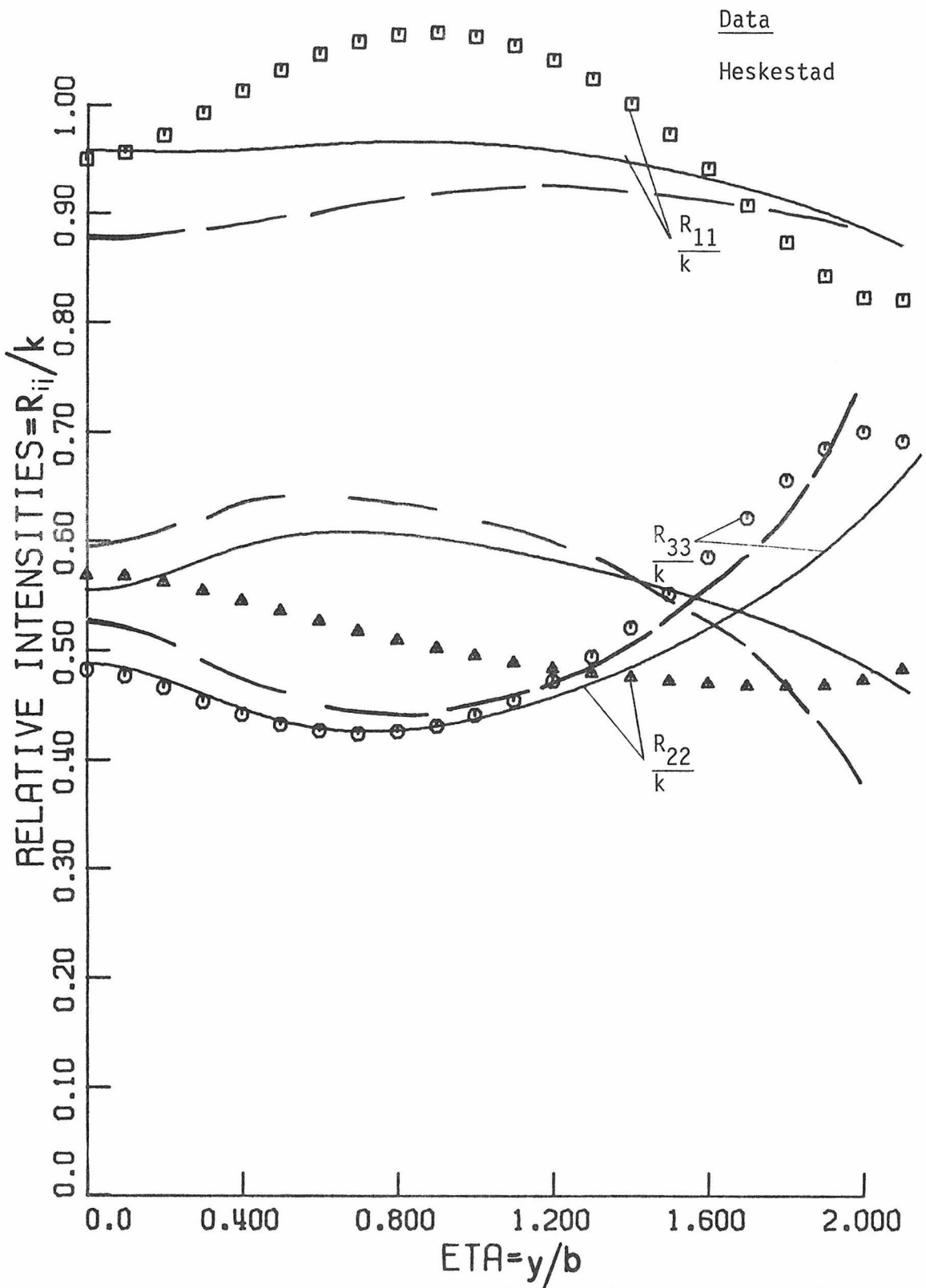

Figure 5.16.--MRS Model Calculations of the Relative Reynolds Stresses for the Plane Jet. Lines have same meaning as in Figure 5.14.

mean velocity profile from the present MRS model to the experimental data of Robbins (1971), and the shear stress profile to the data of Gutmark and Wygnanski (1976), Bradbury (1965) and Heskestad (1965). The calculated mean velocity profile agrees well with the data up to $\tilde{\eta} = 1$ but is slightly too high in the outer portion of the jet. The predicted shear stress, on the other hand, agrees well with the data of Heskestad (1965) but is somewhat lower than the remaining data sets in the central part of the jet. Since the shear stress is related to the slope of the mean velocity, any under prediction of the shear stress (for example, near $\tilde{\eta} = 1$ in Figure 5.14) will yield a slope for the mean velocity profile which is too small.

The calculated kinetic energy profile is compared to the envelope of the available data (see section 5.6 for discussion) in Figure 5.15. The qualitative features of the experimental curves are well predicted. Quantitatively, however, the predicted kinetic energy appears to be somewhat low near the jet centerline. The relative intensities of the normal stress components are compared with the experimental data of Heskestad (1965) in Figure 5.16. Again the predictions are in qualitative agreement with the data. In particular the relative ordering $R_{11} > R_{33} > R_{22}$ on the jet centerline is seen to agree with the data. Furthermore, the predicted magnitudes are in reasonable agreement with the data, though the detailed functional dependent on $\tilde{\eta}$ is only fair for R_{11} and R_{33}.

Figures 5.14 to 5.16 also contain predictions obtained using the model of LRR calculated using the present numerical scheme.

From these figures the following points of comparison can be made between the two models:

(1) The model of LRR gives a somewhat better prediction of the mean velocity, but overpredicts the shear stress relative to the present model.

(2) The kinetic energy profiles of the two models are comparable. The slightly higher maximum obtained using the LRR model is due to the larger predicted shear stress values.

(3) The relative intensity profile predictions are comparable, with the present model giving marginally better predictions.

(4) The predicted spreading rates are given in Table 5.8.

Table 5.8.--Spreading Rate Predictions Versus Experiment.

Model	K_1 (Spreading Rate)
Present	.089
LRR - - -	.117
Experiment	.091

The spreading rate is seriously over-predicted using the LRR model, but predicted in good agreement with experiment by the present model. The reasons for the differences in the two predictions will be discussed after the wake solutions are presented. However, it

should be reiterated here that the present model is determined entirely on the basis of homogeneous data (except for the diffusion terms which are identical with those of LRR, see § 2.7), while the LRR model actually utilized jet data in the determination of the model constants. It is thus gratifying (and even somewhat surprising) that our model yields results for the jet which are equally good as the LRR model.

Calculated profiles of the turbulence quantities for a plane turbulent wake are presented in Figures 5.17 to 5.19. In Figure 5.17 the predicted mean velocity profile both for our model and for LRR is compared to Townsend's (1956) experimental curve. In addition, the predicted shear stress distributions are compared to the data of Pfeil and Eifler (1975). In this case the mean velocity is under predicted by both models for $\tilde{\eta} > 1.0$ and the predicted width of the wake is appreciably less than the experimentally determined value. This is better illustrated by considering the eigenvalue λ_1 which is the location of the wake's edge (see § 5.3). The calculated values (for both the present model and LRR) are $\lambda_1 \simeq .40$ whereas the measured value (Townsend, 1956) is $\lambda_1 \simeq .60$. The poor prediction for the mean velocity profile can be traced to the fact that the predicted shear stress profile is considerably below the data. A possible cause of these relatively poor predictions will be discussed at the end of this chapter.

In Figure 5.18 the turbulent kinetic energy predictions are compared to the kinetic energy data of Townsend (1956), Everitt (1971) and Fabris (1974). As was the case for the jet, the

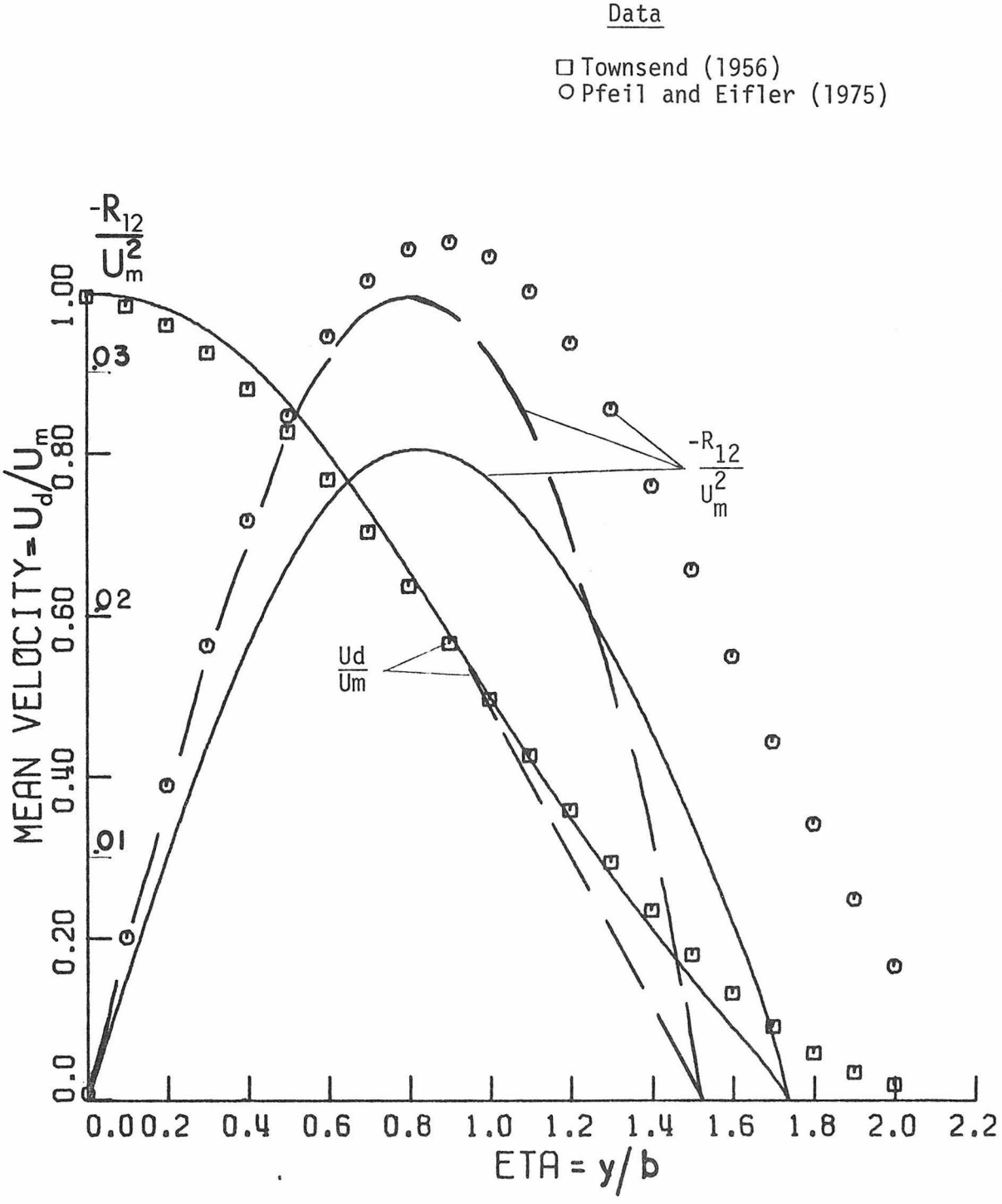

Figure 5.17.--MRS Model Calculations of the Mean Velocity and Shear Stress for the Plane Wake. Lines have same meaning as in Figure 5.14.

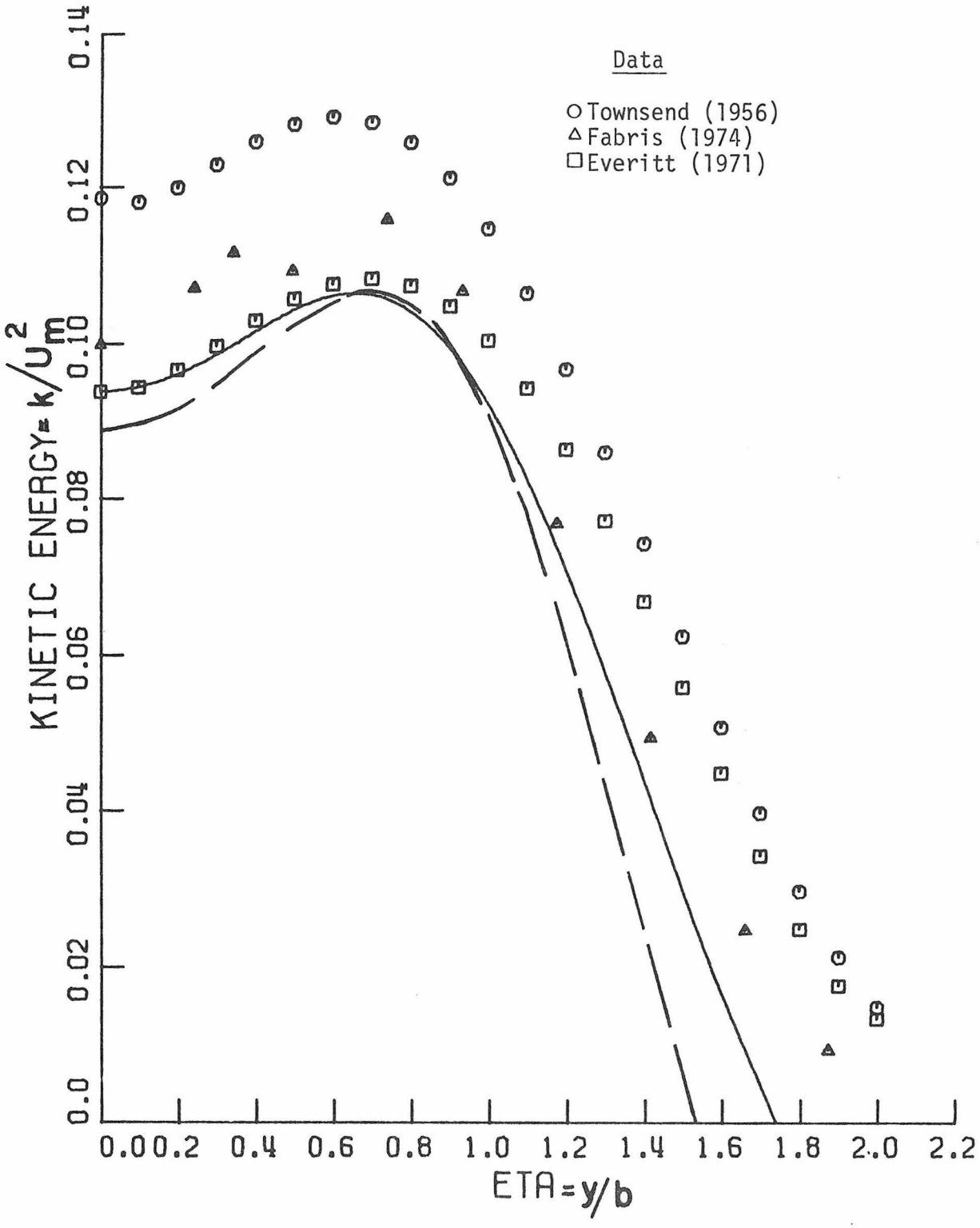

Figure 5.18.--MRS Model Calculations of the Kinetic Energy for the Plane Wake. Lines have Same Meaning as in Figure 5.14.

qualitative agreement is good, allowing for the under-prediction of the wake width. The present model predictions are slightly greater than those of LRR and this fact yields a marginal improvement in the present model relative to the data. The normal components of the Reynolds stress tensor are compared to the data of Townsend (1956) and Pfeil and Eifler (1975) in Figure 5.18. It may be seen that $h(\tilde{\eta}) = (R_{11}/U_m^2)$, is over-predicted and $e(\tilde{\eta}) = (R_{33}/U_m^2)$ is under-predicted relative to the data. However, as suggested in § 5.6, the experiments of Uberoi and Freymuth (1969) and Builtjes (1977) suggest that $h(\tilde{\eta})$ may be greater than the determination of Townsend (1956) or Pfeil and Eifler (1975). Thus the present predictions may not be too bad over the central part of the wake. In addition it should be pointed out that, while it is the Reynolds stresses which are plotted, it is their r.m.s. values that are actually measured. Thus an apparent 20 percent error in the stress prediction reflects only a 10 percent error in its predicted r.m.s. value. With these facts in mind, the predicted stress components (with both models) are in reasonable agreement with the experimental data.

The calculated spreading rates S_1, determined using equation (5.6.12) are compared to the available data in Table 5.9. For the case of the wake, both the present model and LRR under-predict the spreading rate. As in the case of the jet, the spreading rate calculated using the LRR model is greater than that determined using the present model.

Table 5.9.--Wake Spreading Rates, S_1, for Predictions and Experiment.

Model	S_1
Present	.226
LRR - - -	.254
Experiment	.273-.300

5.7.4 Discussion of the Results

The comparison between data and predictions will be discussed in two ways. First, the two models which we have considered are compared with the data, and secondly the predictions of the present model are compared with those determined using the LRR model. Generally speaking, both models provide a useful qualitative prediction for the plane jet, and, in fact, certain qualitative features are modeled very well. However, for the wake, the width of the turbulent region measured in terms of y/b is very poorly predicted. We feel that this is due to the inherent intermittency and unsteadiness of the wake in the experimental situation. The solutions presented for the wake are similarity solutions in which the edge of the turbulent region is inherently assumed to be sharp and steady. Instantaneous photos of the wake (cf. Figure 11, Grant, 1958) show that the edge is sharp but unsteady and intermittent. Of course this is true for the jet as well, but the jet is fully turbulent over a greater fraction of its width than the wake. This is illustrated in Figure 5.20. In this figure, the intermittency factor γ is the fraction of the time that

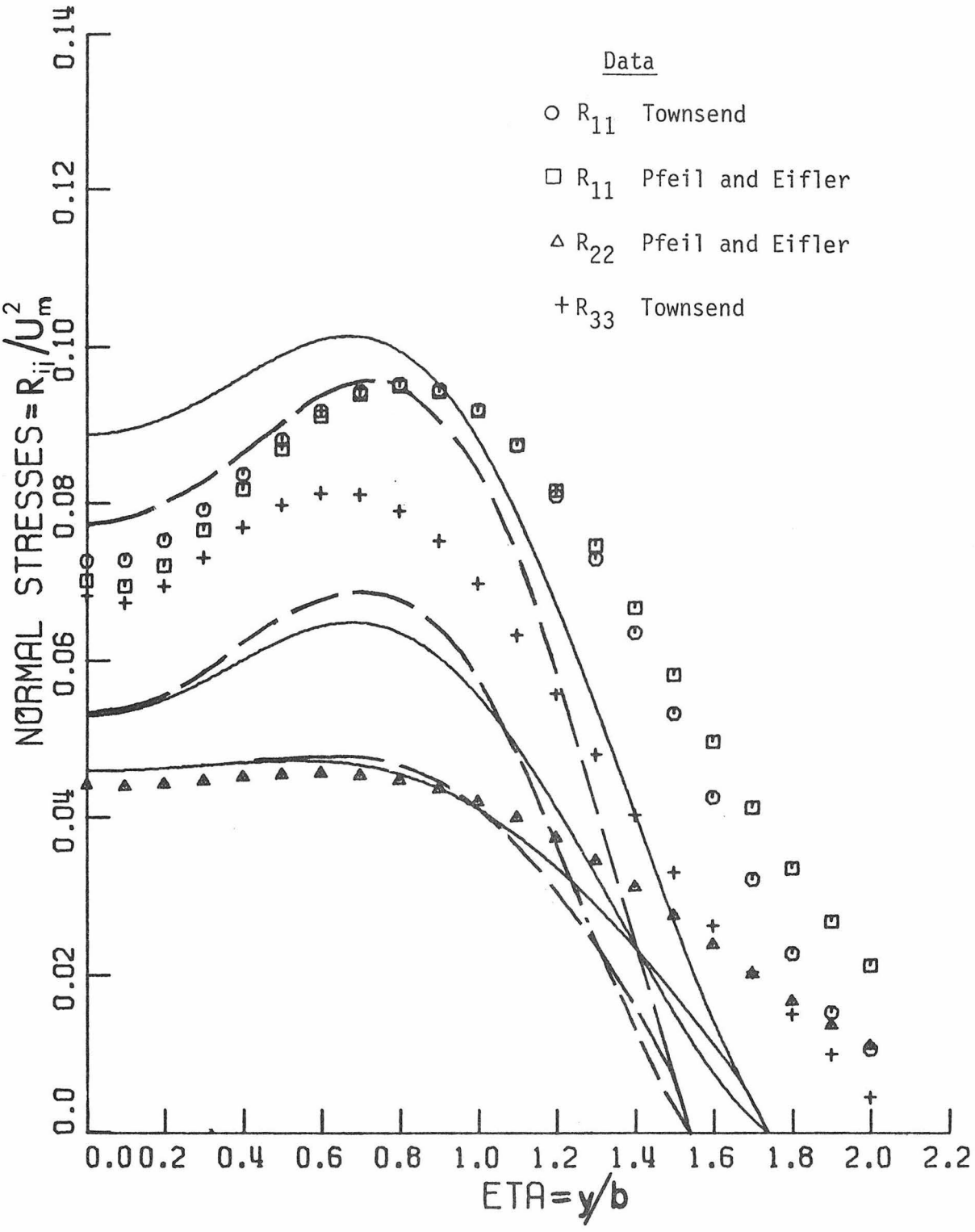

Figure 5.19.--MRS Model Calculations of the Normal Reynolds Stresses for the Plane Wake. Lines Have Same Meaning as in Figure 5.14.

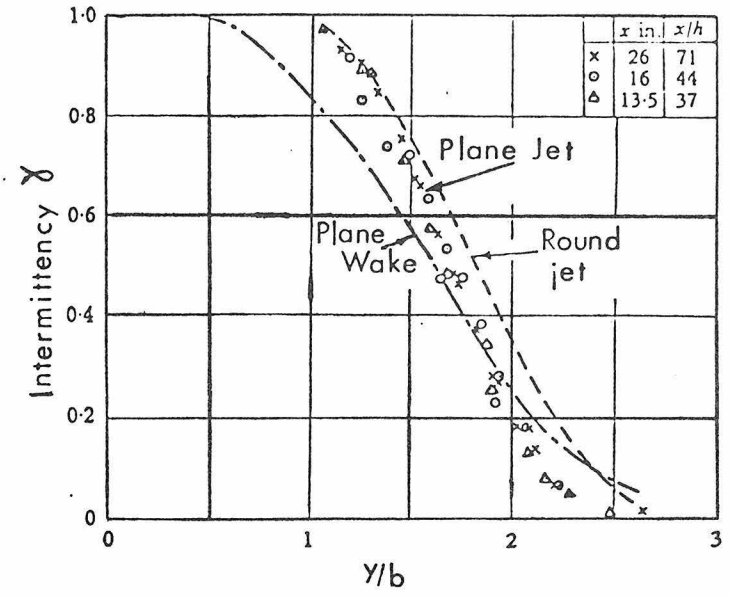

Figure 5.20.--The Intermittency Factor. Source of Data: Plane Jet, Bradbury (1965); Round Jet, Corsin and Kistler (1975); and Plane Wake, Townsend (1956).

the flow is fully turbulent (i.e. when $\gamma = 1$ the flow is turbulent 100 percent of the time. γ is determined by averaging the output of a probe that indicates unity when the flow is turbulent and zero when the flow is irrotation. Saffman (1974) suggests searching for solutions with wavy or unsteady boundaries as a means for obtaining more realistic solutions. A more physical approach would be to include intermittency calculations as part of the solution. Formative steps toward including the intermittency function γ in a turbulence model have recently been taken by Libby (1975, 1976).

The main difference between the present model and that of LRR is the magnitude of the coefficient α_0 in the T_{ij}^{1} equation (equation 2.5.14). Although the difference between the two models is only 15 percent (i.e. $\alpha_0 = -.333$ in the present case and $\alpha_0 = -.291$ for LRR) this coefficient has an important influence on the

predictions of the Reynolds stresses, particularly the shear stress. This can most easily be shown by considering the model for the "rapid" part of the pressure-strain correlation (T_{ij}^{1} - equation 2.5.14). For the shear stress component, this term is;

$$T_{12}^{1} = (\frac{4}{10} + 2\alpha_0)\, k - (\frac{2}{3} + \frac{8}{3}\alpha_0)\, R_{11} - (\frac{1}{3}\alpha_0 - \frac{2}{3})\, R_{22} \frac{dU_1}{dx_2} \quad (5.7.2)$$

To simplify this expression, for illustrative purposes, the values of R_{11} and R_{22} can be expressed in terms of the energy k,

$$R_{11} = a_{11}k$$

$$R_{22} - a_{22}k$$

using the a_{ij}-values given in Table 4.2. Then equation (5.7.2) becomes:

$$T_{12}^{1} = (\frac{4}{10} + 2\alpha_0)k - (\frac{2}{3} + \frac{8}{3}\alpha_0)\cdot 95k - (\frac{1}{3}\alpha_0 - \frac{2}{3})\cdot 45k \frac{dU_1}{dx_2} \quad (5.7.3)$$

For the two values of α_0 under consideration, this term may be written

$$T_{12}^{1} = C_1 k \frac{dU_1}{dx_2} \quad (5.7.4)$$

in which $C_1 = .244$ for $\alpha_0 = -.333$ (present model) and $C_1 = .266$ for $\alpha_0 = -.291$ (LRR). Using the same simplification, the production of the shear stress becomes

$$P_{12} = - R_{22} \frac{dU_1}{dx_2} = .45k \frac{dU_1}{dx_2} \quad (5.7.5)$$

and when combined with T_{12}, the result is a modified production,

$$P_{12} + T_{12}^{1} = - (.45 - C_1)k \frac{dU_1}{dx_2} \qquad (5.7.6)$$

This term illustrates the importance of the energy transfer term. The presence of T_{12}^{1} inhibits the production of the shear stress and inspection of equation (5.7.6) shows that the greater the magnitude of α_0 (and hence the greater the C_1-value), the more production is inhibited. For this reason, the present value of α_0 produces a smaller shear stress than the model of LRR does.

These results suggest that the lower value of α_0 determined by LRR is a reflection of inhomogeneity of the flows considered in their computer optimization of the model constants. To account for flow inhomogeneities on the pressure-strain correlation in the present modeling scheme, more terms must be added to the model for T_{ij} since any change in the present value of α_0 will cause changes in the homogeneous flow predictions discussed in Chapter 3. In our opinion, however, it is extremely encouraging that reasonable predictions of two <u>inhomogeneous</u> shear flows can be determined using the <u>homogeneous</u> representations of T_{ij}^{1}, T_{ij}^{2} and Δ_{ε}.

CHAPTER 6

CONCLUSIONS

In this study we have considered the systematic development of a second-order turbulence model for isothermal, incompressible, turbulent flows, i.e. a Mean Reynolds Stress Model. Specifically, a model for the calculation of homogeneous turbulent flows was derived by considering a rational scheme for the closure of the Reynolds stress transport equations in their homogeneous form. The higher order correlations that appear in these correlations were modeled by forming functional expansions for the unknown correlations in terms of a set of modeling variables ($U_{i,j}$, R_{ij}, ε). A systematic method of considering measurements of the turbulence quantities from experiments on homogeneous turbulent flows was then used to estimate the magnitude of the multiplicative constants that appear in the functional expansions.

The resulting model was then tested by performing a series of dynamic calculations for various kinds of homogeneous turbulent flows (i.e. homogeneous decay, homogeneous strain and homogeneous shear). These calculations were compared to the best available experimental data and it was shown that the model gave excellent predictions relative to the data and out-performed the well known models of Launder, Reece and Rodi (1975) and Donaldson (1972) for the homogeneous shear flow.

It has been suggested by Cormack (1975), Rotta (1975) and Pope (1978) that the homogeneous models for the pressure-strain correlation T_{ij} in the Reynolds stress equation (equation 5.3.6a-d) and the source of dissipation term in the dissipation equation (equation 5.3.6e) can be used in inhomogeneous flow calculations provided the inhomogeneity is not too great. To test this assumption, models suggested by Cormack et al. (1978) for the triple velocity correlation (J_{ijk}, equation 2.7.5) and by Hanjalic and Launder (1972) for the diffusion of dissipation (H_j, equation 2.7.8) were used in addition to the homogeneous models developed here for T_{ij} and Δ_ε to model the plane turbulent jet and wake. To carry out these calculations a numerical scheme was developed that allowed the governing partial differential equations to be solved as a set of similarity (ordinary) differential equations. The homogeneous form of the model (plus the inhomogeneous diffusion terms, of course) gave predictions for the jet and wake that were comparable to those of the model of Launder, Reece and Rodi (1975) which in our opinion is the best existing model for these types of flows. However, a major difference in philosophy exists between the present modeling method and that employed by LRR. In the present case we are <u>extending</u> the present homogeneous model to an inhomogeneous flow situation. If the predictions for inhomogeneous flows are not good, a rational method exists (see Chapter 2) whereby additional terms can be added to the homogeneous ones to account for the inhomogeneities. On the other hand, certain of the constants in the model of LRR have been adjusted by consideration of both homogeneous and inhomogeneous flows.

Thus there is no base state for the model and any additional terms accounting for increasing inhomogeneity must be accompanied by a re-evaluation of the constants in the terms already present.

It was also shown that the predictive capability of the model depended in some way on the inherent unsteadiness or intermittency of the flow being modeled. In future model development the importance of intermittency must be considered in a systematic way and it may be necessary to extend the model to provide the capability of estimating the intermittency. This would allow the conditionally averaged measurements of the turbulence quantities currently being determined experimentally to be used in model development.

Finally, the model developed here needs further testing on other free shear flows and boundary layer flows for the purposes of determining the limits of its predictive capability. In particular, three dimensional mean flow fields should be considered since only these flows can have mean field vortex stretching. It has recently been suggested by Pope (1978) that these flows will not be well predicted by MRS models, such as the present one, because the models do not take into account the effect of vortex stretching of the mean flow.

REFERENCES

Alexopoulos, C.C. and J.F. Ketter. "Extended Measurements of the Two-Dimension Turbulent Wake." University of Toronto, Mechanical Eng. Rept. UTME - TP 6811, (1968).

André, J.C.; G. DeMoore; P. Lacarrére; and R. DuVachat. "Turbulence Approximation for Inhomogeneous Flows: Part I. The Clipping Approximation." J. Atmos. Sci., 33 (1976): 476.

Bashir, J. "Experimental Study of the Turbulent Structure and Heat Transfer of a Two-Dimensional Heated Jet." Ph.D. Dissertation, University of Colorado, (1973).

Batchelor, G.K. "The Theory of Homogeneous Turbulence." Cambridge University Press. London, England, 1953.

Batchelor, G.K. and I. Proudman. "The Effect of Rapid Distortion on a Fluid in Turbulent Motion." Quart. J. Mech. Appl. Math., 7 (1954): 83.

Batchelor, G.K. and A.A. Townsend. "Decay of Isotropic Turbulence in the Initial Period." Proc. Roy. Soc. A, 193 (1948): 539.

Bradbury, L.J.S. "The Structure of a Self-Preserving Plane Jet." Journal of Fluid Mechanics (J.F.M.), 23 (1965): 31.

Bradshaw, P. "The Turbulence Structure of Equilibrium Boundary Layers." J.F.M., 29 (1967): 625.

_____. "Outlook for Three Dimensional Procedures. In Proc. Computation of Turbulent Boundary Layers - 1968. AFOSR-ITP-Stanford Conference. (Ed. Kline, Markovia, Sovran and Cockrell), Vol. 1 (1968): 427.

_____. "The Understanding and Prediction of Turbulent Flow." Aeronaut. J., 76 (1972): 403.

_____. "Effect of External Disturbances on the Spreading Rate of a Plane Turbulent Jet." J.F.M., 80 (1977): 795.

_____. Discussion of Launder and Pridden paper. "The Calculation of Turbulent Boundary Layers on Spinning and Curved Surfaces." J. Fluids. Eng., Trans. ASME, Ser. I, Vol. 99 (1977): 435.

Bradshaw, P.; D.H. Ferris; and N.P. Atwell. "Calculation of Boundary Layer Development Using the Turbulent Energy Equation." J.F.M., 28 (1967): 593.

Bradshaw, P.; D.H. Ferris; and R.F. Johnson. "Turbulence in the Noise Producing Region of a Circular Jet." J.F.M., 19 (1964): 591.

Brown, G.L. and A. Roshko. "One Density Effects and Large Structure in Turbulent Mixing Layers." J.F.M., 64 (1974): 775.

Builtjes, P.J.H. "Memory Effects in Turbulent Flows." Ph.D. Thesis. Delft University of Tech. Delft, The Netherlands, 1977.

Champagne, F.H.; V.G. Harris; and S. Corrsin. "Experiments on Nearly Homogeneous Turbulent Shear Flow." J.F.M., 41 (1970): 81.

Chevray, R. and Kovasznay, L.S.G. "Turbulence Measurements in the Wake of a Thin Flat Plate." AIAA J., 7, (1969): 1641.

Chou, P.Y. "On the Velocity Correlations and the Solution of the Equations of Turbulent Fluctuations." Q. Appl. Math., 3 (1945): 38.

Coleman, B.D. and W. Noll. "Recent Results in the Continuum Theory of Viscoelastic Fluids." Ann. N.Y. Acad. Sci. 89 (1961): 672.

Comte-Bellot, G. and S. Corrsin. "The Use of a Contraction to Improve the Isotropy of Grid Turbulence." J.F.M., 25 (1966): 657.

Cormack, D.E. "Topics in Geophysical Fluid Dynamics: II. Studies of a Phenomenological Turbulence Model." Ph.D. Thesis. Calif. Inst. of Tech., 1975.

Cormack, D.E., L.G. Leal, and J.H. Seinfeld. "An Evaluation of Mean Reynolds Stress Turbulence Models: The Triple Velocity Correlation." J. Fluids Eng., Trans ASME, Ser. I. Vol. 100 (1978): 47.

Corrsin, S. "Limitations of Gradient Transport Models in Random Walks and in Turbulence." Adv. Geophysics., 18A (1974): 25.

Daly, B.J. "A Numerical Study of Turbulence Transitions in Convective Flow." J.F.M., 64 (1974): 129.

Daly, B.J. and F.H. Harlow. "Transport Equations in Turbulence." Phys. Fluids, 13 (1970): 634.

Deardorff, J.W. "A Numerical Study of Three-Dimensional Turbulent Channel Flow at Large Reynolds Numbers." J.F.M., 41 (1970): 453.

_____. "Numerical Investigation of Neutral and Unstable Planetary Boundary Layers." J. Atmos. Sci., 29, (1972): 91.

_____. "The Use of Subgrid Transport Equations in a Three-Dimensional Model of Atmospheric Turbulence." J. Fluids Eng., Trans. ASME, Ser. I, Vol. 95 (1973): 429.

Donaldson, C. duP. "Calculation of Turbulent Shear Flows for Atmospheric and Vortex Motions." AIAA J., 10 (1972): 4.

Ermshaus, R. "Eigen tum lichkeiten turbulenter Nachlauf stromungen." Mitt. a.d. Max-Planck Inst. fur Stromungsforschung, No. 46, 1970.

Everitt, K. Ph.D. Thesis. University of London, 1971.

Fabris, G. Ph.D. Thesis. Illinois Inst. of Tech., 1974.

Gessner, F.B. and A.F. Emergy. "A Reynolds Stress Model for Turbulent Corner Flows--Part 1: Development of the Model." J. of Fluids Eng., Trans ASME, Ser. I, Vol. 98 (1976):261.

Gutmark E. and I. Wygnanski. "The Planar Turbulent Jet." J.F.M., 73 (1976): 465.

Halleen, R.M. "Literature Review of Subsonic Free Turbulent Shear Flow." Stanford University. Mech. Eng. Rep. MD-11, 1964.

Hanjalic, K. "Prediction of Turbulent Flow in Annular Ducts with Differential Transport Model of Turbulence." Warmeund Stoff., 7 (1974): 71.

Hanjalic, K. and B.E. Launder. "A Reynolds Stress Model of Turbulence and its Application to Thin Shear Flows." J.F.M., 52 (1972): 609.

_____. "Contribution Toward a Reynolds-Stress Closure for Low-Reynolds Number Turbulence." J.F.M., 74 (1976): 593.

Harris, V.G., J.A.H. Graham, and S. Corrsin. "Further Experiments in Nearly Homogeneous Turbulent Shear Flow." J.F.M., 81 (1977): 657.

Heskestad, G. "Hot-Wire Measurements in a Plane Turbulent Jet." J. Appl. Mech., 32 (1976): 721.

Hwang, W.S. "Experimental Investigation of Turbulent Shear Flows." Ph.D. Thesis. University of Virginia, 1971.

Irwin, H.P.A.H. "Measurements of a Self-Preserving Plane Wall Jet in a Positive Pressure Gradient." J.F.M., 61 (1973): 33.

Irwin, H.P.A.H. and P.A. Smith. "Prediction of the Effect of Streamline Curvature on Turbulence." Vol. 18 (1975): 624.

Keller, H.B. "Accurate Difference Methods for Nonlinear Two-Point Boundary Value Problems." S.I.A.M. J. Numer. Anal. 11 (1974): 305.

Klebanoff, P.S. "Characteristics of Turbulence in a Boundary Layer with Zero Pressure Gradient." N.A.C.A. Rep. No. 1247, 1955.

Kotsovinos, N.E. "A Note on the Spreading Rate and Virtual Origin of a Plane Turbulent Jet." J.F.M., 77 (1976): 305.

_____. "Plane Turbulent Boyant Jets" Part I, Integral Properties." J.F.M., 81 (1977): 25.

Kwak, D., W.C. Reynolds, and J.H. Ferziger. "Three Dimensional Time Dependent Computation of Turbulent Flow." Stanford University Dept. Mech. Eng., Rep. TF-6, 1975.

Landau, L.D. and E.M. Lifshitz. "Fluid Mechanics." Pergamon Press, Oxford, 1959.

Laufer, J. "Investigation of Turbulent Flow in a Two-Dimensional Channel." N.A.C.A., Rep. No. 1053, 1950.

_____. "The Structure of Turbulence in Fully Developed Pipe Flow." N.A.C.A. Rep. No. 1174, 1955.

Launder, B.E. "Progress in Modeling of Turbulent Transport." Lecture Series, No. 76, von Karman Inst., Belgium, 1975.

Launder, B.E. and A. Morse. "Numerical Prediction of Axisymmetric Free Shear Flows with a Second Order Reynolds Stress Model." Symposium on Turbulent Shear Flows. Penn. State University, April 1977.

Launder, B.E., G.I. Reece and W. Rodi. "Progress in the Development of a Reynolds Stress Turbulence Closure." J.F.M., 68 (1975): 537.

Leslie, D.C. "Developments in the Theory of Turbulence." Clarendon Press, Oxford, 1973.

Lewellen, W.S. "Use of Invariant Modeling." A.R.A.P. Report No. 243, Princeton University, 1975.

Libby, P.A. "On the Prediction of Intermittent Turbulent Flows." J.F.M., 68 (1975): 273.

_____. "Prediction of the Intermittent Turbulent Wake of a Heated Cylinder." Phys. Fluids, 19 (1976):494.

Liepmann, H.W. and J. Laufer. "Investigation of Free Turbulent Mixing." N.A.C.A. T.N. 1257, 1947.

Lin, A. and M. Wolfshtein. "Theoretical Study of the Reynolds Stress Equations." Symposium on Turbulent Shear Flows. Penn. State University, April 1977.

Lumley, J.L. "On a Rational Approach to Relations Between Motions of Different Scales in Turbulent Flows." Phys. Fluids, 10 (1967): 1405.

_____. "Toward a Turbulent Constitutive Relative." J.F.M., 41, (1970): 413.

_____. "Pressure-Strain Correlation." Phys. Fluids, 18 (1975a): 750.

_____. "Prediction Methods for Turbulent Flows." Lecture Series No. 76, von Karman Inst., Belgium, 1975b.

_____. "Simulating Turbulent Transport in Urban Air Pollution Models." Unpublished, 1976.

Lumley, J.L. and B. Khajeh-Nouri. "Computational Modeling of Turbulent Transport." Adv. in Geophysics, 18A (1974): 193.

Lumley, J.L. and G.R. Newman. "The Return to Isotropy of Homogeneous Turbulence." J.F.M., 82 (1977): 161.

Lumley, J.L., O. Zeman and J. Siess. "The Influence of Buoyancy on Turbulent Transport." J.F.M., 84 (1978): 581.

Marechal, J. "Etude Experimentale de la Deformation plane d'une Turbulence Homogene." J. Mecanique, 11 (1972): 263.

Meroney, R.N. "An Algebraic Stress Model for Stratified Turbulent Shear Flows." Computers and Fluids, 4 (1976): 93.

Mills, R.R. and S. Corrsin. "Effects of Contraction on Turbulence and Temperature Fluctuations Generated by a Warm Grid." NASA Memo. No. 5-5-59 W, 1959.

Mjolsness, R.C. and A.G. Petschek. "Positivity of the Reynolds Stress Tensor in the Harlow-Daly Turbulence Model." Submitted to J.F.M., 1977.

Monin, A.S. and A.M. Yaglom. "Statistical Fluid Mechanics." MIT Press, Cambridge, Mass, 1971.

Mulhearn, P.J. and R.E. Luxton. "Experiments on Uniformly Sheared Turbulence to Large Total Strains." Chas. Kolling Res. Lab. Tech. Note. F-19, November, 1970.

_____. "The Development of Turbulence Structure in a Uniform Shear Flow." J.F.M., 68 (1975): 577.

Naot, D.; A. Shavit; and M. Wolfshtein. "Two-Point Correlation Model and the Redistribution of Reynolds Stresses." Physics of Fluids, 16 (1973):6.

Newman, B.G. "Turbulent Jets and Wakes in a Pressure Gradient." In: "Fluid Mechanics of Internal Flow" (G. Sovran, ed). Elsevier, 1967, p. 170.

Okamoto, T.; M. Yagita; and K. Ohtsuka. "Experimental Investigation of the Wake of a Wedge." Bulletin J.S.M.E., 20 (1977): 323.

Orszag, S.A. "Numerical Methods for the Simulation of Turbulence." Phys. Fluids Supplement II, 1969, pp. II-250.

Patankar, S.V. and D.B. Spalding. "Heat and Mass Transfer in Boundary Layers." Intertext Books, London, 1970.

Patel, R.P. "A Study of Two-Dimensional Symmetric and Asymmetric Turbulent Shear Flows." Ph.D. Thesis. McGill University, Montreal, Canada, 1970.

Pfeil, H. and J. Eifler. "Messungen im Turbulente n Nachlauf des einzelzylinders." V.D.I. Forschung im Ing.-Wes., 41, (1975): 137.

Pope, S.B. "A More General Effective-Viscosity Hypothesis." J.F.M., 72 (1975): 331.

_____. "The Statistical Theory of Turbulent Flames." Submitted to Proc. Roy. Soc. A., 1978.

Reichardt, H. "Gesetz massigkeiten der freien Turbulenz." V.D.I. Forschungsheft, Heft 494, 1942.

Reynolds, A.J. and H.J. Tucker. "The Distortion of Turbulence by General Uniform Irrotational Strain." J.F.M., 68 (1975): 673.

Reynolds, W.C. "Computation of Turbulent Flows." A.I.A.A. Paper No. 74-556, 1974.

_____. "Computation of Turbulent Flows." Ann. Rev. of Fluid Mech., 8 (1976): 183.

Richards, H.K. "Experimental Investigation of Turbulent Shear Flow with Quadratic Mean Velocity." Ph.D. Thesis. University of Virginia, 1972.

Richards, H.K. and J.B. Morton. "Experimental Investigation of Turbulent Shear Flow with Quadratic Mean-Velocity Profiles." J.F.M., 73 (1976): 165.

Robbins, A. "The Structure and Development of a Plane Turbulent Free Jet." Ph.D. Thesis. University of London, 1971.

Rodi, W. "The Prediction of Free Turbulent Boundary Layers by Use of a Two-Equation Model of Turbulence." Ph.D. Thesis. University of London, 1972.

_____. "A New Algebraic Relation for Calculating the Reynolds Stress." Z.A.M.M., 56 (1976): T219.

_____. "A Review of Experimental Data of Uniform Density Free Turbulent Boundary Layers." In "Studies in Convection." B. Launder, ed. Academic Press, London, 1976.

Rodi, W. and D.B. Spalding. "A Two-Parameter Model of Turbulence and its Application to Free Jets." Warme und Stoff. 3 (1970): 85.

Rose, W.G. "Results of an Attempt to Generate a Homogeneous Turbulent Shear Flow." J.F.M., 25 (1966): 97.

_____. "Interaction of Grid Turbulence with a Uniform Mean Shear." J.F.M., 44 (1970): 767.

Rotta, J. "Statistische Theorie Nichtomogener Turbulenz." Z. Physik, 129 (1951): 547.

Rotta, J.C. "Prediction of Turbulent Shear Flow Using the Transport Equations for Turbulence Energy and Turbulence Length Scale." Lecture Ser. No. 76, von Karman Inst., Belgium, 1975.

Sabot, J. and G. Comte-Bellot. C.R. Aead. Sci. Paris, A 275 (1972): 667.

Saffman, P.G. "A Model for Inhomogeneous Turbulent Flow." Proc. Roy. Soc. A, 317 (1970): 417.

_____. "Model Equations for Turbulent Shear Flow." Stud. Appl. Math., 53 (1974): 17.

Schlichting, H. z "Uber das ebene Windschattenproblem." Ing. Archiv, 1 (1930): 533.

Schumann, U. and G.S. Patterson. "Numerical Study of Pressure and Velocity Fluctuations in Nearly Isotropic Turbulence." Submitted to J.F.M., April, 1975a.

_____. "Numerical Study of the Return of Axisymmetric Turbulence to Isotropy." Submitted to J.F.M., April, 1975b.

Shaanan, S.; J.H. Ferziger; and W.C. Reynolds. "Numerical Simulation of Homogeneous Turbulence with Rotation." Stanford University Dep. Mech. Eng. Rep. TF-6, 1975.

Tennekes, H. and J.L. Lumley. "A First Course in Turbulence." Cambridge, Mass.: MIT Press, 1972.

Townsend, A.A. "The Fully Developed Turbulent Wake of a Circular Cylinder." Aust. J. Sci. Res. 2 (1949): 451.

_____. "The Uniform Distortion of Homogeneous Turbulence." Quart. J. Mech. Appl. Math., 7 (1954): 104.

_____. "The Structure of Turbulent Shear Flow." 1st Ed. Cambridge University Press, London, England, 1956.

_____. "The Structure of Turbulent Shear Flow." 2nd Ed. Cambridge University Press, London, England, 1976.

Tucker, H.J. "The Distortion of Turbulence by Irrotational Strain." Ph.D. Thesis. McGill University, Montreal, Canada, 1970.

Tucker, H.J., and A.J. Reynolds. "The Distortion of Turbulence by Irrotational Plane Strain." J.F.M., 32 (1968): 657.

Uberoi, M.S. "Effect of Wind Tunnel Contraction on Free Stream Turbulence." J. Aero. Sci., 23 (1956): 754.

_____. "Equipartion of Energy and Local Isotropy in Turbulent Flows." J. Appl. Phys., 29 (1967): 1165.

Uberoi, M.S. and P. Freymuth. "Spectra of Turbulence in Wakes Behind Circular Cylinders." Phys. Fluids, 12 (1969): 1359.

von Karman, T. and L. Howarth. "On the Statistical Theory of Isotropic Turbulence." Proc. Roy. Soc. A, 164 (1938): 192.

Warsi, Z.U.A. and B.B. Amlicke. "Improved Algebraic Relation for the Calculation of Reynolds Stresses." A.I.A.A. J., 14 (1976): 1779.

White, A.B. "Numerical Solution of Two-Point Boundary Value Problems." Ph.D. Thesis. California Inst. of Tech., 1974.

Wolfshtein, W. "On the Length Scale of Turbulence Equation." Israel J. of Tech., 8 (1970): 87.

Wyngaard, J.C. "Modeling the Planetary Boundary-Layer, An Extension to the Stable Case." Boundary Layer Met., 9 (1975):441.

Zeman, O. "The Dynamics of Entrainment in Planetary Boundary Layers: A Study in Turbulence Modeling and Parameterization." Ph.D. Thesis. Penn. State University, 1975.

Zeman, O. and J.L. Lumley. "Modeling Buoyancy Driven Mized Layers." J. Atmos. Sci., 33 (1976): 1974.

Zeman, O. and H. Tennekes. "A Self-Contained Model for the Pressure Terms in the Turbulent Stress Equations of the Neutral Atmospheric Boundary Layer." J. Atmos. Sci., 32 (1975): 1808.

APPENDIX A

Determination of $B_{ij\ell m}$

Determination of $B_{ij\ell m}$

From equation (2.5.11), $T_{ij}^{1} = 2\frac{dU_\ell}{dxm} B_{ij\ell m}$ and because of continuity, $B_{ii\ell m} = 0$ and $B_{ij\ell\ell} = 0$. Furthermore in the isotropic case, there is symmetry in the indices i,j and ℓ,m. Thus, $B_{ij\ell m} = B_{ji\ell m}$. $B_{ij\ell m} = B_{ij\ell m}$. Finally, using Green's theorem it may be shown (Rotta, 1951) that $B_{ijjm} = R_{im}$. These conditions are sufficient to determine $B_{ij\ell m}$.

If we assume that $B_{ij\ell m}$ is isotropic, then

$$B_{ij\ell m} = [\alpha_1\delta_{ij}\delta_{\ell m} + \alpha_2\delta_{i\ell}\delta_{jm} + \alpha_3\,\delta_{im}\delta_{\ell j}]q^2 \qquad \text{(A-1)}$$

and symmetry in i and j requires that $\alpha_2 = \alpha_3$. Further, since $B_{ii\ell m} = 0$,

$$3\alpha_1 + 2\alpha_2 = 0 \qquad \text{(A-2)}$$

and

$$R_{11} = B_{1jj1} = (\alpha_1 + 4\alpha_2)q^2 = \frac{1}{3}\,q^2 \qquad \text{(A-3)}$$

Solving (A-2) and (A-3) for α_1 and α_2 yields, $\alpha_1 = -\frac{1}{15}$, $\alpha_2 = \frac{1}{10}$.

The most general fourth order tensor that contains terms that are linear in b_{ij} is

$$B_{ij\ell m} = \text{isotropic part} + \alpha_4\delta_{ij}b_{\ell m} + \alpha_5\delta_{im}b_{j\ell} + \alpha_6\delta_{i\ell}b_{jm} + \alpha_7\delta_{\ell m}b_{ij}$$

$$+ \alpha_8\delta_{j\ell}b_{im} + \alpha_9\delta_{jm}b_{i\ell}\,.$$

Using symmetry, $\alpha_5 = \alpha_9$ and $\alpha_6 = \alpha_8$. Using continuity and the relation $R_{11} = B_{1jj1}$, gives the following set of equations for α_4, α_5, α_6 and α_7.

$$3\alpha_4 + 2\alpha_5 + 2\alpha_6 = 0 \tag{A-4}$$

$$2\alpha_5 + 2\alpha_6 + 3\alpha_7 = 0 \tag{A-5}$$

$$\alpha_4 + \alpha_5 + 4\alpha_6 + \alpha_7 = 1 \tag{A-6}$$

Solving (A-4) to (A-6) gives

$$\alpha_4 = \alpha_7$$

$$\alpha_5 = -\frac{1}{3}(1 + 4\alpha_7)$$

$$\alpha_6 = \frac{1}{6}(2 - \alpha_7)$$

Hence the final model is

$$B_{ij\ell m} = -\frac{1}{15}\delta_{ij}\delta_{\ell m} + \frac{1}{10}(\delta_{i\ell}\delta_{jm} + \delta_{im}\delta_{\ell j}) + \alpha_7(\delta_{ij}b_{\ell m} + \delta_{\ell m}b_{ij}) - \frac{1}{3}(1 + 4\alpha_7)(\delta_{im}b_{j\ell} + \delta_{jm}b_{i\ell}) + \frac{1}{6}(2 - \alpha_7)(\delta_{i\ell}b_{jm} + \delta_{j\ell}b_{im}) , \tag{A-7}$$

and contains only <u>one</u> undetermined coefficient, α_7.

To determine $T_{ij}{}^1$, $B_{ij\ell m}$ is multiplied by $2\frac{dU_\ell}{dx_m}$. However, $\frac{dU_\ell}{dx_m} = S_{\ell m} + \Omega_{\ell m}$, so

$$T_{ij}{}^1 = 2\frac{dU_\ell}{dx_m} B_{ij\ell m} = 2(S_{\ell m} + \Omega_{\ell m})\, B_{ij\ell m} \tag{A-8}$$

$$= (\frac{4}{10} + 2\alpha_7)S_{ij}q^2 - 3\alpha_7(R_{ik}S_{kj} + R_{jk}S_{ki} - \frac{2}{3} R_{jk}\frac{dU_j}{dx_k}) - \frac{2}{3}(2 + \frac{7}{2}\alpha_7)(R_{ik}S_{kj} + R_{jk}\Omega_{ki})$$

For convenience, α_7 will be changed to α_0 in the main text.

APPENDIX B

Isotropic Form of the Pressure-Velocity Correlation

Isotropic Form of the Pressure-Velocity Correlation

It will be shown that, for isotropic turbulence, the pressure gradient-velocity correlation may be written:

$$\left(\overline{u_j \frac{\partial p}{\partial x_i}} + \overline{u_i \frac{\partial p}{\partial x_j}}\right) = -\frac{4}{10} q^2 S_{ij} \tag{B-1}$$

It was shown in equation (2.5.10) that,

$$\overline{u_j \frac{\partial p}{\partial x_i}} = \frac{dU_m(\underline{x})}{\partial x_n} \left[\frac{1}{2\pi} \int \frac{\partial}{\partial r_i \partial r_m} R_{jn} \frac{d\underline{r}}{r}\right]. \tag{B-2}$$

If we express the correlation tensor R_{jn} in terms of its spectrum tensor, Φ_{jn} where,

$$R_{jn}(\underline{r}) = \int \Phi_{jn}(\underline{k}) e^{i\underline{k}\cdot\underline{r}} \, d\underline{k} \tag{B-3}$$

then, after an elementary integration over $\underline{r}$, (B-2) becomes

$$\overline{u_j \frac{\partial p}{\partial x_i}} = \frac{-2dU_m(\underline{x})}{dx_n} \int \frac{k_i k_m}{k^2} \Phi_{jn}(\underline{k}) \, d\underline{k} \tag{B-4}$$

The spectrum function for isotropic turbulence is (Batchelor, 1953)

$$\Phi_{jn}(\underline{k}) = \frac{E(k)}{4\pi^2 k} \left(\delta_{jn} - \frac{k_j k_n}{k^2}\right) \tag{B-5}$$

Here, $E(k)$ is normalized so that $\int_0^\infty E(k)\, dk = \frac{q^2}{2}$. Defining the unit vector $\underline{n} = \frac{\underline{k}}{k}$, then

$$I_1 = \int \frac{k_i k_m}{k^2} \Phi_{jn}(\underline{k}) d\underline{k} = \int n_i n_m \frac{E(k)}{4\pi k^2} (\delta_{jn} - n_j n_n)\, d\underline{k} \qquad \text{(B-6)}$$

The unit volume is $d\underline{k} = k^2 \sin\theta\, dk\, d\theta\, d\phi$. Hence (B-6) is,

$$\begin{aligned} I_1 &= \int_0^\infty E(k)\, dk \oint \frac{1}{4\pi} [n_i n_m \delta_{jn} - n_i n_m n_j n_m]\, d\ell \\ &= \frac{q^2}{2} \left[\frac{1}{3}\delta_{im}\delta_{jn} - \frac{1}{15}(\delta_{ij}\delta_{mn} + \delta_{im}\delta_{jn} + \delta_{in}\delta_{jm})\right] \end{aligned} \qquad \text{(B-7)}$$

Hence,

$$\begin{aligned} \overline{u_j \frac{\partial p}{\partial x_i}} &= -2\frac{dU_m}{dx_n} I_1 \\ &= -\frac{dU_m}{dx_n} \left[\frac{4}{15}\delta_{im}\delta_{jn} - \frac{1}{15}(\delta_{ij}\delta_{mn} + \delta_{in}\delta_{jm})\right] \end{aligned} \qquad \text{(B-8)}$$

The form corresponding to $\overline{u_i \frac{\partial p}{x_j}}$ is obtained by interchanging the indicies i and j. Hence, the final model is

$$\overline{u_i \frac{\partial p}{\partial x_j}} + \overline{u_j \frac{\partial p}{\partial x_i}} = \frac{-2dU_m}{dx_n} \left[\frac{1}{15}\delta_{ij}\delta_{mn} + \frac{1}{10}(\delta_{im}\delta_{jn} + \delta_{in}\delta_{jm})\right] q^2 \qquad \text{(B-9)}$$

Equation (B-9) is exactly the same as that obtained in appendix A (cf. equation A-1) using the modeling scheme outlined in Chapter 2. Contracting the indices in (B-9) and using continuity gives

$$\overline{u_i \frac{\partial p}{\partial x_j}} + \overline{u_j \frac{\partial p}{\partial x_i}} = -\frac{2}{5} q^2 S_{ij}$$

APPENDIX C

The Non-Linear Return-to-Isotropy Model of Lumley and Newman (1977)

The Non-Linear Return-to-Isotropy Model of Lumley and Newman (1977)

Recently the problem of return to isotropy was studied analytically by Lumley and Newman (1977). In this appendix, the final form of their model is given along with a brief description of its derivation.

The governing Reynolds stress equations for a decaying, anisotropic homogeneous isothermal turbulence field may be written:

$$\dot{\overline{u_i u_j}} = -(\overline{p_{,i}u_j} + \overline{p_{,j}u_i})/\rho - 2\nu\,\overline{u_{i,k}u_{j,k}} \qquad \text{(C-1)}$$

$$= -\left[(\overline{p_{,i}u_j} + \overline{p_{,j}u_i})/\rho - 2\nu\,\overline{u_{i,k}u_{j,k}} + \frac{2}{3}\varepsilon\delta_{ij}\right] - \frac{2}{3}\varepsilon\delta_{ij}$$

$$= -\varepsilon\phi_{ij} - \frac{2}{3}\varepsilon\delta_{ij}$$

The formulation, C-1, is valid over the whole range of Reynolds number, hence in general the function ϕ_{ij} contains the anisotropic part of the dissipation tensor in addition to the pressure gradient-velocity correlation. (Recall that in the limit of infinite Reynolds number, we assume that the last two terms in the square brackets sum to zero.) Following the analysis of Chapter 2, it may be shown that

$$\phi_{ij} = \phi_{ij}(b, R_\ell) = b_{ij}\beta + \gamma(b_{ij}^2 - \delta_{ij}II/3) \qquad \text{(C-2)}$$

where $\beta = \beta(II, III, R_\ell)$, $\gamma = \gamma(II, III, R_\ell)$ and $R_\ell = \frac{q^4}{9\varepsilon\nu}$.
The functions β and γ must be expressed in invariant form and Lumley and Newman attempt to determine the asymptotic behavior of these

invariant functions. The first asymptotic state is that of small Reynolds numbers. In the final period of decay (Batchelor 1953, p. 92), (C-1) becomes

$$\overline{u_i u_j} = 2\nu\overline{u_{i,k}u_{j,k}} = -\varepsilon(2b_{ij} + \frac{2}{3}\delta_{ij}),\ R_\ell \to 0 \qquad \text{(C-3)}$$

hence

$$\phi_{ij} \to 2b_{ij},\ R_\ell \to 0 \qquad \text{(C-4)}$$

For the case of axisymmetric turbulence (which is the most useful since the majority of return-to-isotropy experiments have been carried out on such turbulence) we have

$$b = \begin{bmatrix} b & 0 & 0 \\ 0 & -\frac{1}{2}b & 0 \\ 0 & 0 & -\frac{1}{2}b \end{bmatrix} \qquad \text{(C-5)}$$

and in the final period we have

$$\frac{\phi_{11}}{b} \to 2 \quad \text{as } R_\ell \to 0 \qquad \text{(C-6)}$$

In the asymptotic limit of high Reynolds number and vanishing anisotropy, Lumley and Newman used the experiments of Comte-Bellot and Corrsin to show that

$$\frac{\phi_{11}}{b} \to 2 + 8.0/R_\ell^{\frac{1}{2}},\ R_\ell \to \infty,\ II \to 0 \qquad \text{(C-7)}$$

Although the form (C-2) is completely general , Lumley and Newman chose a slightly less general form, namely that ϕ_{ij} is a polynomial of arbitrary order in b_{ij} (i.e. of the form $a_0 b^0 + a_1 b^1 + a_2 b^2 + \ldots$, where $b_{ij}^n = b_{ip} b_{qp} \ldots b_{qj}$ with n factors and the a_i constants) minus the trace of the polynomial, then in principal axes.

$$\phi_{ij} = \frac{1}{3} \begin{pmatrix} 2f(b_1) - f(b_2) - f(b_3) & 0 & 0 \\ 0 & 2f(b_2) - f(b_1) - f(b_3) & 0 \\ 0 & 0 & 2f(b_3) - f(b_1) - f(b_2) \end{pmatrix} \qquad \text{(C-8)}$$

where b_2 are the eigenvalues of the b_{ij} matrix (of course the principal axes are the cartesian co-ordinate axes here) and f(x) is the polynomial function. To ensure realizability (i.e. if one component of the energy (in principal axes) vanishes, the time derivative of that component must also vanish, in order to avoid subsequent negative values of that component), if any eigenvalue takes on the value -1/3 then the corresponding eigenvalue of ϕ_{ii} takes on the value -2/3, regardless of the value of the eigenvalues. Thus,

$$[2f(-1/3) - f(b_2) - f(1/3 - b_2)]/3 = -2/3 \; . \qquad \text{(C-9)}$$

This is a functional equation for f(x), which may be solved to give

$$f(x) = g(x - 1/6), \; g(x) = -g(x), \; g(\tfrac{1}{2}) = 1 \qquad \text{(C-10)}$$

Lumley and Newman use a Fourier series expansion of g(x), and the asymptotic conditions (C-6) and (C-7) to determine that

$$g(x) = 2x + \exp(-DR_\ell^{-\frac{1}{2}})\{a[4\sin(2\pi x) - \sin(4\pi x) + \sin(6\pi x)]$$

$$+ 1.70\, R_\ell^{-\frac{1}{2}}[1.28\sin(2\pi x) - .112\, \sin(4\pi x)]\} \qquad \text{(C-11)}$$

The parameters D and a were determined from the strongly anisotropic decay experiments of Uberoi (1956, 1957) and Mills and Corrsin (1959).

The model of Lumley and Newman is shown graphically for two Reynolds numbers, namely $R_\ell = 100$ and $R_\ell = 400$, for the case of axisymmetric return-to-isotropy in Figure 3.8.

APPENDIX D

Determination of Initial Values of Turbulence Quantities for Homogeneous Strain Flows

Determination of Initial Values of Turbulence Quantities for Homogeneous Strain Flows

In these flows, the beginning of the distorting duct was chosen as the starting point for the numerical integration and the model equations were integrated in the streamwise direction in increments of Δ = 1 inch. The magnitude of the Reynolds stresses was read directly from their profiles determined by Tucker (1970) and were made dimensionless with U_0, the constant, upstream mean velocity. The magnitudes of the dimensionless Reynolds stresses, for the various ducts considered, are given in Table 3.12.

In most cases the mean streamwise velocity increases as the flow proceeds through the duct. The single exception is the plane lateral distortion where x_2 is the streamwise co-ordinate (recall that the x_1-direction is always chosen such that an extension occurs in this direction) and the mean velocity coefficients are given by,

$$U_2 = \text{constant}, \quad U_3 = - bU_2x_3, \quad U_1 = bU_2x_1 \ . \tag{D-1}$$

Hence, the mean rates of strain are

$$\frac{\partial U_2}{\partial x_2} = 0, \quad \frac{\partial U_3}{\partial x_3} = - bU_2, \quad \frac{\partial U_1}{\partial x_1} = bU_2 \tag{D-2}$$

where b = .01854 inches $^{-1}$.

For flows which have the axis of the duct in the x_1-direction, namely the axisymmetric contraction and the longitudinal plane strain, the mean streamlines are given by

$$x_2 = (x_2)_A\ (1 + cx_1)^F$$
$$x_3 = (x_3)_A\ (1 + cx_1)^{-1-F} \qquad \text{(D-3)}$$

where F is the "strain type" parameter defined in § 3.3 and $(x_2)_A$, $(x_3)_A$ are the precontraction values. The mean streamwise velocity at a point x is inversely proportional to the ratio of the area of the duct at the point x to the precontraction area, i.e.

$$\frac{U_1}{(U_1)_A} = \frac{(x_2)_A\ (x_3)_A}{x_2 x_3} = (1 + c_1)x \qquad \text{(D-4)}$$

Thus, the mean streamwise velocity increases linearly through the duct. Following the same analysis, it may be shown that a similar equation is true for the equivalent diffuser, namely

$$\frac{U_2}{(U_2)_A} = (1 + c_1)x \qquad \text{(D-5)}$$

The value c_1 is calculated from the mean velocity profiles given in Tucker (1970). The mean rates of strain are determined by differentiating (D-4) and (D-5). The coefficients c_1 and the maximum total strain attainable in each distorting duct are summarized in Table D.1.

Table D.1.--Mean Velocity and Total Strain: Homogeneous Strain.

Duct	c_1	Max. Strain τ max	Max. Extent inches
axisymmetric contraction	.056	5.78	86
longitudinal strain			
a. strong strain	.056	5.50	80
b. weak strain	.018	2.53	84
equivalent diffuser	.015	2.30	84

The dissipation rate at the beginning of the test section can be determined from a consideration of the kinetic energy profile (Figure 3.17). The kinetic energy is described by,

$$U_1 \frac{dq^2}{dx_1} = - 2R_{ij} \frac{dU_i}{dx_j} - 2\varepsilon \qquad \text{(D-6)}$$

Defining the dimensionless quantities,

$$q^{2'} = \frac{q^2}{U_0^2} , \; R_{ij}' = \frac{R_{ij}}{U_0^2} , \; \varepsilon' = \frac{\varepsilon \Delta}{U_0^3} , \; U_1' = \frac{U_1}{U_0} , \; x' = \frac{x}{\Delta} , \; y' = \frac{y}{\Delta} \qquad \text{(D-7)}$$

where Δ = grid spacing = 1 inch and U_0 is the constant precontraction velocity, equation (D-6) may be rewritten:

$$\frac{\partial q^{2'}}{\partial x_1'} = - \frac{2}{U_1'} (R_{ij}' \frac{dU_i'}{dx_j'} + \varepsilon') \qquad \text{(D-8)}$$

Upstream of the contraction, the energy profile is described by the straight line

$$q^{2'} = q_0^{2'} (x - x_0)^{-n}$$

where $q_0^2 = 9.33 \times 10^{-2}$ and n = 1.2. The production term is zero in this region and the initial dissipation rate is determined from

$$\varepsilon_0' = -\frac{1}{2}\left(\frac{\partial q^{2'}}{\partial x_1}\right) = \tfrac{1}{2}n(q_0^{2'})(x-x_0)^{-n-1} \quad . \qquad \text{(D-9)}$$

Hence, for the lateral plane distortion (experiment #1) of Tucker (1970), $\varepsilon_0' = 0.75 \times 10^{-4}$. The same procedure was followed for all of the flows and the values determined for ε_0' in each case are listed in Table 3.12.